Identification of degradation pathways for HSP90 client proteins

A thesis submitted to the University of Sussex for the Degree of Doctor of Philosophy

Zhaobo Li

December 2016

Declaration

I hereby declare that this thesis has not been and will not be submitted, in whole or in part to another University for the award of any other degree.

Acknowledgements

First, I would like to express my appreciation to Professor Laurence H. Pearl and Dr Chrisostomos Prodromou who provided me with the opportunity to pursue a PhD degree at the University of Sussex, Genome Damage and Stability Centre. Their patients, continuous support and immense knowledge guided me through my PhD.

Secondly, I would like to thank to my father and mother for believing in me and supporting me throughout my studies both financially and emotionally. I am extremely grateful.

I would also like to thank Dr Velibor Savic for calibrating the siRNA screen experiment with me, Dr Lihong Zhou who helped me through the tissue culture techniques. Finally, I also would like to express my pleasure to my fellow colleagues from Laurence Pearl ‘s laboratory and all members of the GDSC for stimulating discussions and encouragement during my PhD.

University of Sussex

Zhaobo Li

Doctor of Philosophy Biochemistry

Identification of degradation pathways for HSP90 client proteins

Summary

Heat shock protein 90 (HSP90) is an ATP-dependent molecular chaperone that plays critical roles in regulating the folding, stabilization, post-translational modification, activation and maturation of its various client proteins, of which many are oncoproteins. Impairing the function of HSP90 by the inhibition of its ATPase cycle with inhibitors such as AUY922 promotes the ubiquitylation and proteasomal degradation of its client proteins. However, we currently do not fully understand the mechanism for ATPase-inhibited triggered degradation of client proteins, and which E3 ligase systems are involved.

Although previous studies revealed a number of E3 ligases including CHIP and CUL5 as potentially E3 ligases involved in the degradation of HSP90-dependent client protein, these have often used cancer cells that may have dysregulated systems. Additionally, other components of such E3 ligase systems have not been well characterised.

Using a Reverse Transfection Format (RTF) siRNA screen system we identified

two E3 ligases that are involved in two independent pathways for mediating proteasomal degradation of the HSP90-dependent protein kinase CRAF in HEK293 cells. The elongin BC-CUL5-SOCS-box protein (ECS) complex operates one pathway for the degradation of CRAF, while a novel but poorly described HECTD3 from the HECT-family was identified as the main E3 ligase for degrading CRAF following the pharmaceutical inhibition of HSP90. We revealed a potential complexes consisting of CRAF, HSP90 and HECTD3, which may contribute towards identifying the pathway for the degrading of such HSP90-dependent client protein kinases. We were also able to show that depriving access of CRAF to CDC37 and therefore HSP90 resulted in an HECTD3 and CUL5 independent degradation pathway. These studies form the basis of establishing the complex network of pathways that help to regulate CRAF protein levels.

Table of Contents

Abbreviations

17-AAG	17-N-allylamino-17-demethoxygeldanamycin/ Tanespimycin
17-DMAG	17-Dimethylaminoethylamino-17-demethoxygeldanamycin
A549	Adenocarcinomic human alveolar basal epithelial cells
ADARs	Adenosine deaminases acting on RNA
Ago	Argonaute
AHA	L-azidohomoalanine
AHA1	ATPase homolog 1
AKT	v-Akt Murine Thymoma Viral Oncogene
AMP-PNP	5′-Adenylylimidodiphosphate
AMPL	AMP-activated protein kinases
ANT1	Adenine Nucleotide Translocase 1
ASB	Ankyrin repeat and SOCS box protein
ATP	Adenosine triphosphate
ATPase	Adenosine triphosphatase
BAY 43-9006	Sorafenib
BONCAT	Bio-orthogonal non-canonical amino acid tagging
BRAF	v-RAF murine sarcoma viral oncogene homolog B
BSA	Bovine serum albumin
BTB	Bric-a-brac-tramtrack-broad
c-Kit	Mast/stem cell growth factor receptor
C-terminus	Carboxyl terminus
CAND1	Cullin-associated NEDD8-dissociated protein 1
CDC20	Cell-division cycle protein 20
CDC37	HSP90 chaperone protein kinase-targeting subunit

CDH1	CDC20 homologue 1
CDK4/6/11	Cyclin dependent kinase 4/6/11
CFTR	Cystic Fibrosis Transmembrane Conductance Regulator
CHIP	C terminus of HSC70-Interacting Protein
CK2	Casein kinase 2
cMET/MET	MET proto-oncogene, receptor tyrosine kinase
CO_2	Carbon dioxide
COS7	African green monkey fibroblast-like cell line 7
CR2/3	Complement receptor type 2/3
CRAF	Proto-oncogene serine/threonine-protein kinase
CRLs	Cullin-RING ligase
CTD	C-terminal domain
CUL	Cullin
CYP3A4	Cytochrome P450 3A4
DAPI	4',6-diamidino-2-phenylindole
DCAF	CUL4-associated factor
DCCR	DharmaFECT cell culture reagent
DDB1	DNA damage-binding protein 1
DIC	Differential interference contrast
DMSO	Dimethyl sulfoxide
DNA	Deoxyribonucleic acid
DOC1	Destruction of cyclin B protein 1
dsRNA	Double-stranded Ribonucleic acid
DTT	Dithiothreitol
DUBs	Deubiquitylating enzymes
E. coli	Escherichia coli
E1	Ubiquitin-activating enzyme

E2	Ubiquitin-conjugating enzymes
E3	Ubiquitin ligase
E6AP	Ubiquitin-protein ligase E3A
ECS	ElonginBC-CUL2/5-SOCS-box protein complex
EDD	Ethylenediamine Dihydrochloride
EDTA	Ethylenediaminetetraacetic acid
EGFR	Epidermal growth factor receptor
ErbB2	Receptor tyrosine-protein kinase erbB-2
ERI-1	3'-5' exoribonuclease 1
ERK	Extracellular signal-regulated kinases
FBXW8	WD40 domain 8
FCS	Foetal calf serum
FGFR-1	Fibroblast growth factor receptor 1
FITC	Fluorescein isothiocyanate
FKBP	Peptidyl-prolyl cis-trans isomerase FKBP
FUNCAT	Fluorescent non-canonical amino acid tagging
G2E3	G2/M phase-specific E3 ubiquitin-protein ligase
G418	Geneticin
GAPDH	Glyceraldehyde 3-phosphate dehydrogenase
GB	Glioblastoma
GDP	Guanosine diphosphate
GEF	Guanine nucleotide exchange factor
GFP	Green fluorescence protein
GI50	Growth inhibition 50
GRP	Glucose-regulated protein
GTP	Guanosine triphosphate
GTPase	Guanosine triphosphatase

HACE1	HECT domain and ankyrin repeat-containing E3 ubiquitin-protein ligase 1
Hch1	High-copy HSP90 suppressor protein 1
HCT116	Human colorectal carcinoma cell line
HECT	Homologous to the E6-AP Carboxyl Terminus
HECTD1/2/3	HECT domain-containing protein 1/2/3
HEK293	Human Embryonic Kidney 293 cells
HERC1/2	HECT domain and RCC1-like domain-containing protein 1/2
HOP/STIP1	Septin and tuftelin-interacting protein 1
HSP70	Heat shock protein 70
HSP90	Heat shock protein 90
HT29	Human colorectal adenocarcinoma grade II
HTPG	Chaperone protein HtpG
HUWE1	Homologous to E6AP carboxyl terminus homologous protein 9
IL4	Interleukin 4
IRS1/2	Insulin receptor substrate 1/2
ITC	Isothermal titration calorimetry
ITCH	E3 ubiquitin-protein ligase Itchy homolog
JAK2	Janus kinase 2
JNK	c-Jun N-terminal kinases
JUNB	Transcription factor jun-B
K48	Lysine 48
K63	Lysine 63
Kan	Kanamycin
K_d	Kilobase
kDa	Kilodalton
K_i	Inhibitory constant

KIAA0317	Apoptosis-resistant E3 ubiquitin protein ligase 1
KIAA0614	Probable E3 ubiquitin-protein ligase HECTD4
LAMP2	Lysosome-associated membrane glycoprotein 2
LB	Luria-Bertani
LKB1	Liver kinase B1/ Serine/threonine-protein kinase STK11
LOF	loss-of-function
MALT1	Mucosa-associated lymphoid tissue 1
MAPK	Mitogen-activated protein kinase
MAPKK	Mitogen-activated protein kinase kinase
MAPKKK	Mitogen-activated protein kinase kinase kinase
MASTL	Microtubule associated serine threonine kinase
MC4R	Melanocortin receptor 4
MD	Middle domain
MEK1/2	Dual specificity mitogen-activated protein kinase kinase 1/2
MG132	Carbobenzoxy-Leu-Leu-leucinal
$MgCl_2$	Magnesium chloride
Mia	PaCa2 human pancreatic cancer cells
min	minute
MLK3	Mixed-lineage protein kinase 3
mRNA	Messenger ribonucleic acid
MUF1/LRRC41	Leucine-rich repeat-containing protein 41
NCI-H460	human non-small cell lung cancer cells
NEDD8	Neural precursor cell expressed developmentally down-regulated protein 8
NEDL1	NEDD4-like E3 ubiquitin-protein ligase 1
nM	Nanomolar
NOTCH1	Neurogenic locus notch homolog protein 1

NTD	N-terminal domain
AUY922	Luminespib
Oca2	Melanocyte-specific transporter protein
ORF	Open reading frame
PBS	Phosphate buffered saline
PDGFR	Platelet-derived growth factor receptors
PDK1	Phosphoinositide-dependent kinase-1
PET	Photoinduced electron transfer
pH	potential of hydrogen
piRNA	Piwi-interacting ribonucleic acid
PIWI	P-element Induced WImpy testis
PKB	Protein kinase B
PLA	Proximity ligation assay
PLA	Proximity ligation assay
PP1	Protein phosphatase 1
PP2A	Protein phosphatase 2
PP5	Serine/threonine-protein phosphatase 5
Ras	Guanosine-nucleotide-binding protein
RBX1	RING finger protein 75
RBX2	RING finger protein 7
RCC1	Regulator of chromosome condensation 1
RDRP	RNA-dependent RNA polymerase
RET	Proto-oncogene tyrosine-protein kinase receptor Ret
RHEB	RAS homologue enriched in brain
RIP	Receptor-interacting serine/threonine-protein kinase 1
RISC	RNA-induced silencing complex
RLC	RISC-loading complex

RLD	Regulator of chromosome condensation 1-like domain
RNA	Ribonucleic acid
RNAi	Ribonucleic acid interference
RNase-III	Ribonuclease III
RP	Ribosomal protein
Rpb1	DNA-directed RNA polymerase II subunit A
rpm	Revolutions per minute
RTF	Reverse transfection format
RTK	Receptor tyrosine kinase
SAPK	Stress-activated protein kinases
SAXS	Small angle X-ray scattering
SCFs	Skp, Cullin, F-box containing complex
SDS	Sodium dodecyl sulphate
SGT1	Small glutamine-rich tetratricopeptide repeat-containing protein alpha
SH2	Sequence homology 2
siRNA	Single strand ribonucleic acid
siRNA	Small interfering ribonucleic acid
SKP1/2	S-phase kinase-associated protein 1/2
SMAD	Mothers against decapentaplegic homolog
Smurf1	SMAD-specific E3 ubiquitin-protein ligase 1
SOC	Super optimal broth
SOCS	Suppressor of cytokine signaling
SOS	Son of sevenless
Spc1	Signal peptidase complex subunit SPC1
SPSB 1	SplA/ryanodine receptor domain and SOCS box containing 1
SRC	Proto-oncogene tyrosine-protein kinase
T20	Tween 20

TCEB1/2/3	Transcription elongation factor B polypeptide 1/2/3
TFA	Trifluoroacetic acid
TIFF	Tagged Image File Format
TPR	Tetratricopeptide repeat
Trap1	Tumor necrosis factor type 1 receptor-associated protein
TRIP12	Thyroid receptor-interacting protein 12
U2OS	Human Bone Osteosarcoma Epithelial Cells
Ub	Ubiquitin
UBE3B	Ubiquitin-protein ligase E3B
UBE3C	Ubiquitin-protein ligase E3C
UPS	Ubiquitin proteasome system
UV	Ultraviolet
v/v	Volume per volume
VEGFR1	Vascular endothelial growth factor receptor 1/2/3
WD-40	Beta-transducin repeats
WSB	WD repeat and SOCS box-containing protein
WT	Wild type
WWP1/2	NEDD4-like E3 ubiquitin-protein ligase WWP1/2
YFP	Yellow fluorescence protein

List of figures

CHAPTER ONE

Introduction

1.1: Heat shock protein 90

1.1.1: A brief overview

Proteins that protect against thermal stress, or other such proteotoxic stresses, are called heat shock proteins (HSPs) and various human HSP families have been classified including HSP100, HSP90, HSP70, HSP60, HSP40, and HSP10. HSP90 is a 90-kDa chaperone protein that has the ability to assist folding, stabilization, post-translational modification, maturation and activation of vast array of proteins, otherwise known as client proteins. HSP90 is found in many multiprotein complexes, and works together with co-chaperones, but its role in the activation and maturation of client proteins is very poorly understood (Wiech et al., 1992; Dey et al., 1996; Chang et al., 1997; Prodromou et al., 1997b; Panaretou et al., 1998; Prodromou et al., 1999; Lee et al., 2002; Mayer, Nikolay and Bukau, 2002; Pearl and Prodromou, 2001; Siligardi et al., 2002; Meyer et al., 2004; Ali et al., 2006;). HSP90 is an ATP-dependent chaperone (Prodromou et al., 1997a), and the binding and hydrolysis of ATP drives a chaperone cycle that involves the dimerization of the N-terminal domains of HSP90 (Prodromou et al., 1997b; Panaretou et al., 1998). The ATPase activity of HSP90 has shown to be an essential property of this chaperone (Obermann et al., 1998; Panaretou et al., 1998; Young and Hartl, 2000).

Many of the HSP90 client-proteins are involved in cell signaling for growth, proliferation and migration; thus these signal transduction pathways rely on this remarkable chaperone. It is thus not surprising that HSP90 is found in the cytosol, nucleus and various organelles, as well as on the cell surface, suggesting that it also has possible extracellular roles (Trepel et al, 2010; Sidera et al, 2008; Eustace et al, 2004).

Client proteins include kinases; steroid hormone receptors, transcription factors and a list of clients can be found at https://www.picard.ch/downloads/HSP90interactors.pdf. In order to understand the diverse mechanistic roles that HSP90 plays, it is becoming apparent that a detailed structural knowledge of various HSP90 complexes is required.

Because of HSP90's involvement in the activation of key signaling proteins, HSP90 has become a major anti-cancer target (Trepel et al., 2010). Inhibition, by targeting the N-terminal ATP binding site results in the ubiquitylation of client protein and their subsequent proteasomal degradation (Whitesell et al., 1997). However, the components involved in such pathways are very poorly described and it is the aim of this study to identify such potential components that lead to the proteasomal degradation of the protein kinases CRAF.

1.1.2: Structure of HSP90

1.1.2.1: Introduction

The structure of full-length yeast Hsp90 was determined by x-ray crystallization in complex with its co-chaperone Sba1p (Ali et al, 2006) (**Figure** 1.1). The yeast form Hsp90 consists of three domains, an N-terminal domain, responsible for the binding of ATP and a variety of inhibitors (Prodromou et al., 1997a&b and 2000; Stebbins et al., 1997; Pearl and Prodromou, 2000), which is followed by a charged linker that leads to a middle domain that is thought to form a major client protein interaction site (Meyer et al., 2003). The C-terminal domain provides the basis of the inherent dimerization of the chaperone (Harris et al., 2004; Minami et al., 1994). Various other conformational structures of HSP90, either with or without nucleotides, have been characterized by biophysical techniques such as electron microscopy, small angle X-ray scattering

(SAXS) analysis and X-ray crystallography (Ali et al., 2006; Vaughan et al., 2006; Shiau et al., 2006; Southworth et al., 2008; McLaughlin et al., 2004; Meyer et al., 2004). These structures suggest a highly flexible and dynamic HSP90 structure.

1.1.2.2: The N-terminal domain

The first structural insight of HSP90 was through the determination of the X-ray crystallographic study of the N-terminal domain for human (Stebbins et al., 1997) and yeast (Prodromou et al., 1997b) (**Figure** 1.2 A). The 25kDa N-terminal domain consists of a two-layer sandwich alpha/beta structure that possesses a cleft into which ATP and inhibitors, such as geldanamycin.

Binding of ATP leads to a conformational change involving a loop structure, known as the lid, that binds over the bound ATP and through a series of conformational and co-operative structural changes leads to N-terminal dimerization and the formation of a catalytically active state (Prodromou et al., 1997a and 2000; Panaretou et al., 1998; Keramisanou et al., 2016). Subsequent hydrolysis of ATP induces the dissociation of the ATPase domains, and completes the chaperone cycle of HSP90, which is also subject to regulatory control by a variety of co-chaperones.

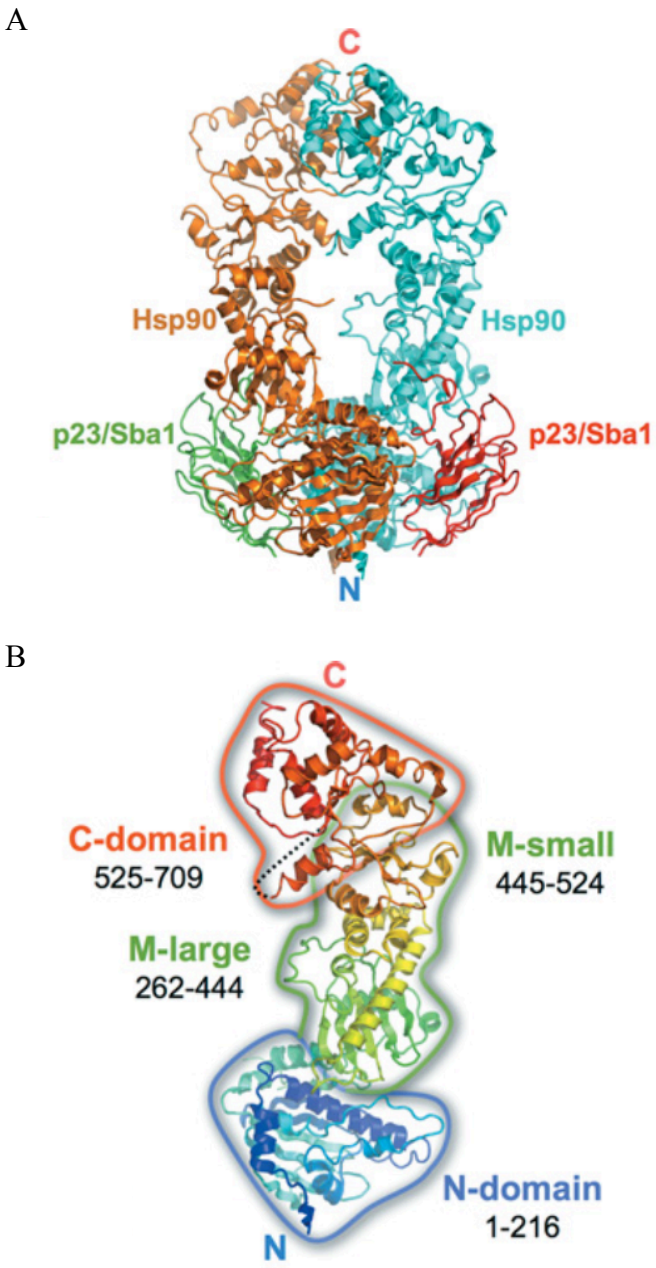

(Pear, Prodromou and Workman, 2008)

Figure 1.1 Crystal structure of HSP90 in complex with p23/Sba1p. (A) The two HSP90 molecules (orange and blue) interact respectively at C-terminus via a constitutive dimer interface and the N-terminus through a transient ATP-dependent interface. The HSP90 molecules twist around each other in the closed conformation. The co-chaperone p23/Sba1p binds at the junction of the two HSP90 N terminal domains in ATP-bound HSP90. **(B)** The domain structure of a singe monomeric HSP90 molecule.

1.1.2.3: The HSP90 middle domain

The structure of the middle segment of HSP90 was determined some time after the N-terminal domain structures (Meyer et al, 2003). The middle segment has a molecular mass of 35 kDa and is composed of three sub-domains. The N-terminal region consists of a large alpha-beta-alpha fold. At the C-terminal end there is a second alpha-beta-alpha fold but this sub-domain is much smaller than the N-terminal one. Theses sub-domains are linked together by a tight coil of 3 short alpha helices (**Figure** 1.2 B). Mutagenesis studies suggest the middle domain appears to be a client protein interaction site (Meyer et al., 2003). This is supported by the observation that the binding site for protein kinase PKB/Akt appears to map to the middle domain of HSP90 (Sato et al., 2000), and by electron microscopy studies (EM) that revealed CDK4 bound to this domain (Vaughan et al., 2006; Cara et al., 2006). However, other reports suggest that client proteins also interact with several other regions of HSP90. The precise details by which HSP90 recognizes client protein are still poorly understood. Recently it has been suggested that HSP90 recognizes proteins, such as kinases, that have an inherently unstable fold (Keramisanou et al., 2016).

1.1.2.4: The HSP90 C-terminal domain

The C-terminal domain of HSP90 (**Figure** 1.2 C&D) has the molecular mass of 12-kDa and is essential for the inherent dimerization of the chaperone (Toft et al., 1998; Chiosis et al., 2004; Harris et al., 2004). At the extreme C-terminus is a teratricopeptide repeat (TPR) motif responsible for recruiting TPR domain containing co-chaperones, such as HOP (also known as Stip1 in yeast), FKBP proteins, PP5 and AIP/Xap2/ARA9. HOP scaffolds the association between HSP90 and HSP70 through its TPR domains (Scheufler et al., 2000).

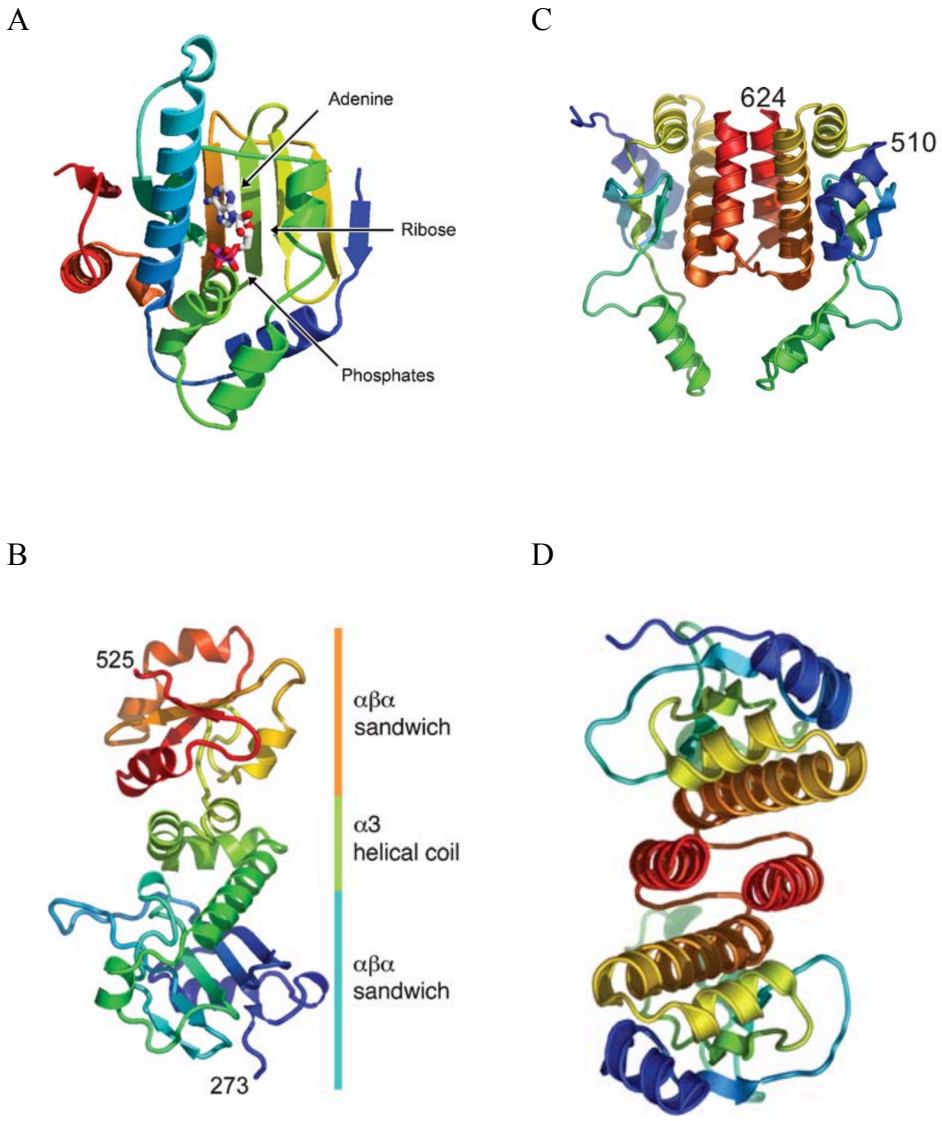

(Pearl and Prodromou, 2006)

Figure 1.2 Domain crystal structures of HSP90. (A) The N-terminal domain of yeast Hsp90 with AMPPNP bound to the ATP/ADP binding site. **(B)** The three sub-domain crystal structure of the middle segment of yeast Hsp90. **(C)** Crystal structure of the *E.coli* Hsp90 (Hptg) homologue C-terminal domain, responsible for the inherent dimerization of HtpG (left). **(D)** HtpG C-terminal domains viewed down the local pseudotwofold symmetry axis of panel (C). All structures are coloured from the N to the C terminus in rainbow (blue to red, respectively).

1.1.3: ATPase chaperone cycle of HSP90

HSP90 is an ATP-dependent chaperone protein, and its ATPase activity has been shown to be essential for the activation and folding of client proteins (Panaretou et al., 1998 and 2002) (**Figure** 1.3 A&B). Previous studies revealed that the ATP-binding pocket is located in the N-terminal domain (NTD) of HSP90 (Prodromou et al., 1997a), and multiple conformational changes are required to form a catalytically active unit that is able to hydrolysis ATP. A critical structural element in the NTD of HSP90, called the 'lid', controls the dimerization of NTD and its association with the middle domain (MD) of HSP90 upon ATP binding. The 'lid' traps bound ATP by closing over the ATP-binding pocket, while simultaneously exposing a hydrophobic surface required for dimerization (Panaretou et al., 1998). The docking of the NTDs with the middle domains of HSP90 allows the middle domain catalytic loop to interact with bound ATP, which is essential ATPase activity (Prodromou et al., 2000; Meyer et al., 2003 and 2004; Pearl and Prodromou, 2006). Recently, these motions were directly observed using one-nanometer fluorescence probes based on photo-induced electron transfer, and found to act cooperatively (Schulze et al., 2016) (**Figure** 1.4). A two-step mechanism for lid closure over the bound nucleotide was apparent and the co-chaperone AHA1 could mobilize the lid of apo HSP90, suggesting an early role in the catalytic cycle (Schulze et al., 2016). The ATPase competent state of HSP90 is stabilized by casein kinase 2 (CK2), which phosphorylates threonine 22 of HSP90 in the α–helix 1 of the NTD of yeast HSP90 (Mollapour et al., 2011).

A

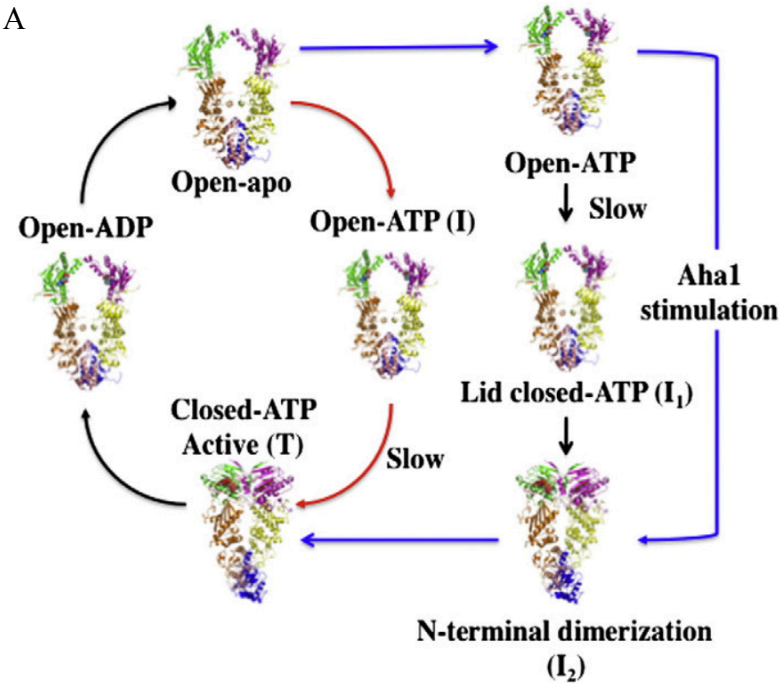

B

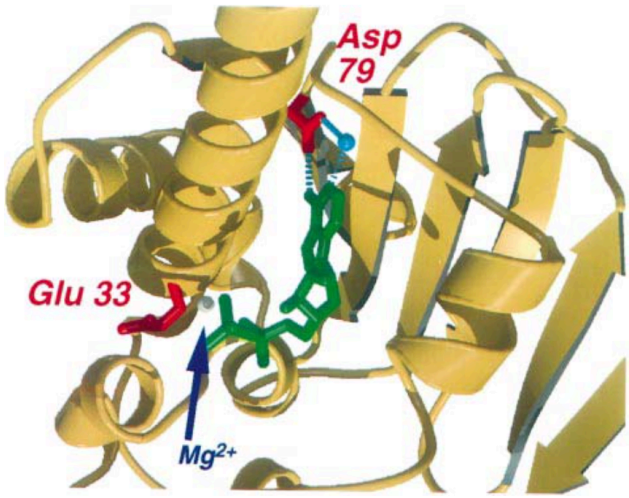

(Prodromou, 2012;Panaretou et al., 1998)

Figure 1.3 ATPase chaperone cycle of HSP90. (A) The ATPase kinetic cycle of S.cerevisiae Hsp90 and *E.coli* HtpG. The blue and black arrows indicate the ATPase cycle in yeast. During this cycle of conformation change, two intermediate conformations, I1 and I2, are involved that lead to the catalytically state (closed-ATP Active) (T). The I1 sate is bypassed by co-chaperone AHA1 to accelerate the cycle. In contrast, the formation of the closed-ATP active state of the *E.coli* (red and black

arrows) involves by a two-phase transition through an intermediate conformation (I). ‘Slow’ indicates the rate-limiting step in both cycles. **(B)** Binding and hydrolysis of ATP is necessary for the activation of HSP90-dependent kinases. The amino acid residues, Asp79 and Glus33 (shown in red) of the NTD of HSP90 are essential for nucleotide binding and hydrolysis of ATP.

1.1.4: Co-chaperones of HSP90

1.1.4.1: Introduction

There are numerous co-chaperones that operate with HSP90 that associate with specific types of client proteins and thus form defined chaperone complexes (Riggs et al., 2004; Taipale et al., 2012). These include those that deliver client proteins to HSP90, such as HOP (yeast Sti1p) and CDC37, those that regulate the chaperone cycle, such as AHA1, and p23 (yeast Sba1p), those that play a structural role (i.e. Pih1) or those that display a specific enzymatic activity, such as PP5 and immunophilins. However, even though a given co-chaperone may be involved in specific process such as client protein delivery, it may also be able to regulate the cycle to achieve client protein activation for example. The next section will cover the roles of such co-chaperones in more detail.

1.1.4.2: The co-chaperone CDC37

A wide range of its client proteins has been identified and the number is continually increasing (http://www.picard.ch/downloads/HSP90interactors.pdf). These clients can be approximately divided into three classes including protein kinases, transcription factors (ie, the nuclear receptors for steroid hormones) and structurally unrelated clients (Pratt et al., 2004 and 2006).

CDC37, also known as p50, is a co-chaperone that specifically recognizes client protein kinases and recruits them to HSP90 (Shao et al., 2003a&b; Caplan et al., 2007; Karnitz and Felts, 2007; Taipale et al., 2012). CDC37 was previously shown to interact with CDK4 and form a complex with HSP90 (Dai et al., 1996; Vaughan et al., 2006) (**Figure** 1.5 A). The structure of the HSP90-CDC37-CDK4 complex has also been determined to 3.9 angstrom by cryo-electron microscopy (Verba et al., 2016). Surprisingly, C- and N-

terminal lobes of CDK4 are separated with the unfolding of the β4-β5 sheet. The open kinase is stabilized by CDC37, which mimics part of the kinase N lobe, by wedging itself between the two kinases lobe. Finally, HSP90 was seen to be clamped around the unfolded kinase β5 strand and interacting with both the exposed N- and C-lobe interfaces, thus protecting the kinase in a trapped unfolded state (Verba et al., 2016) (**Figure** 1.5 B). CDC37 has also been shown to bind CRAF (Stancato et al., 1993; Grammatikakis et al., 1999), LKB1 (Boudeau et al., 2003; Nony et al., 2003), MLK3 (Zhang et al., 2004), EGFRvIII (Lavictoire et al., 2003), SAPK, Spc1 (Tatebe and Shiozaki, 2003) and CDK11 (Mikolajczyk et al., 2004) amongst others.

The reorganization of CRAF by CDC37 has been controversial. The binding site was previously reported to be the C-terminal domain of CDC37 between residues 1 to 163 (Grammatikakis et al., 1999). However, another study revealed that CDC37 residues 181 to 200 were able to recognize client proteins kinases such as CRAF, Akt1, Aurora B and CDK4. In particularly, residues 191 to 195 of CDC37 were particularly required for CRAF interaction (Terasawa and Minami, 2005) and that N-terminal lobe of the kinase proteins was critical for this interaction (Mort-Bontemps-Soret et al., 2002; Scroggins et al., 2003; Zhao et al., 2004; Prince et al., 2004).

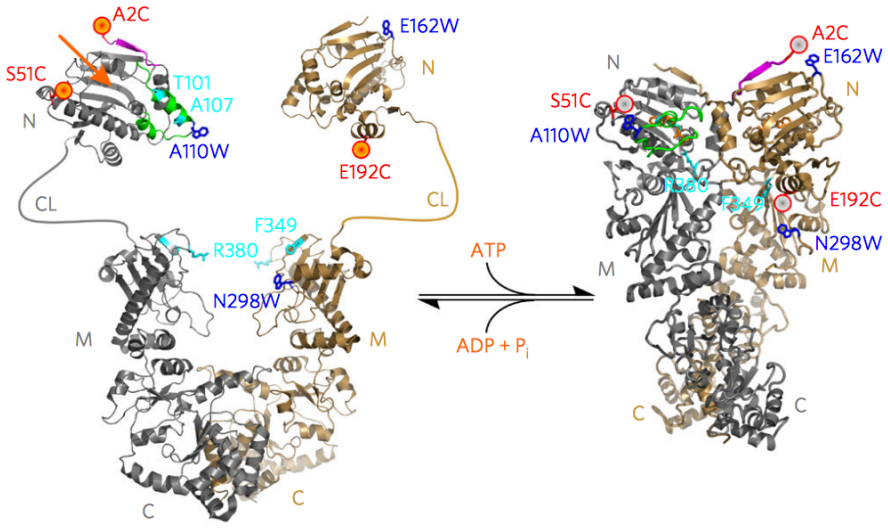

(Schulze et al., 2016)

Figure 1.4 Tracking the conformational change of HSP90 ATPase cycle by PET fluorescence quenching. (Left) The nucleotide free state of HSP90. The ATP binding site is indicated (Orange arrow). **(Right)** The binding of ATP induces the closed-clamp conformation. Magenta and green indicates the N-terminal β-strand and the lid, respectively. The red spheres and blue sticks represent the PET reporters.

The crystal structure of the Middle and C-terminal domain (MC) of CDC37 in complex with the N-terminal domain of HSP90 has been determined (Vaughan et al., 2006; Pearl and Prodromou, 2006) (**Figure** 1.6 A & B). This showed a 1:1 stoichiometric complex (Roe et al., 2004), with CDC37 bound to the lid segment of the NTD of HSP90 (**Figure** 1.6 C). Consequently, the NTD is prevented from conformational movement and the ATPase activity of the chaperone is inhibited. Furthermore, Arg 167 of CDC37 also interacts with the catalytic Glu 33 of the ATPase domain of HSP90, thus preventing hydrolysis of any bound ATP (**Figure** 1.6 C) (Prodromou et al., 1997a; Panaretou et al., 1998; Obermann et al., 1998). Following delivery of the client protein and inhibition of the chaperone cycle, it is thought that the chaperone and kinase are now in specific conformational states that allow molecular recognition between them. It appears that CRAF binds to HSP90 through the C-terminal catalytic domain of the kinase (Stancato et al., 1993). Furthermore, the stabilization of CRAF was reported to depend on the activity of HSP90 (Eccles et al., 2008). The chaperone cycle is thought to progress following the binding of ATP and the ATPase stimulating co-chaperone AHA1 (**Figure** 1.5 B). The details of the mechanism leading to disengagement of CDC37 and Kinase form the chaperone complex are not understood.

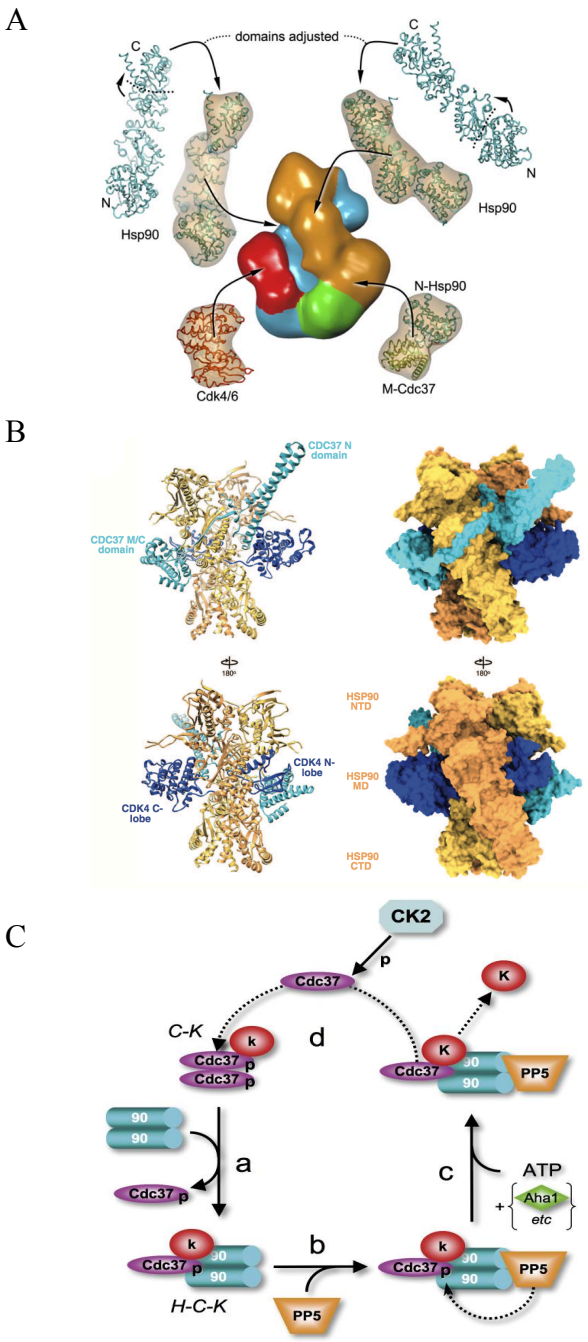

(Vaughan et al., 2006; Verba et al., 2016)

Figure 1.5 Kinase client activation. (A) The EM reconstruction of HSP90 in complex with CDK4/6 and CDC37. In this 20 A˚ resolution atomic models, CDK6 is used to illustrate how its larger C-terminal lobe is associated with one of the meddle-domains of a HSP90 monomer. The N-terminal domain of CDK6 associates with the N-terminal domain of HSP90 and/or CDC37. The middle domain of CDC37 interacts with one of the N-terminal domains of HSP90. **(B)** The closed conformation HSP90 (Yellow) in

complex with CDK4 (Teal) and CDC37 (Blue). This HSP90-CDC37-CDK4 complex was revealed by a 3.9-angstrom cryo-electron microscopy and represented in ribbon (left) and surface structure (right). **(C)** A schematic of a proposed mechanism of kinase client activation and the co-chaperones involved. (a) A stable HSP90-CDC37-inactive kinase (H-C-K) is formed after CDC37-inactive kinase (C-K) complex binds to a dimeric HSP90 with loss of one CDC37 monomer. (b) CDC37 is dephosphorylated upon binding of PP5/Ppt1. (c) The binding of ATP and other co-chaperones such as AHA1 may occur either prior to or concomitantly with the process of the dephosphorylation of CDC37. (d) Following the hydrolysis of ATP active kinase dissociates from the complex. CK2 rephosphorylates CDC37 at Ser 13 for the next HSP90 cycle.

The mechanism by which CDC37 recognizes a client protein kinase was recently reported (Keramisanou et al., 2016). The authors suggest that CDC37 acts as a scanning factor and is able to selectively bind kinases that are inherently unstable. Binding of the kinase further destabilizes its structure leading to a stable CDC37-kinase complex, in which the kinase can then interact with HSP90 following CDC37 binding (**Figure** 1.7 A, B & C).

Thus, induced conformational stability of the kinase acts as the determinant for selection by CDC37 and binding to HSP90. Stable formation of an HSP90-CDC37-kinase ternary complex is promoted by Ser 13 phosphorylation of CDC37 (Miyata and Nishida, 2004; Polier et al., 2013; Shao et al., 2003b; Vaughan et al., 2008). The phosphorylation of CDC37 at Ser13 is dependent on the Ser/Thr kinase, CK2 (**Figure** 1.5 C) (Bandhakavi et al., 2003; Shao et al., 2003b: Miyata and Nishida, 2004), while the protein phosphatase PP5/Ppt1 dephosphorylates p-Ser 13 (Vaughan et al., 2008) (**Figure** 1.5 C). It has also been reported that the phosphorylation of various Tyr residues on CDC37 abolishes the association with different client protein kinases (Xu et al., 2012).

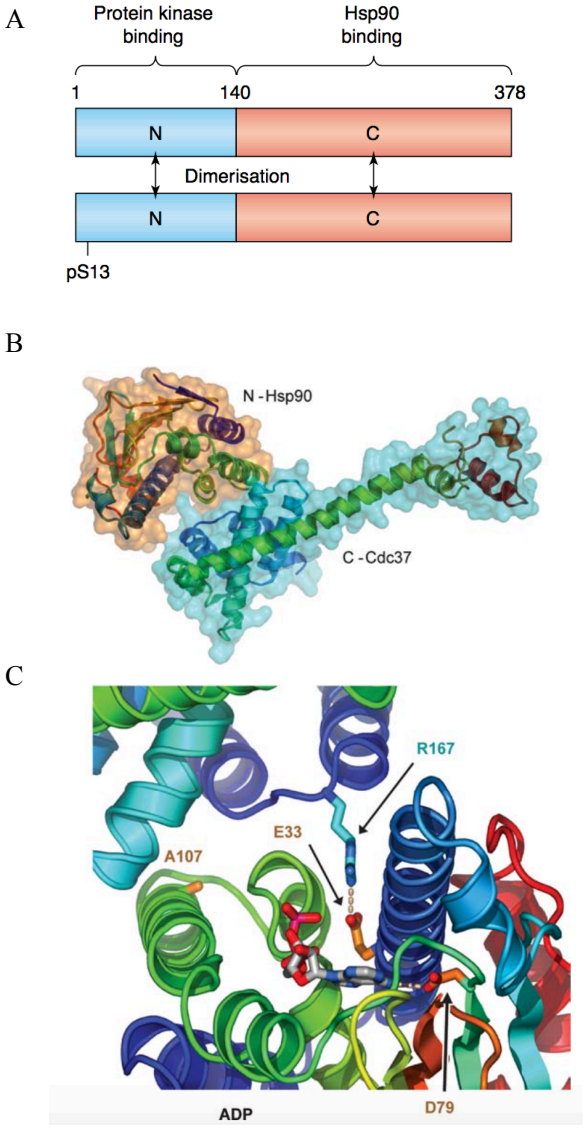

(Pearl, 2005; Pearl and Prodromou, 2006)

Figure 1.6 Schematic domain structure of CDC37 and the crystal structure of the MC-CDC37 – NTD-HSP90 complex. (A) The NTD (blue) of CDC37 is essential for kinase binding, while the central and C-terminal region (red) is the HSP90 and kinase binding domain. The assembly and stability of HSP90-CDC37-kinase complex is regulated by a CKII phosphorylation located in N-terminal region. **(B)** Crystal structure of CDC37 C-terminal region (blue) in complex with the NTD (orange) of HSP90. **(C)** The "lid" segment in the NTD of HSP90 provides the binding surface for CDC37. CDC37 inserts the guanidinium side chain of Arg 167 into the HSP90 nucleotide-binding pocket and interacts with catalytic residue Glu 33.

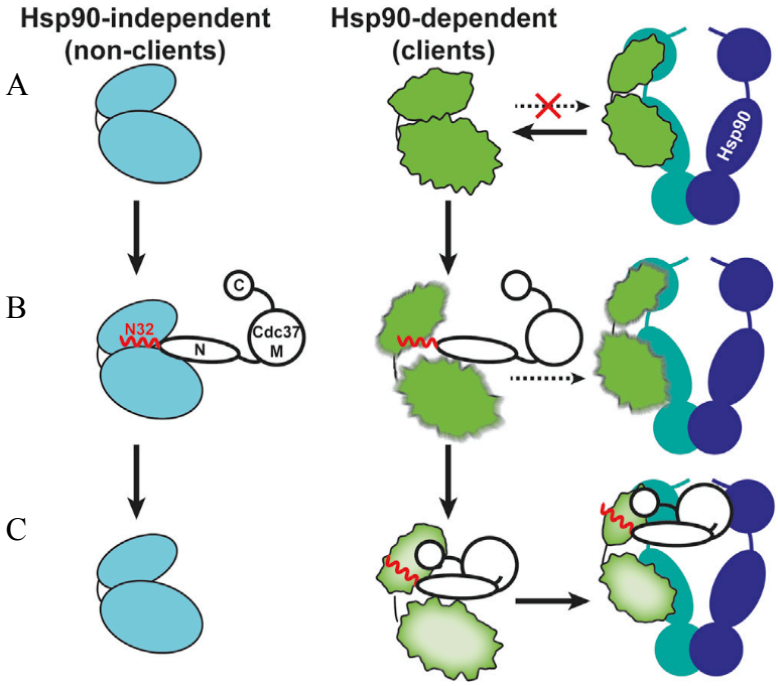

(Keramisanou et al., 2016)

Figure 1.7 Recognition and sorting schema of protein kinase by CDC37. (A) Non-clients (blue filled) obtain a native conformation without HSP90 (dark green and blue) assistance. Such kinases (cyan) display a high level of thermodynamic stability. **(B)** Clients (green) with a low thermodynamic stability fail to interact fully with CDC37 and are therefore not recruited to HSP90. They simply interact with the NTD of CDC37 (N-CDC37) (black outline) with helix a1 (N32) tail (red) recognizes. The conformational properties of non-clients are therefore not affected by binding with N-CDC37. **(C)** Client protein kinases stably associated with both the N-terminal and C-terminal of CDC37 are recruited to HSP90. The conformational properties of kinase clients are destabilized upon the association with N-CDC37.

1.1.4.3: The co-chaperone AHA1

AHA1 is the most potent protein activator of the ATPase activity of HSP90 (Panaretou et al., 2002; Meyer et al., 2003&2004; Retzlaff et al., 2010). Structural studies using the NTD of AHA1 revealed the mechanism by which this domain could activate the ATPase activity of HSP90 (**Figure** 1.8). The NTD of AHA1 is able to modulate the conformation of a catalytic loop, found in the MD of the chaperone, and thus facilitates engagement of Arg 380 with the γ-phosphate of ATP bound in the NTD (Meyer et al., 2003; Prodromou, 2012). However, for full activation the C-terminal domain of AHA1 is also required (Panaretou et al., 2002). The C-terminal domain of AHA1 was shown to bind between the NTDs of HSP90, at a site overlapping that for Sba1p binding, This might provide stabilization of the N-terminally dimerised state (Retzlaff et al., 2010).

AHA1, Unlike STIP1/HOP and CDC37, is not involved in client protein delivery and most likely partakes in a role downstream of client protein binding. AHA1 has been implicated in the activation and maturation of protein kinases, steroid-hormone receptors, CFTR, MC4R and ANT1 (Panaretou et al., 2002; Lotz et al., 2003; Harst et al., 2005; Koulov et al., 2010; Wang et al., 2006; Meimaridou et al., 2011; Holmes et al., 2008; Swick and Kapatos, 2006; Ran, Gadura and Michels, 2010; Sun et al., 2008; Zhong et al., 2009). AHA1 appears to be a regulatory co-chaperone of HSP90 activation of client proteins in general or alternatively is specifically required for the regulation and assembly of oligomeric HSP90 complexes (Sun et al., 2012).

In addition to AHA1, budding yeast possesses a small AHA1 paralogue, Hch1 (Nathan et al., 1999) resembling the N-terminal domain of AHA1. Hch1 can activate HSP90 ATPase activity (Panaretou et al., 2002), but its biological function is very different to

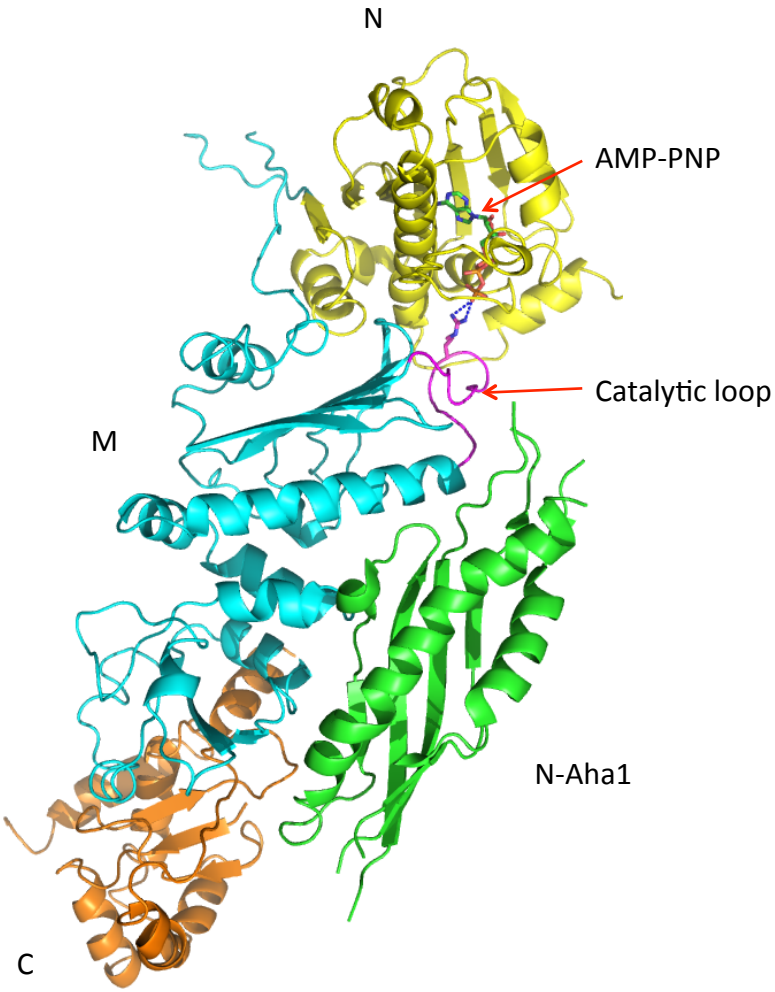

Fig 1.8 Structure of AHA1-HSP90 complex showing activation of the catalytic loop. The monomeric structure of HSP90 with N-terminal (yellow), Middle (light blue) and C-terminal (brown) domains are shown. Bound AMP-PNP bound to the N-terminal domain is in stick representation (green). The catalytic loop of HSP90 is shown in magenta. The N-terminal domain of AHA1 (green) interacts with the middle domain of HSP90 and promotes an open state of the catalytic loop of HSP90 and thus allows Arg 380 to interact with γ -phosphate of ATP (AMP-PNP in this case). Hydrogen bonds are presented as a broken blue line.

that of AHA1 (Armstrong et al., 2012). Deletion of Hch1, but not AHA1, mitigates the temperature sensitive phenotype of two HSP90 mutations, G313S and A587T, while overexpression increases sensitivity to the HSP90 inhibitor AUY922 (Armstrong et al., 2012).

1.1.4.4: The co-chaperone PP5

The human serine/threonine protein phosphatase type 5 (PP5) has a three-domain structure (Swingle et al., 2004) and appears to be required for the activation and maturation of HSP90 kinase client proteins. The dephosphorylation of CDC37 by PP5 at Ser 13 causes the dissociation of kinase from the HSP90 complexes. (Vaughan et al., 2006 & 2008; Mayer, Prodromou and Frydman, 2009) (**Figure** 1.5 C)

The N-terminal domain of PP5 consists of three tetratricopeptide repeat (TPR) motifs, while the C-terminus is an auto-inhibitory domain, and the middle domain is the phosphatase catalytic domain (**Figure** 1.9 A). The N-terminal TPR domain is responsible for binding the conserved MEEVD motif at the C-terminal end of HSP90 and three specific residues (Lys32, Lys97 and Arg101) within the TPR cleft of PP5 have been identified as important for the binding HSP90 (Das et al., 1998; Blatch and Lassle, 1999; Russell et al., 1999; Scheufler et al., 2000; Ramsey et al., 2000) (**Figure** 1.9 B).

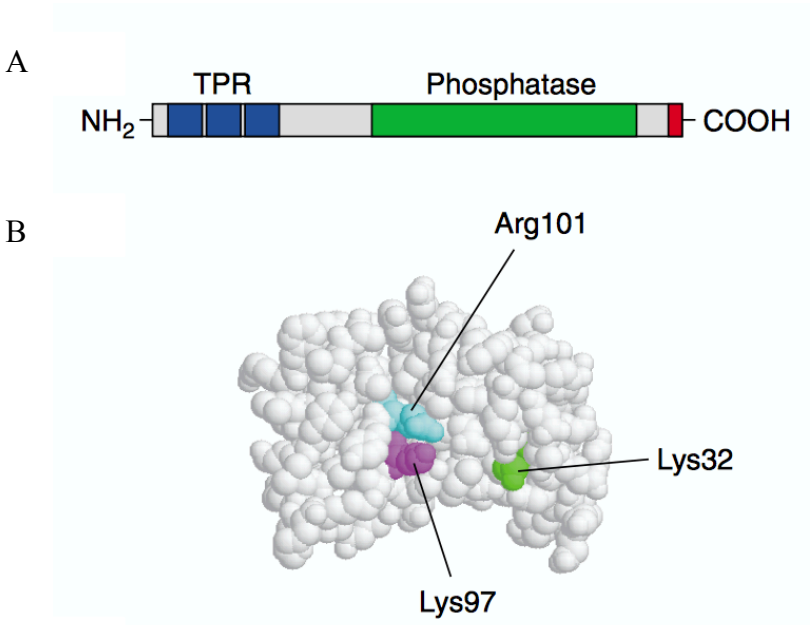

(Chinkers, 2001)

Figure 1.9 Domain structure and the activation of phosphatase type 5 (PP5). (A) The N-terminus of PP5 contains three TPRs (blue). The phosphatase catalytic domain (green) is upstream of the C-terminal auto-inhibitory domain (red). **(B)** Lys32 (green), Lys97 (purple) and Arg101 (cyan) are the three basic residues in the TPR domain (white fill) of PP5 for associating with HSP90.

1.1.5: Inhibition of HSP90

1.1.5.1: Overview

The chaperone cycle of HSP90 is dependent on the binding and hydrolysis of ATP by its N-terminal domains (Prodromou et al., 1997a). Many of HSP90's client proteins not only contribute to normal cell maintenance but also when mutated, help to drive oncogenesis. HSP90 itself can be highly expressed (Pick et al., 2007), which helps and supports oncoprotein function. Furthermore, nutrient stress, proteotoxicity, hypoxia or genetic instability in cancer cells could further drive up the levels of HSP90. HSP90 is itself involved in processes that lead to tissue invasion, abnormal angiogenesis, avoidance of cellular apoptosis and immune destruction (Workman et al., 2007; Trepel et al., 2010; Neckers and Workman, 2012) (**Figure** 1.10). Because of HSP90's central role is not only maintaining oncoprotein function, but also promoting oncogenic processes, it is no wonder that HSP90 is a major anticancer target (Powers and Workman, 2006; Neckers and Workman, 2012). Initial worries about cytotoxicity in targeting HSP90 due to its housekeeping role in cells (Kim et al., 2009) have subsided and it has been demonstrated that targeting HSP90 leads to inhibition of cell proliferation, degradation of client proteins and apoptosis using inhibitors such as 17-AAG (Hostein et al., 2001). .

1.1.5.2: Development of HSP90 inhibitors

In 1994, HSP90 was discovered as the molecular target of geldanamycin. This inhibitor prevented association of the client protein SRC with HSP90, which consequently destabilized the kinase by ubiquitylation and proteasomal degradation (Whitesell et al., 1994).

The molecular details of the interaction between geldanamycin and HSP90 were finally observed when the structure of the NTD of HSP90 was crystallized in complex with this inhibitor (Stebbins et al., 1997; Roe et al., 1999). Although geldanamycin can arrest the function of HSP90 by inhibiting its ATPase activity (Roe et al., 1999), geldanamycin has many limitations due to its hepatotoxicity and poor solubility. Therefore, geldanamycin has not progressed far in clinical trials. But, it has provided a basic chemical structure that can be further developed.

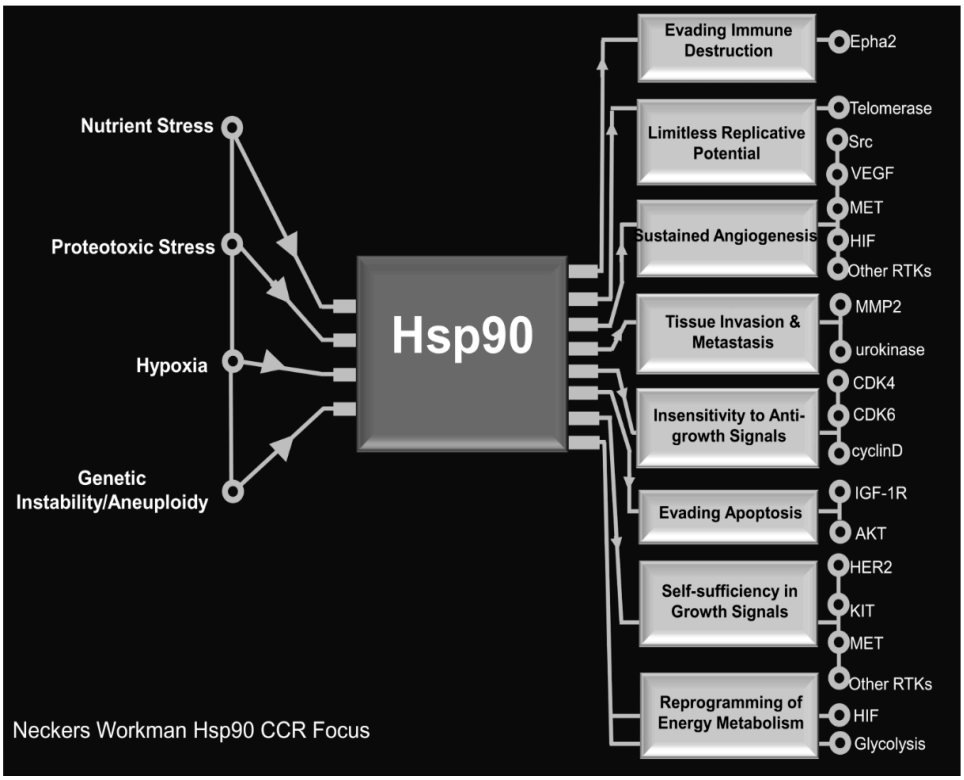

(Neckers and Workman, 2012)

Figure 1.10 Schema for HSP90 responding to stress conditions in cancer cells. In responds to the various environmental stresses, HSP90 in cancer cells acts as a buffer for mediating the expression of numerous client proteins, regulating biological signaling and pathways (list on the right) that then promotes the cell survival.

17-allylamino-17-demethoxy-geldanamycin (17-AAG) and 17- (dimethylamino - ethylamino)-17-demethoxygeldanamycin (17-DMAG) are the two next generation inhibitors (Taldone et al, 2009; Neckers and Workman, 2012). In contrast to geldanamycin, 17-AAG and 17-DMAG possess less toxicity and are more soluble than geldanamycin (Ge et al., 2006; Sausville et al, 2003). Additionally, both have progressed in phase I and II clinical trials, and the results showed they both suppressed and stabilized tumors (Banerji et al, 2005; Pacey et al, 2006; Modi et al, 2007). However, this class of inhibitor still retains limitations, including hepatotoxicity, poor pharmacokinetics, and polymorphic metabolism via CYP3A4 (Cytochrome P450 3A4). Additionally, the formulation of these drugs is difficult (Egorin et al, 1998).

1.1.5.3: Potent activity of AUY922: A novel HSP90 inhibitor

Among the HSP90 inhibitors, AUY922, 5-(2,4-Dihydroxy-5-isopropylphenyl)-4-(4-morpholin-4-yl- methylphenyl) isoxazole-3-carboxylic acid ethylamide (also named as Luminespib), is a novel isoxazole amide inhibitor that is the most potent synthetic small molecule inhibitor so far developed against the NTD of HSP90 (Brough et al., 2008; Eccles et al., 2008; Gao et al., 2010) (**Figure** 1.11). Previous studies showed AUY922 exhibited the ability to regulate the activity of glioblastoma (GB) and that continual drug exposure does not result in resistance to AUY922 (Gaspar et al., 2009 and 2010). AUY922 was also found to be potent against breast cell lines (Jensen et al., 2008), xenograft tumor (Eccles et al., 2008), early antiangiogenic tumor (Nagengast et al., 2010), glioblastoma (Gaspar et al., 2010) and non-small cell lung cancers (Ueno et al., 2012; Garon et al., 2013; Park et al., 2016).

The structure of AUY922 in complex with the N-terminal domain of human HSP90 in has been determined (Brough et al., 2008) and the IC50 against HSP90 α is 7.8 ± 1.8

nmol/L and 21 ± 16 nmol/L for HSP90 β (Brough et al., 2008). The K_i values are 9.0 ± 5.0 nmol/L (HSP90 α) and 8.2 ± 0.7 nmol/L (HSP90 β). The *K*d value determined by isothermal titration calorimetry (ITC) for HSP90 β is 1.7 ± 0.5 nmol/L (Sharp et al., 2007b) and this data shows that the binding is mainly enthalpically driven (Eccles et al., 2008). In contrast to binding cytoplasmic HSP90, binding to the endoplasmic HSP90, GRP94 and the mitochondrial Trap1 appears to be weaker (Grp94, IC50 535 ± 51 nmol/L and K_i = 108 nmol/L) and TRAP-1 (IC50 85 ± 8 nmol/L and K_i = 53 nmol/L) (Eccles et al., 2008). Inhibition of HSP90 by AUY922 shows typical client protein degradation of kinases such as ErbB2, CRAF, LKB1 and CDK4 within 24 hours after the treatment of HEK293 and HCT116 human cancer cells (Eccles et al., 2008). The cell cycle of HCT116 cells was arrested by AUY922 in G1 and G2-M phase (Eccles et al., 2008). Research on the effects of HSP90 inhibitors has helped us to understand the molecular mechanism of HSP90 to some degree. Pre-treatment with AUY922 has helped identify HSP90 client-proteins and has been shown to induce their degradation. Such proteins include ErbB2, MASTL, LKB1, CDK1, CDK4, Akt, pAkt, CRAF and $BRAF^{V600E}$, which are critical components for cell proliferation, growth and survival. Loss of important client proteins such as these impacts greatly on cellular processes leading to increased DNA damage and impairment of the cell cycle (Stingl et al., 2010).

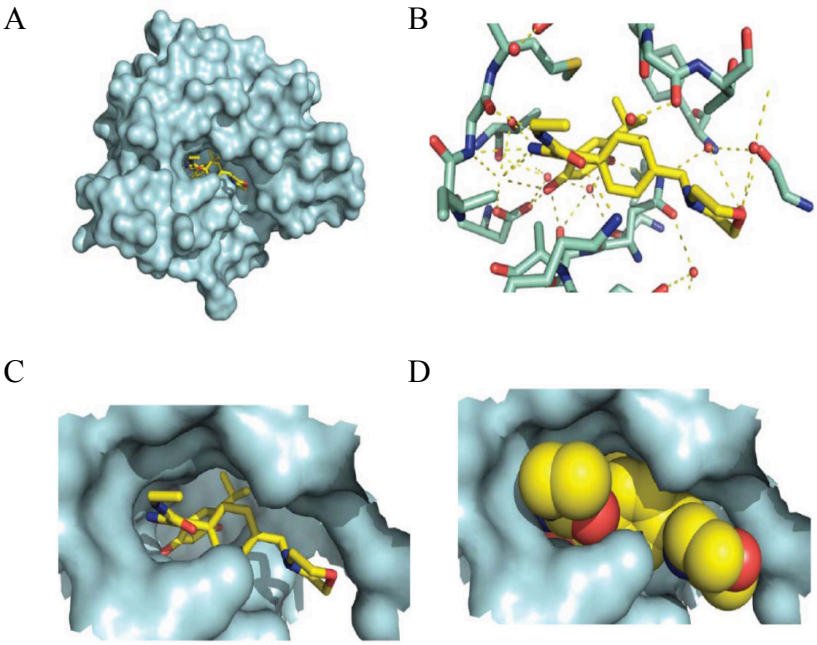

(Neckers and Workman, 2012)

Figure 1.11 X-ray crystal structure of AUY922 bound in the NTD of HSP90. (A) Space filled model of the NTD of human HSP90α (blue) with bound AUY922 inhibitor (yellow) in the ATP pocket. **(B)** Detail of AUY922 (yellow) binding to the NTD of HSP90 (green), including hydrogen bonding (dotted yellow) and water molecules (red spheres). **(C)** A close up of the space filled view of AUY922 in the ATP pocket of HSP90 (blue) with hydrogen-bonding interaction removed. **(D)** A space filled model of AUY922 within the solvent-accessible surface of HSP90 (blue).

1.2: The protein kinase CRAF

1.2.1: The RAF-MEK-ERK pathway

The activation of RAF kinase by the HSP90 chaperone cycle is detailed in Section 1.1.4.2. The Mitogen-activated protein kinase (MAPK) cascade is a cellular signaling pathway involved in cell proliferation, differentiation and survival (**Figure** 1.12 A). The MAPK signaling pathway is a highly conserved intracellular pathway, which consists of a series of protein kinases including a MAPK kinase kinase (MAPKKK), a MAPK kinase (MAPKK) and a MAPK (Johnson and Lapadat., 2002). There are four MAPK pathways in mammalian cells (**Figure** 1.12 B). In particularly, the pathway that includes the RAF family kinase is described as the RAF-MEK-ERK MAPK cascade (Wellbrock et al., 2004; Schreck and Rapp, 2006) and is usually activated by growth factors. The other three are commonly known as the JNK, p38 and ERK5 pathways and normally activated by stress stimulators (Roberts and Der, 2007). Thus, these pathways are activated by extracellular signals detected by a receptor tyrosine kinase (RTK) (Wellbrock et al., 2004).

The RAF-MEK-ERK cascade is activated by the G-protein RAS (Wilhelm et al., 2004). HRAS, KRAS and NRAS are the three classes of RAS that share 85% similarity in their amino acid sequence (Lowy and Willumsen, 1993). The activation of RAS depends on the turnover of GDP and GTP, which is controlled by GTPase activating proteins (GAPs) and guanine nucleotide exchange factors (GEFs) (Campbell et al., 1998). There are three members from the RAF serine/threonine protein kinase family; ARAF, BRAF and CRAF (also known as RAF-1) (Rapp et al., 1983; Jansen et al., 1984; Sutrave et al., 1984). Activated G-protein RAS signals recruit RAF kinase to the plasma membrane,

where it in turn becomes activated (Leevers et al., 1994; Stokoe et al., 1994). A phosphorylation cascade then follows that results in active ERK1/2, which finally enters the nucleus via translocation to activate, by phosphorylation, transcription factors that are responsible for the expression of specific genes (Wellbrock, 2004).

A

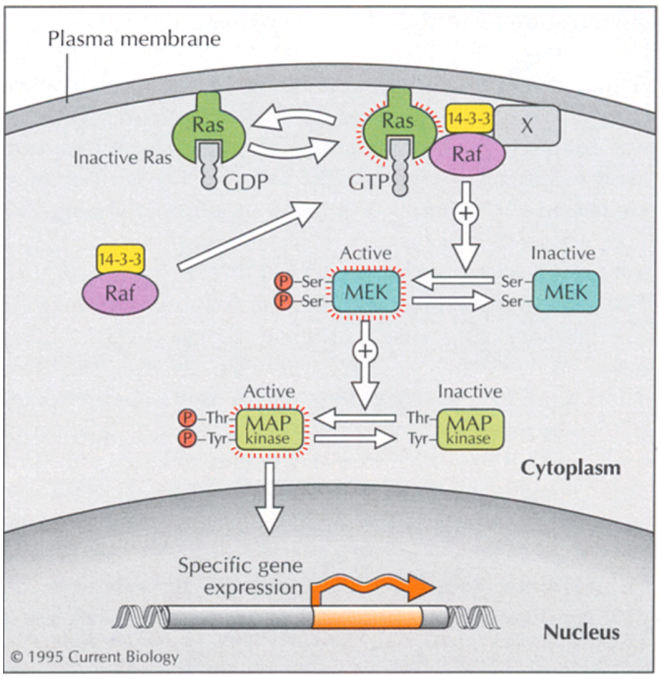

B

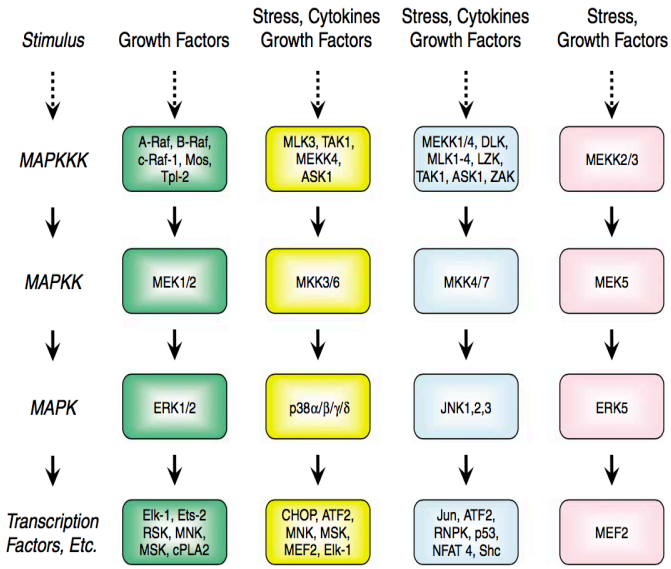

(Burbelo and Hall, 1995; Roberts and Der, 2007)

Figure 1.12 The RAS-RAF-MEK-ERK signaling pathway. (A) Binding growth factors (ligands) to receptor tyrosine kinase (RTK) induce a dimerization change, leading to intrinsic tyrosine-kinase activity. The intracellular portion of the receptor gets autophosphorylated on specific tyrosine residues, which initiates binding to adaptor proteins such as GRB2 via the sequence homology 2 (SH2) domains. This complex then recruits the son of sevenless (SOS) closely to RAS kinase. Interaction RAS with SOS

induces a conformational change on RAS, which promotes the dissociation of GDP from RAS and replaces it with GTP for activation. Activated RAS recruits and phosphorylates CRAF. CRAF then binds ATP and phosphorylates MEK MKKs (MEK1 and MEK2), which finally in turn phosphorylates the ERK MAPKs (ERK1 and ERK2). Activated ERKs phosphorylates specific substrates in nucleus for regulating various cellular responses. The CRAF becomes inactivated by dephosphorylation and associates with 14-3-3 protein, which a conformational change of CRAF is induced. The inactive state CRAF is then translocated to the cytoplasm. 14-3-3 disassociates from CRAF after the configuration of CRAF is changed by phosphorylation/ dephosphorylation events. **(B)** The MAPK cascades in Mammalian cells consist of four major MAPKKK-MAPKK-MAPK protein kinase pathways. The growth factors commonly activate the ERK1/2 pathways, whereas environmental stress activates the signaling pathway for JNK, p38 and ERK5.

1.2.2: The scaffold protein 14-3-3 regulates CRAF protein kinase activity

The highly conserved, acidic 30 kDa adaptor scaffold protein, 14-3-3, has been shown to modulate the maturation of CRAF (Fantl et al., 1994; Freed et al., 1994; Fu et al., 1994; Irie et al., 1994; Yamamori et al., 1995) (**Figure** 1.12 A). A recent study has shown CRAF is not the only kinase to be regulated by 14-3-3 and a large number of client proteins have been identified that interact with 14-3-3 (Aitken et al., 1995; Muslin et al., 2000). This scaffold protein has some specific short peptide motifs, which are responsible for binding client proteins. Phosphorylation may be required for some interactions but it is not essential (Muslin et al., 1996; Petosa et al., 1998; Yaffe et al., 1997). 14-3-3 can suppress the activity of its kinase protein by forming an inactive subcellular complex (Muslin et al., 2000). As well as the maturation of CRAF, 14-3-3 can also regulate the activity of CRAF (Fantl et al., 1994; Freed et al., 1994; Irie et al., 1994; Li et al., 1995; McPherson et al., 1999; Roy et al., 1998; Thorson et al., 1998; Yip-Schneider et al., 2000), but this remains controversial (Fu et al., 1994; Michaud et al., 1995; Suen et al., 1995). CRAF possesses two binding sites (CR2 and CR3) for 14-3-3 interactions and the activity of CRAF depends on which site is occupied by 14-3-3 (Thorson et al., 1998). Binding to the CR2 site requires phosphorylation of Ser 259, which leads to suppression of CRAF activity. In contrast, activity is promoted by binding to the CR3 site, which is dependent on the phosphorylation of Ser 621 (Muslin et al., 1996; Petosa et al., 1998; Yaffe et al., 1997). The dimeric nature of 14-3-3 does, however, allow it to bind both the CR2 and CR3 sites of CRAF (Petosa et al., 1998; Yaffe et al., 1997). This conformation locks CRAF into an inactive state (Rommel et al., 1996; Tzivion et al., 1998). It has been shown that Ser 259 can be phosphorylated by Protein kinase B, and dephosphorylated by protein phosphatase 1 (PP1) and protein

phosphatase 2 (PP2A) (Jaumot et al., 2001). In contrast to the activation of CRAF and ARAF, the activation of BRAF is quite different (Wellbrock, 2004). BRAF lacks the complex set of regulatory events for activation. The activation of ERK1/2 is mainly due to the participation of BRAF, and the basal activity that it possesses, which is significantly higher than the other two isoforms of this kinase (Jaiswal et al., 1994; Catling et al., 1994; Moodie et al., 1994; Pritchard et al., 1995; Wojnowski et al., 2000; Mason et al., 1999).

1.2.3: The inhibition of RAF protein kinase

The classical route to inhibiting RAF serine/threonine kinase is by small molecule inhibitors. Bayer and Onyx developed a very effective RAF kinase inhibitor in 1995 called Sorafenib (Smith et al., 2001). Sorafenib, is a bi-aryl urea compound (3-trifluoromethyl-4-chlorophenyl)-N′ - (4-(2-methylcarbamoyl pyridin-4-yl) (BAY 43-9006, Nexavar) (Smith 2006) (**Figure** 1.13 A & B). Sorafenib can target the activity of protein kinase CRAF (Wilhelm et al., 2006; Lyons et al., 2001), wild type BRAF and $BRAF^{V600E}$ mutant (Wilhelm et al., 2004). Crystallographic analysis, confirms that Sorafenib targets the ATP-binding pocket of the kinase domain (Wan et al., 2004). Sorafenib can also inhibit the activity of other kinases including c-Kit, Flt-3, platelet-derived growth factor receptor (PDGFR) β, vascular endothelial growth factor (VEGFR) 1, VEGFR-2, VEGFR-3, RET and fibroblast growth factor receptor 1 (FGFR-1), of which some play a critical role in angiogenesis (Wilhelm et al., 2004; Carlomagno et al., 2006). While Sorafenib inhibits the phosphorylation of ERK in various human tumor cell lines, including human colon tumor cell lines HCT116 and HT29 and the human pancreatic tumor cell line Mia PaCa2, it does not inhibit non-small lung cancer cell lines such as NCI-H460 and A549 (Wilhelm et al., 2004).

Recently a study revealed that such ATP-competitive kinase inhibitors disrupt the interaction between CDC37 and $BRAF^{V600E}$, which in turn blocks access of the kinase to HSP90. Consequently, without HSP90's chaperoning activity this leads to the ubiquitylated degradation of the kinase (Polier et al., 2013).

A

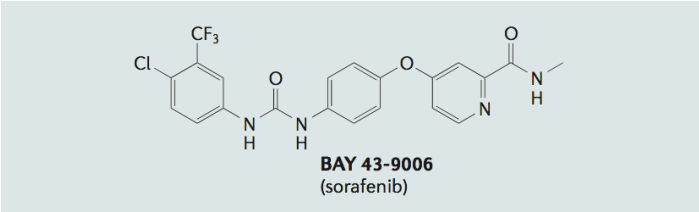

B

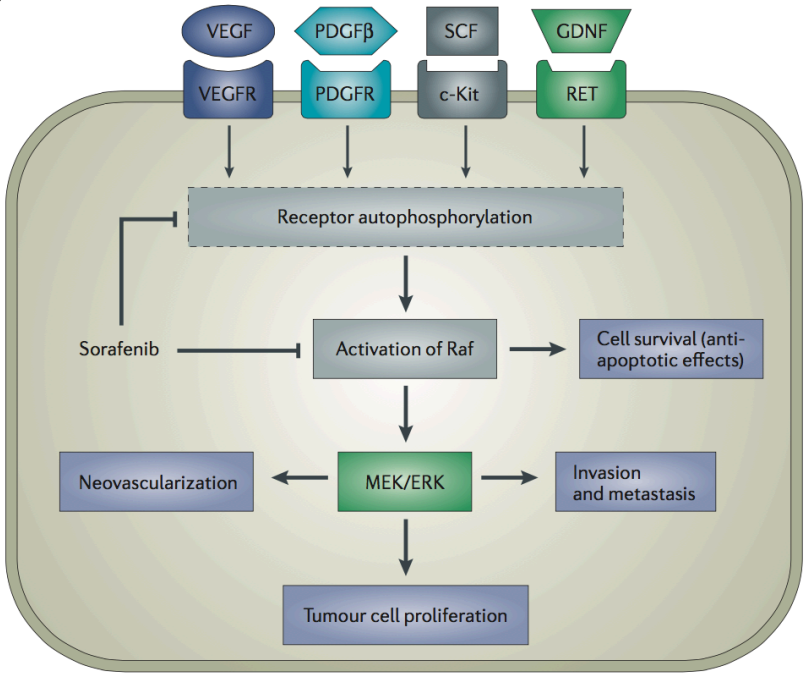

(Wilhelm et al., 2006)

Figure 1.13 Structure and cellular function of BAY43-9006 (Sorafenib). (A) The chemical structure of BAY 43-9006 (Sorafenib). **(B)** Sorafenib is a multi-kinase inhibitor. It binds and inhibits the activation of RAF kinases (see Wan et al., 2004 for more details of the interaction between inhibitor and RAF kinase), and also blocks the autophosphorylation of the receptor tyrosine kinases such as VEGFR, PDGFR, c-Kit and RET. The inhibition by Sorafenib modulates downstream signaling for cell surviving, neovascularization, tumour cell proliferation, invasion and metastasis.

1.3: Protein degradation

1.3.1: Brief overview

Protein synthesis and degradation are major mechanisms in protein homeostasis. The lysosomal and ubiquitin-proteasome pathways are the two major pathways for mediating the degradation of proteins or cellular molecules in eukaryotic cells. The proteolysis pathway degrades proteins or cellular molecules in lysosomes that contain digestive enzymes. The target substrate is taken up into autophagosome vesicles and these fuse with lysosomes that then digest the contents (Adams, 2004) (**Figure** 1.14). The ubiquitin-proteasome degradation pathway is a selective mechanism that ubiquitylates targets proteins targeting them to the proteasome for degradation (Lu and Hunter, 2009). The degradation of CRAF by the ubiquitin-proteasome pathway is the main focus of the project.

1.3.2: A brief outline of the ubiquitin system

The Ubiquitin Proteasome System (UPS) is critical for many cellular processes (Mani et al., 2005), for degrading target protein substrates, it ensures cellular processes function correctly. The UPS is an ATP-dependent process (Hershko et al., 1971&1980; Simpson et al., 1953; Ciechanover et al., 1980; Schlesinger et al., 1975; Wilkinson et al., 1980), and consists of many protein components, including ubiquitin, three different ubiquitylation enzymes (E1, E2 and E3) and the 26S proteasome, that co-operate to bring about the degradation of the targeted protein (**Figure** 1.15 B). Machinery involved in such protein degradation is present in both the nucleus and the cytosol. Ubiquitin, the 9-kDa protein is central to the UPS system as it acts as the primary signal leading to

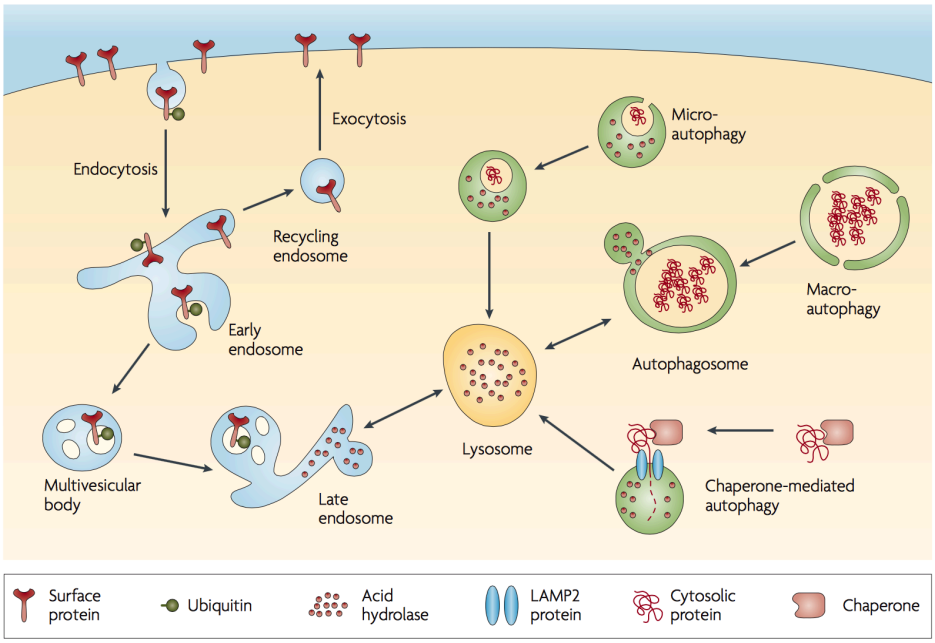

(Tai and Schuman, 2008)

Figure 1.14 The lysosomal proteolysis pathways. Lysosomes are cellular organelles that break down biopolymers and biomolecules by acid hydrolases. Endocytosed membrane proteins associate with early endosomes for delivery back to cell membrane through exocytosis, or by fusing into multivesicular bodies, which are then transported to late endosomes or lysosomes. Intracellular materials are digested via either micro- (through lysosomal invagination) or macro- (through autophagosome) autophagic mechanisms. The lysosome-associated membrane protein 2 (LAMP2) translocates unfolded proteins delivered by chaperons to the lysosome for digestion.

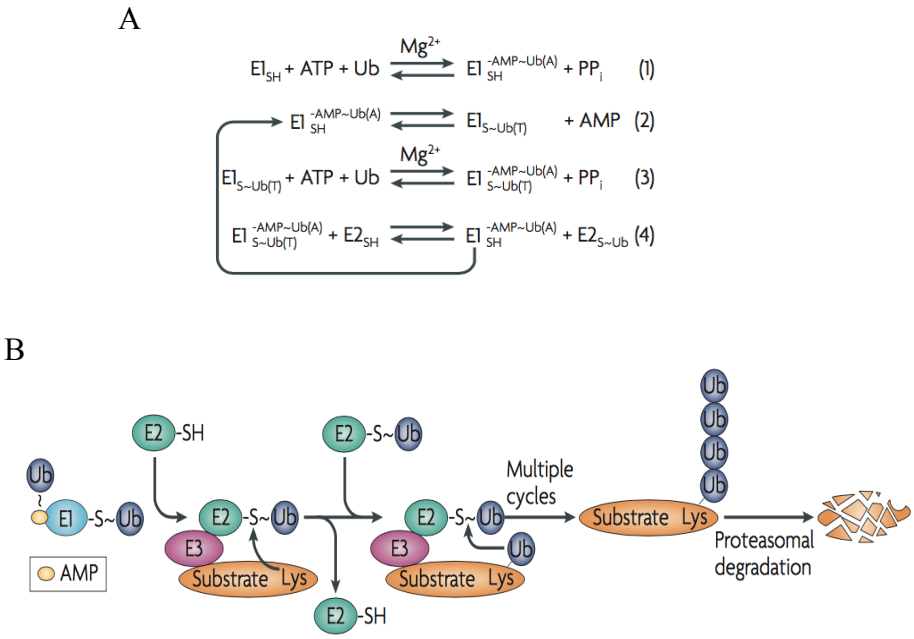

(Schulman and Harper, 2009)

Figure 1.15 Ubiquitin-Proteasome pathway. (A) Free ubiquitin is produced either by ribosomal protein (RP), or hydrolyses of the isopeptide bond between polyubiquitin molecules with deubiquitylating enzymes (DUBs). Activation of ubiquitin through E1 is an ATP-dependent reaction. ATP hydrolysis produces a non-covalently associated ubiquitin at the adenylation active site of the E1 enzyme. Then, a high-energy thiolester bond between the ubiquitin carboxy-terminal Gly residue and a conserved E1 cysteine side-chain in the catalytic domain is formed. A second ubiquitin can then enter the first step, binding to the E1 adenylation domain to become an adenylated ubiquitin. **(B)** The fully loaded E1 then transfers the cysteine-linked ubiquitin to the E2 enzyme. The E2 continuously passes on the activated ubiquitin to E3, where it is finally attached to substrate. The target protein that is polyubiquited (usually via a Lysine 48 link) is then degraded by the 26S proteasome.

proteasomal association and degradation. Uubiquitin is covalently attached to a primary amino group (usually a lysine side-chain) of the target protein through an isopeptide bond. It has been noted that defective translational modification by ubiquitin can induce disease (Ciechanover, 2005; Goldberg, 2007), which illustrates the importance of this system in protein homeostasis.

Lys 48 and Lys 63 are the most common sites for ubiquitin-linked chains (Tenno et al., 2004). However, Lys48 linked chains are usually degraded by the proteasome, whereas polyubiquitin or monoubiquitin at Lys 63 appear to be involved in different cellular processes (Hicke and Dunn, 2003; Feng and Chen, 2012; Nelson, Randle and Laman, 2013) (**Figure** 1.16).

There are 9 UBL conjugation pathways conjugates with 8 structuraly and functionaly related E1 and approximately 40 E2 enzymes (Schulman and Harper, 2009). The first step in the cascade (**Figure** 1.15 A) of ubiquitin transfer involves hydrolyses of ATP by the E1 enzyme, and the adenylation of the C-terminal glycine residue of ubiquitin, which then links to the active site cysteine of the E1 enzyme to form the activated E1 thioester bonded complex. However, full activity of the E1 enzyme is dependent on the non-covalent binding to and adenylation of a second ubiquitin molecule. The E1 enzyme then transfers the thioester-linked ubiquitin to the conserved cysteine residue of an E2 conjugating enzyme, which eventually binds to an E3 ligase with substrate for downstream processing (Hershko et al., 1983). Three main classes of E3 ubiquitin ligase enzymes have been classified to date and can be distinguished on the basis of their E2-recruiting domains (**Figure** 1.17). The cullins, which combine with a RING finger-containing protein, form the cullin-ring ubiquitin ligases (CRLs) (Lorick et al., 1999; Freemont, 2000; Joazeiro and Weissman, 2000) (**Figure** 1.17 C). The U box family (Aravind and Koonin, 2000; Hatakeyama et al., 2001; Cyr et al., 2002)

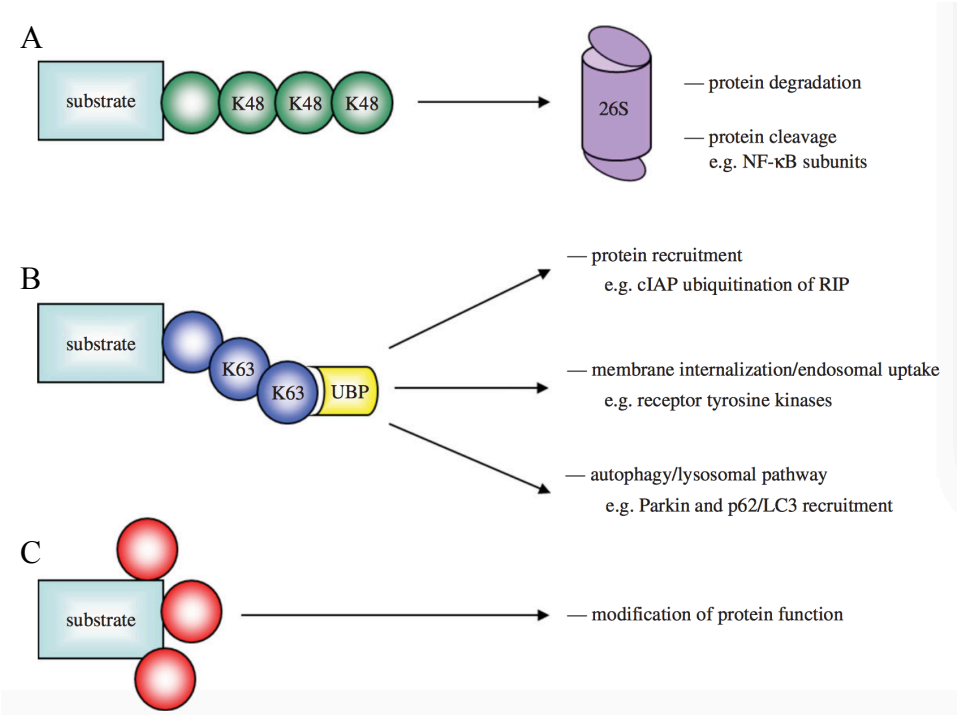

(Nelson, Randle and Laman, 2013)

Figure 1.16 The common linkages of the ubiquitin chain. (A) Degrading target protein via the 26S proteasome usually requires the formation of the polyubiquitin chains via lysine 48 (K48) linkages. **(B)** Lysine 63 (K63) is another common linkage for polyubiquitin chain. The ubiquitylated proteins (UBPs) use this chain as a scaffold for recruiting proteins or complexes, mediating cell signaling, regulating the endosomal pathway and autophagic/lysosomal pathway. **(C)** The cellular function, localization or binding property of the target substrate can be changed by monoubiquitylation or multi-monoubiquitylation.

and single RING finger form the second family of enzyme (**Figure** 1.17 B), while the U-box and RING E3 ligases act as scaffolding molecules that recruit both the Ub-charged E2 and the target substrate (Aravind and Koonin, 2000; Hatakeyama et al., 2001). Substrate recruitment involves protein interaction modules such as a WD-40 repeat, TPR, and armadillo repeat domains. The U-box and RING domains are similar in that they posses a common domain organization (Ohi et al., 2005; Ballinger et al., 1999; Mudgil et al., 2004). The RING-domains structure is built around two zinc-binding sites, whereas U-boxes have a network of hydrogen bonds and salt bridges in the corresponding location (Ohi et al., 2003). In contrast, homologous to E6-associated protein (E6-AP) C-terminus (HECT) E3 ligases contain a HECT-domain for accepting ubiquitin from the E2 ubiquitin-conjugate by forming a thioester bond with the ubiquitin (an intermediate step) before transferring it to the target protein (**Figure** 1.17 A). The conserved cysteine is located within the last 32-36 aa of the HECT-domain (Huibregtse et al., 1995), while E2 binding occurs at the amino-terminal part of the HECT-domain (Hatakeyama et al., 1997). The RING between RING (RBR) fingers protein is another E3 ligase has been identified recently, which this class of E3 could occupy the activity from both RING and HECT E3s (Aguilera et al., 2000).

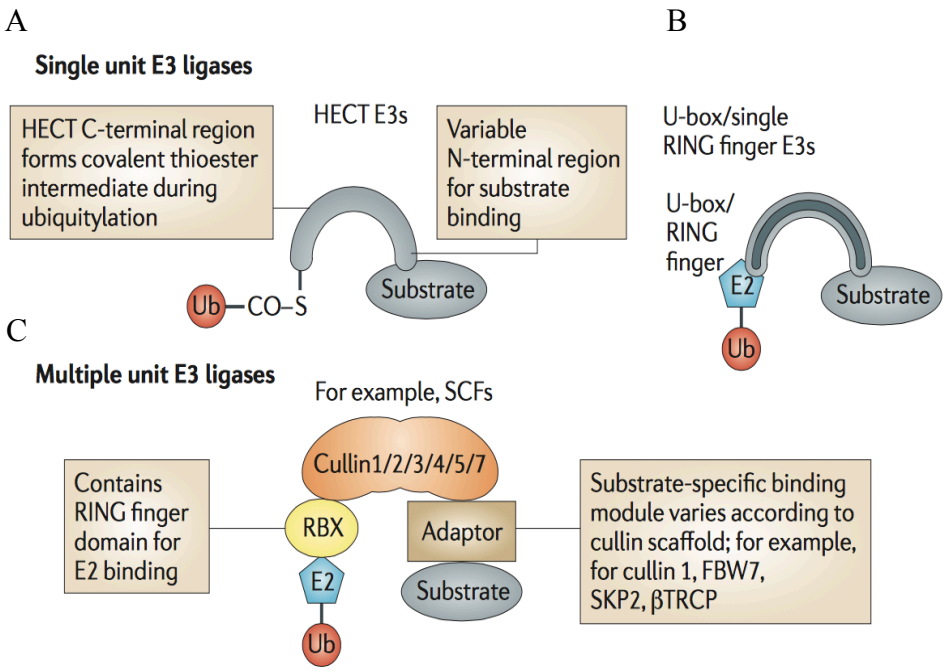

(Bedford et al., 2011)

Figure 1.17 Structural differences between major classes of E3 ubiquitin ligases. (A) The HECT domain E3 ligases are single unit ligases that do not transfer ubiquitin from E2 to the substrate directly, but involve an intermediate step. The ubiquitin is firstly delivered to a conserved cysteine residue on the E3 through the process of trans-thiolation, and then transferred to the amino group of the target substrate. **(B)** The U-box or monomeric RING finger E3s are also a single unit E3 ligase. They are structurally similar to each other, except that the RING finger relays on a Zn^{2+} binding domain for its structure, and both bind an E2 and substrate. However, there is a Zn^{2+} binding domain on RING finger motif for E2s binding, whereas U-box is metal ion indepndent. **(C)** The multimeric RING finger complexes include anaphase promoting complex/cyclosome and cullin-RING ligases (CRLs). SCFs complexes have a RING box protein (RBX) for E2 binding and an adaptor protein for substrate recognition. Ubiquitin is directly transferred to substrate once in close proximity.

1.3.3: Cullin-Ring ubiquitin E3 complexes

Cullins are a family of scaffold protein that most commonly includes CUL1, CUL2, CUL3, CUL4A/B, CUL5, CUL7, CUL9 and each of them are assembled into cullin-RING ligase (CRL) family complexes with different adaptor and substrate-recognized proteins (Skaar, Pagan and Pagano, 2013) (**Figure** 1.18). Generally, they consist of four components; the cullin core, the RINGs, adaptor proteins and substrate recognition proteins. There are two human RING components known as RBX1 and RBX2, which are required by the E3 ligase for activity. In addition, each cullin contains a key conserved lysine residue at its C-terminal end that is neddylated and is essential for E3 ligase activity (Pan et al., 2004). Neddylation involves the transfer of the NEDD8 protein, which is an ubiquitin like protein, to the cullin target. Neddylation of cullins disrupts the inhibitory binding of CAND1, and is brought about by an analogous reaction to that of ubiquitylation involving an E1 NEDD8-activating enzyme that activates NEDD8, an E2 NEDD8-conjugating enzyme, which carries the NEDD8 protein and finally an E3 NEDD8 ligase that transfers NEDD8 to the cullin (Rabut and Peter, 2008; Soucy et al., 2010)

1.3.3.1: Cullin 1 assembled complex

One of the best-described CRL complexes is the S phase kinase associated protein 1 (SKP1)-Cullin1 (CUL1)-F-box protein complex (CRL1) (Petroski et al., 2005) (**Figure** 1.18). The scaffold protein CUL1 holds all these components in complex. Substrate recognized by this complex undergoes post-translational modification and degradation (Lipkowitz and Weissman, 2011). The C-terminal end of CUL1 binds RBX1 (or RBX2), which is responsible for the recruitment of an E2 enzyme, while its N-terminal domain binds SKP1, which in turn recognizes the F-box domain found in a variety of proteins,

such as the S phase kinase associated protein 2 (SKP2). Such proteins contain in turn a WD40 or leucine rich repeat domain that is responsible for the recognition of protein substrate (**Figure** 1.18) (Petroski et al., 2005). The human genome contains at least 69 identified F-box proteins (Jin et al., 2004), which carry the distinct 40 amino acid F-box domain (Frescas and Pagano, 2008; Welcker and Clurman, 2008)

Recently it was suggested that SGT1, which also binds SKP1, acts as an adaptor protein that might link HSP90 to the CRL1 complex. The CS-domain of SGT1 was previously shown to interact with the N-terminal domains of HSP90 (Zhang et al., 2010)

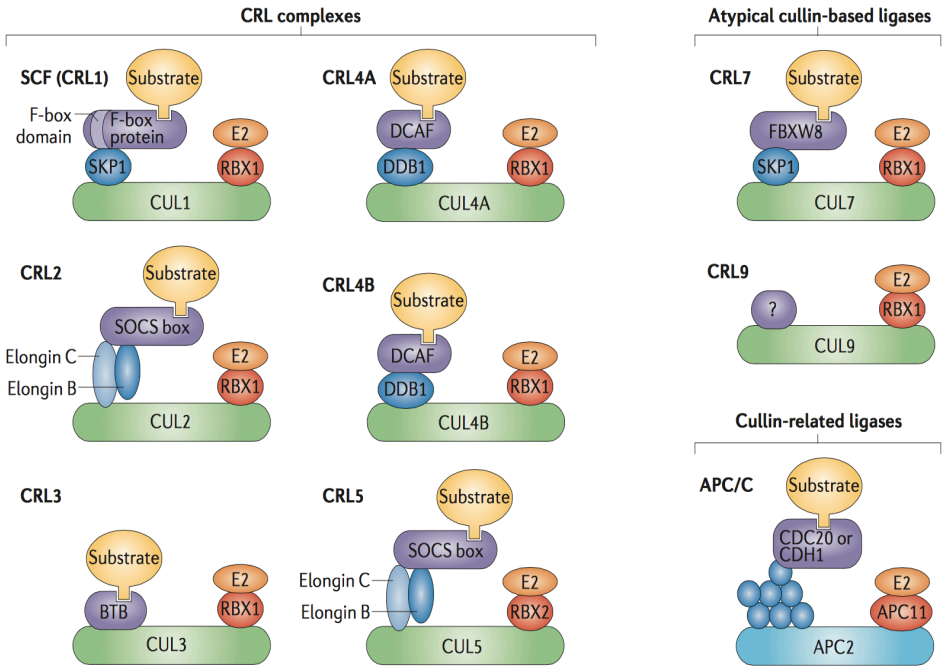

(Skaar, Pagan and Pagano, 2013)

Figure 1.18 Overview of the Cullin-RING ligases. Components of Culin-RING ligases include RBX1, RBX2 and E2 enzyme, an adaptor protein (SKP1, DDB1, BTB and elongin BC complex) amongst others and a substrate recognition module (F-box protein, and SOCS box proteins) amongst others.

1.3.3.2: Cullin 2, Cullin 5 and other cullin systems

The elongin BC and a variety of SOCS box proteins operate with the CRL2 and CRL5 E3 ligase systems, and are responsible for recruiting substrate (Kile et al., 2002) (**Figure** 1.18). The elongin BC complex binds to the N-terminal domain of the E3 ligase, which in turn acts as the adaptor for a specific SOCS box containing proteins, which include the cytokine-inducible Src homology 2 domain-containing protein (CIS), SOCS1-7, WSB1, SPSB1, ASB1, Rab40, elongin A and MUF1 amongst others (Okumura et al., 2016). The elongin BC complex of CUL5 can interact with SOCS protein through the specific box-binding domain (Piessevaux et al., 2008). These contain a variety of other domains thought to be involved in substrate recruitment, which include the SH2 domains of SOCS 1-7, WD40 domains of WSB1, ankaryn domains of ASB1 as well as leucine rich repeats of MUF1. However, although these SOCS proteins may selectively assemble with CUL5 for post-translational modification of the specific substrate, the affinities for each SOCS protein is differently, such as SOCS1 and SOCS3 are weaker than others, and the precise role of these interactions remains questionable (Babon et al., 2009).

In general, the other cullins include CRL4A and B use DNA damage-binding protein 1 (DDB1) and DDB1-and CUL4-associated factor (DCAF) as the substrates adaptors (**Figure** 1.18). In contrast, CRL3 only has bric-a-brac-tramtrack-broad complex (BTB) as the adaptor for its substrates. CRL7 and CRL9 are atypical cullin-based ligases complexes. SKP1 and WD40 domain 8 (FBXW8) F-box protein was identified as the substrate adaptor for CRL7 (**Figure** 1.18). No substrate adaptors have been identified for CRL9. Cell-division cycle protein 20 (CDC20) or CDC20 homologue 1 (CDH1) are the substrates adaptors that have been revealed for APC/C so far, but still unclear for the entire complex (Skaar, Pagan and Pagano, 2013).

Recent work has implicated CUL5 in the proteasome directed degradation of HSP90 client proteins. Efficient silencing of CUL5 in the human cancer cell line HT29, using custom designed siRNA significantly stabilized the degradation of the HSP90 client kinases, ERBB2, $BRAF^{V600E}$, AKT and CDK4, in response to the HSP90 inhibitor. Interestingly, CUL5 silencing also increased resistance to HSP90 inhibitors in a variety of cancer cell lines (Samant, Clarke and Workman, 2014).

1.3.3.3: U-box containing E3 ubiquitin ligases

The homodimeric protein CHIP is a U-box E3 ligase (Murata et al., 2001) that possesses an N-terminal tetrotricopeptide (TPR) domain that binds directly to the conserved MEEVD and IEEVD motifs at the extreme C-terminus of HSP90 and HSP70, respectively. CHIP directs Lys 63-linked polyubiquitylation with Ubc13-Uev1a (Zhang et al., 2005; Komander and Rape, 2012). CHIP also direct Lys 48-linked polyubiquitylation for facilitating the quality control of chaperone client proteins (Cyr, Höhfeld and Patterson, 2003). As such it is a prime candidate for the ubiquitylation of HSP90 client proteins. CHIP has been implicated in the ubiquitylation of ErbB2 (Xu et al 2002; Zhou et al, 2003), cystic fibrosis transmembrane regulator (Meacham et al, 2001, Younger et al 2004), Nitric Oxide synthase (Jiang et al, 2003; Peng et al, 2004; Pertrucelli et al., 2004; Shimura et al, 2004), and E2A transcription factors (Huang et al, 2004) and SMAD proteins (li et al, 2004). Many of these are now known to be HSP90 client proteins. The structure of CHIP in complex with an MEEVD peptide of HSP90 (**Figure** 1.19 A) and the Ubc13-Uve1 (**Figure** 1.19 B) has been determined (Zhang et al., 2005). CHIP displays an inherent asymmetry that ensures one U-box E3 ligase is involved in the polyubiquitylation of substrate (Zhang et al., 2005).

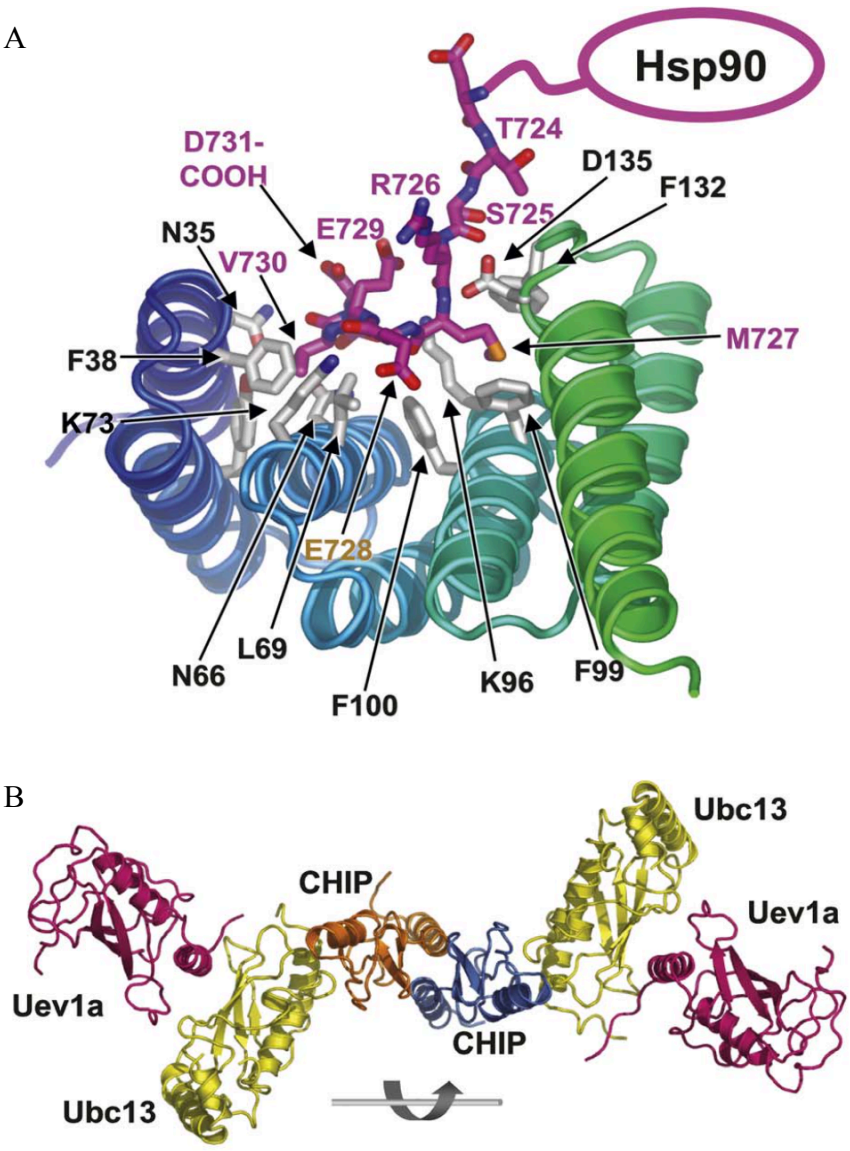

(Zhang et al., 2005)

Figure 1.19 Crystal structure of CHIP in various complexes. (A) CHIP TPR domain associated with the decapeptide of the C-terminal domain of HSP90. The MEEVD sequence of the C-terminal domain lies along the TPR channel with an extended conformation. The binding of Met727 from the side-chain into a hydrophobic pocket, which projects the upstream sequence out of the TPR domain. **(B)** The dimer U box domains (orange and blue) of CHIP independently interact with Ubc13 (yellow), which in turn is bound to Uev1 (magenta).

1.3.4: HECT ubiquitin E3 ligases

The third major family of E3 ubiquitin ligase is homologous with E6-associated protein C-terminus (HECT) domain E3 ligase. Unlike, RING finger E3 ligases, HECT E3 ligase do not directly transfer the ubiquitin from the E2 conjugating enzyme to substrate but form a covalent thioester intermediate directly via a conserved cysteine residue (Spratt et al., 2014). HECT domain E3 ligases have been classified into three families (Rotin and Kumar, 2009) (**Figure** 1.20). These are the HERC family (HERC1 to 6), which contain a regulator of chromosome condensation 1 (RCC1)-like domain (RLD), the NEDD4 family (NEDD4, NEDD4L, SMURF1/2, ITCH, WWP1, WWP2, NEDL1 and NEDL), which contain two to four WW domains and finally the remaining HECT proteins (E6AP, HECTD2, KIAA0614, TRIP12, G2E3, EDD, HACE1, HECTD1, UBE3B, UBE3C, KIAA0317, HUWE1 and HECTD3) that contain a myriad of domains, including Ankaryn, zinc-finger, RING and DOC domains amongst others (Rotin and Kumar, 2009) (**Figure** 1.20).

In common, the HECT proteins all contain a C-terminal HECT domain, which regulates a variety of processes. For example, the ITCH E3 ligase from the NEDD4 family was reported to regulate the immune system through the adjustment of JUNB levels in cells, which in turn affects the expression level of interleukin 4 (IL4) (Gao et al., 2004). ITCH can also down-regulate the level of NOTCH1, which is thought to bind the WW domain of ITCH, leading to its ubiquitylation (Spana et al., 1996; McGill et al., 2003). In contrast, HERC1 plays a role in membrane trafficking (Garcia-Gonzalo and Rosa, 2005). HERC2 appears to affect human eye color variation via the regulation of Oca2 locus (Sturm et al., 2008; Eiberg et al., 2008). HUWE1 appears to regulate the degradation of p53 (Chen et al., 2005) and myeloid cell leukemia sequence 1 (MCL-1) (Zhong et al., 2005).

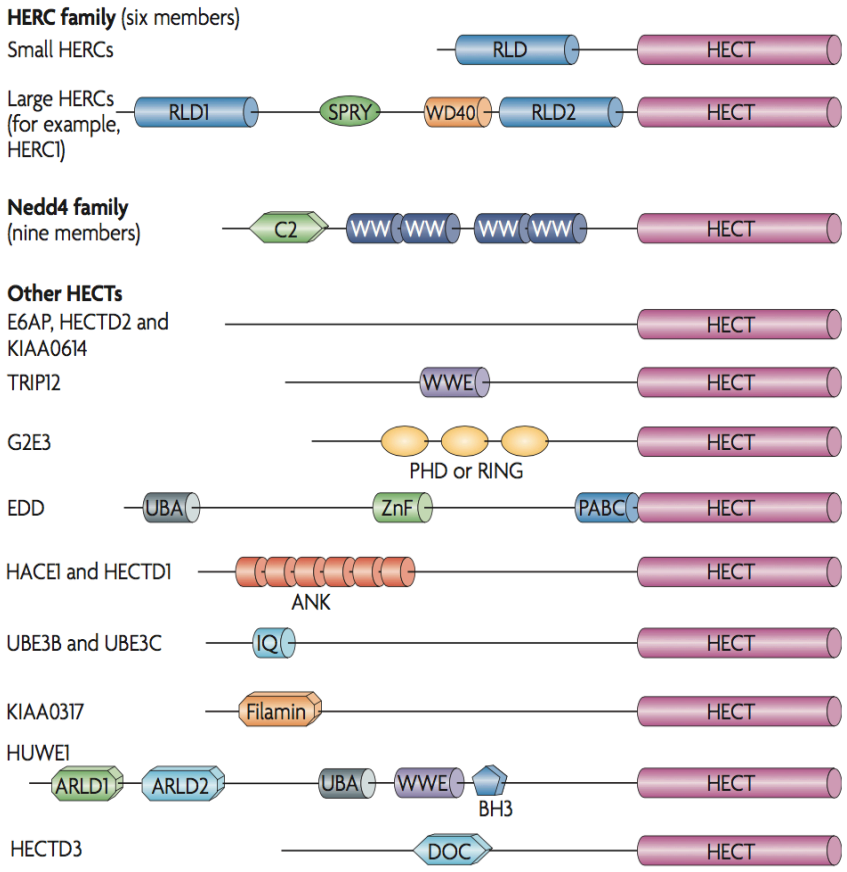

(Rotin and Kumar, 2009)

Figure 1.20 Family of human HECT domain E3 ligases. So far 28 human HECT E3 ligases have been identified and are divided into three classes: HERC, NEDD4 and other HECTs families. The HERC family has six members and is further divide into small and large HERCs. The small HERCs contain single regulator of chromosome condensation 1 (RCC1) –like domains (RLD), while the large HERCs have more RLDs and additional domains, including SPRY and WD40. NEDD4 family has nine members and they all contain an amino-terminal C2 domain and several WW domains (usually two to four). The rest of the HECTs could be distinguished by unique and myriad domain architecture. The C-terminus HECT region is a common domain for all these 28 HECTs.

1.3.4.1: HECTD3

HECTD3 is characterized as having an unknown N-terminal domain, a middle DOC domain and a C-terminal HECT domain (Rotin and Kumar, 2009). Very little is known about the biological role of HECTD3. Early studies implicate HECTD3 in the ubiquitin directed degradation of Tara (Yu et al., 2008), and later then it was revealed that HECTD3 could interact and promote the ubiquitylation of Syntaxin 8 (Zhang et al., 2009). More recent studies suggest that HECTD3 might interact and promote the polyubiquitylation of caspase-8 (Li et al., 2013a). It was also suggested that HECTD3 interacts with mucosa-associated lymphoid tissue 1 (MALT1) and is required for its stabilization (Li et al., 2013b). The HECT E3 ligase is also important for regulating certain types of cancer cells. For example, the E6AP ligase forms a complex with the onco-protein E6 in human papilloma virus (HPV) infected cells and promotes the proteasomal degradation of HSP90-dependent client protein tumour suppressor protein p53. In turn this promotes oncogenesis and cervical cancer is enhanced (Scheffner et al., 1993). The HUWE1 HECT ligase was also found to regulate the degradation of p53 (Chen et al., 2005) and promotes the survival and transformation of cells.

Some structural information on the HECT domain has been published for E6AP, WWP1 and SMURF2. The N lobe of HECT domain is recognized to be responsible for E2 binding, while the conserved Cys residue in the C lobe accepts ubiquitin from the E2 and forms thioester complexes with ubiquitin (an intermediate step), which is then transferred to the substrates (Huang et a., 1999; Verdecia et al., 2003; Ogunjimi et al., 2005).

1.4: RNA interference

1.4.1: Introduction

RNA interference (RNAi) is a technique that efficiently and reliably knocks down or knocks out target gene expression (Matzke et al., 2005; Huppi et al., 2005). In general, post-transcriptional gene silencing or RNAi describes the complementary interaction between siRNA and messenger RNA (mRNA) (Resnier et al., 2013). RNA silencing was discovered in a *Caenorhabditis elegans,* which is a type of the nematode worm, by exogenously introducing double stranded RNA (dsRNA) into the worm and depressing par-1 mRNA (Guo et al., 1995; Fire et al., 1998). Selective silencing of target gene interrupts the normal expression of the encoded protein and may reveal the biological function of the protein. Short interfering RNAs (siRNAs), micro RNAs (miRNAs) and piwi interacting RNAs (piRNAs) are the three main categories of small RNAs that have been identified so far in eukaryote cells. piRNAs are characterized by its single stranded nature and are mainly found in animals. In contrast, siRNAs and miRNAs are characterized by their double stranded nature (Malone and Hannon, 2009), but whereas miRNAs are expressed from the cell's own genome, siRNAs are derived exogenously from viruses or transposons for example. While siRNAs is excised from long dsRNAs with perfect complementary, miRNAs is produced from incomplete double stranded stem-loop precursors (Tomari and Zamore, 2005) (**Figure** 1.21), but both ultimately silence expression by acting through a common mechanism.

1.4.2: Pathway for maturing RNA precursors

The primary miRNA transcript is initially processed in the nucleus (Lee et al., 2002* and 2003) by Drosha, which specifically excises the miRNA precursor from the primary

miRNA transcript, and subsequently exports a miRNA molecule, as a stem loop structure with a cohesive 5' phosphate and a 2-nucleotide 3' overhang, through the exportin-5 receptor to cytoplasm (Lee et al., 2003; Basyuk et al., 2003; Bohnsack et al., 2004; Lund et al., 2004; Yi et al., 2003; Lee et al., 2002* and 2003) (**Figure** 1.22). The RNase-III like enzyme Dicer is then responsible for the maturation of miRNA precursor in a similar way to dsRNA and siRNA in the cytoplasm (Hutvágner et al., 2001; Grishok et al., 2001; Lee et al., 2004; Xie et al., 2004; Bernstein et al., 2001) (**Figure** 1.22). The number of Dicer genes in organisms is variable. For example, there are two paralogues of Dicer (Dice-1 and Dice-2) in *Drosophila melanogaster*, while S. pombe C. elegans and mammalas only contain one. In *Drosophila melanogaster*, Dicer-1 is responsible for processing miRNA precursor, while long dsRNA is processed by Dice-2 (Lee et al., 2004; Liu et al., 2003; Pham et al., 2004).

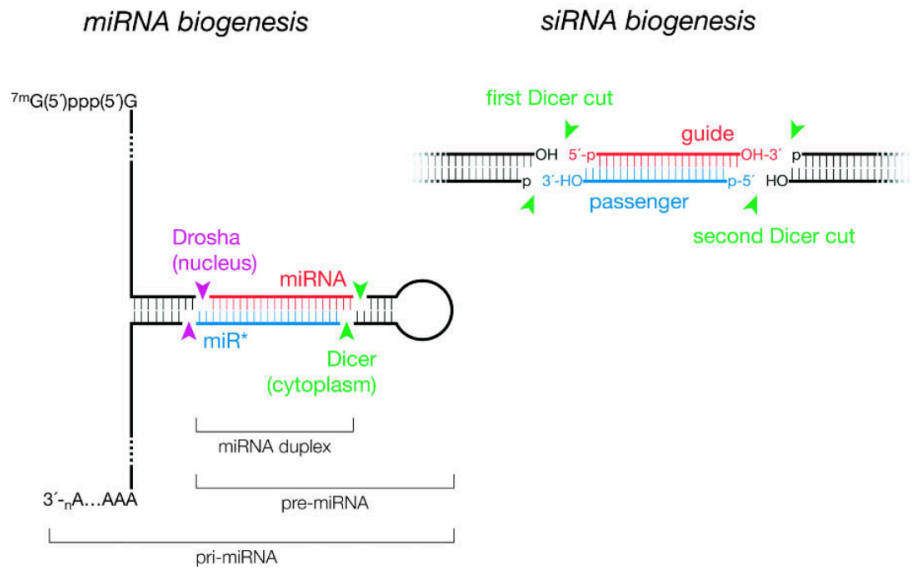

(Tomari and Zamore, 2005)

Figure 1.21 Biogenesis of small RNA in animals. (Left) RNase-III-like enzyme Drosha cleaves the primary miRNA (pri-miRNA) in nucleus to generate the pre-miRNA (miRNA with precursors), which it is exported to the cytoplasm after the binding with Exportin 5. Dicer binds and cleavages the pre-miRNA to release a miRNA duplex. **(Right)** Drosha is not required for long double-stranded RNAs (dsRNAs). Successfully cleaving the long dsRNA by a pairs of Dicer generates a siRNA duplex. The cleavage is preferentially initiated at the ends of dsRNA. Both miRNA and siRNA is then selectively assembled into RISC by specific machinery.

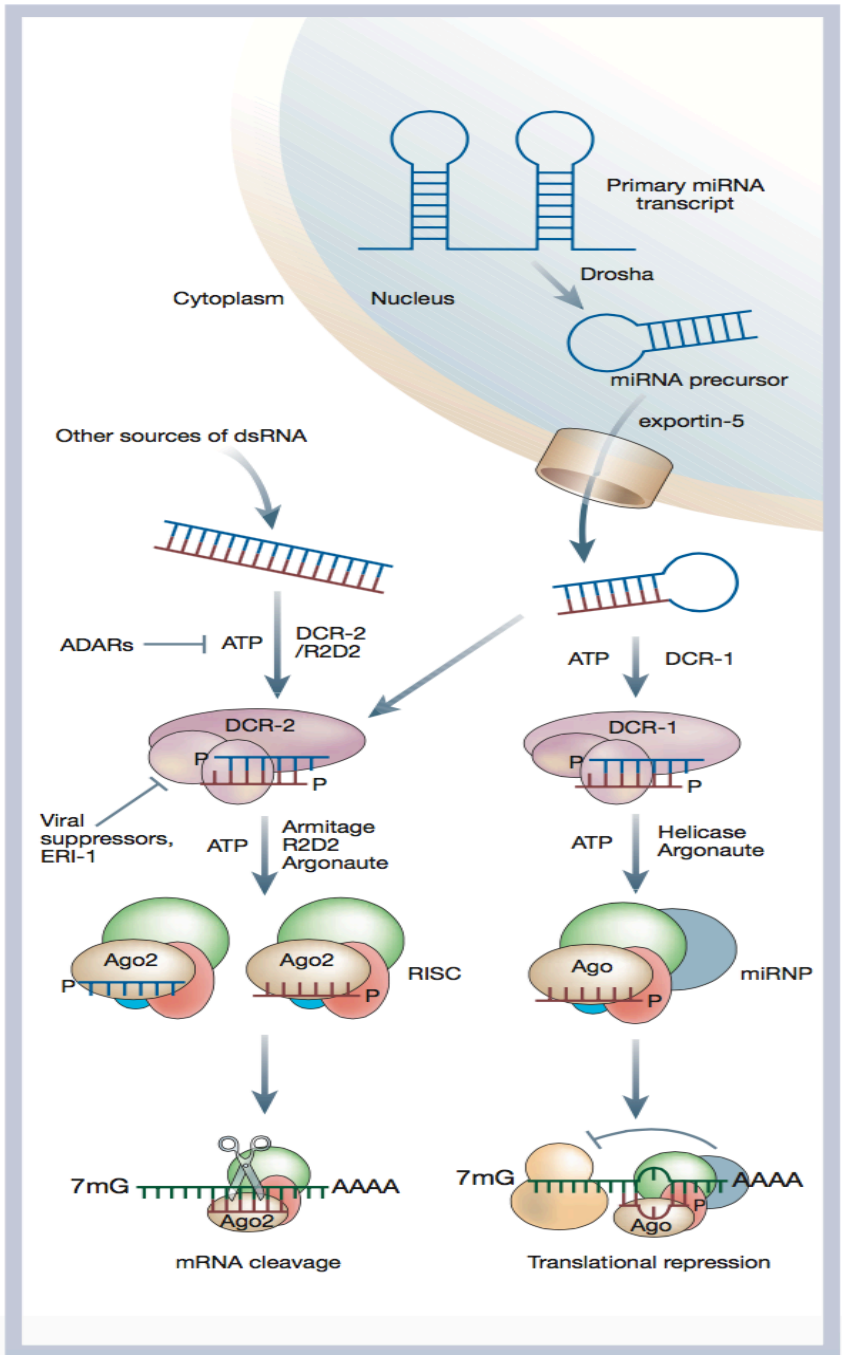

(Meister and Tuschl, 2004)

Figure 1.22 Maturation pathway of small-RNA in *Drosophila melanogaster*. RNase-III-like enzyme Drosha cleavages the primary miRNA in the nucleus. The miRNA precursor (pre-miRNA) is produced after the cleavage and subsequently exported into cytoplasm via exportin-5 receptor. The miRNA precursor is further cleaved by Dicer to generate siRNA-duplex-like intermediates. The siRNA duplex assembles into miRNP/RISC after unwinding the double strand. Ago proteins bind to the mature

miRNAs for regulating the translational repression or guiding the cleavage of the target mRNAs. For the other sources long dsRNA in cytoplasm (usually includes: artificially introduced dsRNA, viral RNAs, RDRPs generated dsRNA, and genomic sense and antisense transcripts), the RNase III enzyme Dicer processes the long dsRNA into 21 to 23 nucleotide long dsRNA intermediates. This dsRNA is then unwound and assembled into RISC with help from RNA helicase Armitage and R2D2. The exonuclease ERI-1 and the adenosine deaminase acting on RNA (ADARs) are the two negative regulators of this pathway.

The RISC assembly consists of duplex RNAs loaded onto the Ago protein and unwinding of the duplex (Kawamata and Tomari, 2010). RISC assembly in *Drosophila* using Ago2-RISC is the best-studied system. In this, the RNA duplex is initially captured by the RISC-loading complex (RLC), consisting of Dicer-2 and the R2D2 protein in a polarity determined by the higher affinity for the RNA duplex by R2D2. Thus, Ago2 binds the RNA duplex with a prefixed orientation (Tomari et al., 2004; Matranga et al., 2005) (**Figure** 1.22). The chaperone protein, HSP90 assists Ago loading in an ATP-dependent manner (Iwasaki et al., 2010) (**Figure** 1.23). It is thought that the initial loading of the RNA duplex involves a chaperone mediated conformational change in Ago (stretching) (Kawamata and Tomari, 2010; Meister, 2013). Subsequently, as Ago releases the tension by returning to its closed conformation, which is ATP independent, the duplex RNA is unwound and the passenger strand is discarded. In the mammalian genome there are four different Ago proteins that are similar to fly Ago1 rather than to fly Ago2. Although there is some debate concerning the precise details, the processing of the RNA also appears to be different and involves a RISC loading complex (RLC), comprised of Ago, Dicer, and TRBP (Maniataki and Mourelatos, 2005). The Dicer-Ago components bind and cleave the pre-miRNA and the product is then oriented by the Dicer-TRBP heterodimer while handling off to Ago (**Figure** 1.23).

1.4.3: Gene silencing via siRNA

Exogenous dsRNA that is introduced into a cell can be processed by Dicer into a 21 nucleotide fragment with a 2 nucleotide base overhang at the 3′ ends of the dsRNA molecule (Bernstein et al., 2001; Elbashir et al., 2001). Synthetic siRNA bearing this structure can be introduced into cells and is then assembled into siRISC complexes for

gene silencing of complementary mRNA, by cleaving the central section of the complementary mRNA (Martinez et al., 2002 and 2004). Cleavage is achieved by the Ago PIWI-domain, which acts as a non-ATP dependent reaction (Nykänen et al., 2001; Hutvágner et al., 2002). The endonucleolytic cleavage of the mRNA can be suppressed if siRNA is mismatched to its target mRNA (Tomari and Zamore, 2005).

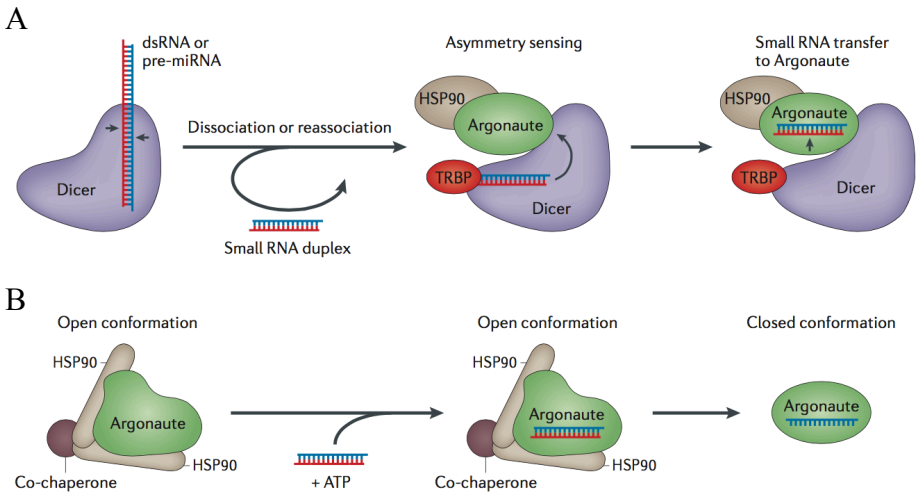

(Meister, 2003)

Figure 1.23 Model for assembly of small RNAs into Ago clade proteins. (A) Dicers two RNase III domains engage with dsRNA or pre-miRNA to generate a 21 to 23 nucleotides dsRNA. Such short dsRNA repositions its location on Dicer by reloading itself. During this step, the dsRNA-binding protein makes sure the loading and the strand selection is correct. The heat shock protein 90 (HSP90) is thought to keep Argonaute in an open conformation for dsRNA transfer. **(B)** Ago binds HSP90 and is converted to its open conformation. This process is assisted by co-chaperones. Upon the binding of small RNA to Ago, the double strand is unwound and the passenger strand is cleaved and removed, while ATP is hydrolyzed by HSP90. Ago protein then shifts to its closed conformation with only the guide single strand RNA. Finally, HSP90 and co-chaperones dissociate from the complex.

1.5: Hypothesis and Aims

HSP90 functions a chaperone protein that regulates the stability of its client proteins for downstream signaling, and inhibition of HSP90 disrupts its biological function and induces the degradation of client proteins through the proteasome system. E3 ligases are a large and structurally diverse class of molecules that collectively co-operate with hundreds of protein components required for the degradation or regulation of a vast array of substrates. Many of these substrates are known HSP90 clients, but how they are delivered to E3 ligases complexes is still unknown. Identifying specific E3 ligases involved in the degradation of HSP90 client proteins is the initial step towards understanding such complex degradation pathways. Finally, determining the mechanisms that operate may help us understand their role in carcinogenesis.

CHAPTER TWO

Materials and Methods

2.1: Reagent and Buffer

Full growth DMEM medium:

DMEM (life technologies, 21969-035) medium supplemented with 10% FCS and 1% v/v L-glutamine (Life Technologies, 25200-056)

Full growth DMEM plus medium:

DMEM media supplemented with 10% v/v Foetal Calf Serum (FCS), 1% v/v non-essential amino acid (life technologies, 11140-035) and 1 % v/v L-glutamine

FCS free DMEM:

DMEM medium supplemented with 0% FCS and 0% v/v L-glutamine

GFP-trap pull down lyses buffer:

0.5 mM EDTA, 25 mM HEPES pH 7.8, 150 mM NaCl, 10% v/v Glycerol, 1/100 protease inhibitor, 1mM DTT, and 0.5% v/v Triton X-100

GFP-trap pull down washing buffer:

0.5 mM EDTA, 25 mM HEPES pH 7.8, 150 mM NaCl, 10% v/v Glycerol, 1/100 protease inhibitor and 1mM DTT

Western blot transfer buffer:

10% 10x Tris-Glycine, 20% methanol and 70% SQ water

AHA-labeling GFP pull down lyses buffer:

0.5 mM EDTA, 25 mM HEPES pH 7.8, 150 mM NaCl, 10% Glycerol 1/100 protease inhibitor and 0.5% Triton X-100

AHA labeling G25 column equilibrium/washing buffer:

0.5 mM EDTA, 25 mM HEPES pH 7.8, 150 mM NaCl, 10% Glycerol and 1/100 protease inhibitor

Iodoacetamide solution:

Dilute 50mM iodoacetamide in 25mM NH_4HCO_3

Trypsin buffer:

Dilute trypsin with acidic buffer to give 1 µg/ µl concentration

2.2: DNA cloning and amplification

2.2.1: DNA restriction digests and gene synthesis

All restriction enzymes and buffers were purchased from New England Biolabs (NEB, Hitchin, UK). Double restriction digest were conducted as recommended by the restriction enzyme manufacturer. Typically for each double digest reaction, 1 µl of DNA was mixed with 4 µl of restriction buffer (contain 100x BSA) in 33 µl of ultra-pure water. Restriction enzymes (1 µl for each enzyme) were added to the solution just prior to incubation at 37° C for 1 hr. Digestion with XhoI and BamHI were found to be the most suitable restriction enzymes for cloning CRAF into the pEYFP-C1 vector. The gene for the full-length human CRAF was designed with XhoI-BamHI cloning sites (**Appendix** 1). The construct was synthesized and inserted into pEYFP-C1 by Genscript (Piscataway, NJ 08854 USA).

2.2.2: Transformation of E. coli

Competent cells were deforested on ice and gently mixed with 1 µl of pEYFP-C1-CRAF plasmid DNA. The cells were then incubated on ice for 25 min, heat shocked for 30 sec at 45°C and immediumtely replaced on ice for 2 min. 1 ml of Super Optimal Broth medium (Invitrogen, 15544-034) without antibiotics was then added with gently

mixing and the cells incubated for 45 min at 37°C with shaking at 250rpm. The transformed cells were then evenly spread on LB (Lauria broth) agar plates containing kanamycin (Fisher Scientific, 25389-94-0) at 50 μg/ml. The plate was subsequently incubated over night at 37° C to allow transformed cells to form colonies.

2.2.3: Amplification of plasmid DNA

Single colonies were picked and cultured in 5 ml LB medium containing 100 μg ampicillin at 37° C with shaking at 220 rpm. This starter culture was then diluted 1/40 into a sterile flask containing 50 ml LB medium with 100 μg kanamycin and grown at 37°C over night with shaking at 220 rpm. Cells were then harvested by centrifugation at 5000 rpm for 20 min at 4°C. Plasmid was prepared with the Midi Plasmid Kit (QIAGEN, 12943), as described by the manufacturer. Once the DNA pellet was dry, it was dissolved in a suitable volume of TE pH 8.0 buffer.

2.3: Maintenance and growth of human Cell lines

The HCT116 human colorectal carcinoma and HT29 human colorectal adenocarcinoma cell lines were a kind gift from Paul Workman (The Institute of Cancer Research). Both HCT116 and HT29 cells were grown in full culture DMEM plus medium. NHE1, HEK293, COS7 and A549 cell lines were obtained from the Genome Damage and Stability Centre, University of Sussex. These cell lines were cultured in full culture DMEM medium. All cells were grown in either a 75 cm^2 (with 25 ml medium in total) or a 175 cm^2 (with 50 ml medium in total) flask (Corning, T75, T175), at 37° C with a 5% CO_2 humidified atmosphere in a NuAire Microbiological CO_2 incubator as described by the manufacturer (NuAire Company, Caerphilly, UK).

Cell lines were maintained by washing once in 37°C PBS and then incubating for 5 min with 0.25% trypsin-EDTA (Life Technologies, 25200-056), at 37°C and a 5% CO_2 humidified atmosphere. Cells were then transferred into a 50 ml Falcon tube (Thermo Fisher Scientific) and pelleted at 1500 rpm for 5min. The cell pellet was washed with 37° C PBS and re-suspended in 10 ml full culture DMEM medium. Subsequently, 10 µl of cell suspension was loaded onto a Marienfeld counting chamber (haemocytometer) and dispersed with an ultra thin glass coverslip. Cell numbers were determined by counting individual cells in each 4x4 square at each corner and averaged by 4. Next, $1.5x10^6$ cells were then inoculated into fresh medium as appropriate and grown at 37°C in a 5% CO_2 humidified atmosphere. The procedure was then repeated every three days.

To prepare cell line stocks for long-term storage, a confluent monolayer of cells was grown in a 175 ml flask (Corning, T175). The cells were then made de-adherent with 0.25% trypsin-EDTA for 5 min and then pelleted at 1500 rpm. The cell pellet was subsequently suspended in FCS medium containing 10% v/v DMSO and $1x10^6$ cells aliquoted per tube and stored frozen in a container (NALGENE, 5100-0001) at -80 °C for 24 hr before moving into liquid N_2 for longer term storage.

2.4: Generation of a HEK293 cell line stably expressing pEYFP-CRAF

HEK293 cells were grown in full culture DMEM medium. $1x10^5$ cells in a total volume of 3 ml were seeded into a 6 well plate. After 24 hr incubation at 37°C and a 5% CO_2 humidified atmosphere, various concentrations of G418 (50, 100, 200, 400, 800 and 1600 µg/ml) were added to the cells. The culture medium containing G418 was replaced every 3 days. The growth of the cells was observed for two weeks and the

highest concentration of G418 was chosen for the selection of a stable cell line.

For each transfection reaction, 2 µg of plasmid DNA (pEYFP-C1-CRAF or pEYFP-C1) was mixed with sterile nuclease free water to give a final volume of 10 µl. The DNA was then added to an eppendorf containing 100 µl of FCS free DMEM medium, and 4 µl of transfection reagent TurboFect (Thermo Fisher, R0531), and gently mixed before incubating for 20 min at room temperature. Finally, the DNA mixture was gently added drop by drop to $7.5x10^4$ HEK293 cells which were previously seeded into 6 well plates and incubated for 24 hr to allow cells to reach 50% confluence. After 24 hr growth at 37° C with a 5% CO_2 humidified atmosphere, expression of pEYFP-CRAF was checked by western bot analyses (**Section** 2.6.2) and 800 nM of G418 was then added to maintain selection for 2-3 days growth. Cells were then harvested and transferred into a 10 cm plastic plate for further selection with 800 nM G418. Once cells had reached 80% confluence they were split into 2-3 10 cm plates and the full culture DMEM medium containing G418 refreshed at least twice a week. Further selection was did in 96 well plate with single colony picked up from 10 cm plates. After a month of selection, the expression level of eYFP-CRAF and the eYFP control protein was analysed from each colony of wells. All cell samples showing expression of eYFP-CRAF and eYFP were selected and further stored at -80° C (**Section** 2.3).

2.5: Development of an in vivo plate fluorescence-based assay

2.5.1 Determination of the GI_{50} for HEK293 cells with the HSP90 inhibitor, AUY922

$1.5x10^4$ of either wild type or stably eYFP-CRAF over expressing HEK293 cells in total volume of 160µl of full culture DMEM medium was seeded in to a flat-bottomed 96 well plate that allowed adherence of cells to the well bottom (Ibidi, 250210). The wells on the outermost edge of the plate were not seeded but filled with PBS in order to buffer the innermost cells against temperature changes otherwise known as the side effect. The plates were then incubated at 37° C with a 5% CO_2 humidified atmosphere and grown for 24 hr. Subsequently, 40 µl of FCS and L-glutamine free DMEM medium containing 0, 2.5, 5, 10, 20, 40, 80, 160 and 320 nM of AUY922 was added to test wells. One well in each column contained DMEM medium and inhibitor but was void of cells and represented the control. Plates were then incubated for 24 hr at 37° C in a 5% CO_2 humidified atmosphere. Subsequently, 10x AlamarBlue (Thermo Fisher, DAL1100), cell viability reagent was added to each well to all development of the fluorescence signal from living cells. The absorption from AlamarBlue from both control and test wells was measured immediately at 450 nm in a POLARstar Omega micro-plate reader (BMG Labtech, Germany). The GI_{50} was determined by plotting cell survival against drug concentration and then applying a logarithmic regression to allow estimation of the concentration of the AUY922 required to inhibit 50% growth of cells.

2.5.2: Determination of the AUY922 concentration required for promoting eYFP-CRAF proteasome dependent degradation

Having determined the GI_{50} for AUY922 for HEK293 cells we next investigated the amount of AUY922 required for stimulation of eYFP-CRAF proteasomal degradation. HEK293 cells were grown in full culture DMEM medium and $6x10^5$ cells in a total volume of 3 ml were seeded in to 2x6 well plates and grown up to 50% confluence at 37° C with a 5% CO_2 humidified atmosphere. AUY922 was then added at 1x, 2x, 3x, 4x and $5xGI_{50}$ concentration (**Section** 2.5.1) and the cells incubated for growth. At 24 hr cells were harvested from one plate to check for the expression of eYFP-CRAF by western blot analysis (**Section** 2.6.2). The second duplicate plate was allowed to grow for 72 hr incubation and cell numbers reflecting viability were counted as the described in Section 2.3.

2.5.3: Fluorescence assay for performing the proteasome degradation of eYFP-CRAF induced by AUY922

$1.5x10^4$ of stably expressing eYFP-CRAF HEK293 cells in a total volume of 160 µl DMEM medium were grown in a flat-bottomed 96 well plate. The wells on the outermost edge of the plate were not seeded but filled with PBS in order to buffer the innermost cells against temperature changes otherwise known as the side effect. The last well of each column was devoid of cells and acted as the control. At 50% confluence of cell density, $3xGI_{50}$ (determined from section 2.5.2) of AUY922 diluted with FCS free DMEM medium in a total volume of 40 µl was added to all experimental wells. At each indicated time point following AUY922 treatment (0, 3, 6, 9 and 12 hr), medium from the well was aspirated, the cells washed twice with 200 µl PBS, and then 100 µl of PBS was added. The total eYFP fluorescence intensity from the well was immediately

analysed using the POLARstar Omega (BMG Labtech, Germany) micro-plate reader at 485 nm excitation and 520 nm emission. Cell viability was also analysed with 10x AlamarBlue (**Section** 2.5.1).

2.6: In vivo cell biology techniques

2.6.1: EYFP-CRAF Pull down assay

Stably transfected HEK293 cells expressing full-length eYFP tagged human CRAF or eYFP itself were grown in a 10cm plastic plate in full culture DMEM medium to 60-80% confluence. 2 μM of MG132 was then added to each plate, incubated for 3 hr in a 5% CO_2 humidified atmosphere at 37^{o}C, followed by the addition of a 3xGI_{50} concentration of AUY922. Cells were then re-incubated at 37° C with a 5% CO_2 humidified atmosphere and cells from individually plates harvested at specific time points (0, 2, 4, 8, 16 and 24 hr) by washing twice with warm PBS and then finally by scrapping cells to detach them from the plates, without trypsinization. The cell number was then determined by a haemocytometer count and a total of 5x10^6/ml cells transferred to a 15ml Falcon tube (Thermo Fisher Scientific). Cells were then pelleted at 1500 rpm for 5 min at room temperature, washed with 5 ml room temperature PBS, and finally re-suspended in 1ml ice cold PBS before transferring to a 1.5 ml eppendorf tube. The cells were then pelleted at 8000 rpm for 3 min at 4°C, the supernatant was discarded and the cell pellet re-spin at 10000 rpm for 1min at 4°C to remove traces of PBS. The cell pellet was then frozen in liquid N_2 and stored in -80°C freezer.

For pull down assays cells were defrosted on ice for 30 min in lysis buffer (400 μl/7.5x10^6 cells) and then allowed to lyse on a rotating wheel for 1 hr at 4°C. Cell debris

and insoluble material were then removed by centrifugation at 13400 rpm for 20 min at 4°C. 500 µl of the supernatant was then transferred into eppendorfs with 30 µl pre-equilibrated GFP-trap agarose beads (Chromotek, gta-20), and incubated on the rotating wheel at 4°C for 45 min. The GFP-trap agarose beads were then pelleted at 3200 rpm for 2 min at 4°C and then washed three times with 120 µl of washing buffer, re-pelleted at 3200 rpm for 2 min at 4°C. After the final wash, 60 µl of 2x NuPAGE LDS sample buffer (Life technologies, NP0007) was added to the resin and the sample and control samples (30 µl of the supernatant and all flow through fractions) boiled for 5 min at 100°C. Finally, 20 µl of each sample was analysed by SDS-PAGE gel electrophoresis (Invetrogen, NuPAGE) and visualized by staining with instant blue (expedeon, ISB1L).

2.6.2: Western blots

In each well from 6 well plate, cells were lysed with 500 µl of 2X NuPAGE LDS sample Buffer, and then the lysate transferred to an eppendorf. Cell lysates were boiled at 100º for 10-15 min, cooled on ice briefly and then pipetted up and down to reduce viscosity before boiling for another 2 min. 10-20 µl of sample was analysed by SDS-polyacrylamide gel electrophoresis (Life technologies NuPAGE 4-12%Bis-Tris Gel NP0321BOX) at 160 V and 400 mA for 60-90 min. Subsequently, proteins were transferred to Amersham Hyperfilm ECL membrane (GE Healthcare, 10600034) using the Xcell II Blot Module (Invitrogen, EI9051) at 210 V and 120 mA for 60-90 min or follow the manufacturer instructions.

For detection, the membrane was pre-incubated in 5% milk-PBS with 0.1% v/v Tween 20 (T20) for 30 min and then transferred to a 50ml falcon tube containing 10 ml 3% milk-PBS-T20. The primary antibody was then added and membranes incubated on rotating wheel over night at 4°C. The incubation for ErbB2 was performed for 2 days

with 1% milk since the expression level for endogenous ErbB2 is quite low in the HEK293 cell line. After incubation with primary antibody, membranes were washed for 3 x 15 min with PBS-T20, and then incubated with the appropriate secondary antibody in 3% milk-PBS-T20 for 1-2 hr at room temperature. The membrane was finally washed 3 x 15 min with PBS-T20, and soaked in ECL western blot reagent (Thermo Fisher, 32106) to develop a specific chemiluminescent signal, which was detected on amersham hyperfilm ECL (GE Healthcare, 28906836). The dilutions for primary and secondary antibodies used are summarized (**Appendix** 2).

2.6.3: Azide and alkyne pulse-labelling reaction for newly synthesized eYFP-CRAF

HEK293 cells stably expressing eYFP-CRAF were grown in full culture DMEM medium and $5x10^5$ cells were then seeded into 10 cm plastic plates and grown to 50% confluence. Subsequently, cells were transfected with HECTD3 siRNA for 48 hr with the method described in Section 2.6.5. All cell samples were then washed twice with warm PBS and cultured in L-methionine free DMEM medium (Invitrogen, 21013-024) for 1 hr to remove traces of methionine. Cells were then washed twice with warm PBS and labelled with 30 μM Click-iT AHA L-azidohomoalanine (Invitrogen, C10102) for 3 hr, before washing with warm PBS. Cells were then re-grown in full culture DMEM medium for 24 hr. Samples were harvested at 8, 16 and 24 hr as described previously (**Section** 2.6.1). Finally, cell pellets were frozen in liquid nitrogen and stored at -80°C.

As required cell pellets were defrosted and lysed for 90 min at 4 °C in AHA-labelling GFP pull down lyses buffer. Cell lysate was then clarified by centrifugation at 13,000 rpm for 25 min at 4°C and 50 μL of the supernatant (up to 200 μg of AHA labeled protein) was used for the AHA-azide and biotin-alkyne (Thermo Fisher, B10185)

conjugation in the absence of DTT, which is a potent inhibitor of the reaction by using the Click-iT protein reaction buffer kit (Invitrogen, C10276). Conjugation reactions between AHA-azide and biotin-alkyne were performed by rolling the sample in the dark for 20 min at room temperature. Subsequently, the sample was desalted on a PD SpinTrap G-25 column (GE, 28-9180-04), which was pre-equilibrated with AHA-labelling equilibrium washing buffer. The AHA-Biotin labelled protein was then subjected to pull down assays using GFP-Trap to sequester AHA-Biotin labeled eYFP-CRAF from the entire protein mixture. Samples of AHA-Biotin labeled eYFP-CRAF were then analysed by western blot (**Section** 2.6.2).

2.6.4: siRNA experiment

2.6.4.1: Control siRNA oligos against eYFP-CRAF in HEK293 cells

80 µl of $1.2x10^4$ of stably expressing eYFP-CRAF HEK293 cells in full culture DMEM medium were seeded in to a 96 well plate and incubated for 24 hr at 37° C with a 5% CO_2 humidified atmosphere. On-target plus GFP siRNA (Dharmacon), which target YFP and On-target plus Non-targeting siRNA (Dharmacon) (**Appendix** 3.2), used as the negative control were transfected into the stably expressing eYFP-CRAF HEK293 cells. Briefly, stock siRNA was gently spin down and diluted with 1x siRNA buffer (Dharmacon, B-00200-UB-100) and prepared in Nuclease free water (Fisher scientific, 7732-18-5) to give a final concentration of 5 µM siRNA, which could be stored at -20° C. For each siRNA transfection, which was triplicated, 0.5 µl of 5µM siRNA was added to 9.5 µl of FCS free DMEM medium and incubated for 5 min at room temperature. The contents were then gently mixed with 0.2 µl of DharmaFECT reagent 1 (Dharmacon, T-2001-01) diluted in 9.8 µl of FCS free DMEM and incubated for 25-30 min at room

temperature. Finally, the transfection mixture was added to a well containing the 80 µl of $1.2x10^4$ of HEK293 cells and the plate incubated for 72 hr at 37°C with a 5% CO_2 humidified atmosphere. Cells were then washed and fixed for 10 min using 4% paraformaldehyde in PBS, then permeabilised using 0.3% Triton X-100 in PBS and stained with 0.5µg/ml DAPI in PBS for 15 min. DAPI was replaced by PBS after the staining. The effectiveness of the siRNA knockdown was confirmed by imaging using the Olympus ScanR microscope at 10x magnification and images were analysed using ScanR Analysis proprietary software. A minimum of 10,000 cells was imaged per individual sample. For analysis, the images were subjected to a standardized background correction with a 50-pixel window and image segmentation analysis anchored to nuclei as main objects in order to obtain the total eYFP-CRAF intensity per nucleus and the nucleus-associated cytoplasmic region. To eliminate potential image segmentation artifacts, we only included the analysis for cells associating with a cell segment smaller than 9,000 pixels - roughly equivalent to the observed cell size on the raw image. We also excluded high DNA content artifacts (>4N) as they predominantly represented unresolved multi-nucleated cell aggregates. The filtered data was then exported and analysed using Microsoft Excel. All other immunofluorescence experiments imaged and analysed on the Olympus ScanR were subjected to the same image analysis protocol.

2.6.4.2: High throughput screening with a ubiquitin ligase siRNA library

High throughput siRNA screening was conducted using E1-E2-E3 (Cullin and HECT domain E3) ubiquitin ligase library subset1 from Dharmacon, consisting of 6 siRNA-coated plates (Dharmacon) (**Appendix** 3.1). Plates were used to reverse-transfect format

at 50 nM final siRNA concentration into optical imaging plates. For each siRNA plate screen, 7.9 ml of DharmaFECT cell culture reagent (Thermo scientific, B-004500-100) was mixed with 80 µl of Dharmacon transfection reagent 1 and stored at room temperature under sterile conditions for no longer to 2 hr prior to use. 25 µl of the mixture was then added to each experimental well containing smart-pool siRNA and incubated 30 min at room temperature. 100 µl of full culture DMEM medium containing $2.4x10^4$ HEK293 cells stably expressing eYFP-CRAF were gently added into wells and incubated for 72 hr at 37° C with a 5% CO_2 humidified atmosphere. Following transfection, eYFP-CRAF degradation was initiated by addition of $3xGI_{50}$ of AUY922 for 8 hr at 37° C with a 5% CO_2 humidified atmosphere. Subsequently, cells were washed, fixed and stained with DAPI as described (**Section** 2.6.4.1). The eYFP intensity from each experimental well was analyses as previously described (**Section** 2.6.4.1)

2.6.4.3: Validation of high-throughput siRNA screen hits

HEK293 cells stably expressing eYPF-CRAF were grown in full culture DMEM medium. $1.2x10^4$ cells in a total volume of 80 µl were seeded into 96 well plates and incubated for 24 hr at 37°C with a 5% CO_2 humidified atmosphere. The wells on the outermost edge of the plate were not seeded but filled with PBS in order to buffer the innermost cells against temperature changes otherwise known as the side effect. A 250 nM siRNA for each potential positive hit from the high through put screen (**Section** 2.6.4.2) were prepared as previously described and 20 µl of each siRNA was added to a each well to a final concentration of 50 nM in total 100 µl. Cells were then incubated for 72 hr at 37°C with a 5% CO_2 humidified atmosphere. Each siRNA knockdown was repeated six times in a single plate. Subsequently a $3xGI_{50}$ of AUY922 was added to

each well and incubated for an additional 8 hr. The cells were then washed, fixed and stained with DAPI (**Section** 2.6.4.1). The eYFP intensity from cells were analysed by microscopy as previously described (**Section** 2.6.4.1). All quantitative data measurements were at least in triplicated and error bars represent standard deviation from the mean. Individual cell data were averaged where appropriate and averages were used in subsequent analyses. Significance was tested using a Paired Student T-test and stars denote the levels of significance. All such analyses were done using Microsoft Excel.

2.6.4.4: Western blot analysis of that endogenous CRAF levels following siRNA knockdown of Cullin 5 and HECTD3

$3x10^5$ HEK293 cells grown in full culture DMEM medium in a total volume of 3 ml were seeded into 6-well plates and grown to a 40% confluence. The siRNA for CUL 5 and HECTD3 (**Appendix** 3) were prepared at 50 nM, respectively, and added to cells as described in Section 2.6.4.1. The plate was then incubated for 48 hr (HECTD3) or 72 hr (CUL5) at 37°C with a 5% CO_2 humidified atmosphere. A double siRNA treatment for HECTD3 was suggested after 24 hr transfection. Degradation of endogenous CRAF was subsequently induced by the addition of $3xGI_{50}$ of AUY922. Cells were then harvested at 0, 8, 16 and 24 hr drug treatment. Both the level of endogenous CRAF depletion, and the knock down level Cuillin5 and HECTD3 were analysed by western blot analysis (Section 2.6.2).

2.6.5: Proximity Ligation Assay for detection of co-localization between HSP90, CRAF, and HECTD3

HEK293 cells stably expressing eYFP-CRAF and eYFP were grown in full culture DMEM medium. $4.5x10^5$ cells in a total volume of 3 ml were seeded on cover slips (Thermo scientific, A67761333) in 6-well plates and grown to 40-60% confluence and followed by $3xGI_{50}$ of AUY922 for another 18hr incubation. The cells were then fixed with 4% paraformaldehyde in PBS for 10 min and subsequently washed for 3x5 min with warm PBS buffer (2ml). Cells were then permeabilized with 0.3 % Triton X-100 in PBS (200µl) for 10 min, washed for 3x5 min wash with warm PBS buffer and then blocked with 200µl BlockAid blocking solution for 20 min. The primary antibodies were prepared with BlockAid blocking solution (Life Technologies, B10710) (100 µl per coverslip). Cells were then incubated for 1 hr with primary antibodies (**Appendix** 2) as appropriate. Slides were then washed with 1x PLA Buffer A for 2x5 min while shaking. The proximity ligation experiment between HSP90/eYFP, HSP90/CRAF, HSP90/HECTD3 and CRAF/HECTD3 was performed by using the Duolink® In Situ Red Starter Kit (Sigma-Aldrich, DUO92101). The PLA probes (secondary antibodies), MIUS and PLUS, was diluted 1:5 with BlockAid blocking solution. For each reaction, 24 µl of the PLA probes were mixed with 72 µl BlockAid blocking solution and subsequently added onto the cells. Slides were incubated 1 hr at 37°C in a pre-heated humidity chamber. The cells were then gently washed for 2x5 min with 1x PLA Buffer A in preparation for the ligation and PCR steps of the PLA assay.

The Ligation buffer from the kit was then diluted 1:5 in RNAse free water and used to dilute the ligase by 1:40. The ligation-ligase mix (120 µl) was then added to the cells and the sample incubated at 37^oC in a humidified chamber for 30 min. Meanwhile, amplification buffer was then diluted 1:5 in with RNAse free water and used to dilute

the DNA polymerase by 1:80. The cells were then washed with 1x PLA buffer A for 2x5 min, the amplification-DNA polymerase mix (120 µl) was added to the cells, and the sample incubated at 37°C for 100 min. The cells were then wash with 1x PLA Buffer B for 2x10 min, with 0.01x PLA Buffer B for 1 min and the slides allowed to dry at room temperature in the dark.

The slides were eventually stained with DAPI and VECTASHIELD. 10 µl of DAPI containing mounting medium (Sigma, DUO82040) was placed onto a glass slide, and the coverslip containing the treated cells was then applied to the mounting solution cell side down. The edges of the coverslip were sealed with colourless nail varnish. The Leica TCS SP8 Confocal Microscope was used to capture all images from the cell sample using a 63x magnification oil objective, or stored at -20° C for short periods of time. Using a confocal microscope (Leica TCS SP8) the nuclei of cells were imaged using a UV light setting and the PLA signal using a 555 nm laser source. A series of stacked images were taken in both channels. The images from each stack were processed by IMAGE J using the Z project plug and analysed with *Macros for PLA foci counting* (**Appendix** 4).

2.7: In vitro cell biology techniques

2.7.1: Mass spectrometry

Protein samples from pull down assays were analysed by SDS-PAGE gel and stained with Instant Blue (**Section** 2.6.1). Protein bands were cut from the gel using a clean scalpel, fragmented to increase the surface area to volume ratio and then transfer into an eppendorf tube. The gel fragments were then de-stained with 25 mM NH_4HCO_3 diluted with 50% MeCN for 5 min with shaking. These washes were repeated three times and

the gel fragments then further dehydrated in a spin vacuum for 5 min without heating. Subsequently, the gel pieces were incubated for 45 min at 50°C with sufficient 10mM DTT that just covered the gel until the gel was rehydrated. After the gel cool back to room temperature, aspirating all the liquid and replaced with iodoacetamide solution. The eppendorf tube was then incubated for 45 min in dark room at room temperature. Liquid was aspirated from the eppendorf tube and repeated the step of dehydrated. After that, the pieces of gel were rehydrated in trypsin solution with the volume just enough to fully rehydrate the gel back to full size, and leave on ice for 10 min. 25mM NH_4HCO_3 was then added to the eppendorf tube to cover the gel and incubated overnight at 37°C. TFA (just enough to cover the gel) was added to eppendorf tube with vortex. Peptides were eluted by spin down the pieces of gel and remove the supernatant (peptides) to a clean tube. Finally, the volume of peptide was concentrated to 10 µl using speed vacuum with heat on or off.

CHAPTER THREE

Degradation of HSP90-dependent client kinases in HEK293 cells following HSP90 inhibition

3.1: Introduction

Most biological components involved in the ubiquitylation of HSP90 client-proteins remain unknown. The automated siRNA screening provides a reliable route by which such components, including the E3 ligase, could be identified following the inhibition of HSP90, which is known to induce ubiquitylation of protein substrates. The HSP90 inhibitor AUY922 competitively binds with a high affinity to the ATP pocket of the N-terminal domain of HSP90 (Brough et al., 2008; Eccles et al., 2008; Gao et al., 2010). Previous studies revealed that treatment of the tumor cells lines HT29 and HCT116 with 17-AAG and AUY922 promoted ubiquitylation of the proto-oncogene kinases BRAF and CRAF (Sharp et al., 2007). The survival of such cancer cell lines is highly dependent on RAF kinase stimulated MAP kinase signaling.

Selection of the cell line for this study was carefully considered. We firstly tried to over express eYFP-BRAF^{V600E} kinase domain in Hela cells, but the expression is unstable and the protein tended to degrade (**Appendix** 5). HCT116 and HT29 cell lines were also investigated, but none of them showed stable transfection of the kinase domain of BRAF^{V600E} or the full length of CRAF. However, ultimately we wanted to avoid cell lines that are driven by RAF kinases. We reasoned that such cell lines might have altered E3-ubiquitylation systems that aid their survival and that cells might be sensitive to apoptosis following HSP90 inhibition. We also considered very carefully the choice of HSP90 client protein; its sensitivity and most importantly that it displayed a significant depletion in response to HSP90 inhibition. CRAF in HEK293 cells fulfilled these requirements and was therefore selected for this study. Consequently, we developed an eYFP-CRAF stably over-expressing HEK293 cell line that was suitable for use in siRNA screens.

3.2: Methodology

3.2.1: Live cell imaging with the DeltaVision microscopy imaging system

The Olympus inverted microscope was used for live cell imaging of over-expressed eYFP-CRAF in HEK293 cells. Cells were grown for 24 hr in a sterile chamber (Thermo Fisher, 155379), washed with warm PBS and then incubated in cell imaging solution pre-heated to 37^{o}C (Thermo Fisher, A14291DJ). The Köhler illumination was adjusted for high quality imaging and the filter for FITC and transmitted light channel were selected. The exposure time was minimized to reduce bleaching of the eYFP protein. The focus was auto-adjusted based on the channel of transmitted light. A 10x objective was used and imaging was conducted over a 24 hr period. Cells were selected at 10 different locations in the chamber and images captured every 5 min. 288 images were captured at each location, which were processed by OMERO and FIJI (Image J) software as required.

3.2.2: Plate reader assay modifications

Plate readers are often used to quantify signals from assays or directly from cells (see Material and Method 2.5). Using HEK293 cells in a 96-well plate we encountered two problems. The first issue came from the culture environment. Cells that were seeded in wells at the edge of the plate gave a relative low reading compared with cells cultured in wells situated in the middle region of the plate. This is probably due to changes in temperature and CO_2 tension during the incubation, which tends to be more extreme at the plate edges. Thus the temperature at the edge wells can cool faster during manipulations. Furthermore, changes in airflow can affect the CO_2 tension, which may

in turn alter the pH of the medium. Another issue encountered was that of weak attachment of HEK293 cells to the bottom of the plate. Replacement of the medium or washing with PBS removed substantial numbers of cells. This seriously influenced the measurement of the signal from the eYFP-CRAF protein in the fluorescence-based assay. To address these issues an enhanced cell attachment plate was used. Furthermore, when replacing medium or PBS buffer a specific amount was left in wells to limit any environmental changes and reducing the pressure from incoming solution, while the outermost wells of each plate contained medium or PBS and were not seeded with cells. This acted as a buffer to environmental changes during manipulations of the plate.

3.3: Results

3.3.1: Over-expression of eYFP-CRAF in HEK293 cells

Human full-length CRAF was cloned into the Kan/Neo resistance pEYFP-C1 vector as an XhoI-BamHI fragment (**Figure** 3.1). A stable cell line expressing eYFP-CRAF was selected on medium containing 800 μg/ml G418 antibiotic (see Materials and Methods 2.4). The expression of eYFP-CRAF in HEK293 cells was checked by immunobloting with α-GFP antibody, which identified a band corresponding to the expected relative molecular mass of the eYFP-CRAF fusion protein. No considerable level of free eYFP expression was detected (**Figure** 3.2). Live cell imaging over a 24 hr period (see Section 3.2.1), revealed a high level of eYFP-CRAF expression and a cytosolic distribution (**Figure** 3.3).

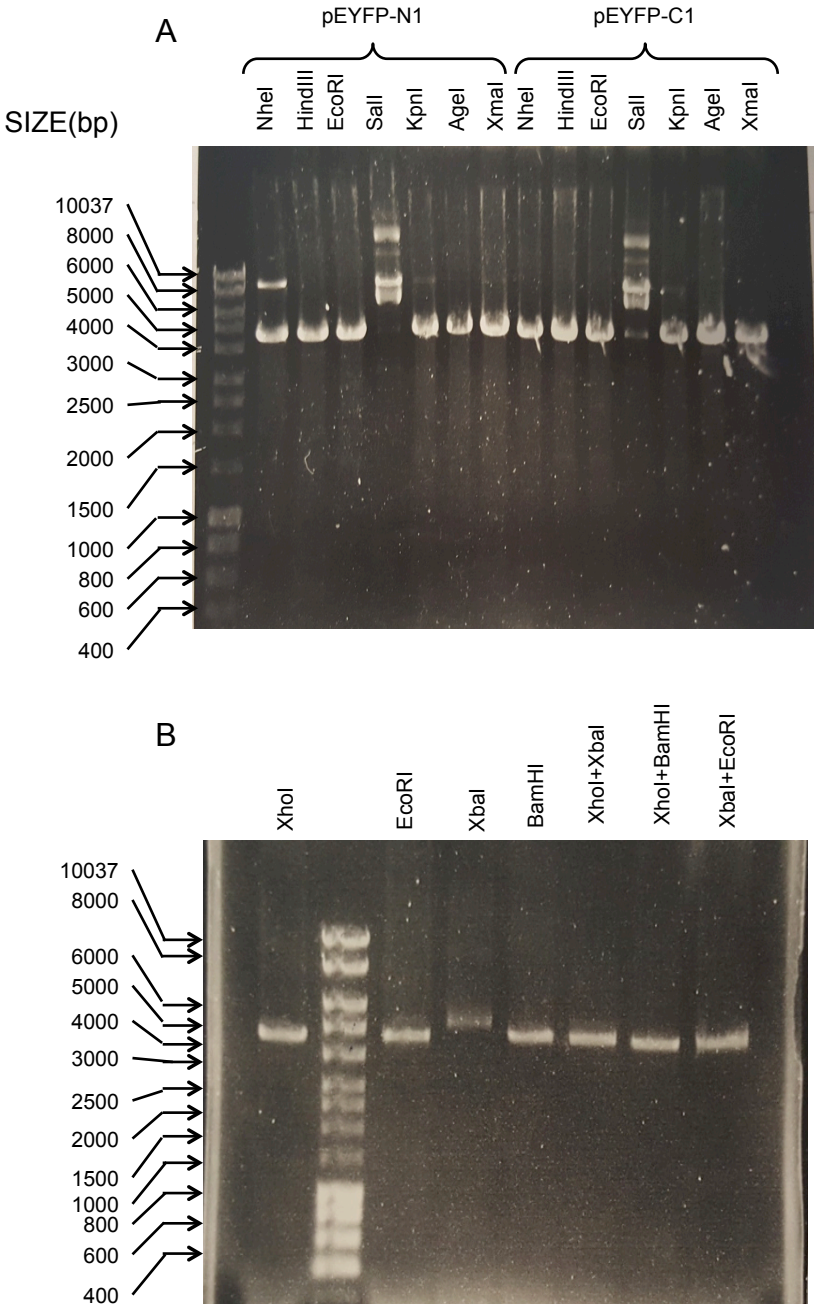

Figure 3.1 Restriction enzyme digests for the cloning of CRAF. Restriction enzymes used to digest vector and insert. **(A)** Both the pEYFP-C1 and N1 vector was tested with single NheI, HindIII, EcoRI, SalI, KpnI, AgeI and XmaI restriction enzymes of their ability to cleave the DNA. **(B)** The pEYFP-C1 vector was further tested with double restriction enzyme digests.

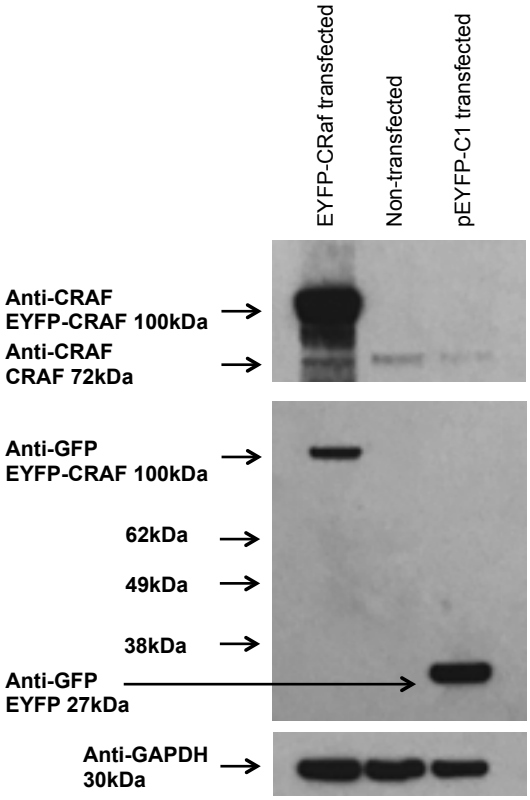

Figure 3.2 Exogenous eYFP-CRAF stably expressed in HEK293 cells. Expression levels of eYFP-CRAF, native CRAF and eYFP were detected by immunoblotting of stably transfected and none-transfected HEK293 cells with α-GFP antibody. GAPDH was used as the loading control. The same amount of eYFP-CRAF was detected by both anti-CRAF and Anti-GFP botibodies.

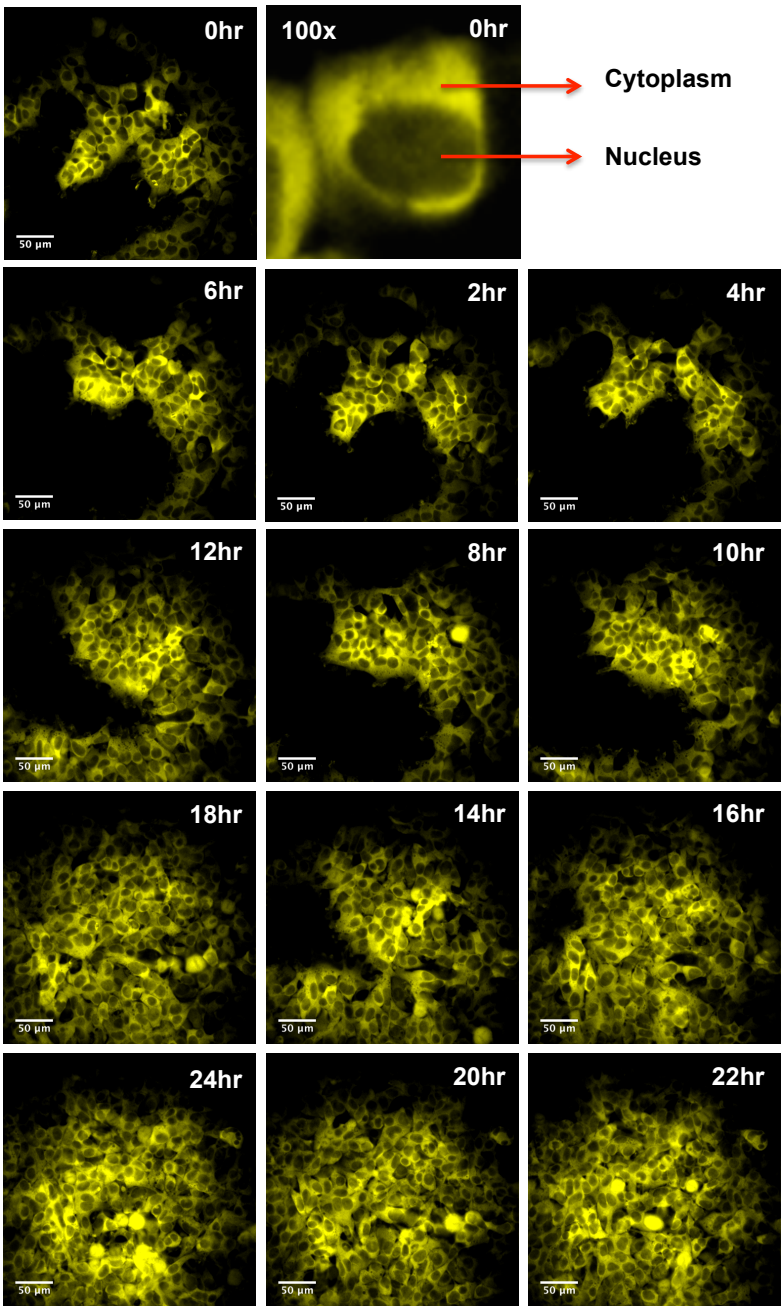

Figure 3.3. Live cell imaging of stably expressing eYFP-CRAF transfected HEK293 cells. Stably eYFP-CRAF expressed HEK293 cells were cultured in a chamber suitable for live cell imaging. The microscope was set up to captured the cell for every 5 min up to 24 hr. Images were processed by FIJI (Image J). A 100x time image from 0hr was provided to present a view of cytoplasm and nucleus. Scale bar = 50 µm.

3.3.2: Determining the AUY922 GI_{50} for WT and eYFP-CRAF overexpressing HEK293 cells

The GI_{50} concentration of AUY922 was determined for both wild type and stably transfected HEK293 cell lines (see Materials and Methods 2.5.1). The initial range of the inhibitor concentration tested was between 2.5 and 1600 nM. Cells exposed to concentrations above 360 nM were stressed and did not survive. Consequently, an upper limit of 320 nM of AUY922 was used in subsequent experiments. No substantial drop in cell viability was observed at 2.5, 5.0, 10.0 and 20 nM of inhibitor (**Figure** 3.4 A & B). However, the cell viability decreased to 44% when cells were exposed to 40 nM inhibitor concentrations. Viability continued to decrease with concentrations of AUY922 increasing to 320 nM. All measurements were conducted in triplicate and repeated at least 5 times. AUY922 is now in Phase II clinical trial and the given concentration to patient per week is 70mg/m^2. More information is available on clinicaltrials.gov.

To determine the GI_{50}, a logarithmic trend line was applied to the graph between the AUY922 concentrations of 2.5 to 320 nM. The equation, y=-12.23In(x)+98.315 was derived from the logarithmic trend line. The GI_{50} for wild type HEK293 cells was found to be 28±5 nM (**Figure** 3.4 A). The GI_{50} for cells containing overexpressed eYFP-CRAF was 27±5 nM (F**igure** 3.4 B). The GI_{50} reading for both the cell lines are quite similar, suggesting that the over-expression of eYFP-CRAF in HEK293 cells does not affect its response to AUY922.

A

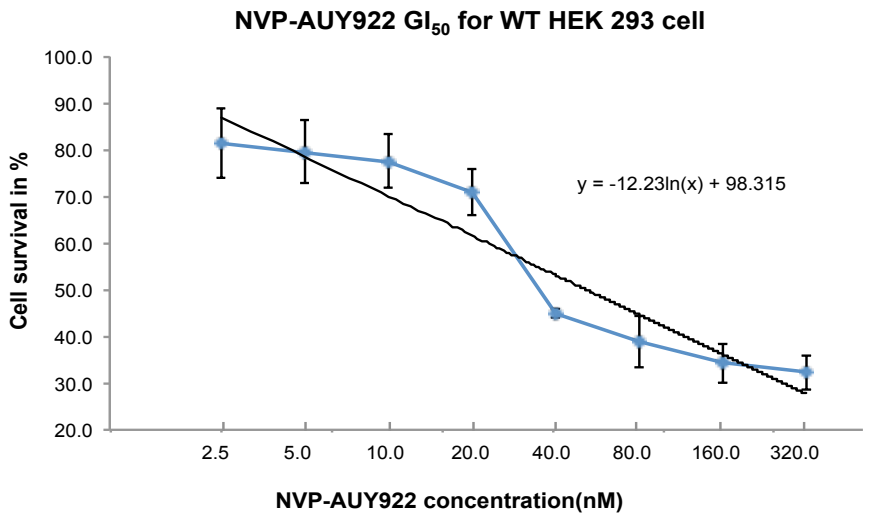

Drug Concentration (nM)	2.5	5.0	10.0	20.0	40.0	80.0	160.0	320.0
Data Average	81.3	79.5	77.5	71.0	44.9	38.7	34.3	32.2
Standard Deviation	7.3	6.7	5.9	5.0	0.9	5.5	4.2	3.6

B

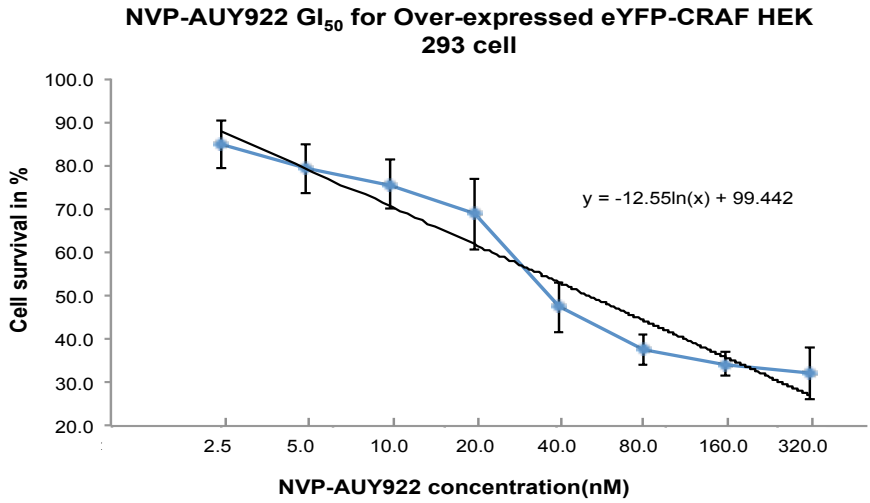

Drug Concentration (nM)	2.5	5.0	10.0	20.0	40.0	80.0	160.0	320.0
Data Average	85.0	79.3	75.6	68.8	47.4	37.6	34.2	32.2
Standard Deviation	5.6	5.6	5.6	8.2	5.8	3.5	2.7	6.0

Figure 3.4 GI50 determinations. The AUY922 GI_{50} for **(A)** wild type and **(B)** eYFP-CRAF over-expressing HEK293 cells were respectively determined by cell viability assay. Logarithmic equation was applied for the cure for calculating the GI_{50} for wild

type HEK293 cells and eYFP-CRAF over-expressing HEK293 cells. Each measurement was repeated at least 5 times and the standard deviation was applied and showed in error bar. A table for presenting the drug concentration and cell survivability was followed at the bottom of each graph.

3.3.3: Degradation of eYFP-CRAF in response to AUY922 treatment

The concentration (GI_{50} = 28 ±5 nM) of AUY922 that inhibited 50% growth of HEK293 cells in 24 hr might not be sufficient at promoting the degradation of eYFP-CRAF. To determine the concentration required for inducing the degradation of eYFP-CRAF, HEK293 cells stably expressing eYFP-CRAF were incubated with 1, 2, 3, 4 and 5 x the GI_{50} of AUY922, and the level of eYFP-CRAF depletion was evaluated using α -GFP antibody (see materials and methods 2.6.2). Cells incubated with 1 and 2 x GI_{50} did not show substantial depletion of eYFP-CRAF, whereas those treated with 3, 4 and 5 x GI_{50} showed a dramatic degradation of the fusion protein (**Figure** 3.5 A).

Cell survival was also tested with the same concentrations of AUY922 (**Figure** 3.5 B). 1 x GI_{50} did not affect the viability of the cells after a 72 hr incubation. Cell numbers dropped approximately 40% when incubated with 2 x GI_{50} and cell proliferation was almost totally inhibited at 3 x GI_{50}. Cell numbers dropped below the initial seeded levels when cells were treated with 4 and 5 x $GI_{50,}$ as observed microscopically. At 4 and 5 x GI_{50} cells were visibly stressed or dead. Consequently, we decided to use a concentration of 3 x GI_{50} in future experiments as this gave a substantial depletion of eYFP-CRAF without causing significant visible stress or death to cells.

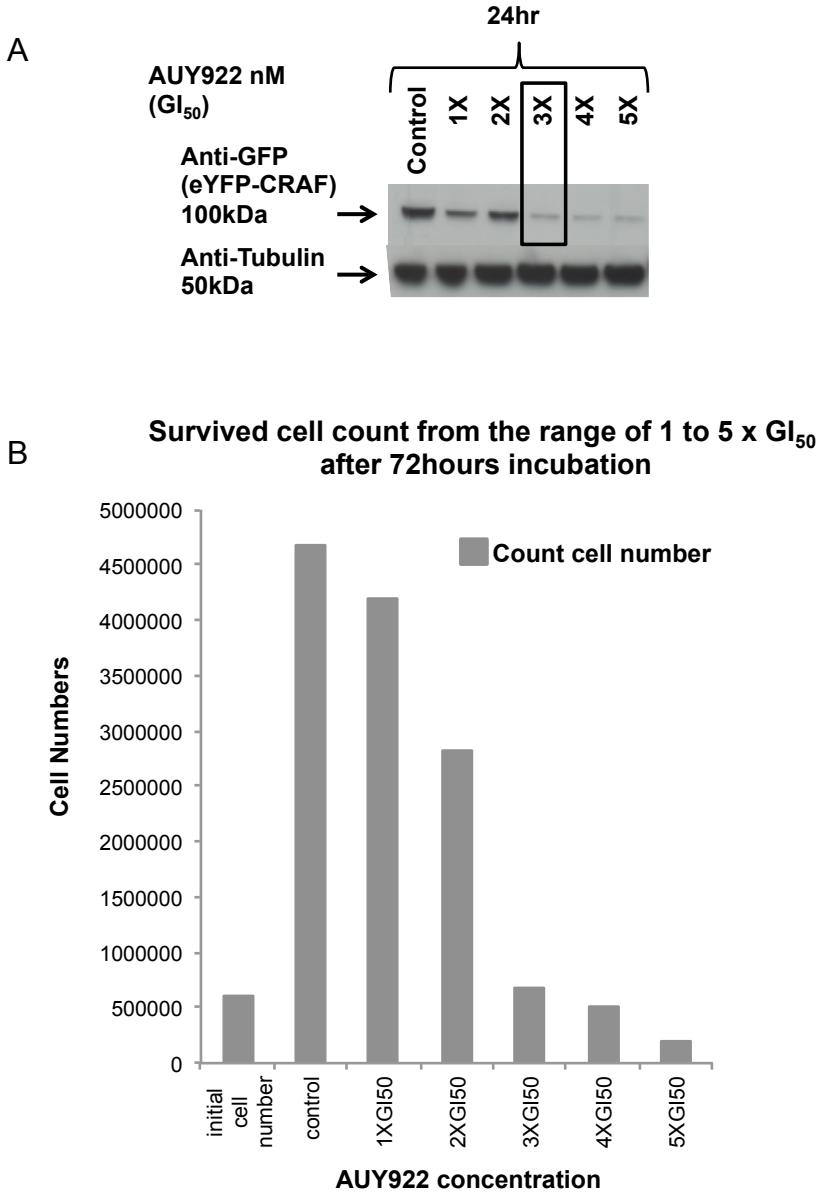

Figure 3.5 Protein stability and cell survival following AUY922 treatment. (A) Cells were exposed to 1-5 x GI_{50} of AUY922 for 72 hr and the expression of eYFP-CRAF was quantified by a western blot analysis. Most of the eYFP-CRAF was depleted at 3 x GI_{50} of NVP-AUY92 after 24hr. **(B)** Cell survival was determined by counting the total cell numbers from each experimental well. The growth of 293 cells was mostly inhibited at 3 x GI_{50} of NVP-AUY92 after 72 hr treatment. Cells died at 4 and 5 x GI_{50} of AUY922.

3.3.4: AUY922 promotes the degradation of multiple kinase proteins

Previous experiments revealed that a 3 x GI_{50} concentration of AUY922 would efficiently promote the degradation of the eYFP-CRAF fusion protein in HEK293 cells. We next tested the same concentration of AUY922 on HEK293 cells and noted the depletion of several other HSP90-dependent protein kinases. These included ErbB2, MASTL, BRAF, CRAF, RIP, PDK1, LKB1 and CDK4 (**Figure** 3.6). Low levels of ErbB2 expression where seen in HEK293 cells, which turned out to be the most sensitive kinase to AUY922 treatment. Depletion of ErbB2 almost reached 100% after 4 hr incubation with the HSP90 inhibitor, and no recovery was detected within 24 hr. In contrast, MASTL, which was also expressed at low levels, was not particularly sensitive to HSP90 inhibition, only showing substantial depletion after 24 hr treatment. For wild type BRAF, a high endogenous level was detected, but it is was not much more HSP90-dependent in HEK293 cells, and it appears that only the mutant type $BRAF^{V600E}$ in tumour cells relay on HSP90 In contrast, CRAF, which belongs to the same RAF family, was found to be very sensitive. The degradation of CRAF was constant over the first 16 hr of inhibitor treatment, but showed signs of recovery after 18 hr. Although BRAF and CRAF are both upstream regulators of the RAF-MEK-ERK cascades (Lowy and Willumsen, 1993), they clearly respond differently to HSP90 inhibition in HEK293 cells as has been seen in previous studies (Wellbrock, Karasarides and Marais, 2004). For RIP, detected as a double band with a 5 to 10-kDa difference, only the upper band was found to be sensitive to HSP90 inhibition, while an increase in the levels of the lower band were simultaneously observed following HSP90 inhibition (**Figure** 3.6). Strangely, for PDK1 an increased expression level was observed following inhibitor treatment. The significance of this remains unknown.

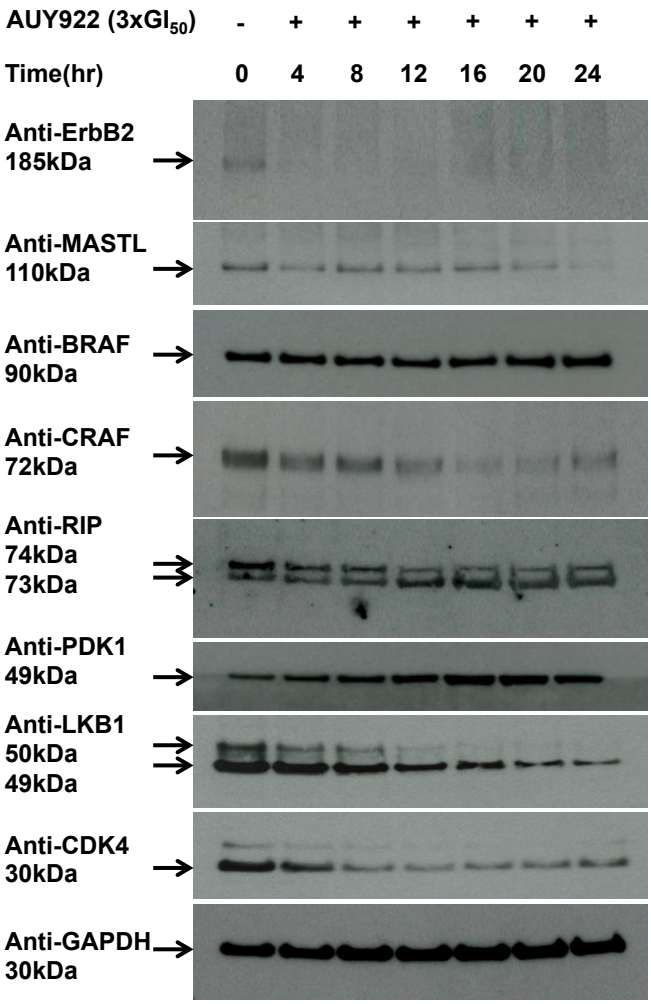

Figure 3.6 Sensitivity of kinases to HSP90 inhibition. Immunoblotting of cellular kinase levels for ErbB2, MASTL, BRAF, CRAF, RIP, PDK1, LKB1 and CDK4 in HEK293 cells with kinase specific antibodies during a 24 hr AUY922 treatment. ErbB2, CDK4, MASTL and LKB1 levels declined during AUY922 treatment. GAPDH was used as a loading control.

The stabilization of the tumor suppressor LKB1 was previously found to depend on the activity of HSP90 (Boudeau et al., 2003). An apparent constant rate of LKB1 degradation was observed following AUY922 treatment (**Figure** 3.6). Two LKB1 bands were detected by immunoblotting, and both bands showed a substantial time dependent degradation with no observable recovery within 24 hr treatment. The endogenous expression level of CDK4 in HEK293 cells was identified as the highest among the kinase tested. Recovery of CDK4 levels was observed after 20 hr treatment.

3.3.5: A Fluorescence-based assay for eYFP-CRAF degradation in HEK293 cells

Prior to the development of the assay it was necessary to confirm whether HEK293 cells in the presence or absence of AUY922 produced any measurable signal that would interfere with eYFP detection (**Figure** 3.7 A). The readout signals from wild type cells with or without AUY922 were similar to that of PBS alone. This suggested non-transfected HEK293 cells and AUY922 did not generate any considerable interference signal.

It was also necessary to determine the linear range over which the eYFP signal could be detected using a POLARstar Omega micro-plate reader. Cell densities of 25, 50, 75 and 100% confluence were used. As expected, these results showed that as the cell densities used in the experiment increased the eYFP signal increased in a linear fashion (**Figure** 3.7 B).

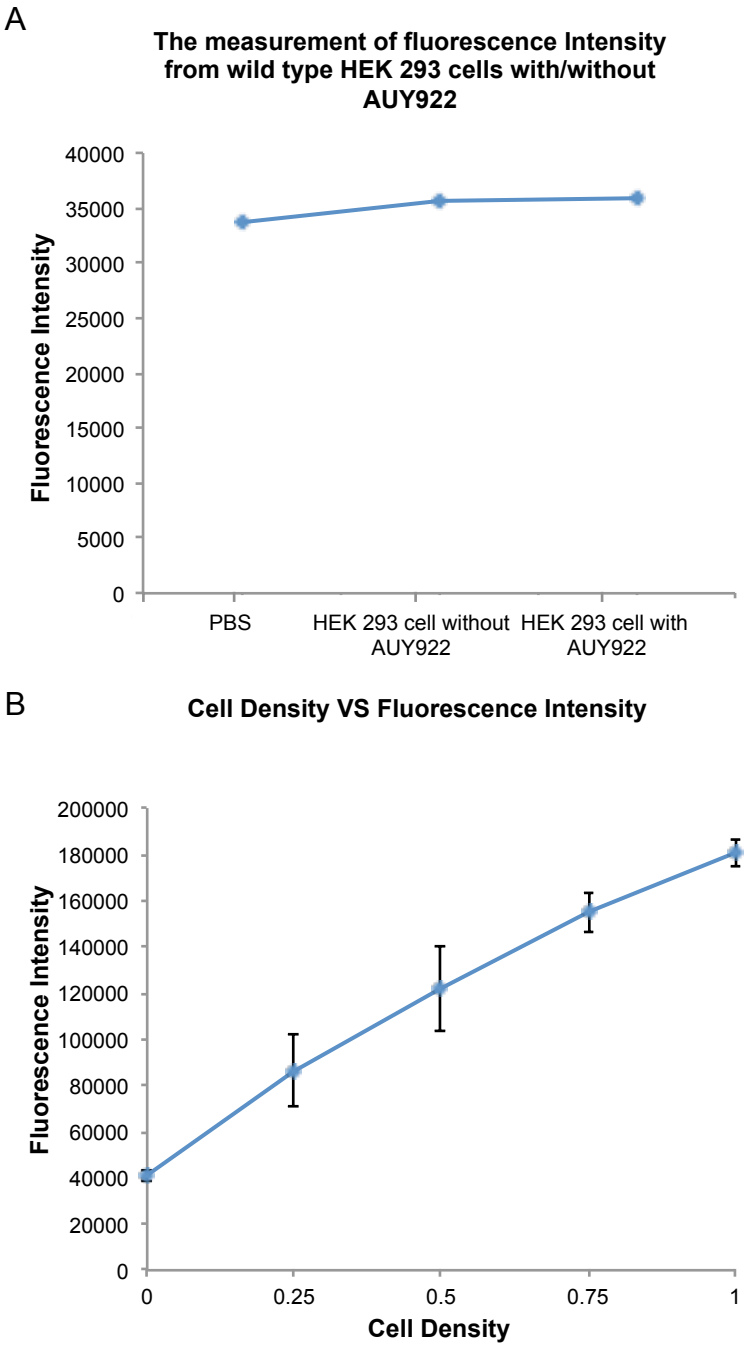

Figure 3.7 Control experiments for the fluorescence based assay in the HEK293 cell line. Background fluorescent signal from, **(A)** Wild type HEK293 cells with/without AUY922 treatment was examined. Either the WT cells or AUY922 did not contribute any significant readout signal. **(B)** The fluorescence intensity of eYFP-CRAF over-expressing HEK293 cells with increasing cell density.

Next the effect of AUY922 on the fluorescence intensity of eYFP-CRAF was tested (see Materials and Methods 2.5.2). The total fluorescence signal from cells expressing eYFP-CRAF was measured from each experimental well and plotted against time (**Figure** 3.8 A). Measurements from non-transfected HEK293 cells were used as control readout, and wells containing PBS represented the blank (background) readout. There was no considerable readout signals detected from the non-transfected cells either with or without inhibitor at each selected time point. In contrast, transfected cells produced a consistent and significant loss of the eYFP-CRAF signal within 12 hr post AUY922 treatment and no subsequent recovery was observed. As expected, non-drug treated cells showed an increase in the total signal (**Figure** 3.8 A**)**. No significant cell death was observed during the course of the experiment (**Figure** 3.8 B).

The decrease in fluorescence for AUY922 treated cells suggests depletion of eYFP-CRAF. This was also confirmed by a western blot analysis (**Figure** 3.8 C). The endogenous expression of CRAF and HSP90 was also analysed (**Figure** 3.8 C). The results showed efficient depletion of both eYFP-CRAF and endogenous CRAF with drug treatment.

3.3.6: Inhibition of HSP90 leads to the proteasomal degradation of eYFP-CRAF.

Previous experiments demonstrated considerable cellular degradation of eYFP-CRAF by quantifying the eYFP fluorescence intensity in transfected HEK293 cells following treatment with AUY922 (see section 3.3.3). This suggests that following HSP90 inhibition eYFP-CRAF might be subject to ubiquitylation and degradation by the ubiquitin system.

Consequently, stably expressing eYFP-CRAF HEK293 cells were treated with MG132 or DMSO control prior to AUY922 treatment. Subsequently, eYFP-CRAF was immunoprecipitaed with GFP-trap beads (see Material and Methods 2.6.1) and the degree of eYFP-CRAF ubiquitylation was analysed. Cells not treated with 1μM MG132 (treated with DMSO) showed some ubiquitylation of eYFP-CRAF, but those treated with the proteasome inhibitor displayed a substantially higher level of ubiquitylation (**Figure** 3.9). This indicated that the fusion protein was ubiquitylated in response to HSP90 inhibitor treatment and was subject to proteasome degradation.

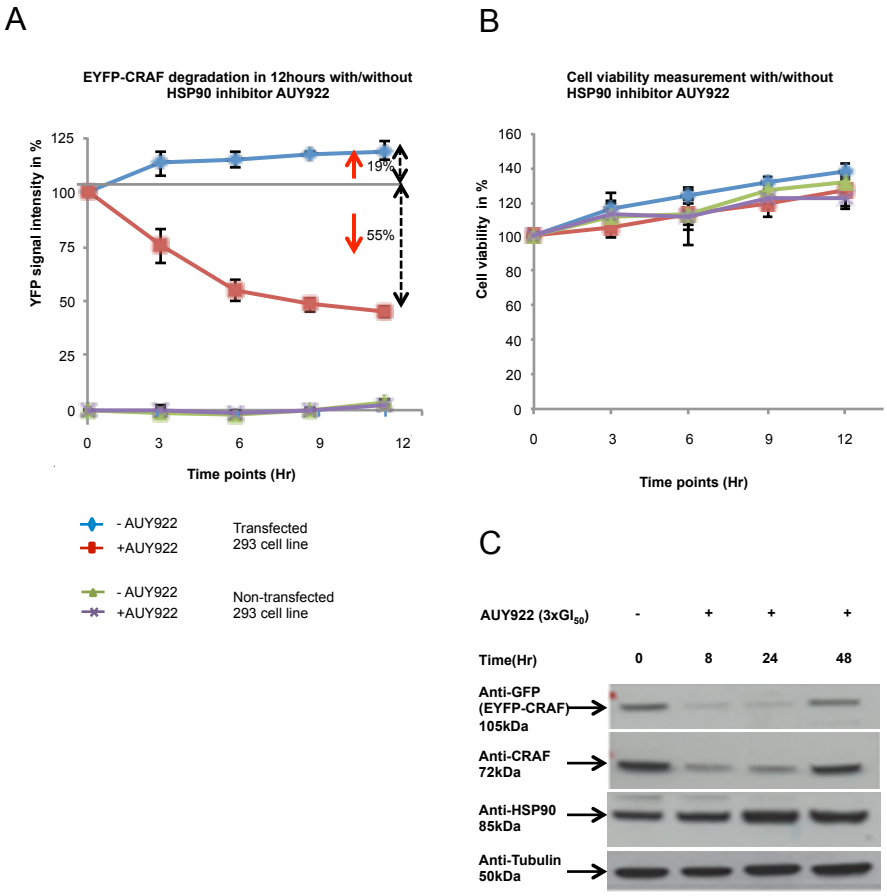

Figure 3.8 Fluorescence-based assay quantifying the degradation of eYFP-CRAF following AUY922 treatment. (A) Both the stably eYFP-CRAF over-expressing and wild type (WT) HEK293 cells were treated with 3 x GI_{50} of AUY922 for 12 hr. The remaining (non-degraded) eYFP-CRAF signal was quantified for each 3 hr time period. A significant decrease of the eYFP signal was observed with the treatment of inhibitor. The WT HEK293 cells did not contribute any considerable readout. **(B)** The viability of cells was quantified for each 3 hr time period during the inhibitor treatment. 3 x GI_{50} of AUY922 did not effect the cell viability within this period of time. **(C)** Corresponding antibodies confirmed the cellular expression level of eYFP-CRAF, endogenous CRAF and HSP90 after 8, 24 and 48 hr AUY922 treatment. Both the endogenous and exogenous CRAF went down by responding to the inhibition of HSP90 and started to recover after 24 hr treatment. Tubulin was used as the loading control.

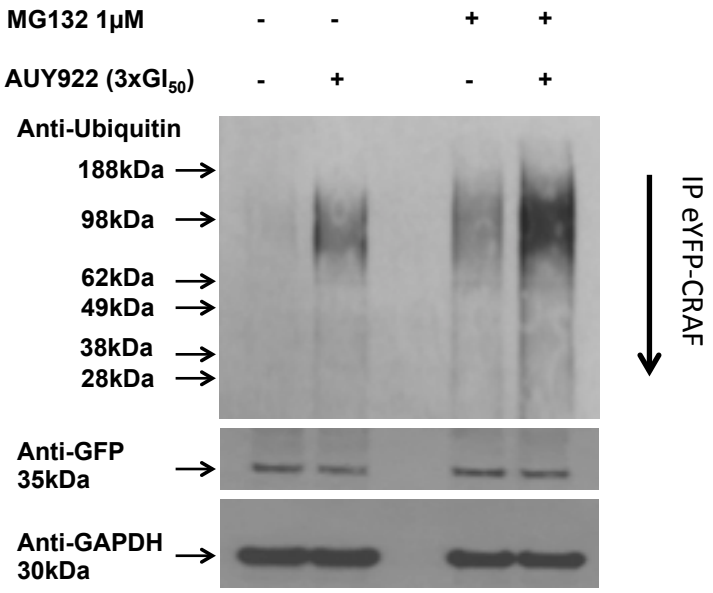

Figure 3.9 Ubiquitylation of eYFP-CRAF. EYFP-CRAF over-expressing HEK293 cells were pre-treated with MG132 and then AUY922. EYFP-CRAF was subsequently immunoprecipitated with GFP-trap beads and evaluated for the degree of eYFP-CRAF ubiquitylation using an α-ubiquitin antibody. The eYFP-CRAF fusion was showed by α-GFP antibody. The GAPDH from flow through was used as the loading control.

3.4: Discussion

Previous studies revealed the ubiquitylation and degradation of CRAF through the proteasome system in cells treated with geldanamycin, a natural-product inhibitor of HSP90 (Schulte et al., 1995; Chavany et al., 1996). When these inhibitors were initially discovered, they were not known to competitively bind to the ATP pocket of HSP90. However, once their target was identified (Prodromou et al., 1997a; Roe et al., 1999) many different HSP90 inhibitor chemotypes were developed that could promote the proteasomal degradation of HSP90-dependent protein kinases (Sharp et al., 2006 and 2007; Chiosis et al., 2001; Banerji et al., 2005). Similarly, the ATP-competitive protein kinase inhibitors such as Vemurafenib could also promote the ubiquitiylation dependent degradation of HSP90 client protein kinases. Such inhibitors are now known to prevent kinase association with the co-chaperone CDC37 and therefore recruitment to HSP90 (Polier et al., 2013). However, whether kinase degradation following kinase inhibitor treatement proceeds through the same pathway, as the HSP90 inhibitor-triggered degradation remains uncertain.

Previous work by Paul Workman's group indicates the stabilization of HSP90 client proteins, including ErbB2, CRAF, CDK4, CDK6 and p-AKT in human colon cancer cells, depends on the expression of CDC37. Furthermore, knockdown of CDC37 promotes the proteasome-mediated degradation of these protein kinases, which indicates that the involvement of HSP90 is not a prerequisite for degradation and that separate pathways might exist. The loss of CDC37 in cells also increases the sensitivity of such kinases to the HSP90 inhibitor 17-AAG (Smith et al., 2009). Clearly, CDC37 is a critical scaffold protein in HSP90 complexes, and an essential component for HSP90 dependent kinase stability.

$BRAF^{V600E}$ is one of the most common mutations able to drive cancer and consequently it has been heavily studied (Davies et al., 2002). Mutated $BRAF^{V600E}$ was previously shown to form an HSP90-CDC7 complex (Polier et al., 2013). The HSP90 inhibitor 17-AAG has been shown to promote the degradation of the mutated $BRAF^{V600E}$, but not the $BRAF^{WT}$ in melanoma and other human cancer cells, leading to the inhibition of cell proliferation and an increase cell apoptosis and antitumor activity (da Rocha Dias et al., 2005; Grbovic et al., 2006). Two other HSP90 inhibitors, PF-4470296 and PF-3823863, were also shown to promote the degradation of $BRAF^{V600E}$, as well as cMET, ErbB2, CRAF and AKT, in several human tumor cell lines (Mehta et al., 2011).

In summary, our data show that in HEK293 cells, eYFP-CRAF and endogenous CRAF, and a number of other HSP90 dependent protein kinase, are sensitive to the anticancer HSP90 inhibitor AUY922. We see a consistent loss of eYFP-CRAF, CRAF, ErbB2, MASTL, LKB1 and CDK4 following treatment of cells with AUY922.

CHAPTER FOUR

Automated siRNA screening of a human ubiquitin library

4.1: Introduction

In chapter three, a fluorescence-based assay using stably eYFP-CRAF over-expressed HEK293 cells was described. We found that the eYFP-CRAF fusion product could undergo degradation in response to AUY922 treatment, by observing the fluorescence change as a detectable output. In this chapter, the first subset of the human ubiquitin library is used to identify potential components that may regulate the proteasomal degradation of eYFP-CRAF in HEK293 cells.

The human siRNA library used in this study is known as Subset 1. It contains the human E1, E2, cullins and HECT domain E3 ligases and was used in an automated screening procedure, using a reverse transfection format (RTF) system. A specifically adjusted cell Vivo Olympus microscope from Dr Velibor Savic ‘s laboratory (Genome Damage and Stability Center, University of Sussex) was used for processing the siRNA screen and analyzing the data (**Figure** 4.1).

The loss-of-function (LOF) screen technique is the most direct application that is used to identify the function of a gene of interest, based on the phenotype observed. Typically, a large number of expressing genes can be targeted with a large-scale siRNA library, which potentially identifies the role of such genes upon a specific biochemical process. The knockdown of gene products in such a screen has been shown to be effective against the expression of structural components, enzymes, transcriptional factors and cell membrane receptors (Echeverri and Perrimon, 2006). However, it is critical to distinguish the difference between knockdown (transient) and knockout (stable) (Echeverri and Perrimon, 2006).

The modifier and synthetic lethal screen approach offers an additional step for modifying the LOF phenotype screen. Following silencing, a specific drug treatment

can be introduced and the phenotypic effect observed using a florescent readout. The screen of the human ubiquitin library in this project was developed based on this application using eYFP-tagged CRAF. One recent study based on this approach, identified a novel tumor suppressor (Kolfschoten et al., 2005; Westbrook et al., 2005). More details for high throughput RNAi screening in cultured cells can be found in the user's guide written by Echeverri and Perrimon in 2006.

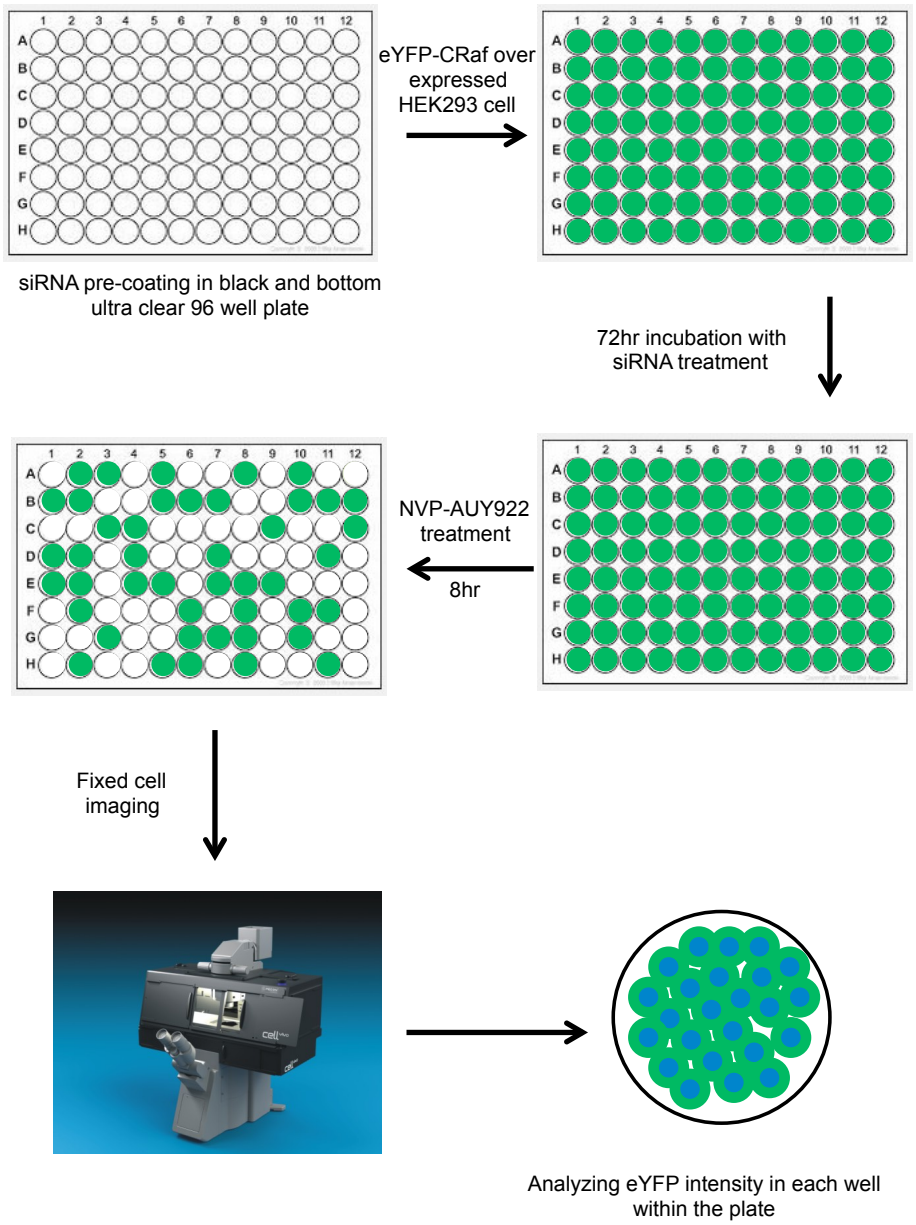

Figure 4.1 The imaging strategy for quantifying the eYFP intensity from individual cells. Stably eYFP-CRAF over expressing HEK293 cells were transfected and incubated for 72hr in a 96 well plate with pre-coated siRNA. Cells were then treated for an additional 8hr with the HSP90 inhibitor, AUY922. The cells were then fixed and the eYFP intensity from individual cells in each well was captured and analysed by Olympus cell Vivo microscope (see Material and methods 2.6.4 for details).

4.2: Results

4.2.1: Normalizing control siRNA

Control siRNA experiments were conducted ahead of the automated screen so that the cellular effect from both the positive and negative control siRNA treatment could be normalized. The on-target plus non-targeting smart-pool (siCTRL) and GFP duplex I siRNA (siGFP) were selected as the negative and positive control, respectively. Stably expressing eYFP-CRAF HEK293 cells were transfected with either negative or positive control siRNA (see Material and Methods 2.6.4), and the average GFP intensity from each individual cell was quantified and plotted as a histogram against the normalized frequency of cells using the Scan R software (**Figure** 4.2 A). Non-siRNA transfected cells had a total distribution of average GFP intensity between 180 and 1200, with a peak frequency at 450. Non-targeting siRNA treated cells showed similar range of GFP intensity, with a peak frequency of cells close to 440 (**Figure** 4.2 A). As expected, the GFP siRNA treated cells showed a peak frequency at around 260, which was substantially lower than for the control cells (**Figure** 4.2 A).

The level of eYFP-CRAF expression following negative or positive control siRNA transfection was also determined by immunobloting with GFP antibody and compared to that of non-siRNA transfected cells The results showed that transfecting with non-targeting siRNA did not influence the expression of eYFP-CRAF, whereas the GFP siRNA substantially reduced the expression of eYFP-CRAF (**Figure** 4.2 B).

Next the effect of AUY922 triggered degradation of eYFP-CRAF on siRNA treated cells was also investigated. Stably expressing eYFP-CRAF HEK293 cells were treated with negative control or positive siRNA followed by the addition of

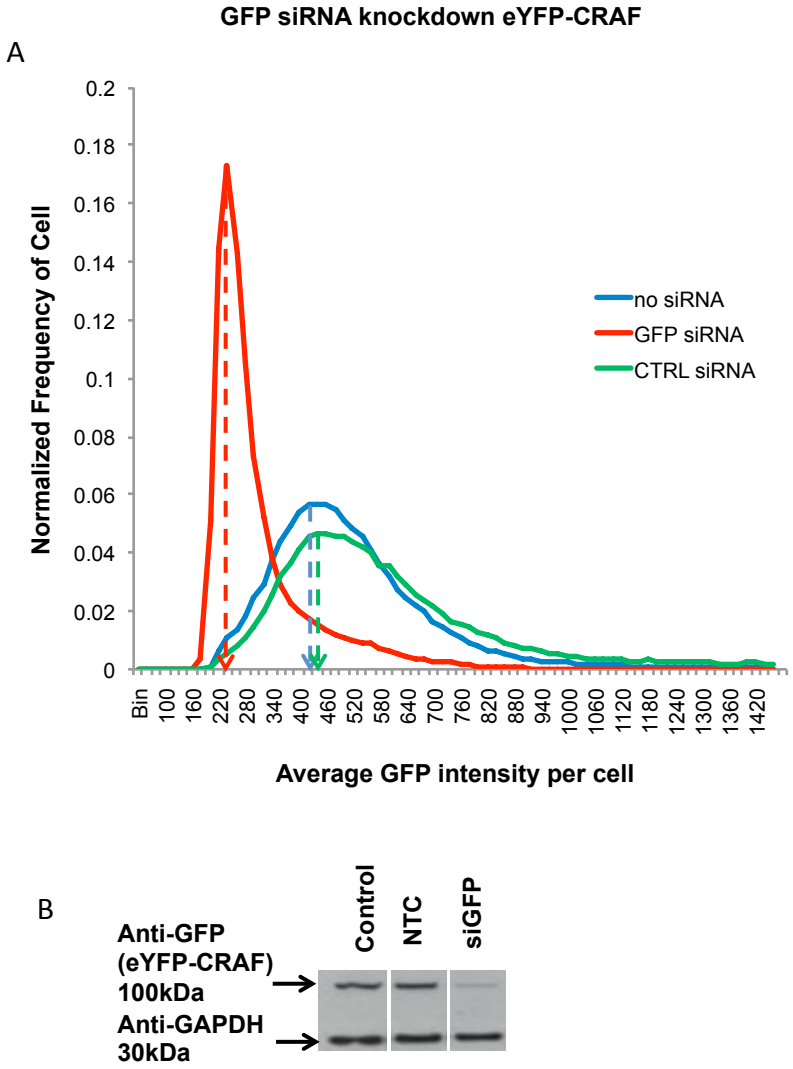

Figure 4.2 Determination of normalized GFP frequency of cells treated with negative or positive siRNA. (A) Stably eYFP-CRAF over expressing HEK293 cells were respectively transfected with GFP siRNA (positive control) and non-targeting siRNA (negative control) for 72 hr. The total eYFP intensity from each cell was arranged in a distribution graph. Cells treated with GFP siRNA dramatically decreased the intensity of eYFP in comparison with non-targeting siRNA and non-transfected cells. **(B)** The expression of eYFP-CRAF from positive, negative and non-transfected cells was clarified by immunoblotting. GAPDH was used as the loading control for all samples.

AUY922 (see Material and Methods 2.6.4). The effects were analysed by counting cell numbers with high, intermediate and low GFP intensity levels (**Figure** 4.3). The non-siRNA transfected cells (CTRL) gave a relative even distribution of cells between high and intermediate eYFP-CRAF intensity, and less than 1% cells were found in the range of low GFP intensity prior to AUY922 treatment. Cells transfected with non-targeting siRNA (siCTRL) showed a similar distribution to that of the CTRL. However, the GFP siRNA (siGFP) transfected cells showed a substantial decrease of cells displaying high eYFP-CRAF intensity (10%) with a corresponding increase on the number of cells with low intensity (30%).

With AUY922 treatment a substantial decrease in eYFP-CRAF signal with high intensity and a corresponding increase in the number of cells displaying low levels was observed (**Figure** 4.3). As expected cells treated with GFP siRNA and AUY922 showed the largest number of cells with low eYFP-CRAF levels. These results suggest that siRNA GFP reduces eYFP-CRAF levels in cells and that treating with AUY922 can further decreases these levels.

4.2.2: Automated siRNA screening for mediators of CRAF degradation

Stably expressing eYFP-CRAF HEK293 cells were screened against the human conjugation ubiquitin library subset 1 (see Materials and Methods 2.6.4.1). The treatment of AUY922 in each experimental well initiated the degradation of eYFP-CRAF, and the change in the total eYFP intensity of non-drug and AUY922 treated cells evaluated after 8 hr (see Materials and Methods 2.6.4.1).

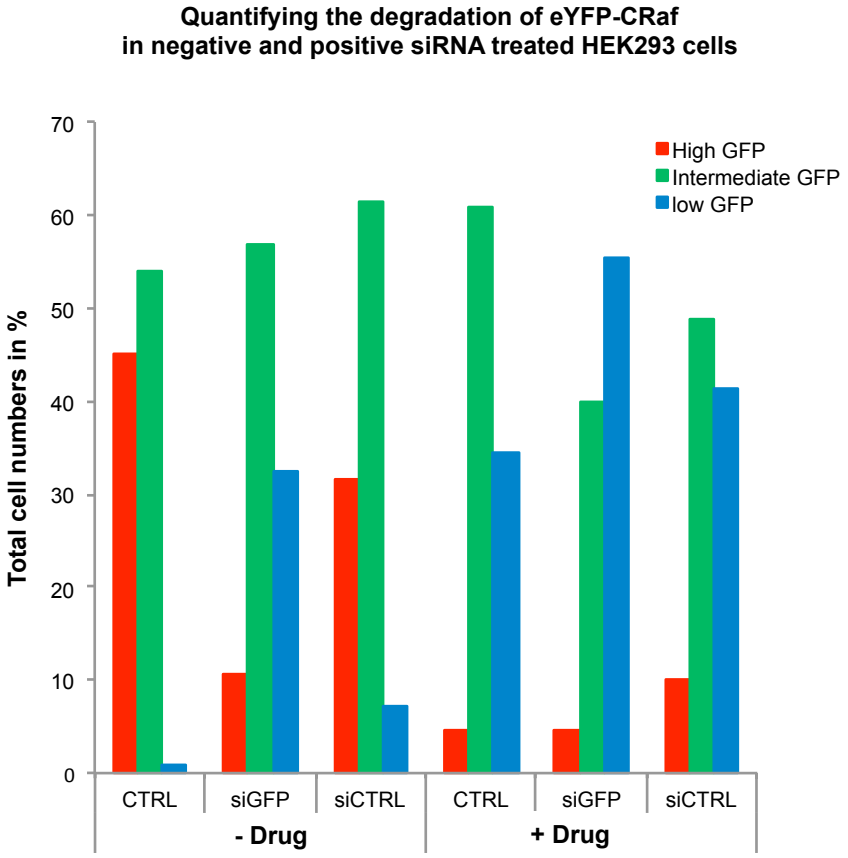

Figure 4.3 Quantifying the degradation of eYFP-CRAF with control siRNAs. GFP and non-targeting control siRNA were respectively transfected into eYFP-CRAF over expressing HEK293 cells followed by additional treatment of 3 x GI_{50} of AUY922. The eYFP intensity per cell is shown as high (Red), intermediate (Green) and low (Blue) level intensity. The shift of the cell population between red and blue bar indicates there were a dramatically drop of eYFP-CRAF level in non-transfected and non-targeting siRNA transfect cells after the drug treatment.

Genes were ranked according to the relative fluorescence stabilization following AUY922 treatment and knock down of the encoded protein, compared to levels following AUY922 treatment of cells transfected with non-targeting control siRNA (**Figure** 4.4) (**Appendix** 3.1 for the list of the gene). From the 87 genes screened, 10 potential hits were identified that stabilized the degradation of eYFP-CRAF by at least 15 % compared to control cells. The top hits stabilizing eYFP-CRAF levels included HECTD3, UBA1, UBE1DC, UBE2G1, UBE2D3, CUL5, NEDD4, TSG101, UBE1L2 and UBE2E1. As expected, the E1 ubiquitin activating enzymes UBE1 (also known as UBA1) and UBE1L2 (also known as UBA6), and the ubiquitin-like-protein E1 enzyme UBE1DC1 (also known as UBA5) were amongst the top hits. The identification of E1 components in the top list provides a critical positive validation of the automated siRNA screen, since E1 enzymes are the essential for initializing all ubiquitylation processes. Furthermore, three E2 ubiquitin-conjugating enzymes featured in the top hits. These included the an E2 enzyme UBE2D3 (also known as UbcH5C) that can act as the initiator of ubiquitin chains as well as in K11 and K48 site specific chain elongation (UniProt P61077), UBE2G1 (also known as Ubc7), which catalyzes the elongation of K48 or K63 chains (UniProt P622520), and UBE2E1 (also known as UbcH6), which is specific for K48 chain elongation (UniProt P51965). Four E3 ligases also featured amongst the highest ranked genes. The best described was the CUL5 protein, which is the core scaffold protein involved in a large group of Cullin-Ring E3 ligases (CLRs) (Kile et al., 2002; Lydeard et al., 2013). Others included TSG101 an ubiquitin-binding component of the endosomal-sorting complex required for transport-I (ESCRT-I) system (Zhang et al., 2014), and HECTD3 and NEDD4, which belong to the HECT-domain E3 ligase family. NEDD4 has been implicated in the regulation of a variety of membrane-associated signaling proteins and ion-channels (Zou et al., 2015), whereas

the role of HECTD3 remains poorly defined. However, previous research has revealed a role for HECTD3 in mediating the degradation of several non-HSP90 dependent client proteins, including Tara, Syntaxin 8, caspase-8 and MALT1 (Yu et al., 2008; Zhang et al., 2009; Li et al., 2013a and 2013b)

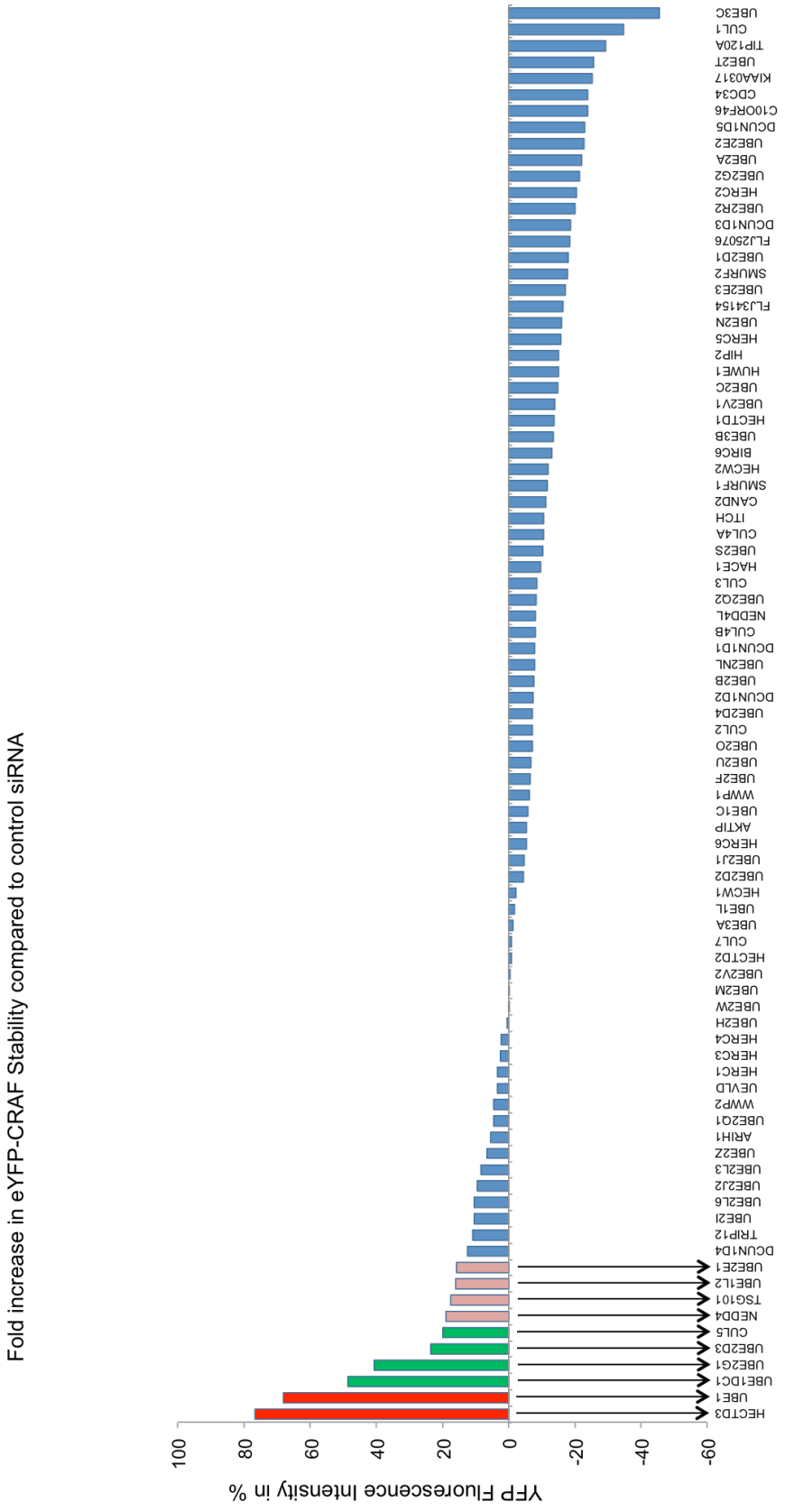

Figure legend on following page

Figure 4.4 Automated siRNA screen of the Human ubiquitin library subset 1. The Human ubiquitin library subset 1 contains E1, E2, Cullins and HECT domain E3 ligases (**Appendix** 3.1) and was used to identify the components involved in AUY922 induced degradation of eYFP-CRAF. HEK293 cells were transfected with 50nM pre-coated smart-pool siRNA (4 unique siRNA oligonucleotides targeting to its complementary sequence for the same gene) to respectively knockdown a specific gene for 72 hr and subsequently incubated with 3 x GI_{50} AUY922. The level of eYFP-CRAF protein remaining was determined using the previously discussed imaging system (**Figure** 4.1). Following subtraction of the mean background value from each cell, the total eYFP signal for each experimental siRNA transfection was normalized as a percentage and compared to the value of the non-targeting negative control siRNA transfected cells. Values on y-axis above or below the negative control indicate the effect of stabilization and destabilization, respectively. Genes were ranked from left to right according to the efficiency of stabilization of eYFP-CRAF, and the top 10 components that gave the most stabilization were highlighted by colour from RED to GREEN and PINK.

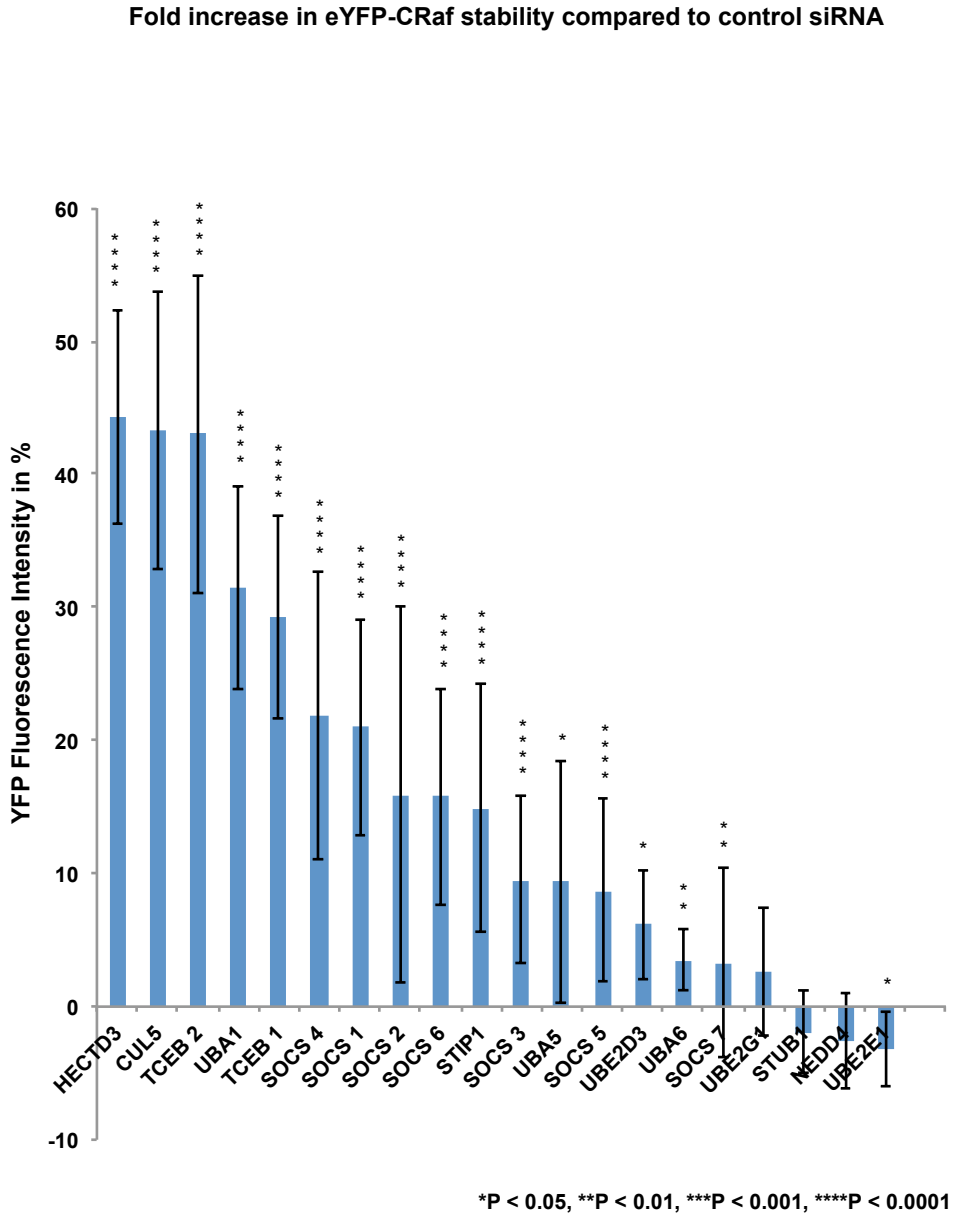

Figure 4.5 Validation of the top positive hits and associated proteins. For each positive hit from the top ten, a single siRNA was used to target the gene (**Appendix** 3.2), followed by 3 x GI_{50} AUY922 treatment. The eYFP intensity from each cell was quantified and analysed as described in Figure 4.4. Each siRNA transfection experiment was repeated at least 5 times. The significant difference for each gene was statistically analysed (*P<0.05, **P<0.01, ***P<0.001, ****P<0.0001) using the Paired student's t-test. The stabilization effect from HECTD3, CUL5 and UBA1 was reproducible. The individual knockdown of TCEB1 and TCEB2 also prevent the degradation of eYFP-

CRAF. None of the SOCS protein contributed a competitive effect then HECTD3 or CUL5. The additional associated protein: STUB1 and STIP1 did not stabilize the degradation of eYFP-CRAF.

4.2.3: Validation of the positive hits

To verify the involvement of these genes identified in the siRNA screen, which may mediate the degradation of eYFP-CRAF, we used individually designed ON-TARGET plus single siRNAs (GE Dharmacon) distinct from the pools used in the screens. Robust repeatable and highly statistically significant (with P value < 0.0001 in paired t-test) stabilization of eYFP-CRAF fluorescence was obtained for CUL5 and HECTD3. The level of stabilization was compared to that obtained with repeat siRNA knockdown of UBA1 (**Figure** 4.5).

The validation experiments showed that UBE2E1 and UBE2G1 (with P value >0.05), UBE2D3 (P value < 0.005), NEDD4 (P value > 0.05), UBA5 (with P value < 0.05) and UBA6 (with P value < 0.001) from the top ranked genes did not significantly stabilize the degradation of eYFP-CRAF, showing only 10% stabilization (**Figure** 4.5). Not surprisingly, the knockdown of UBA1 consistently prevented the loss of eYFP-CRAF (with P value < 0.0001) (**Figure** 4.5).

Previous studies revealed that siRNA silencing of the HSP90/HSP70 associated U-Box E3 ligase, STUB1/CHIP, mediated the degradation of ErbB2 following HSP90 inhibition (Xu et al., 2002; Zhou et al., 2003). However, these experiments were not reproducible in the current study involving the degradation of eYFP-CRAF (with P value > 0.05). The knockdown of STIP1, a co-chaperone that mediates the association between HSP90 and HSP70, was shown not to significantly stabilize eYFP-CRAF following HSP90 inhibition (with P value <0.0001) (**Figure** 4.5).

CUL5 is the scaffold protein for the elongin BC-CUL5-SOCS-Box (ECS) complexes, and operates with the catalytic RING finger proteins (RBX1/2) and NEDD8. The elongin BC complex (also known as TCEB2&1 complex) mediates the assembling of

the SOCS-box substrate recognized adaptor proteins, SOCS1-7 (Lydeard et al., 2013). Single knockdown of CUL5, TCEB1 or TCEB2 was found to have a consistent stabilization affect on eYFP-CRAF levels (**Figure** 4.5), which contradicts a previous study in the HT29 tumor cell line. This study revealed that the degradation of the HSP90 client proteins ErbB2 and $BRAF^{V600E}$ by CUL5 was independent of TCEB1&2 (Ehrlich et al., 2009; Samant et al., 2014). The significance of this apparent contradiction remains unknown, but could be cell line specific. We also found that the knockdown of individual SOCS-Box proteins such as SOCS 1 and 4 could stabilize the degradation of eYFP-CRAF by more than 20% over control siRNA, but this effect was not as strong as that seen from HECTD3 and CUL5 knockdown (**Figure** 4.5).

Taken together, the results so far suggest that the degradation of eYFP-CRAF in the HEK293 cell line was mediated by the elongin BC-CUL5 core and HECTD3 E3 ligase. A clear single SOCS-box protein specific for selecting eYFP-CRAF was not identified suggesting either, a large degree of redundancy between SOCS proteins in this role, or that some unidentified non-SOCS adaptor protein might be responsible.

4.2.4: Validation of endogenous CRAF degradation by CUL5 and HECTD3

The results so far suggest that the knockdown of CUL5 and HECTD3 leads to the stabilization of eYFP-CRAF following by AUY922 treatment. However, it was possible that this observation is due to some idiosyncratic feature of the eYFP-CRAF fusion protein. In order to address this, the effect on endogenous CRAF protein kinase was investigated following the knockdown of CUL5 and HECTD3. The CUL5 siRNA transfected HEK293 cells showed a delayed degradation of endogenous CRAF at 8 hr post AUY922 treatment and then leveled off towards 24 hr, while the non-targeting

siRNA treated cells showed a consistent degradation of CRAF (**Figure** 4.6). The knockdown of HECTD3 dramatically stabilized the degradation of CRAF (**Figure 4.7)**, thus implicating HECTD3 in the degradation of endogenous CRAF.

Since the degradation of ErbB2 was previously reported to be dependent on CUL5, but not TCEB2 (Ehrlich et al., 2009). We also tested the effect of CUL5 and TCEB2 knockdown on ErbB2 levels. The data revealed that the cells transfected with control siRNA or targeting the knockdown of TCEB2 or CUL5 gave similar levels of ErbB2 degradation in wild type HEK293 cells (**Figure** 4.8). Suggesting that ErbB2 is not subject to proteasomal degradation by the CUL5 pathway. Taken as a whole these experiments suggest that the degradation of CRAF in HEK293 cells is dependent on both the CUL5 and HECTD3 systems, although HECTD3 appears to be the main route for the degradation of CRAF.

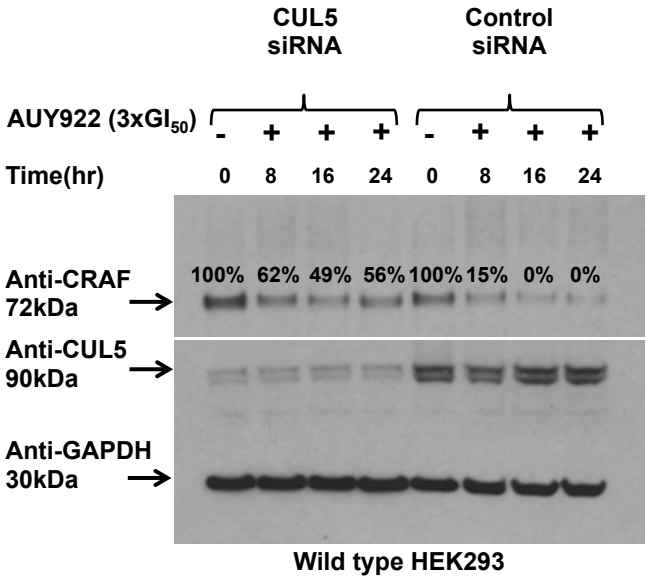

Figure 4.6 Silencing CUL5 delays AUY922 induced degradation of CRAF. Wild type HEK293 cells were transfected with non-targeting negative control or CUL5 siRNA for 72 hr and subsequently treatment with $3xGI_{50}$ AUY922 for between 0 to 24 hr. The protein level of CRAF was immunoblotted and analysed. GAPDH was used as a loading control. A more accumulation of CRAF was observed at 0 hr and the HSP90 inhibitor induced degradation of CRAF was delayed and stabilized to compare with negative control siRNA transfected cells. The CRAF remaining level was corrected with GAPDH level at 0hr and displayed in percentage.

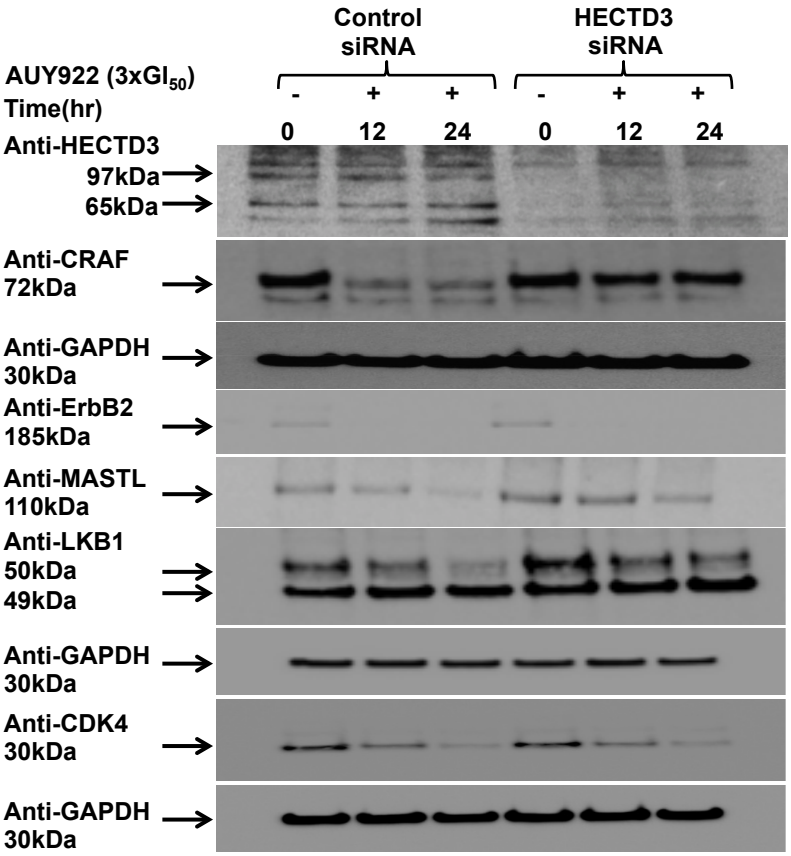

Figure 4.7 The effect of HECTD3 knockdown on multiple protein kinases. Immunoblotting analysis of HSP90-dependent client proteins in both negative control and HECTD3 siRNA transfected HEK293 cells after 48 hr transfection and subsequent treatment with 3 x GI_{50} AUY922 for between 0 to 24 hr. GAPDH was used as the loading control for all samples. The degradation of CRAF, MASTL and LKB1 were implicated after 12 and 24 hr treatment. No significant affect was observed for the degradation of ErbB2 and CDK4.

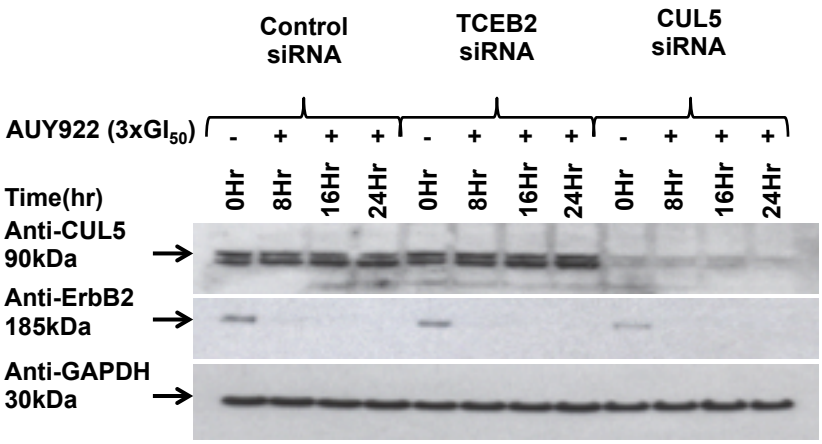

Figure 4.8 Silencing TCEB2 and CUL5 did not delay the loss of ErbB2. Immunoblotting analysis of ErbB2 in negative control, TCEB2 and CUL5 siRNA targeted HEK293 cells after 72 hr transfection and subsequent treatment with 3 x GI_{50} AUY922 for between 0 to 24 hr. GAPDH was used as the loading control for all samples. The degradation of ErbB2 was not effected by the siRNA knockdown of CUL5 or TCEB2.

4.2.5: HECTD3 dependency in the degradation of multiple HSP90 dependent protein kinases

Although HECTD3 was shown to be involved in the degradation of CRAF, its effects on other client kinases remains unknown. Consequently, we tested a series of such kinases, and the level of stabilization in response to HECTD3 knockdown. The expression of ErbB2, MASTL, LKB1, and CDK4 was detected at reasonable levels by immunoblotting in wild type HEK293 cells (**Figure** 4.7). The degradation of MASTL, LKB1 was diminished with the knockdown of HECTD3, while ErbB2 and CDK4 was not affected (**Figure** 4.7). We did not include BRAF, PDK1 and RIP because none of them responded to AUY922 in previous experiments (see section 3.2.5, Figure 3.6). These observations suggest that HECTD3 may represent a common degradation pathway for AUY922 triggered degradation in HEK293 cells for CRAF, MASTL and LKB1, which are all serine/threonine protein kinases.

4.2.6: HECTD3 and CUL5 are not involved in kinase inhibitor dependent degradation of eYFP-CRAF

Previous studies revealed that ATP-competitive kinase inhibitors could block the association between various HSP90 client kinases and the kinase-specific recruitment co-chaperone, CDC37, which ultimately deprives access of the kinase to HSP90 (Polier et al., 2013). Consequently, the inhibited kinases undergo ubiquitin directed proteasomal degradation. However, it is still not fully understood how this HSP90-independent degradation pathway differs to the HSP90-dependent pathway, which involves HSP90 inhibition.

Results previously indicated that incubating HEK293 cells with Sorafenib could

promote degradation of eYFP-CRAF over 24 hours (**Figure** 4.9), as observed for Vemurafenib and $BRAF^{V600E}$, lapatinib and ErbB2 and erlotinib and EGFRG719S (Polier et al., 2013). Moreover Sorafenib treatment substantially inhibited the MAP-kinase pathway and depleted phospho-p44/42 (ERK) levels. However, knockdown of HECTD3 in HEK293 cells did not affect the degradation of eYFP-CRAF and phospho-ERK levels, relative to that seen with control siRNA (**Figure** 4.9 A), and the knockdown of CUL5 also did not show any dependently affect on Sorafenib induced degradation (**Figure** 4.9 B). Consequently, it appears that HECTD3 and CUL5 do not play a major role in kinase degradation triggered by chaperone deprivation in response to kinase inhibitor blockade of CDC37 binding.

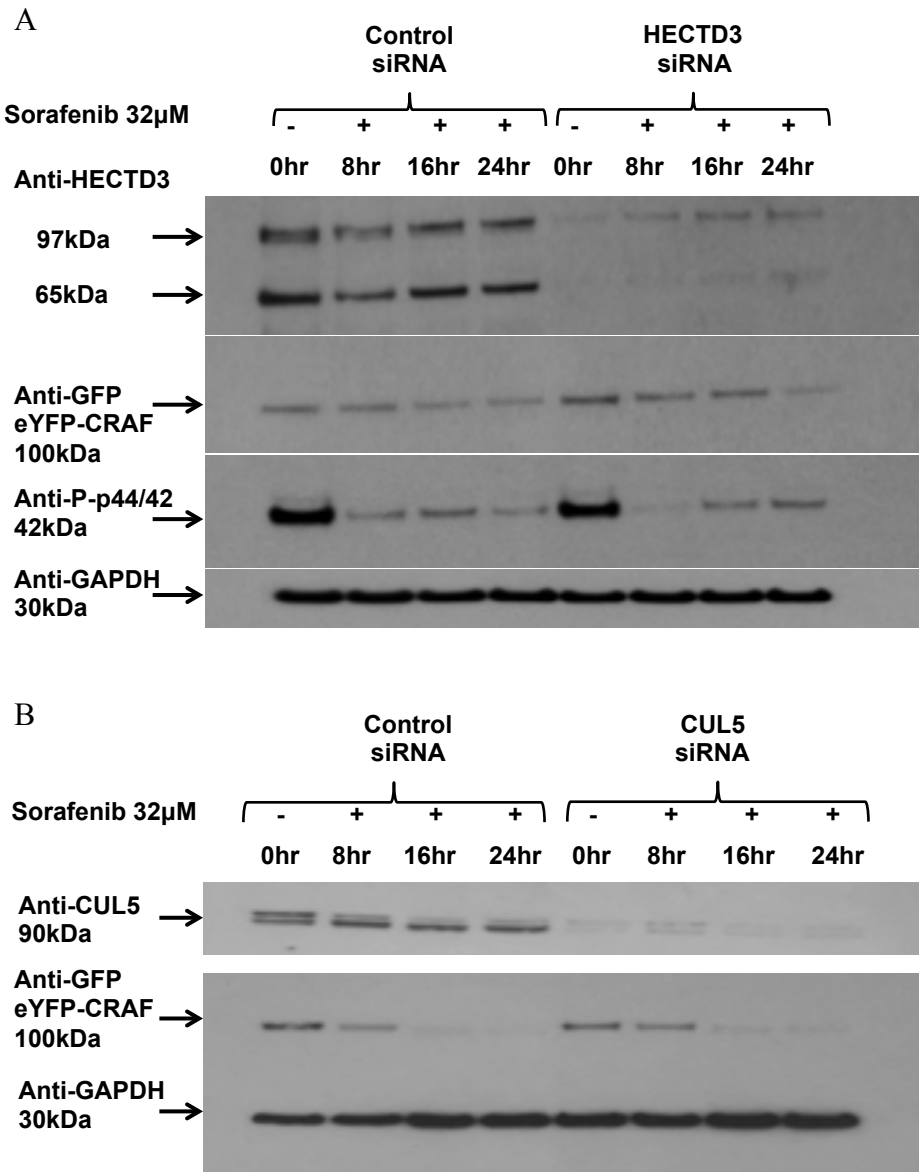

Figure 4.9 Silencing HECTD3 and CUL5 does not influence kinase inhibitor induced loss of eYFP-CRAF. Immunoblotting analysis of eYFP-CRAF and P-p44/42 in negative control, CUL5 and HECTD3 siRNA targeted HEK293 cells after 48 hr transfection and subsequent treatment with 32 μM of Sorafenib for between 0 to 24 hr. GAPDH was used as the loading control for all samples. **(A)** The kinase inhibitor triggered degradation of eYFP-CRAF and downstream signaling of P-p44/42 in 293 cells was observed and it was not influenced by the knockdown of HECTD3 and **(B)** CUL5.

4.3: Discussion

In this chapter, the human ubiquitin conjugation subset 1 library was automatically screened for effects on eYFP-CRAF stability when over-expressed in HEK293 cells. The results revealed several E1s, E2s and E3s might participate in the HSP90 inhibitor AUY922 triggered degradation of eYFP-CRAF. Further validation experiments confirmed the stabilization effect on eYFP-CRAF and endogenous CRAF were specifically related to the E3 ligases HECTD3 and CUL5, but that HECTD3 appears to be the main E3 ligase involved.

Previously the role of CUL5 in HSP90 inhibitor induced degradation of client kinase in HT29 and HCT116 cancer cell lines was shown, but this appeared to be independent of a TCEB2&1 (elongin BC) requirement (Ehrlich et al., 2009; Samant et al., 2014). However, in the current study we observed that knockdown of either TCEB2 or TCEB1 could stabilize the degradation of eYFP-CRAF. We hypothesized that the elongin BC complex is critical for linking substrate recognition to CUL5. This is consistent with a recent study suggesting that siRNA knockdown of CUL5, RBX1, CUL3, RNF7 (also termed RBX2) and SOCS5 could significantly reduce the HSP90 inhibitor, 17-AAG, triggered degradation of ErbB2 in HT29 tumor cells. Furthermore, the degradation of $BRAF^{V600E}$, AKT and CDK4 was also reduced by knockdown of CUL5 or RBX2 (Samant, Clarke and Workman, 2014). Although degradation of the over-expressed ErbB2 in HEK293T (Ehrlich et al., 2009), and endogenous ErbB2 in HT29 cells was previously reported to be dependent on CUL5 (Samant, Clarke and Workman, 2014), we did not observe any stabilization effect on ErbB2 in HEK293 cells following CUL5 or TCEB 2 knockdown (**Figure** 4.8). The reasons for this discrepancy remain unknown and further work is now required in order to address this.

Our analysis suggests both SOCS 4 and SOCS 1 might influence the degradation of eYFP-CRAF, but the effect was far less than the adaptor protein complex TCEB1/2 (elongin BC) or the newly identified HECTD3. Failure to observe strong stabilization effects following SOCS protein knockdown might be due to degeneracy in the recognition system. A variety of different CRL5 complexes specifically for recognizing various substrates, such as $CRL5^{ASB}$, $CRL5^{Cis/SOCS}$, $CRL5^{WSB1}$, $CRL5^{Elongin\ A}$, $CRL5^{SSB}$ and $CRL5^{RAB-40C}$ complexes have been identified (Okumura et al., 2012).

HECTD3 is a poorly characterized E3 ligase. This 97-kDa protein contains a middle domain, which is homologous to the DOC domain of APC10, and a C-terminal HECT domain. The domain structure and function of the N-terminal domain has not yet been defined. To date, although HECTD3 was reported to mediate the ubiquitylation of multiple proteins, none of these appear to be HSP90 dependent protein kinase (Li et al., 2013a and 2013b; Zhang et al., 2009; Yu et al., 2008). Moreover, most previous studies were based around over-expressed HECTD3, which may result in non-specific activity against protein substrates. In contrast, the present study used endogenous levels of HECTD3 and CRAF to show CRAF dependency on HECTD3. In fact, this study suggests that HECTD3 dependency only present in response to HSP90 inhibition and not kinase inhibitor treatment.

The knockdown of E2s alone did not show any considerable influence on the degradation eYFP-CRAF when triggered by AUY922. However, amongst these E2s, UBE2D3 appears to show some moderate effect. The UBE2D3 (also termed as UBCH5C) is a well-known E2 conjugating enzyme that cooperates with various E2 or E3 components for substrate proteasomal degradation. Further work would have to be carried out to confirm whether UBE2D3 is an E2 conjugating enzyme that can co-operate with HECTD3. In conclusion, HECTD3 knockdown contributes to a robust

stabilization effect on CRAF above that seen for CUL5 knockdown in HEK293 cells, following HSP90 inhibition. UBE2D3 is tentatively identified as a potential E2 that might co-operate with HECTD3. An E2 screen with HECTD3 could confirm this hypothesis.

The lack of the specificity or off-target activity from the rapid use of siRNA technology could effect and complicate the gene silencing phenotype. There are three main categories of off-target effects, which include immune stimulation effects (Karikó et al., 2004; Judge et al., 2005), endogenous RNAi machinery saturation effects (Grimm et al., 2006; Khan et al., 2007) and microRNA-like off-target effects (Jackson et al., 2003 and 2006; Birmingham et al., 2006). Sequences causing pro-inflammation can be removed to help avoiding immune stimulation effects (Judge et al., 2005). No known strategy had been identified to mitigate the effect caused from the saturation of the RNAi machinery. The most appropriate strategies to address microRNA-like off-target effects include to reduce siRNA redundancy, process rescue experiments (Hüttenhofer, 2003; Cullen, 2006; Echeverri et al., 2006), use pool siRNA (Kittler et al., 2007) and modify the seed region. Alternatively, the off-target activity effects could be significantly mitigated by both CRISPR and TALEN gene editing methods to knockout target genes. One of the best approaches to improve the specificity of HECTD3 is to rescue the observed phenotype by expressing a functional vector in a HECTD3 knockout cell line.

CHAPTER FIVE

Co-localization of HSP90 HECTD3 and CRAF

5.1: Introduction

In the last chapter we presented our results validating the role of HECTD3 in the ubiquitin-dependent proteasomal degradation of CRAF, following inhibition of HSP90. Consequently a number of predictions can be made from this observation. There should be a shift of CRAF from HSP90 to HECTD3 complexes following HSP90 inhibition; a decrease in the association of CRAF with HSP90; and finally there may be an increase in HSP90-HECTD3 association. This chapter investigates changes in the association of HSP90, HECTD3 and CRAF in response to HSP90 inhibitor using the proximity ligation assay (PLA) and confocal microscopy. This technique allows us to identify the physical proximity between two components at specific times after HSP90 inhibitor treatment and reports on distances between molecules of 0 to 40 nm separation (**Figure** 5.1 A). Briefly, the PLA assay or in particularly the Duolink In Situ from Sigma is a new technique that can be applied to adherent cells prepared on a slide, tissue or other cytospin samples. This is a proximity ligation technique, which allow us to not only detect, but also visualize and quantify the potential interaction or relation between individual proteins. The availability of this technique is limited by the need for primary antibodies from different species and a wavelength for efficiently detecting the PLA signal. So far, $\lambda_{abs}554/\lambda_{em}579$ and $\lambda_{abs}594/\lambda_{em}624$ are the only two wavelength options from the Sigma-Aldrich. Our PLA assay was performed based on $\lambda_{abs}594/\lambda_{em}624$ (**Figure** 5.1 B) due to the availability of the microscopy facility. More details about Duolink In Situ PLA are available from

https://www.sigmaaldrich.com/content/dam/sigma-aldrich/docs/Sigma-Aldrich/Instructions/1/duolink-fluorescence-user-manual.pdf.

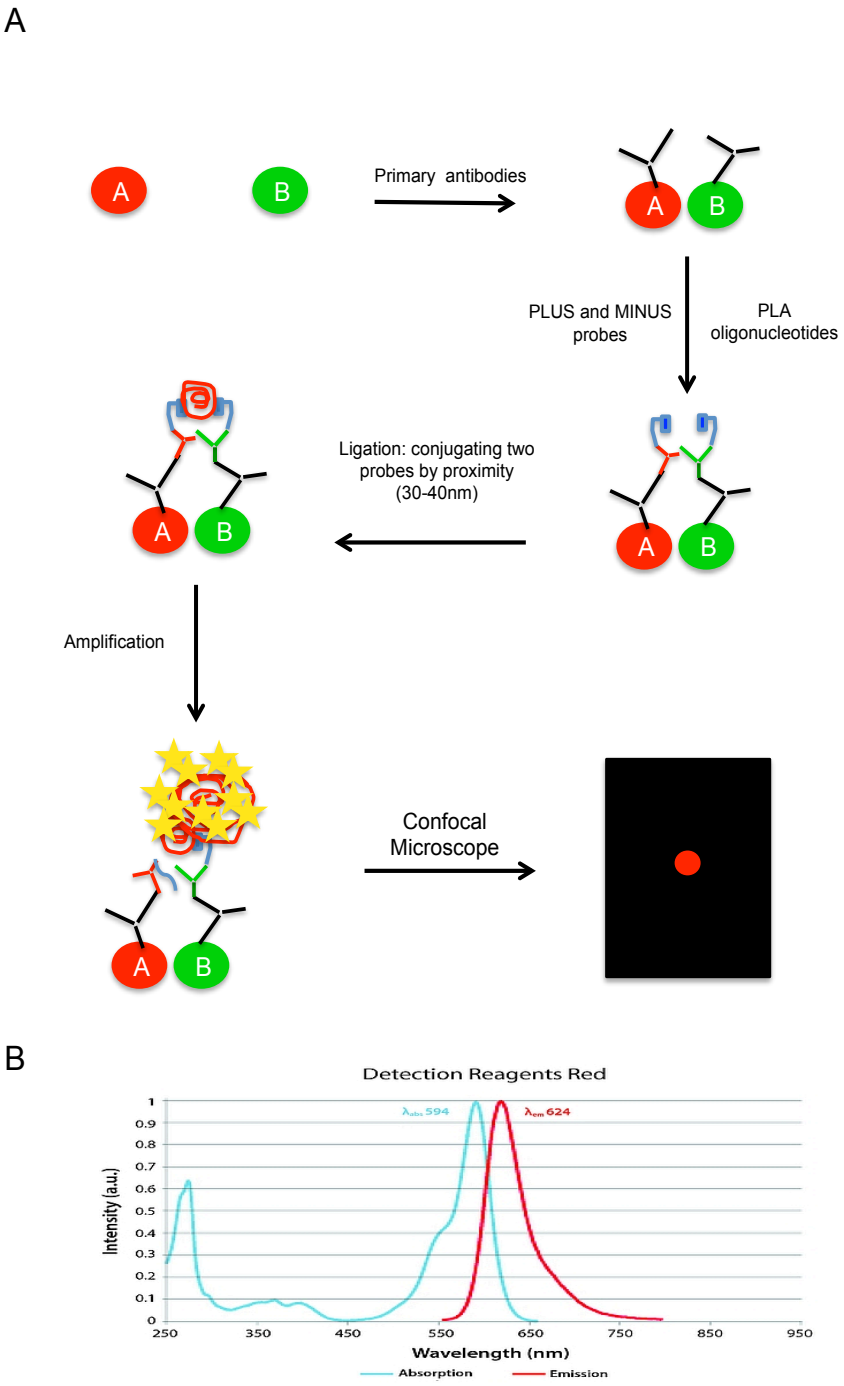

Figure 5.1 The imaging strategy of the Proximity Ligation Assay (PLA). (A) Two proteins of interest are labeled with specific primary antibodies. Cells are then treated with the two PLA PLUS and MINUS probes. During the ligation step, the two probes hybridize and together form a circle piece of DNA, but only if they are physically close enough to each together (within 30-40nm). Finally, the closed circle between the two PLA probes is amplified by a rolling circle amplification reaction to generate a concatemeric repeated sequence product, which the fluorescently labeled

oligonucleotides will hybridize to it. **(B)** Excitation (blue) and emission (red) signal with a peak wavelength at 594nm and 624nm (Image adapted from Sigma-Aldrich).

5.2: Methodology

5.2.1: Confocal microscope for PLA assay

The Leica TCS SP8 confocal microscope was used for co-localization analysis between CRAF, HSP90 and HECTD3 in HEK293 cells. The cells were prepared and labeled with Sigma Doulink PLA probes (see Material and Methods 2.6.5) and Köhler illumination was adopted. The Sigma Duolink® In Situ Red Starter Kit Mouse/Rabbit PLA kit was selected for the PLA assay and ligation signal is dependent on an absorption and emission wavelength of 594 and 624 nm, respectively (**Figure** 5.1 B). A 561 nm laser was the closest available wavelength used for excitation. Although the 561 nm laser did not produce maximum excitation, substantial emission signal could be detected. The 561nm laser power was optimized and decreased to about 3.5% to help minimize the bleaching especially since image stacks were required for co-localization analysis. The use of a low powered laser helped reduce the background signal, which was important because the PLA assay is extremely sensitive, and any non-specific background signal could reduce the effectiveness of the analysis. The sequence imaging method was used to collect signal independently after excitation at 405nm (UV), 561 nm, and for collection of signal with differential interference contrast (DIC) channel. The UV power was minimized to the lowest level since it was noticed that the ligation signal could be slightly excited by UV light. In addition, the imaging speed was set to 200 Hz (imaging time < 5 min) to minimize background signal and improve resolution. Although high scan speeds can further improve resolution and produce high quality images, it requires extended time for analysis (imaging time > 20 min). This could result in PLA signal being bleached before the imaging is completed. Finally, the size of the pin-hole diameter was kept at 1 Airy size to prevent interference from “out-of-focus

light". All images were saved as a TIFF format and processed by FIJI software (see Section 5.2.2).

5.2.2: Image segmentation and foci counting

Segmentation (cell identification) and foci counting (PLA signal) is a critical process in the proximity ligation assay. The identification of proximity ligation foci within each cell was processed and analysed by running a programed macro, which was written by Dr Alex Herbert (Genome Damage and Stability, University of Sussex).

All stack images collected were processed with FIJI software to generate a single layer image that was then saved in TIFF format (see Material and Methods 2.6.5). The PLA and DAPI channel was split and saved individually. The DAPI channel was analysed to identify the numbers of DAPI stained nuclei (one nucleus = one cell). Initially, the threshold level for DAPI intensity was adjusted automatically. However, manual adjustment was always required to increase or decrease the level of the threshold so that single nuclei were identified rather than being counted as two or more separate entities. Any merged nuclei was segmented by applying the *watershed* plugin. The manual adjustment was required to divide any *overlaid* nuclei. The total number of nuclei was finally counted using the *Particle analyses* plugin. The mask plugin was used to exclude background noise.

For PLA imaging the threshold for detecting the signal above background was automated. Any background noise was removed by applying *Remove outliers* and signals less than 1.0 pixels were set as noise and excluded. The *mask* that was created from the complimentary DAPI channel was then overlaid with the PLA image. Finally, the PLA signal was assigned to the nearest nucleus by applying the *Assign Foci To*

Object (Wrote by Dr Alex Herbert) plugin (**Appendix** 4).

5.3: Results

5.3.1: The proximity between CRAF, HSP90 and HECTD3

We used the PLA assay to investigate the distribution and association of HECTD3, HSP90 and CRAF following the treatment of HEK293 cells with AUY922 (see Material and Methods 2.6.5). Two control experiments were conducted in advance to evaluate the background noise from proximity ligation signals. Co-localization between endogenous HSP90 and stably over-expressed eYFP in HEK293 cells was used as a negative control experiment to determine the specificity of the PLA probes for specific proteins (**Figure** 5.2 A). As we expected, less than 1 foci could be detected in cells treated with or without AUY922 when proximity ligation foci within non-cell culture space was excluded.

We next tested the co-localization of protein kinase CRAF and HSP90 (**Figure** 5.2 B). The results showed a strong proximity ligation signal with approximately 9 fluorescent foci on average per cell. As expected, foci numbers dropped almost by half after an18 hr incubation with AUY922 (**Figure** 5.2 E). This result suggests that inhibition of HSP90 results in a decrease in the association of HSP90 and CRAF, due at least in part to CRAF degradation.

Next we investigated the proximity ligation signal for the localization of CRAF and HECTD3 in non-inhibitor treated and AUY922 treated cells (**Figure** 5.2 C). The fluorescent foci were found to more than double after 18 hr incubation with AUY922 (**Figure** 5.2 E). This suggests that inhibition of HSP90 substantially promoted co-

localization between CRAF and HECTD3. An increase in the co-localization between CRAF and HECTD3 in response to AUY922 is supportive of the role of HECTD3 in the ubiquitylation of CRAF and its subsequent degradation by the proteasome.

A significant number of proximity ligation signals, about 4 foci per cell, were also detected between HSP90 and HECTD3 in non-inhibitor treated cells (**Figure** 5.2 D), and the number of foci more than doubled in AUY922 treated cells (Figure 5.4). This observation suggests a potential connection between HSP90 and HECTD3, and might represent a delivery route for the CRAF to HECTD3 for ubiquitylation. Further work would need to be carried out to confirm this hypothesis.

A

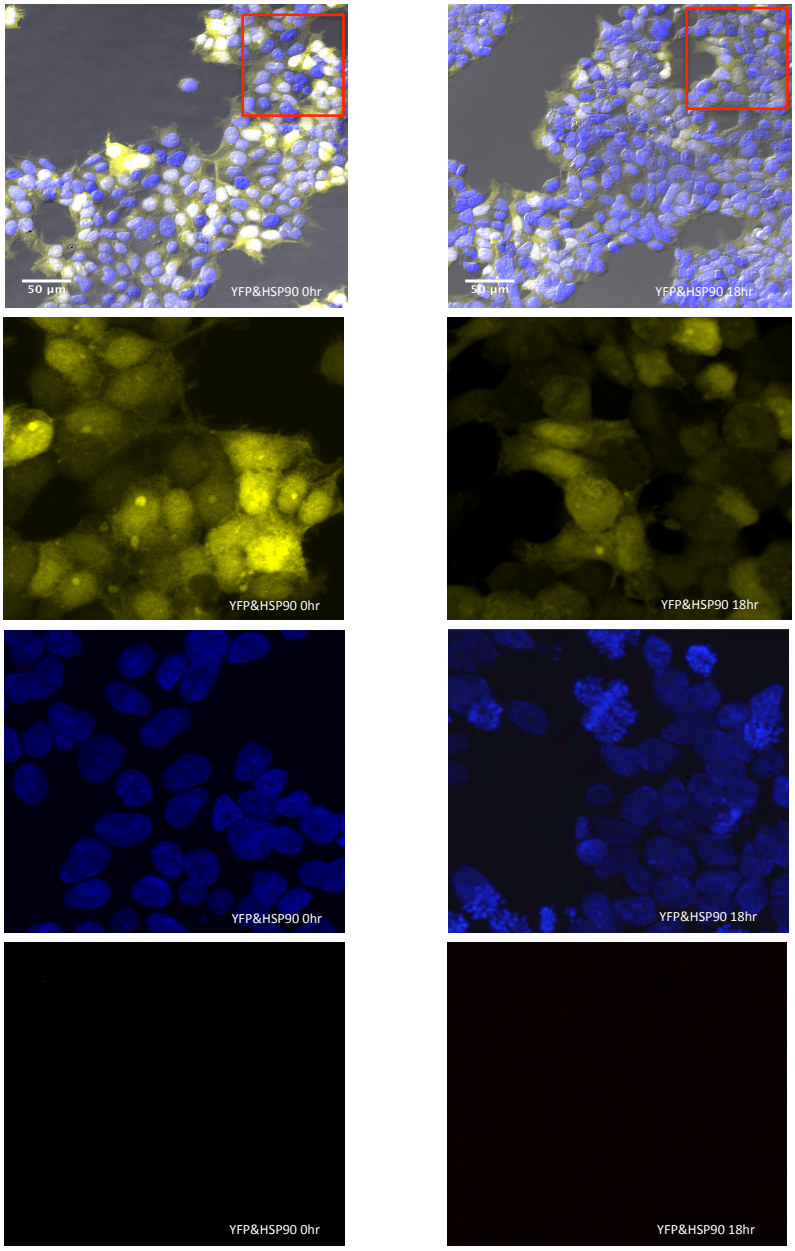
50 µm
YFP&HSP90 0hr
50 µm
YFP&HSP90 18hr
YFP&HSP90 0hr
YFP&HSP90 18hr
YFP&HSP90 0hr
YFP&HSP90 18hr
YFP&HSP90 0hr
YFP&HSP90 18hr

B

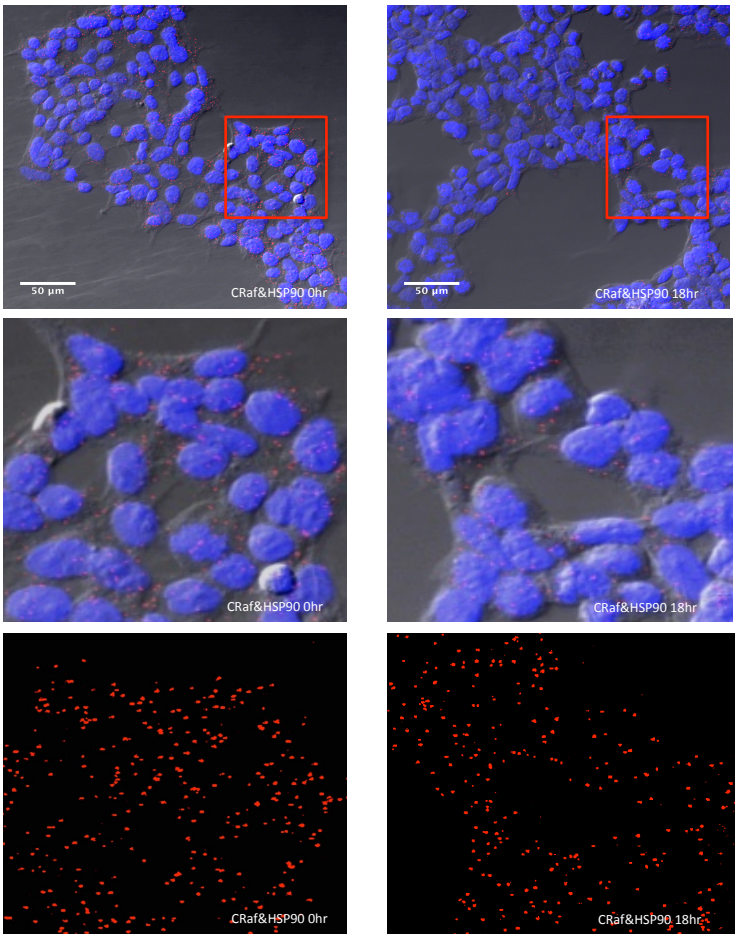
50 μm
CRaf&HSP90 0hr
50 μm
CRaf&HSP90 18hr
CRaf&HSP90 0hr
CRaf&HSP90 18hr
CRaf&HSP90 0hr
CRaf&HSP90 18hr

C

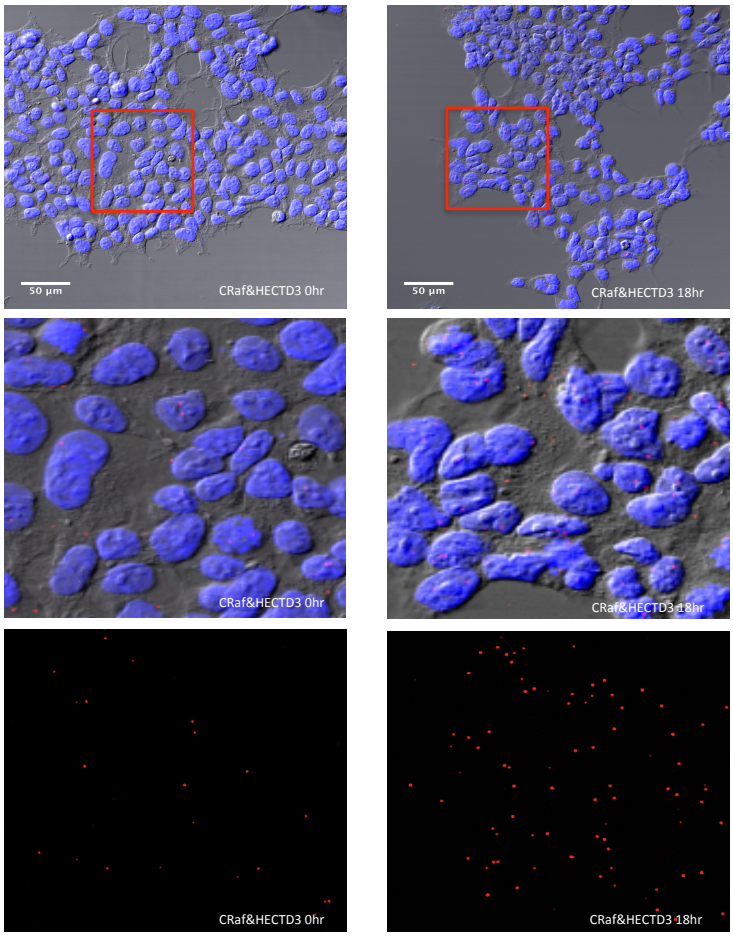
50 μm
CRaf&HECTD3 0hr
50 μm
CRaf&HECTD3 18hr
CRaf&HECTD3 0hr
CRaf&HECTD3 18hr
CRaf&HECTD3 0hr
CRaf&HECTD3 18hr

D

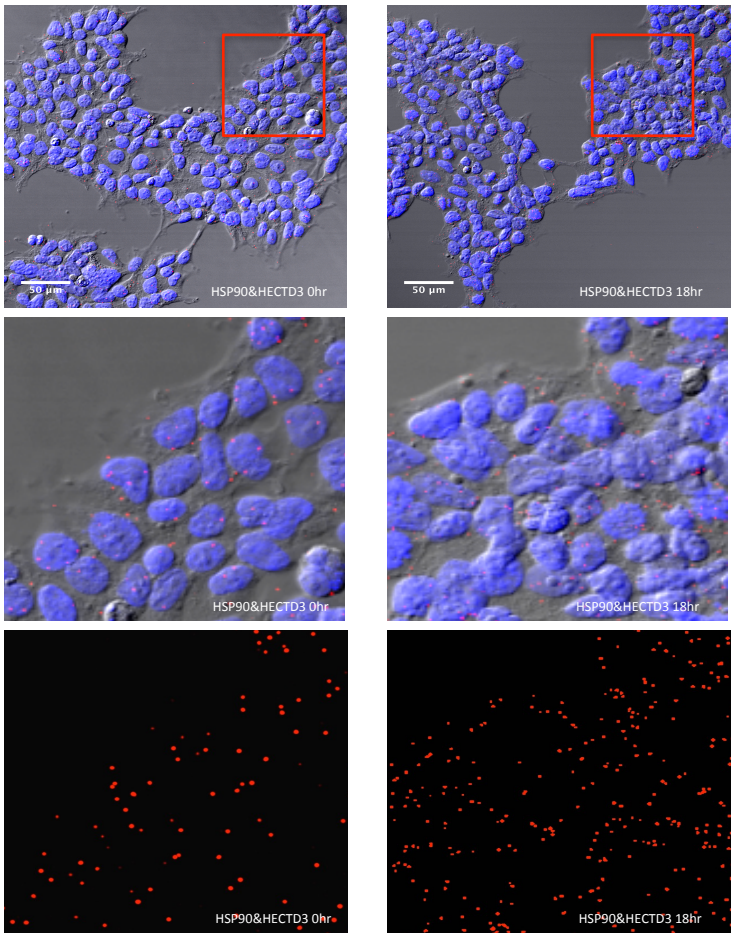
50 µm
HSP90&HECTD3 0hr
50 µm
HSP90&HECTD3 18hr
HSP90&HECTD3 0hr
HSP90&HECTD3 18hr
HSP90&HECTD3 0hr
HSP90&HECTD3 18hr

E

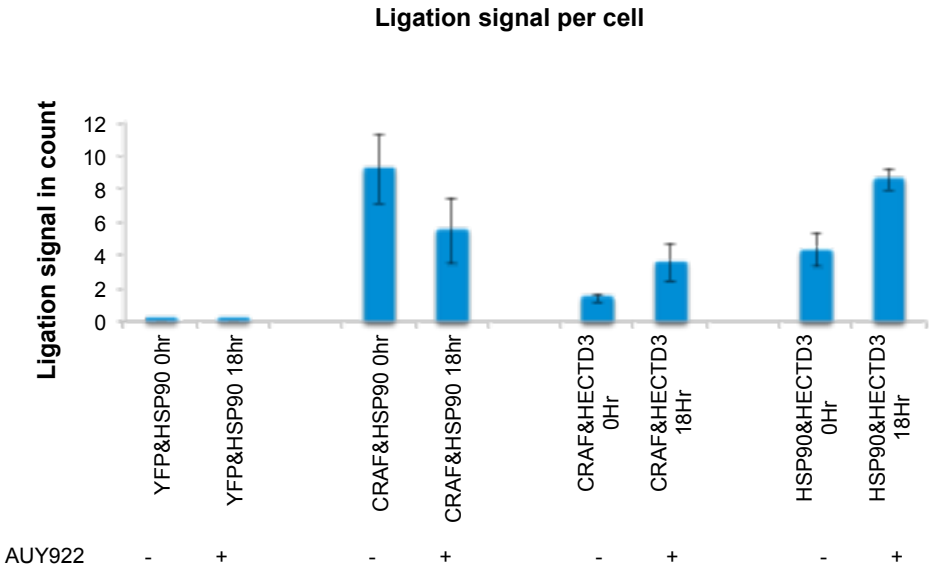
Ligation signal per cell
Ligation signal in count
12
10
8
6
4
2
0
YFP&HSP90 0hr
YFP&HSP90 18hr
CRAF&HSP90 0hr
CRAF&HSP90 18hr
CRAF&HECTD3 0Hr
CRAF&HECTD3 18Hr
HSP90&HECTD3 0Hr
HSP90&HECTD3 18Hr
AUY922
- + - + - + - +

Figure 5.2 Proximity ligation assay (PLA). (A) The ligation reaction between HSP90 and eYFP was used as the negative control, **(B)** while the positive control was set up between HSP90 and CRAF. The experimental proximity ligation assays were taken place between **(C)** CRAF and HECTD3, **(D)** HSP90 and HECTD3. A 10 times zoom in image is provided to have better view of the PLA signal. **(E)** The ligation foci per cell was plotted for each experiment, and the error bar given is for each analysed image. The proximity ligation reaction between HSP90 and eYFP gave no considerable signal with or without 3 x GI_{50} of AUY922 treatment for 18 hr. A large PLA signal was detected for HSP90 and CRAF following AUY922 treatment for 18 hr. An enhanced PLA signal between CRAF and HECTD3 was detected following AUY922 treatment for 18 hr. A potential linkage between HSP90 and HECTD3 was observed. Scale Bar=50 μm.

5.3.2: Co-localization by Immunoprecipitation of eYFP-CRAF

Having shown co-localization of CRAF, HECTD3 and HSP90 we next confirmed these results by immunoprecipitation studies. EYFP-CRAF was immunoprecipitated in cells with or without AUY922 treatment using GFP-trap beads (see Material and Methods 2.6.1). Bands visible on a coomassie stained SDS-gel were characterized by mass spectrometry (**Figure** 5.3 A). The main components that were identified were eYFP-CRAF, HSP90, HSP70, CDC37 and 14-3-3. Although HECTD3 was not observed on SDS–PAGE gels, HECTD3 could be detected by western blot analysis of the precipitated proteins, which appears to be substantially less after 8 hr AUY922 treatment (**Figure** 5.3 B). In contrast, the levels of HSP90 immunoprecipitated did not change, whereas those of HSP70 increased from 0 to 24 hours post AUY922 treatment.

Collectively, the data show that HECTD3 is brought into close physical proximity with both HSP90 and CRAF, following HSP90 inhibitor-induced ubiquitylation and degradation of CRAF. The results suggest that HSP90 and HECTD3 are most likely involved in a physical complex with CRAF.

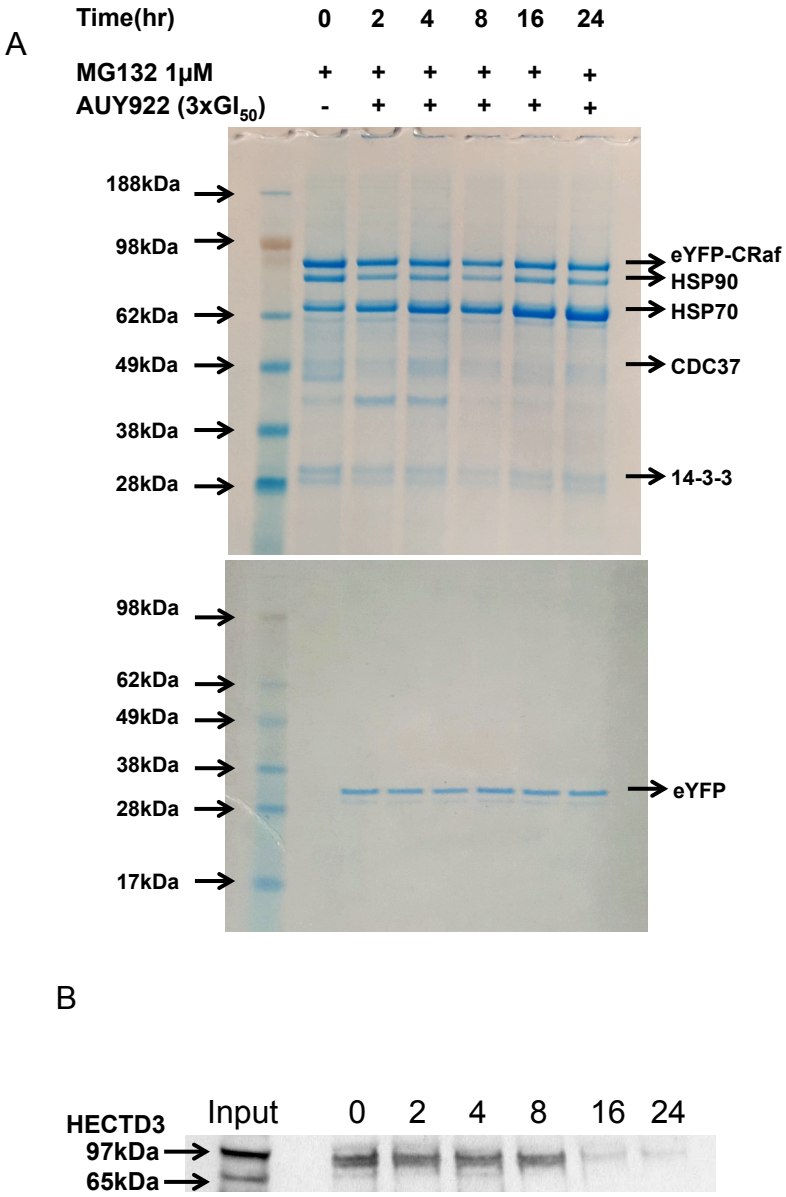

Figure 5.3 Immunoprecipitation of eYFP-CRAF from HEK293 cells reveals potential components in the complex with eYFP-CRAF following AUY922 treatment. (A) HSP90, HSP70, CDC37 and 14-3-3 were identified from the immunoprecipitated eYFP-CRAF by GFP-trap beads. 3 x GI_{50} AUY922 treatment reduced the expression level of eYFP-CRAF, HSP90, CDC37 and 14-3-3, but dramatically increased the level of HSP70. Cells are over-expressing eYFP act as the negative control. **(B)** HECTD3 was immunoprecitated with eYFP-CRAF and identified by immunoblotting with α-HECTD3 antibody.

5.4: Discussion

The PLA assay is a powerful technique that can show the co-localization of proteins within a cell. The results presented herein reveled that treatment of HEK293 cells with the HSP90 inhibitor, AUY922, caused a decrease in HSP90-CRAF co-localization, and an increase in HSP90-HECTD3 and CRAF-HECTD3 co-localization. Co-localization between HSP90 and HECTD3 confirms a previous study suggesting that these proteins associate within cells (Taipale et al., 2012). The same study, however, did not identify CUL5 as an interactor of HSP90, but did identify a strong interaction between CRAF and HSP90, which we have confirmed here. The shift of CRAF from HSP90 to HECTD3 complex suggests a biochemical pathway that leads to the proteasomal degradation of CRAF that is HECTD3 dependent. The significance between these proteins could be improved if the PLA oligonucleotides are designed to directly target the protein without the intermediate step. The appearance of HSP70 in complex with eYFP-CRAF is due to the requirement of HSP70 as an activator of CRAF (Nollen and Morimoto, 2002; Wang et al., 2006), and 14-3-3 is responsible for regulating the activity of CRAF as usual (Li, et al., 1995).

Although the results suggest an interaction between HECTD3 and CRAF, the nature of that interaction and whether other components are required to scaffold that interaction remains to be determined. One route of delivery may involve scaffold components that are responsible for delivering HSP90, and therefore CRAF, to HECTD3. Another possibility is that the DOC domain of HECTD3 directly recognizes the HSP90-CRAF complex by interacting with CRAF. Conformation of this would require further investigation.

CHAPTER SIX

CRAF turnover and cell line variability of HECTD3

6.1: Introduction

In the previous two chapters a poorly described E3 ligase HECTD3 was identified as an important player in the HSP90 inhibitor triggered degradation of CRAF, and co-localization of CRAF and HECTD3 was observed. However, whether CRAF is ubiquitylated by HECTD3 in cells that are not subjected to HSP90 inhibition is still unknown. In this chapter, general turnover of newly synthesized eYFP-CRAF was evaluated by comparing its stability in both control and HECTD3 siRNA treated cells. The variability of the HECTD3 levels in different cancer cell lines is also investigated.

6.1.1: Overview of autophagy

Protein synthesis and autophagic degradation is an ongoing process that responds to various biological processes, such as proliferation, differentiation and metabolism. Protein synthesis is a tightly controlled process at the level of both transcription and translation. Many environmental conditions, such as starvation and external stress alter both protein synthesis and the stability of proteins. Autophagy plays keys roles in cell survival, and tumor suppression (Mizushima et al., 2011; Levine et al., 2008; Mehrpour et al., 2010). Basal levels of autophagy normally operate for the regulation of long-lived proteins during normal growth. Proteins are normally engulfed into phagophores, which are double-membrane structured vesicles that enclose proteins for destruction. These phagophores undergo a process of maturation into autophagosomes that finally fuse with lysosomes, which degrade target protein and turn them into newly available nutrients (Mizushima et al., 2007; Nakatogawa et al., 2009). However, stress can upset this equilibrium and the catabolic process that might in turn help maintain internal nutrient levels.

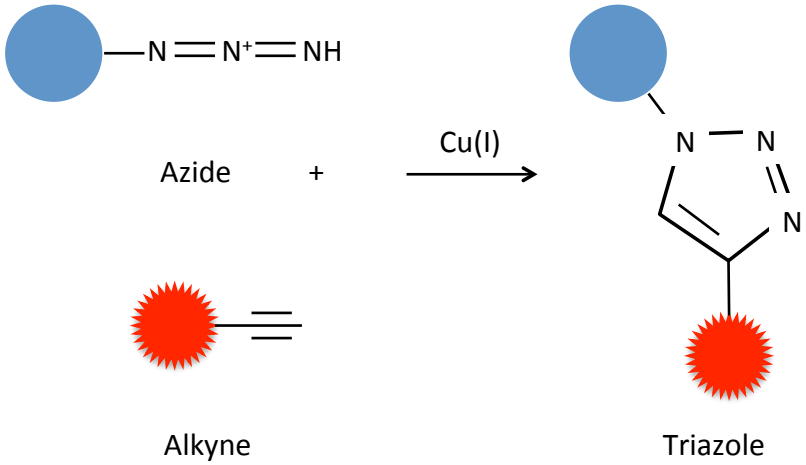

Figure 6.1 Model for copper catalyzed Azide-Alkyne bioconjugation through "Click" reaction. The Azide modified molecules (Blue filled circle) and biomolecule Alkyne (Red filled fuzzy circle) are indicated. The Cu^{I} complex is required for copper catalyzed azide-alkyne cycloaddition (CuAAC). The molecule can be labeled by various biomolecule Alkyne such as Alexa Fluor ® probes (488, 555, 594 or 647), biotin or tetramethylrhodamine depending on applications.

6.1.2: Quantifying autophagic protein

Radioisotope labeling can be used to measure the autophagic flux of a protein. The radioactive amino acid L-(U-^{14}C) valine or L-(U-^{14}C) leucine is used to pulse label cellular proteins, and their degradation rate then quantified (Ogier-Denis et al., 1996; Roberts et al., 2008; Bauvy et al., 2009). However, apart from being radioactive and requiring careful handling, this method may not in fact be sensitive enough for all targets.

Fluorescent non-canonical amino acid tagging (FUNCAT) and bio-orthogonal non-canonical amino acid tagging (BONCAT) are two protein-labeling technologies that have been developed as an alternative means for looking at protein turnover (Best et al., 2009; Dieterich et al., 2006). BONCAT labeling has been recently applied in mammalian cells for detecting newly synthesized proteins. The technique is simply described as a 'CLICK' reaction that is a Cu (I)-catalyzed cyclo-addition reaction between an azide-modified protein and an alkyne affinity tag (Dieterich et al., 2006 and 2007) (**Figure** 6.1). The best azide compound reported to date for the 'Click' reaction is an amino acid analog of methionine, termed L-azidohomoalanine (AHA), which metabolically labels newly synthesized protein and is subsequently linked by a fluorescent or biotin tagged alkyne via chemo-selective ligation (Dieterich et al., 2007). Among other azide compounds, AHA has less cytotoxicity and does not effect or induce autophagy. Furthermore, it has a smaller size that is capable of targeting small biomolecules. The AHA modified protein can be detected in many different ways; including western blots analysis, flow cytometry, mass spectrometry, 2D gel electrophoresis and fluorescence microscopy (Dieterich et al., 2006 and 2007; Schiapparelli et al., 2014). There are numbers of fluorescent alkyne tags that have been developed that allow detection at a variety of wavelengths including 488, 555, 594 and

647 nm. Biotin-tagged alkyne can be detected by western blot analysis.

6.2: Results

6.2.1: The role of HECTD3 in general turnover of CRAF in HEK293 cells

The results so far suggest that HECTD3 plays a role in CRAF degradation following inhibition of HSP90. However, it is equally important to understand the role of HECTD3 in CRAF degradation where access to a functional CDC37/HSP90 chaperone system is uncompromised. Consequently, the half-life of CRAF was analysed.

We pulse-labeled HEK293 cells that stably over-express eYFP-CRAF with the methionine mimetic, azidohomoalanine. Labeled protein, from cells lysed at different times following labeling (see Material and Methods 2.6.3) were tagged, using the "Click" reaction with biotin. EYFP-CRAF was then immunoprecipitated and visualized in an α-biotin western blot (**Figure** 6.2). The levels of AHA-biotin labeled eYFP-CRAF were observed at 6, 12, 18 and 24 hr, for both control siRNA and HECTD3 siRNA treated cells. Both sets of cells showed a constant level of eYFP-CRAF at each time point. This suggests that the knockdown of HECTD3 did not substantially affect the general turnover of eYFP-CRAF when access to an active HSP90-CDC37 complex was uncompromised.

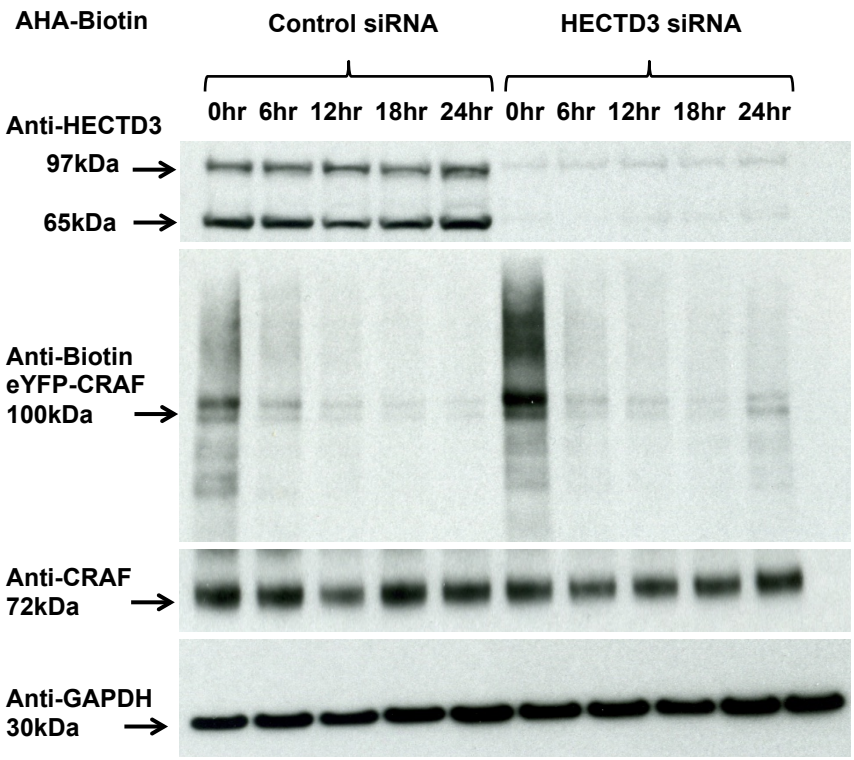

Figure 6.2 Immunoblot analysis of L-Azidohomoalanine (AHA)-Biotin labeled eYFP-CRAF in both wild type and HECTD3 siRNA treated HEK293 cells. HEK293 cells were treated with non-targeting control or HECTD3 siRNA for 48 hr and subsequently newly synthesized proteins were "Click" labeled with AHA-Biotin. EYFP-CRAF was then immunoprecipitated with GFP-trap beads and followed by western blot analysis with α-HECTD3, α-biotin and α-CRAF antibody. Biotinylated eYFP-CRAF was visualized from both wild type and HECTD3 siRNA treated cells that have been individually "Click" labeled for 0, 6, 12, 18 and 24 hr with AHA treatment. No HSP90 or protein synthesis inhibitor was added. The knockdown of HECTD3 gives no significant effect on the turn over of newly synthesized biotinylated eYFP-CRAF. The level of eYFP-CRAF at each time point remained unchanged. GAPDH was used as the loading control.

6.2.2: Cell line isoforms and diversity of HECTD3

Previous studies revealed that HSP90 inhibition in HCT116 and HT29 tumor cell lines triggered the degradation of the HSP90-dependent client protein kinase CRAF. The survival and proliferation of these cell lines critically depends on the MAP-kinase cascade, of which CRAF is part of this signaling pathway (Ehrlich et al., 2009; Samant, Clarke and Workman 2014). It is conceivable that tumor cells may have altered to down regulate processes that limit the activity of CRAF and other kinases of the MAP-kinase cascade. One such route would be the down regulation of the HECTD3 degradation pathway for CRAF and potentially other MAP-kinases. We thus investigated the expression of HECTD3 in a variety of cancer cell lines. We used a C-terminal specific antibody for HECTD3 in immunoblots against HEK293, COS7, U2OS, HT29, HCT116 and A529 cell lines that were not treated with HSP90 inhibitor (**Figure** 6.3). Two specific HECTD3 bands, representing specific isoforms were visible with relative molecular masses of 65 and 97-kDa. However the abundance of each isoform varied depending on the exact cell line (**Figure** 6.3). Full-length HECTD3 was present in both the HEK293 and COS7 non-tumor cell lines. However, this isoform was less abundant in tumor cell lines, and surprisingly no expression was identified in HT29 and HCT116 cells, which only expressed the smaller isoform. These results suggest that the smaller isoform lacks the N-terminal section of full-length HECTD3. Online resources confirmed that the shorter isoform corresponded to a translational product (65,687 Da) of the HECTD3 splice-variant mRNA (NCBI RefSeq XM_011542140.1). This isoform lacks N-terminal exons 1 and 4 and translation begins at Methionine 285. The predicted protein product appears to start midway through a recognizable DOC domain, similar to that of APC10/DOC1-like domain. The DOC1 domain of APC appears to be a subunit in APC complex that can recognize the substrate destruction box of its target proteins

and mutation of this domain reducs the degradation of such substrates *in vivo* (Carroll and Morgan, 2002; Passmore et al., 2003; Carroll, Enquist-Newman and Morgan, 2005). Consequently, the missing DOC domain in this short isoform of HECTD3 would potentially inactivate it, and reducing its capacity to degrade CRAF or other such kinases in cells under stress.

To further confirm this hypothesis, the HCT116 cells were treated with HECTD3 siRNA to knockdown the 65-kDa short isoform (see Material and Methods 2.6.4). AUY922 triggered degradation of CRAF that was similar in both control siRNA and HECTD3 (short isoform) knock down cells and control cells. Failure to show stabilization of CRAF suggests that the minor isoform of HECTD3 is not involved in the ubiquitylation dependent degradation of CRAF (**Figure** 6.4). The result suggests that the loss of the DOC domain of HECTD3 results in a defective ubiquitylation pathway that might promote tumorgenesis by stabilizing and increasing the half-life of specific kinases. It also suggests that an alternative pathway exists for CRAF degradation following HSP90 inhibition, which may rely on CUL5-dependent degradation in cancer cells. For example, the knockdown of CUL5 in HT29 cells, which these cells only expresses the short isoform of HECTD3, stabilizes the degradation of $BRAF^{V600E}$ and ErbB2 (Samant, Clarke and Workman, 2014).

The HSP90 and HECTD3 mRNA level was analysed in breast, lung, ovarian and gastric cancer patient data by Kaplan-meier plotter (**Figure** 6.5). Each data analysis is divided into two groups with low and high expression of the specified mRNA and all restrictions regarding subtypes were included in the final analysis. For high HSP90 mRNA level, survivability was significantly reduced for breast, lung and ovarian cancer (**Figure** 6.5A). However for gastric cancer survival range was improved with higher mRNA levels of HSP90 (**Figure** 6.5 A). Similarly for high HECTD3 mRNA levels

(**Figure** 6.5 B), patients who had lung, ovarian and gastric types of cancer had a low survivability, while breast cancer patients had lower survival range with reduced mRNA levels of HECTD3. The exact details as to why different levels of HSP90 and HECTD3 mRNA in specific cancer cell types differs remains unknown, but it is clear that both proteins can play substantial roles in the survivability of cancer patients. This is particularly apparent in gastric cancers (**Figure** 6.5).

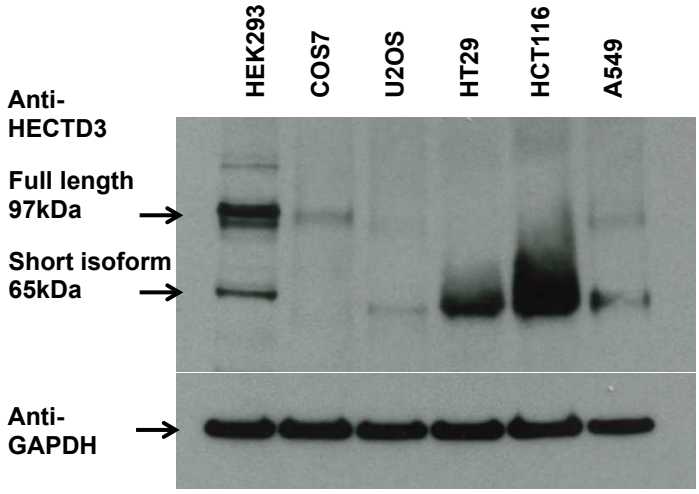

Figure 6.3 HECTD3 in various cell lines. HECTD3 was identified and immunoblotted with α-HECTD3 antiserum against a C-terminal epitope of HECTD3. Lysates were from two non-cancer cell lines, HEK293 and COS7 and four cancer cell lines, U2OS, HT29, HCT116 and A549. HEK293 cells have the both expression of the two isoforms of HECTD3, whereas most the cancer cell lines only mainly express the low molecular weight 65-kDa HECTD3. The COS7 cells only express the 97-kDa HECTD3.

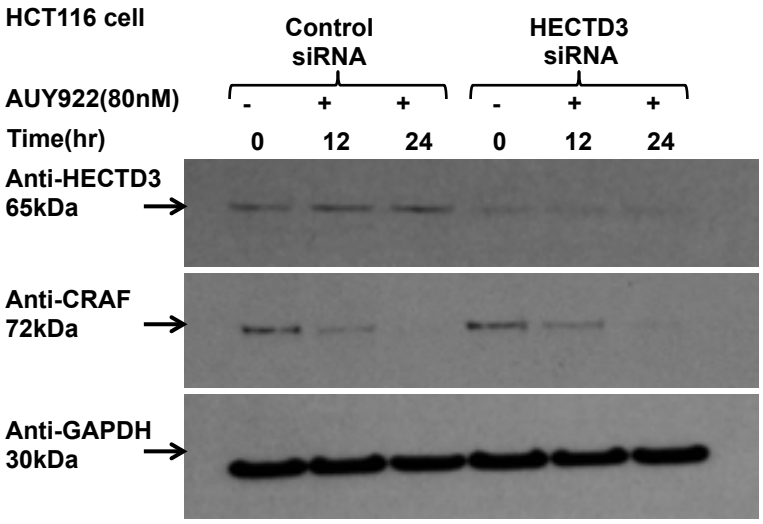

Figure 6.4 The downregulation of HECTD3 in HECT116 cancer cells. HCT116 cells were treated with siRNA to knock down the 65-kDa isoform of HECTD3, and subsequently incubated with 80nM AUY922. Cell samples were harvested after 12 and 24 hr inhibitor treatment. HECTD3 was detected by C-terminal antibody. GAPDH was used as the loading control. Unlike the full-length HECTD3 in HEK293 cells, the truncated splice isoform of HECTD3 does not stabilize the degradation of CRAF in HCT116 cells, which indicates this short isoform is an inactive participant in the ubiquitylation dependent degradation of CRAF.

A

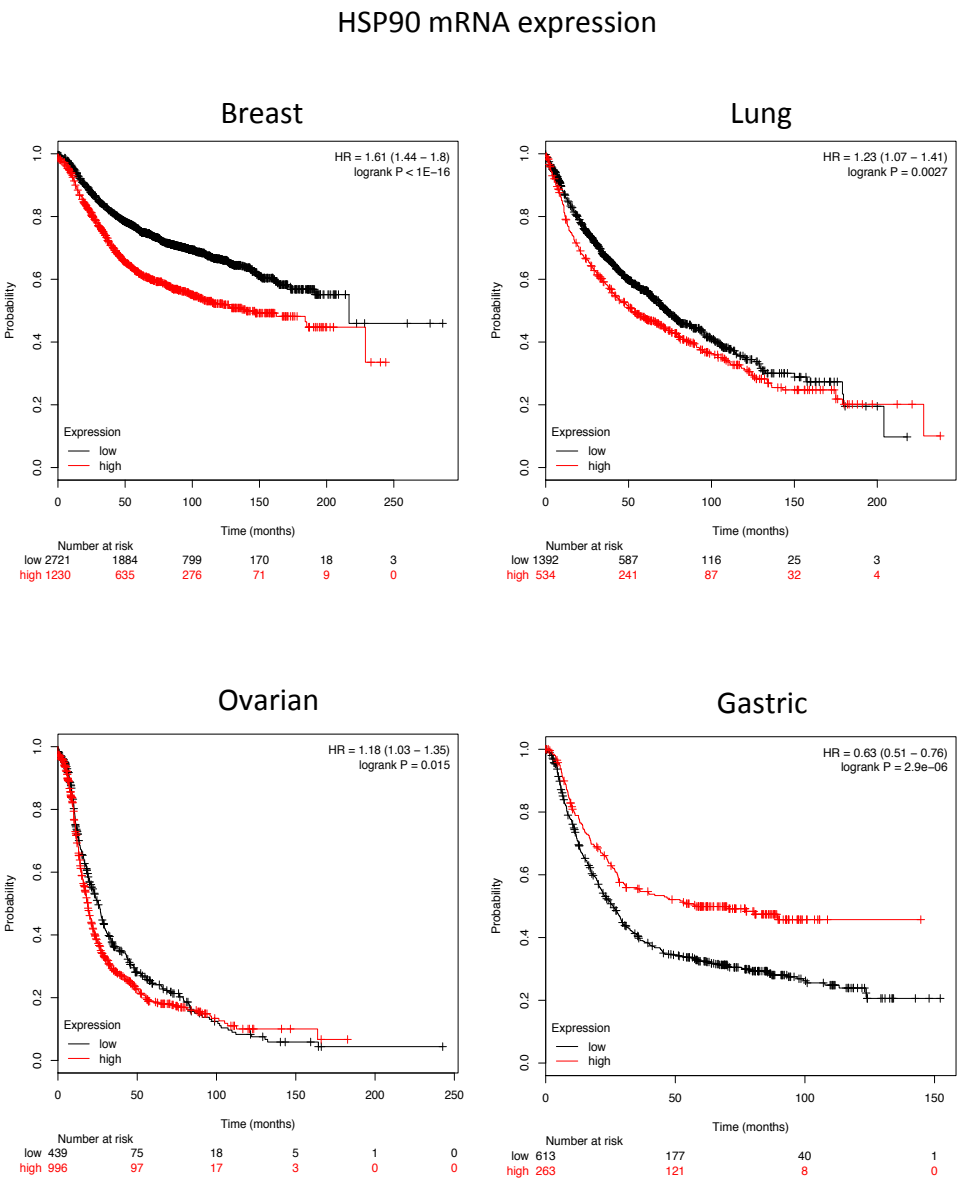
HSP90 mRNA expression
Breast
HR = 1.61 (1.44 – 1.8)
logrank P < 1E–16
Probability
Expression
low
high
Time (months)
Number at risk
low 2721 1884 799 170 18 3
high 1230 635 276 71 9 0
Lung
HR = 1.23 (1.07 – 1.41)
logrank P = 0.0027
Probability
Expression
low
high
Time (months)
Number at risk
low 1392 587 116 25 3
high 534 241 87 32 4
Ovarian
HR = 1.18 (1.03 – 1.35)
logrank P = 0.015
Probability
Expression
low
high
Time (months)
Number at risk
low 439 75 18 5 1 0
high 996 97 17 3 0 0
Gastric
HR = 0.63 (0.51 – 0.76)
logrank P = 2.9e–06
Probability
Expression
low
high
Time (months)
Number at risk
low 613 177 40 1
high 263 121 8 0

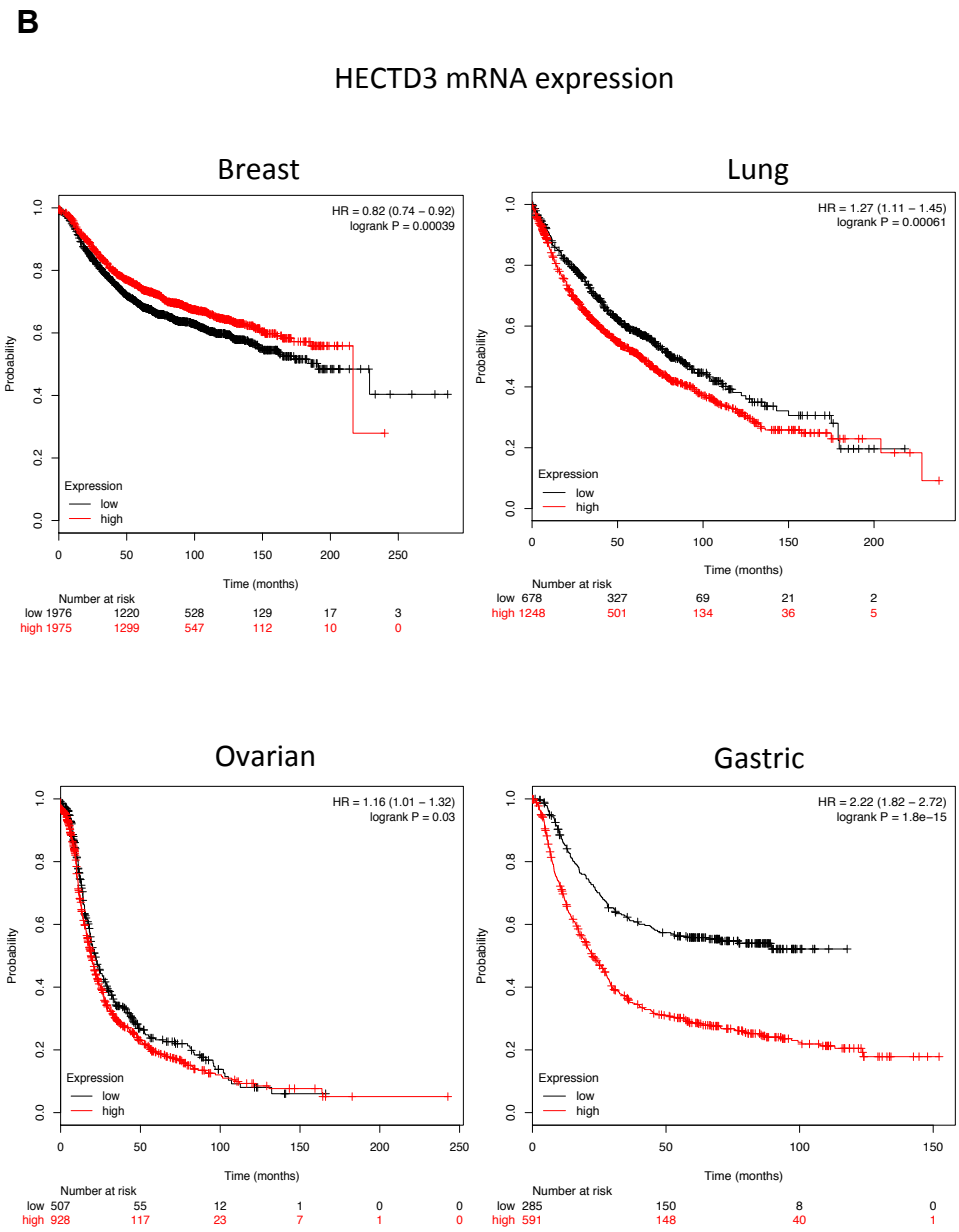

Figure 6.5 The Kaplan-meier plot analysis of HSP90 and HECTD3 mRNA level in various cancers. The expression of HSP90 (A) and HECTD3 (B) mRNA level was respectively analysed with patients had breast, lung, ovarian and gastric types cancer by Kaplan-meier plotter. The horizontal axis indicates the time in month, while the vertical axis presents the survivability of patients during this period of time. The HR and logrank P values are labeled in each graph. All restrictions regarding subtypes were included in each analysis of type cancer.

6.3: Discussion

HECTD3 is s highly conserved E3 ligase whose biological function is largely unknown, and its structure appears to be unique relative to other HECT-domain E3 ubiquitin ligases (Rotin and Kumar, 2009; Marin, 2010). A handful of proteins have been implicated in a HECTD3 dependent degradation, but none of them are protein kinases or known HSP90 clients (Li et al., 2013a; Li et al., 2013b; Zhang et al., 2009; Yu et al., 2008). However, such studies often utilized overexpressed protein where specificity could be impaired, and/or have monitored cellular phenomena that could be downstream of HECTD3 primary E3 ligase activity. In contrast, we show direct HECTD3 involvement in the degradation of CRAF and other kinases, confirmed by knockdown rather than overexpression following treatment with HSP90 inhibitor.

The knockdown of the both the 97 and 65-kDa isoform HECTD3 did not significantly influence the general turnover of the eYFP-CRAF fusion protein in non-drug treated HEK293 cells. This suggests that HECTD3 might not have access to the HSP90/CDC37 complex in its uninhibited state.

The short isoform HECTD3 was shown to have no function on the degradation of CRAF in HCT116 cells and confirmed the functional importance of the missing N-terminus. Although the role of HECTD3 has not been fully resolved yet, the DOC domain of HECTD3 was shown to be structurally related to the APC10 subunit that regulates substrate recognition in the APC/C E3 ligase complex (da Fonseca et al., 2011), and CUL7 and CUL9 (Kominami, Seth-Smith, and Toda, 1998; Dias et al., 2002).

CHAPTER SEVEN

Discussion

7.1: Overall perspective

The overall aim of this study was to identify specific ubiquitylation systems that are responsible for the degradation of HSP90-dependent client proteins, and particularly for CRAF, following inhibition of HSP90 with AUY922. AUY922 has been recognized as one of the most potent inhibitors of HSP90 (Brough et al., 2007; Eccles et al., 2008; Gao et al., 2010), and it is currently in phase II clinical trials. Furthermore, a non-cancerous cell line was chosen that lacked genetic changes associated with cancerous cell lines that might possess altered ubiquitylation systems.

The HSP90 inhibitor AUY922 has been see to bring about client protein degradation of specific kinases, such as ErbB2, EGFR, IGF1R, PDGFR α , PDGFR β , CRAF, C-MET, P-ERK, tyrosine kinase 2 (TYK2), FOP2-FGFR1 fusion onco-protein and phospho-AKT in cancer cell lines (Gaspar et al., 2010; Akahane et al., 2016; Wendel et al., 2016). Our study analysed the cellular behaviour of ErbB2, MASTL, BRAF, CRAF, PDK1, RIP, LKB1 and CDK4 following the inhibition of HSP90 in HEK293 cells. ErbB2, CRAF, LKB1 and CDK4 in HEK293 cells were sensitive to pharmacological inhibition of HSP90 by AUY922. In contrast, wild type BRAF, RIP and PDK1, which were previously described as HSP90 clients (Kim et al., 2012; da Rocha Dias et al., 2005; Palacios et al., 2010), were not degraded in response to AUY922 in HEK293 cells. This suggests that the stability of kinases may vary between cancerous and non-cancerous cell lines and even between different cell types and cancerous cells. However, the mechanisms involved in the degradation of many of these kinase clients remain essentially unknown.

Screening a human ubiquitin library identified HECTD3 and CUL5 as potential components in the degradation of the HSP90-dependent protein kinase client CRAF.

HECTD3 appears to be the major E3 ligase involved in the degradation of CRAF following HSP90 inhibition. Although the kinase inhibitor Sorafenib also promoted CRAF degradation, presumably through a 'chaperone deprivation' mechanism (Polier et al., 2013), this was not prevented by HECTD3 or CUL5 knockdown. This suggests that the pathway for CRAF degradation might be dependent on the point of inhibition and ultimately whether this results in a lack of access to CDC37 or HSP90 for the kinase.

Previous work has suggested that CUL5 plays a role in the degradation of $BRAF^{V600E}$, ErbB2 and phospho-AKT in HT29 cancer cells (Samant, Clarke and Workman, 2014). The $BRAF^{V600E}$ mutation is not present in HEK293 cells and the wild type BRAF in these cells appeared not to be sensitive to the HSP90 inhibitor. However, out data suggests that CUL5 does play a role in the proteolytic degradation of at least some kinases in HEK293 cells. To establish the extent at which CUL5 plays a role in the degradation of HSP90-dependent kinases would require further investigations. This would involve studies that firstly could identify those kinase clients that are sensitive to HSP90 inhibition and then testing the effect of CUL5 knockdown in stabilizing such kinases in response to HSP90 inhibition. Although the structure and biological function of CUL5 has been studied for many years, the delivery pathway for transferring HSP90-dependent client proteins to CUL5 complex is not fully understood, and there is no evidence that suggests a direct interaction between CUL5 and HSP90. Thus the identification of adaptor proteins becomes a critical task. A siRNA screen of SOCS box proteins could identify such adaptors that may be involved. Similarly, tagged CRAF could be used in pull down experiments of cell lysates and the co-precipitating components analysed in order to identify which proteins may act as recruitment factors for CUL5.

A previous high-throughput proximity screen also suggested a possible link between HSP90 and HECTD3 (Taipale et al., 2012). This is clearly supported by our findings. The DOC domain remains the most likely domain of HECTD3 for the recruitment of CRAF. The DOC domain was initially identified in budding yeast Apc10/Doc1 (Hwang and Murray, 1997), and later in the CUL7 (KIAA0076) and CUL9 (KIAA0708) cullin proteins (Kominami, Seth-Smith, and Toda, 1998; Dias et al., 2002). Previous studies revealed that the Doc1 domain is required for the recognition and binding of substrates with the cooperation of Cdh1 and Cdc20 (Carroll and Morgan, 2002; Passmore et al., 2003) in anaphase promoting complex.

CUL7 contains a DOC domain (Dias et al., 2002), and it were previously reported to be the core subunit of the cullin-RING-based SCF E3 complex that interacts with ROC1 (also termed as Rbx1), RING finger protein and SKP1- or FBX29-F-box protein (Patton et al., 1998; Wu et al., 2000,-Tsunematsu et al., 2006). Recently, it was reported Cul7 could regulate the ubiquitylation and degradation of target proteins, such as insulin receptor substrate 1 (IRS-1) (Xu et al., 2008), and hematopoietic progenitor kinase 1 (HPK1) (Wang et al., 2014).

The CUL9 also contains a DOC domain (Dias et al., 2002). Althoug the biological function is not fully understood, it has been suggested that CUL9 might act as tumour suppressor because tumour development was promoted in CUL9 deleted mice (Pei et al., 2011). Recently, the HSP90-dependent protein, survivin (Fortugno et al., 2003), was identified as a substrate of the CUL9 complex and deletion of CUL9 reduced the ubiquitylation of survivin in U2OS cells (Li et al., 2014). It is conceivable that the DOC domain of HECTD3, CUL7, CUL9 and Apc10 is responsible for client protein ligand binding. These previous observations may suggest some similar function of DOC domain for regulating the activity of HSP90-dependent protein.

7.2: Further work

Taken collectively, it appears that HECTD3 may recognize its substrate through its DOC domain, and the loss or mutation of this domain would in turn compromise HECTD3 function. Although time didn't allow us to fully investigate the role of the HECTD3 DOC domain, future work could address this. For example, a GST-DOC fusion could be used in cell lysates of HEK293 cells and pull down experiments conducted to test whether CRAF and HSP90 can be pulled down by the GST-DOC fusion. Although such an experiment does not completely prove that the interaction of the DOC domain is direct with CRAF or HSP90, it does at least show that the DOC domain is involved in recruitment of such HSP90-kinase complexes. Such experiments could also be conducted with or without HSP90 inhibitor. Inversely, pull down experiments could be conducted using a tagged CRAF instead of GST-DOC in pull down experiments from cell lysates. Pulled down material could also be analysed by mass spectroscopy to help identify any components that are pulled down with either GST-DOC or tagged-CRAF. Another screen of E2 conjugation enzymes could also provide more specific information that might help identify essential components in the HECTD3 complex involved in the ubiquitylation of CRAF.

7.3: Concluding remarks

The degradation of proteins by the ubiquitin proteasome system is one of the major pathways for degrading proteins. Inhibiting the activity of HS90 induces the ubiquitylation and degradation of HSP90-dependent client proteins and since many of these are oncogenic proteins, there is a need to understand how such HSP90 client proteins are degraded. Specific details regarding the degradation mechanism for HSP90-

dependent proteins could provide crucial knowledge for the development of anticancer therapies. Targeting HSP90 in cancer cells with ATP competitive inhibitors induces the depletion of various mutated kinase proteins such as $BRAF^{V600E}$, which dramatically displays the importance of HSP90 in cancer. Thus, understanding mechanisms in cancer cells that protect such kinases is critical to understanding the effectiveness of cancer treatments. However, to date very little is known about the degradation systems of such client proteins (Vaughan et al., 2006&2008; Smith et al., 2009&2015; Zhang et al., 2010; Roe et al., 2004; Polier et al., 2013; Keramisanou et al., 2016). This study has now clearly identified two E3 ligases that are involved in client protein degradation. Moreover they have suggested that alternate pathways may exist depending on the point of inhibition. Thus, inhibition of HSP90 leads to a HECTD3 and CUL5 dependent pathway, whereas inhibition of kinase, and thus failure of the kinase to associate with CDC37, leads to a HECTD3 and CUL5 independent pathway that now needs to be identified.

References

Adams, J., 2004. The proteasome: a suitable antineoplastic target. *Nature Reviews Cancer*, *4*(5), pp.349-360.

Aitken, A., 1995. 14-3-3 proteins on the MAP. *Trends in biochemical sciences*, *20*(3), pp.95-97.

Akahane, K., Sanda, T., Mansour, M.R., Radimerski, T., DeAngelo, D.J., Weinstock, D.M. and Look, A.T., 2016. HSP90 inhibition leads to degradation of the TYK2 kinase and apoptotic cell death in T-cell acute lymphoblastic leukemia. *Leukemia*, *30*(1), pp.219-228.

Ali, M.M., Roe, S.M., Vaughan, C.K., Meyer, P., Panaretou, B., Piper, P.W., Prodromou, C. and Pearl, L.H., 2006. Crystal structure of an HSP90–nucleotide–p23/Sba1 closed chaperone complex. *Nature*, *440*(7087), pp.1013-1017.

Andersen, P.L., Zhou, H., Pastushok, L., Moraes, T., McKenna, S., Ziola, B., Ellison, M.J., Dixit, V.M. and Xiao, W., 2005. Distinct regulation of Ubc13 functions by the two ubiquitin-conjugating enzyme variants Mms2 and Uev1A. *The Journal of cell biology*, *170*(5), pp.745-755.

Aravind, L. and Koonin, E.V., 2000. The U box is a modified RING finger—a common domain in ubiquitination. *Current Biology*, *10*(4), pp.R132-R134.

Armstrong, H., Wolmarans, A., Mercier, R., Mai, B. and LaPointe, P., 2012. The co-chaperone Hch1 regulates HSP90 function differently than its homologue AHA1 and confers sensitivity to yeast to the HSP90 inhibitor NVP-AUY922. *PloS one*, *7*(11), p.e49322.

Aguilera, M., Oliveros, M., Martínez-Padrón, M., Barbas, J.A. and Ferrús, A., 2000. Ariadne-1: a vital Drosophila gene is required in development and defines a new conserved family of ring-finger proteins. *Genetics*, *155*(3), pp.1231-1244.

Babon, J.J., Sabo, J.K., Zhang, J.G., Nicola, N.A. and Norton, R.S., 2009. The SOCS box encodes a hierarchy of affinities for Cullin5: implications for ubiquitin ligase formation and cytokine signalling suppression. *Journal of molecular biology*, *387*(1), pp.162-174.

Ballinger, C.A., Connell, P., Wu, Y., Hu, Z., Thompson, L.J., Yin, L.Y. and Patterson, C., 1999. Identification of CHIP, a novel tetratricopeptide repeat-containing protein that interacts with heat shock proteins and negatively regulates chaperone functions. *Molecular and cellular biology*, *19*(6), pp.4535-4545.

Bandhakavi, S., McCann, R.O., Hanna, D.E. and Glover, C.V., 2003. A positive feedback loop between protein kinase CKII and CDC37 promotes the activity of multiple protein kinases. *Journal of Biological Chemistry*, *278*(5), pp.2829-2836.

Banerji, U., O'Donnell, A., Scurr, M., Pacey, S., Stapleton, S., Asad, Y., Simmons, L., Maloney, A., Raynaud, F., Campbell, M. and Walton, M., 2005. Phase I pharmacokinetic and pharmacodynamic study of 17-allylamino, 17-demethoxygeldanamycin in patients with advanced malignancies. *Journal of Clinical Oncology*, *23*(18), pp.4152-4161.

Basyuk, E., Suavet, F., Doglio, A., Bordonné, R. and Bertrand, E., 2003. Human let‐7 stem–loop precursors harbor features of RNase III cleavage products. *Nucleic acids research*, *31*(22), pp.6593-6597.

Bauvy, C., Meijer, A.J. and Codogno, P., 2009. Assaying of autophagic protein degradation. *Methods in enzymology*, *452*, pp.47-61.

Bedford, L., Lowe, J., Dick, L.R., Mayer, R.J. and Brownell, J.E., 2011. Ubiquitin-like protein conjugation and the ubiquitin–proteasome system as drug targets. *Nature reviews Drug discovery*, *10*(1), pp.29-46.

Bernstein, E., Caudy, A.A., Hammond, S.M. and Hannon, G.J., 2001. Role for a bidentate ribonuclease in the initiation step of RNA interference. *Nature*, *409*(6818), pp.363-366.

Best, M.D., 2009. Click chemistry and bioorthogonal reactions: unprecedented selectivity in the labeling of biological molecules.*Biochemistry*, *48*(28), pp.6571-6584.

Birmingham, A., Anderson, E.M., Reynolds, A., Ilsley-Tyree, D., Leake, D., Fedorov, Y., Baskerville, S., Maksimova, E., Robinson, K., Karpilow, J. and Marshall, W.S., 2006. 3′ UTR seed matches, but not overall identity, are associated with RNAi off-targets. *Nature methods*, *3*(3), pp.199-204.

Blatch, G.L. and Lässle, M., 1999. The tetratricopeptide repeat: a structural motif mediating protein‐protein interactions. *Bioessays*, *21*(11), pp.932-939.

Bohnsack, M.T., Czaplinski, K. and GÖRLICH, D., 2004. Exportin 5 is a RanGTP-dependent dsRNA-binding protein that mediates nuclear export of pre-miRNAs. *Rna*, *10*(2), pp.185-191.

Boudeau, J., Maria, D.E.A.K., Lawlor, M.A., Morrice, N.A. and Alessi, D.R., 2003. Heat-shock protein 90 and CDC37 interact with LKB1 and regulate its stability. *Biochemical Journal*, *370*(3), pp.849-857.

Brough, P.A., Aherne, W., Barril, X., Borgognoni, J., Boxall, K., Cansfield, J.E., Cheung, K.M.J., Collins, I., Davies, N.G., Drysdale, M.J. and Dymock, B., 2007. 4, 5-diarylisoxazole HSP90 chaperone inhibitors: potential therapeutic agents for the treatment of cancer. *Journal of medicinal chemistry*, *51*(2), pp.196-218.

Burbelo, P.D. and Hall, A., 1995. 14-3-3 proteins: hot numbers in signal transduction. *Current Biology*, *5*(2), pp.95-96.

Campbell, S.L., Khosravi-Far, R., Rossman, K.L., Clark, G.J. and Der, C.J., 1998. Increasing complexity of Ras signaling. *Oncogene*, *17*(11), pp.1395-1413.

Caplan, A.J., Mandal, A.K. and Theodoraki, M.A., 2007. Molecular chaperones and protein kinase quality control. *Trends in cell biology*, *17*(2), pp.87-92.

Carlomagno, F., Anaganti, S., Guida, T., Salvatore, G., Troncone, G., Wilhelm, S.M. and Santoro, M., 2006. BAY 43-9006 inhibition of oncogenic RET mutants. *Journal of the National Cancer Institute*, *98*(5), pp.326-334.

Carroll, C.W. and Morgan, D.O., 2002. The Doc1 subunit is a processivity factor for the anaphase-promoting complex. *Nature cell biology*, *4*(11), pp.880-887.

Carroll, C.W., Enquist-Newman, M. and Morgan, D.O., 2005. The APC subunit Doc1 promotes recognition of the substrate destruction box. *Current biology*, *15*(1), pp.11-18.

Catling, A.D., Reuter, C.W., Cox, M.E., Parsons, S.J. and Weber, M.J., 1994. Partial purification of a mitogen-activated protein kinase kinase activator from bovine brain. Identification as B-RAF or a B-RAF-associated activity. *Journal of Biological Chemistry*, *269*(47), pp.30014-30021.

Chang, H.C., Nathan, D.F. and Lindquist, S., 1997. In vivo analysis of the HSP90 cochaperone Sti1 (p60). *Molecular and cellular biology*, *17*(1), pp.318-325.

Chavany, C., Mimnaugh, E., Miller, P., Bitton, R., Nguyen, P., Trepel, J., Whitesell, L., Schnur, R., Moyer, J.D. and Neckers, L., 1996. p185 Binds to GRP94 in Vivo DISSOCIATION OF THE p185/GRP94 HETEROCOMPLEX BY BENZOQUINONE ANSAMYCINS PRECEDES DEPLETION OF p185.*Journal of Biological Chemistry*, *271*(9), pp.4974-4977.

Chen, D., Kon, N., Li, M., Zhang, W., Qin, J. and Gu, W., 2005. ARF-BP1/Mule is a critical mediator of the ARF tumor suppressor. *Cell*, *121*(7), pp.1071-1083.

Chin, L., 2003. The genetics of malignant melanoma: lessons from mouse and man. *Nature Reviews Cancer*, *3*(8), pp.559-570.

Chinkers, M., 2001. Protein phosphatase 5 in signal transduction. *Trends in Endocrinology & Metabolism*, *12*(1), pp.28-32.

Chiosis, G., Timaul, M.N., Lucas, B., Munster, P.N., Zheng, F.F., Sepp-Lorenzino, L. and Rosen, N., 2001. A small molecule designed to bind to the adenine nucleotide pocket of HSP90 causes Her2 degradation and the growth arrest and differentiation of breast cancer cells. *Chemistry & biology*, *8*(3), pp.289-299.

Chiosis, G., Vilenchik, M., Kim, J. and Solit, D., 2004. HSP90: the vulnerable chaperone. *Drug discovery today*, *9*(20), pp.881-888.

Ciechanover, A., 2005. Intracellular protein degradation: from a vague idea thru the lysosome and the ubiquitin–proteasome system and onto human diseases and drug targeting. *Cell Death & Differentiation*, *12*(9), pp.1178-1190.

Ciechanover, A., Heller, H., Elias, S., Haas, A.L. and Hershko, A., 1980. ATP-dependent conjugation of reticulocyte proteins with the polypeptide required for protein degradation. *Proceedings of the National Academy of Sciences*, *77*(3), pp.1365-1368.

Cullen, B.R., 2006. Enhancing and confirming the specificity of RNAi experiments. *Nature methods*, *3*(9), pp.677-681.

Cyr, D.M., Höhfeld, J. and Patterson, C., 2002. Protein quality control: U-box-containing E3 ubiquitin ligases join the fold. *Trends in biochemical sciences*, *27*(7),

pp.368-375.

da Fonseca, P.C., Kong, E.H., Zhang, Z., Schreiber, A., Williams, M.A., Morris, E.P. and Barford, D., 2011. Structures of APC/CCdh1 with substrates identify Cdh1 and Apc10 as the D-box co-receptor. *Nature*, *470*(7333), pp.274-278.

da Rocha Dias, S., Friedlos, F., Light, Y., Springer, C., Workman, P. and Marais, R., 2005. Activated B-RAF is an HSP90 client protein that is targeted by the anticancer drug 17-allylamino-17-demethoxygeldanamycin. *Cancer research*, *65*(23), pp.10686-10691.

Dai, K., Kobayashi, R. and Beach, D., 1996. Physical interaction of mammalian CDC37 with CDK4. *Journal of Biological Chemistry*, *271*(36), pp.22030-22034.

Das, A.K., Cohen, P.T. and Barford, D., 1998. The structure of the tetratricopeptide repeats of protein phosphatase 5: implications for TPR‐mediated protein–protein interactions. *The EMBO journal*, *17*(5), pp.1192-1199.

Davies, H., Bignell, G.R., Cox, C., Stephens, P., Edkins, S., Clegg, S., Teague, J., Woffendin, H., Garnett, M.J., Bottomley, W. and Davis, N., 2002. Mutations of the BRAF gene in human cancer. *Nature*, *417*(6892), pp.949-954.

Dey, B., Lightbody, J.J. and Boschelli, F., 1996. CDC37 is required for p60v-src activity in yeast. *Molecular biology of the cell*, *7*(9), pp.1405-1417.

Dias, D.C., Dolios, G., Wang, R. and Pan, Z.Q., 2002. CUL7: A DOC domain-containing cullin selectively binds Skp1‐Fbx29 to form an SCF-like complex. *Proceedings of the National Academy of Sciences*, *99*(26), pp.16601-16606.

Dieterich, D.C., Lee, J.J., Link, A.J., Graumann, J., Tirrell, D.A. and Schuman, E.M., 2007. Labeling, detection and identification of newly synthesized proteomes with bioorthogonal non-canonical amino-acid tagging. *Nature protocols*, *2*(3), pp.532-540.

Dieterich, D.C., Link, A.J., Graumann, J., Tirrell, D.A. and Schuman, E.M., 2006. Selective identification of newly synthesized proteins in mammalian cells using bioorthogonal noncanonical amino acid tagging (BONCAT).*Proceedings of the National Academy of Sciences*, *103*(25), pp.9482-9487.

Eccles, S.A., Massey, A., Raynaud, F.I., Sharp, S.Y., Box, G., Valenti, M., Patterson, L.,

de Haven Brandon, A., Gowan, S., Boxall, F. and Aherne, W., 2008. NVP-AUY922: a novel heat shock protein 90 inhibitor active against xenograft tumor growth, angiogenesis, and metastasis. *Cancer research*, *68*(8), pp.2850-2860.

Echeverri, C.J. and Perrimon, N., 2006. High-throughput RNAi screening in cultured cells: a user's guide. *Nature Reviews Genetics*, *7*(5), pp.373-384.

Echeverri, C.J., Beachy, P.A., Baum, B., Boutros, M., Buchholz, F., Chanda, S.K., Downward, J., Ellenberg, J., Fraser, A.G., Hacohen, N. and Hahn, W.C., 2006. Minimizing the risk of reporting false positives in large-scale RNAi screens. *Nature methods*, *3*(10), pp.777-779.

Egorin, M.J., Rosen, D.M., Wolff, J.H., Callery, P.S., Musser, S.M. and Eiseman, J.L., 1998. Metabolism of 17-(allylamino)-17-demethoxygeldanamycin (NSC 330507) by murine and human hepatic preparations. *Cancer research*, *58*(11), pp.2385-2396.

Ehrlich, E.S., Wang, T., Luo, K., Xiao, Z., Niewiadomska, A.M., Martinez, T., Xu, W., Neckers, L. and Yu, X.F., 2009. Regulation of HSP90 client proteins by a Cullin5-RING E3 ubiquitin ligase. *Proceedings of the National Academy of Sciences*, *106*(48), pp.20330-20335.

Eiberg, H., Troelsen, J., Nielsen, M., Mikkelsen, A., Mengel-From, J., Kjaer, K.W. and Hansen, L., 2008. Blue eye color in humans may be caused by a perfectly associated founder mutation in a regulatory element located within the HERC2 gene inhibiting OCA2 expression. *Human genetics*, *123*(2), pp.177-187.

Elbashir, S.M., Lendeckel, W. and Tuschl, T., 2001. RNA interference is mediated by 21-and 22-nucleotide RNAs. *Genes & development*, *15*(2), pp.188-200.

Eustace, B.K., Sakurai, T., Stewart, J.K., Yimlamai, D., Unger, C., Zehetmeier, C., Lain, B., Torella, C., Henning, S.W., Beste, G. and Scroggins, B.T., 2004. Functional proteomic screens reveal an essential extracellular role for HSP90α in cancer cell invasiveness. *Nature cell biology*, *6*(6), pp.507-514.

Fantl, W.J., Muslin, A.J., Kikuchi, A., Martin, J.A., MacNicol, A.M., Grosst, R.W. and Williams, L.T., 1994. Activation of RAF-1 by 14-3-3 proteins. *Nature*, *371(6498)*, pp.612-614

Feng, L. and Chen, J., 2012. The E3 ligase RNF8 regulates KU80 removal and NHEJ repair. *Nature structural & molecular biology*, *19*(2), pp.201-206.

Fire, A., Xu, S., Montgomery, M.K., Kostas, S.A., Driver, S.E. and Mello, C.C., 1998. Potent and specific genetic interference by double-stranded RNA in Caenorhabditis elegans. *nature*, *391*(6669), pp.806-811.

Fortugno, P., Beltrami, E., Plescia, J., Fontana, J., Pradhan, D., Marchisio, P.C., Sessa, W.C. and Altieri, D.C., 2003. Regulation of survivin function by HSP90. *Proceedings of the National Academy of Sciences*, *100*(24), pp.13791-13796.

Freed, E., Symons, M., Macdonald, S.G., McCormick, F. and Ruggieri, R., 1994. Binding of 14-3-3 proteins to the protein kinase RAF and effects on its activation. *Science, 265(5179),* pp.1713-1716.

Freemont, P.S., 2000. Ubiquitylation: RING for destruction. *Current Biology*, *10*(2), pp.R84-R87.

Frescas, D. and Pagano, M., 2008. Deregulated proteolysis by the F-box proteins SKP2 and β-TrCP: tipping the scales of cancer. *Nature Reviews Cancer*, *8*(6), pp.438-449.

Fu, H., Xia, K., Pallas, D. C., Cui, C., Conroy, K., Narsimhan, R. P., Mamon, H., Collier, R. J., and Roberts. T. M., 1994. Interaction of the protein kinase RAF-1 with 14-3-3 proteins. *Science*, *266*(5182), pp.126–129.

Gao, M., Labuda, T., Xia, Y., Gallagher, E., Fang, D., Liu, Y.C. and Karin, M., 2004. Jun turnover is controlled through JNK-dependent phosphorylation of the E3 ligase Itch. *Science*, *306*(5694), pp.271-275.

Gao, Z., Garcia-Echeverria, C. and Jensen, M.R., 2010. HSP90 inhibitors: clinical development and future opportunities in oncology therapy. *Current opinion in drug discovery & development*, *13*(2), pp.193-202.

Garcia-Gonzalo, F.R. and Rosa, J.L., 2005. The HERC proteins: functional and evolutionary insights. *Cellular and Molecular Life Sciences CMLS*, *62*(16), pp.1826-1838.

Garon, E.B., Finn, R.S., Hamidi, H., Dering, J., Pitts, S., Kamranpour, N., Desai, A.J., Hosmer, W., Ide, S., Avsar, E. and Jensen, M.R., 2013. The HSP90 inhibitor NVP-

AUY922 potently inhibits non–small cell lung cancer growth. *Molecular cancer therapeutics*, *12*(6), pp.890-900.

Gaspar, N., Sharp, S.Y., Eccles, S.A., Gowan, S., Popov, S., Jones, C., Pearson, A., Vassal, G. and Workman, P., 2010. Mechanistic evaluation of the novel HSP90 inhibitor NVP-AUY922 in adult and pediatric glioblastoma. *Molecular cancer therapeutics*, *9*(5), pp.1219-1233.

Gaspar, N., Sharp, S.Y., Pacey, S., Jones, C., Walton, M., Vassal, G., Eccles, S., Pearson, A. and Workman, P., 2009. Acquired resistance to 17-allylamino-17-demethoxygeldanamycin (17-AAG, tanespimycin) in glioblastoma cells. *Cancer research*, *69*(5), pp.1966-1975.

Ge, J., Normant, E., Porter, J.R., Ali, J.A., Dembski, M.S., Gao, Y., Georges, A.T., Grenier, L., Pak, R.H., Patterson, J. and Sydor, J.R., 2006. Design, synthesis, and biological evaluation of hydroquinone derivatives of 17-amino-17-demethoxygeldanamycin as potent, water-soluble inhibitors of HSP90. *Journal of medicinal chemistry*, *49*(15), pp.4606-4615.

Goldberg, A.L., 2007. Functions of the proteasome: from protein degradation and immune surveillance to cancer therapy. *Biochemical Society Transactions*, *35*(1), pp.12-17.

Grammatikakis, N., Lin, J.H., Grammatikakis, A., Tsichlis, P.N. and Cochran, B.H., 1999. p50 CDC37 acting in concert with HSP90 is required for RAF-1 function. *Molecular and cellular biology*, *19*(3), pp.1661-1672.

Grbovic, O.M., Basso, A.D., Sawai, A., Ye, Q., Friedlander, P., Solit, D. and Rosen, N., 2006. V600E B-RAF requires the HSP90 chaperone for stability and is degraded in response to HSP90 inhibitors. *Proceedings of the National Academy of Sciences of the United States of America*, *103*(1), pp.57-62.

Grimm, D., Streetz, K.L., Jopling, C.L., Storm, T.A., Pandey, K., Davis, C.R., Marion, P., Salazar, F. and Kay, M.A., 2006. Fatality in mice due to oversaturation of cellular microRNA/short hairpin RNA pathways. *nature*, *441*(7092), pp.537-541.

Grishok, A., Pasquinelli, A.E., Conte, D., Li, N., Parrish, S., Ha, I., Baillie, D.L., Fire, A., Ruvkun, G. and Mello, C.C., 2001. Genes and mechanisms related to RNA

interference regulate expression of the small temporal RNAs that control C. elegans developmental timing. *Cell*, *106*(1), pp.23-34.

Guo, S. and Kemphues, K.J., 1995. par-1, a gene required for establishing polarity in C. elegans embryos, encodes a putative Ser/Thr kinase that is asymmetrically distributed. *Cell*, *81*(4), pp.611-620.

Harris, S.F., Shiau, A.K. and Agard, D.A., 2004. The crystal structure of the carboxy-terminal dimerization domain of htpG, the Escherichia coli HSP90, reveals a potential substrate binding site. *Structure*, *12*(6), pp.1087-1097.

Harst, A., Hongying, L.I.N. and Obermann, W.M., 2005. AHA1 competes with Hop, p50 and p23 for binding to the molecular chaperone HSP90 and contributes to kinase and hormone receptor activation. *Biochemical Journal*, *387*(3), pp.789-796.

Hatakeyama, S., Jensen, J.P. and Weissman, A.M., 1997. Subcellular localization and ubiquitin-conjugating enzyme (E2) interactions of mammalian HECT family ubiquitin protein ligases. *Journal of Biological Chemistry*, *272*(24), pp.15085-15092.

Hatakeyama, S., Yada, M., Matsumoto, M., Ishida, N. and Nakayama, K.I., 2001. U box proteins as a new family of ubiquitin-protein ligases. *Journal of Biological Chemistry*, *276*(35), pp.33111-33120.

Hershko, A. and Tomkins, G.M., 1971. Studies on the Degradation of Tyrosine Aminotransferase in Hepatoma Cells in Culture INFLUENCE OF THE COMPOSITION OF THE MEDIUM AND ADENOSINE TRIPHOSPHATE DEPENDENCE. *Journal of Biological Chemistry*, *246*(3), pp.710-714.

Hershko, A., Ciechanover, A., Heller, H., Haas, A.L. and Rose, I.A., 1980. Proposed role of ATP in protein breakdown: conjugation of protein with multiple chains of the polypeptide of ATP-dependent proteolysis.*Proceedings of the National Academy of Sciences*, *77*(4), pp.1783-1786.

Hershko, A., Heller, H., Elias, S. and Ciechanover, A., 1983. Components of ubiquitin-protein ligase system. Resolution, affinity purification, and role in protein breakdown. *Journal of Biological Chemistry*, *258*(13), pp.8206-8214.

Hicke, L. and Dunn, R., 2003. Regulation of membrane protein transport by ubiquitin

and ubiquitin-binding proteins. *Annual review of cell and developmental biology*, *19*(1), pp.141-172.

Hofmann, R.M. and Pickart, C.M., 1999. Noncanonical MMS2-encoded ubiquitin-conjugating enzyme functions in assembly of novel polyubiquitin chains for DNA repair. *Cell*, *96*(5), pp.645-653.

Holmes, J.L., Sharp, S.Y., Hobbs, S. and Workman, P., 2008. Silencing of HSP90 cochaperone AHA1 expression decreases client protein activation and increases cellular sensitivity to the HSP90 inhibitor 17-allylamino-17-demethoxygeldanamycin. *Cancer Research*, *68*(4), pp.1188-1197.

Hostein, I., Robertson, D., DiStefano, F., Workman, P. and Clarke, P.A., 2001. Inhibition of signal transduction by the HSP90 inhibitor 17-allylamino-17-demethoxygeldanamycin results in cytostasis and apoptosis. *Cancer research*, *61*(10), pp.4003-4009.

Huang, L., Kinnucan, E., Wang, G., Beaudenon, S., Howley, P.M., Huibregtse, J.M. and Pavletich, N.P., 1999. Structure of an E6AP-UbcH7 complex: insights into ubiquitylation by the E2-E3 enzyme cascade. *Science*, *286*(5443), pp.1321-1326.

Huang, Z., Nie, L., Xu, M. and Sun, X.H., 2004. Notch-induced E2A degradation requires CHIP and Hsc70 as novel facilitators of ubiquitylation. *Molecular and cellular biology*, *24*(20), pp.8951-8962.

Huibregtse, J.M., Scheffner, M., Beaudenon, S. and Howley, P.M., 1995. A family of proteins structurally and functionally related to the E6-AP ubiquitin-protein ligase. *Proceedings of the National Academy of Sciences*, *92*(7), pp.2563-2567.

Huppi, K., Martin, S.E. and Caplen, N.J., 2005. Defining and assaying RNAi in mammalian cells. *Molecular cell*, *17*(1), pp.1-10.

Hutvágner, G. and Zamore, P.D., 2002. A microRNA in a multiple-turnover RNAi enzyme complex. *Science*, *297*(5589), pp.2056-2060.

Hutvágner, G., McLachlan, J., Pasquinelli, A.E., Bálint, É., Tuschl, T. and Zamore, P.D., 2001. A cellular function for the RNA-interference enzyme Dicer in the maturation of the let-7 small temporal RNA. *Science*, *293*(5531), pp.834-838.

Hüttenhofer, A., Schattner, P., Hall, J., Mattick, J.S., Brummelkamp, T.R., Bernards, R. and Martienssen, R.A., 2003. Whither RNAi. *Nat. Cell. Biol*, *5*, pp.489-490.

Hwang, L.H. and Murray, A.W., 1997. A Novel Yeast Screen for Mitotic Arrest Mutants Identifies DOC1, a New Gene Involved in Cyclin Proteolysis. *Molecular biology of the cell*, *8*(10), pp.1877-1887.

Irie, K., Gotoh, Y., Yashar, B.M., Errede, B., Nishida, E. and Matsumoto, K., 1994. Stimulatory effects of yeast and mammalian 14-3-3 proteins on the RAF protein kinase. *Science*, *265*(5179), pp.1716-1719.

Iwasaki, S., Kobayashi, M., Yoda, M., Sakaguchi, Y., Katsuma, S., Suzuki, T. and Tomari, Y., 2010. Hsc70/HSP90 chaperone machinery mediates ATP-dependent RISC loading of small RNA duplexes. *Molecular cell*, *39*(2), pp.292-299.

Jackson, A.L., Bartz, S.R., Schelter, J., Kobayashi, S.V., Burchard, J., Mao, M., Li, B., Cavet, G. and Linsley, P.S., 2003. Expression profiling reveals off-target gene regulation by RNAi. *Nature biotechnology*, *21*(6), pp.635-637.

Jackson, A.L., Burchard, J., Schelter, J., Chau, B.N., Cleary, M., Lim, L. and Linsley, P.S., 2006. Widespread siRNA "off-target" transcript silencing mediated by seed region sequence complementarity. *Rna*, *12*(7), pp.1179-1187.

Jaiswal, R.K., Moodie, S.A., Wolfman, A. and Landreth, G.E., 1994. The mitogen-activated protein kinase cascade is activated by B-RAF in response to nerve growth factor through interaction with p21ras. *Molecular and Cellular Biology*, *14*(10), pp.6944-6953.

Jansen, H.W., Lurz, R., Bister, K., Bonner, T.I., Mark, G.E., and Rapp, U.R., 1984. Homologous cell-derived oncogenes in avian carcinoma virus MH2 and murine sarcoma virus 3611. *Nature*, *307*(5948), pp.281–284.

Jaumot, M. and Hancock, J.F., 2001. Protein phosphatases 1 and 2A promote RAF-1 activation by regulating 14-3-3 interactions. *Oncogene*, *20*(30), pp3949-3958.

Jensen, M.R., Schoepfer, J., Radimerski, T., Massey, A., Guy, C.T., Brueggen, J., Quadt, C., Buckler, A., Cozens, R., Drysdale, M.J. and Garcia-Echeverria, C., 2008. NVP-AUY922: a small molecule HSP90 inhibitor with potent antitumor activity in preclinical

breast cancer models. *Breast Cancer Research*, *10*(2), R33.

Jiang, J., Cyr, D., Babbitt, R.W., Sessa, W.C. and Patterson, C., 2003. Chaperone-dependent regulation of endothelial nitric-oxide synthase intracellular trafficking by the co-chaperone/ubiquitin ligase CHIP. *Journal of biological chemistry*, *278*(49), pp.49332-49341.

Jin, J., Cardozo, T., Lovering, R.C., Elledge, S.J., Pagano, M. and Harper, J.W., 2004. Systematic analysis and nomenclature of mammalian F-box proteins. *Genes & development*, *18*(21), pp.2573-2580.

Joazeiro, C.A. and Weissman, A.M., 2000. RING finger proteins: mediators of ubiquitin ligase activity. *Cell*, *102*(5), pp.549-552.

Johnson, G.L. and Lapadat, R., 2002. Mitogen-activated protein kinase pathways mediated by ERK, JNK, and p38 protein kinases. *Science*, *298*(5600), pp.1911-1912.

Judge, A.D., Sood, V., Shaw, J.R., Fang, D., McClintock, K. and MacLachlan, I., 2005. Sequence-dependent stimulation of the mammalian innate immune response by synthetic siRNA. *Nature biotechnology*, *23*(4), pp.457-462.

Karikó, K., Bhuyan, P., Capodici, J. and Weissman, D., 2004. Small interfering RNAs mediate sequence-independent gene suppression and induce immune activation by signaling through toll-like receptor 3. *The Journal of Immunology*, *172*(11), pp.6545-6549.

Karnitz, L.M. and Felts, S.J., 2007. CDC37 regulation of the kinome: when to hold ‘em and when to fold ‘em. *Science Signaling*, *2007*(385), pp.pe22-pe22.

Kawamata, T. and Tomari, Y., 2010. Making risc. *Trends in biochemical sciences*, *35*(7), pp.368-376.

Keramisanou, D., Aboalroub, A., Zhang, Z., Liu, W., Marshall, D., Diviney, A., Larsen, R.W., LandgRAF, R. and Gelis, I., 2016. Molecular Mechanism of Protein Kinase Recognition and Sorting by the HSP90 Kinome-Specific Cochaperone CDC37. *Molecular Cell*, *62*(2), pp.260-271.

Khan, A.A., Betel, D., Miller, M.L., Sander, C., Leslie, C.S. and Marks, D.S., 2009. Transfection of small RNAs globally perturbs gene regulation by endogenous

microRNAs. *Nature biotechnology*, *27*(6), pp.549-555.

Kile, B.T., Schulman, B.A., Alexander, W.S., Nicola, N.A., Martin, H.M. and Hilton, D.J., 2002. The SOCS box: a tale of destruction and degradation. *Trends in biochemical sciences*, *27*(5), pp.235-241.

Kim, M.G., Moon, J.S., Kim, E.J., Lee, S.H. and Oh, J.W., 2012. Destabilization of PDK1 by HSP90 inactivation suppresses hepatitis C virus replication through inhibition of PRK2-mediated viral RNA polymerase phosphorylation. *Biochemical and biophysical research communications*, *421*(1), pp.112-118.

Kim, Y.S., Alarcon, S.V., Lee, S., Lee, M.J., Giaccone, G., Neckers, L. and Trepel, J.B., 2009. Update on HSP90 inhibitors in clinical trial. *Current topics in medicinal chemistry*, *9*(15), pp.1479-1492.

Kittler, R., Surendranath, V., Heninger, A.K., Slabicki, M., Theis, M., Putz, G., Franke, K., Caldarelli, A., Grabner, H., Kozak, K. and Wagner, J., 2007. Genome-wide resources of endoribonuclease-prepared short interfering RNAs for specific loss-of-function studies. *Nature methods*, *4*(4), pp.337-344.

Kolfschoten, I.G., van Leeuwen, B., Berns, K., Mullenders, J., Beijersbergen, R.L., Bernards, R., Voorhoeve, P.M. and Agami, R., 2005. A genetic screen identifies PITX1 as a suppressor of RAS activity and tumorigenicity. *Cell*, *121*(6), pp.849-858.

Komander, D. and Rape, M., 2012. The ubiquitin code. *Annual review of biochemistry*, *81*, pp.203-229.

Kominami, K.I., Seth‐Smith, H. and Toda, T., 1998. Apc10 and Ste9/Srw1, two regulators of the APC–cyclosome, as well as the CDK inhibitor Rum1 are required for G1 cell‐cycle arrest in fission yeast. *The EMBO Journal*, *17*(18), pp.5388-5399.

Koulov, A.V., LaPointe, P., Lu, B., Razvi, A., Coppinger, J., Dong, M.Q., Matteson, J., Laister, R., Arrowsmith, C., Yates, J.R. and Balch, W.E., 2010. Biological and structural basis for AHA1 regulation of HSP90 ATPase activity in maintaining proteostasis in the human disease cystic fibrosis. *Molecular biology of the cell*, *21*(6), pp.871-884.

Lamphere, L., Fiore, F., Xu, X., Brizuela, L., Keezer, S., Sardet, C., Draetta, G.F. and

Gyuris, J., 1997. Interaction between CDC37 and CDK4 in human cells. *Oncogene*, *14*(16), pp.1999-2004.

Lavictoire, S.J., Parolin, D.A., Klimowicz, A.C., Kelly, J.F. and Lorimer, I.A., 2003. Interaction of HSP90 with the nascent form of the mutant epidermal growth factor receptor EGFRvIII. *Journal of Biological Chemistry*, *278*(7), pp.5292-5299.

Lee, P., Rao, J., Fliss, A., Yang, E., Garrett, S. and Caplan, A.J., 2002. The CDC37 protein kinase–binding domain is sufficient for protein kinase activity and cell viability. *The Journal of cell biology*, *159*(6), pp.1051-1059.

Lee, Y., Ahn, C., Han, J., Choi, H., Kim, J., Yim, J., Lee, J., Provost, P., Rådmark, O., Kim, S. and Kim, V.N., 2003. The nuclear RNase III Drosha initiates microRNA processing. *Nature*, *425*(6956), pp.415-419.

Lee, Y., Jeon, K., Lee, J.T., Kim, S. and Kim, V.N., 2002*. MicroRNA maturation: stepwise processing and subcellular localization. *The EMBO journal*, *21*(17), pp.4663-4670.

Lee, Y.S., Nakahara, K., Pham, J.W., Kim, K., He, Z., Sontheimer, E.J. and Carthew, R.W., 2004. Distinct roles for Drosophila Dicer-1 and Dicer-2 in the siRNA/miRNA silencing pathways. *Cell*, *117*(1), pp.69-81.

Leevers, S.J., Paterson, H.F. and Marshall, C.J., 1994. Requirement for Ras in RAF activation is overcome by targeting RAF to the plasma membrane. *Nature*, *369*(6479), pp.411-414.

Levine, B. and Kroemer, G., 2008. Autophagy in the pathogenesis of disease. *Cell*, *132*(1), pp.27-42.

Li, L., Xin, H., Xu, X., Huang, M., Zhang, X., Chen, Y., Zhang, S., Fu, X.Y. and Chang, Z., 2004. CHIP mediates degradation of Smad proteins and potentially regulates Smad-induced transcription. *Molecular and cellular biology*, *24*(2), pp.856-864.

Li, S., Janosch, P., Tanji, M., Rosenfeld, G.C., Waymire, J.C., Mischak, H., Kolch, W. and Sedivy, J.M., 1995. Regulation of RAF-1 kinase activity by the 14-3-3 family of proteins. *The EMBO Journal*, *14*(4), p.685.

Li, W., Bengtson, M.H., Ulbrich, A., Matsuda, A., Reddy, V.A., Orth, A., Chanda, S.K.,

Batalov, S. and Joazeiro, C.A., 2008. Genome-wide and functional annotation of human E3 ubiquitin ligases identifies MULAN, a mitochondrial E3 that regulates the organelle's dynamics and signaling. *PloS one*, *3*(1), p.e1487.

Li, Y., Chen, X., Wang, Z., Zhao, D., Chen, H., Chen, W., Zhou, Z., Zhang, J., Zhang, J., Li, H. and Chen, C., 2013b. The HECTD3 E3 ubiquitin ligase suppresses cisplatin-induced apoptosis via stabilizing MALT1. *Neoplasia*, *15*(1), pp.39-48.

Li, Y., Kong, Y., Zhou, Z., Chen, H., Wang, Z., Hsieh, Y.C., Zhao, D., Zhi, X., Huang, J., Zhang, J. and Li, H., 2013a. The HECTD3 E3 ubiquitin ligase facilitates cancer cell survival by promoting K63-linked polyubiquitylation of caspase-8. *Cell death & disease*, *4*(11), p.e935.

Li, Z., Pei, X.H., Yan, J., Yan, F., Cappell, K.M., Whitehurst, A.W. and Xiong, Y., 2014. CUL9 mediates the functions of the 3M complex and ubiquitylates survivin to maintain genome integrity. *Molecular cell*, *54*(5), pp.805-819.

Lipkowitz, S. and Weissman, A.M., 2011. RINGs of good and evil: RING finger ubiquitin ligases at the crossroads of tumour suppression and oncogenesis. *Nature Reviews Cancer*, *11*(9), pp.629-643.

Liu, Q., Rand, T.A., Kalidas, S., Du, F., Kim, H.E., Smith, D.P. and Wang, X., 2003. R2D2, a bridge between the initiation and effector steps of the Drosophila RNAi pathway. *Science*, *301*(5641), pp.1921-1925.

Lorick, K.L., Jensen, J.P., Fang, S., Ong, A.M., Hatakeyama, S. and Weissman, A.M., 1999. RING fingers mediate ubiquitin-conjugating enzyme (E2)-dependent ubiquitylation. *Proceedings of the National Academy of Sciences*, *96*(20), pp.11364-11369.

Lotz, G.P., Lin, H., Harst, A. and Obermann, W.M., 2003. AHA1 binds to the middle domain of HSP90, contributes to client protein activation, and stimulates the ATPase activity of the molecular chaperone. *Journal of Biological Chemistry*, *278*(19), pp.17228-17235.

Lowy, D.R. and Willumsen, B.M., 1993. Function and regulation of ras. *Annual review of biochemistry*, *62*(1), pp.851-891.

Lu, Z. and Hunter, T., 2009. Degradation of activated protein kinases by ubiquitylation. *Annual review of biochemistry*, *78*, p.435-475.

Lund, E., Güttinger, S., Calado, A., Dahlberg, J.E. and Kutay, U., 2004. Nuclear export of microRNA precursors. *Science*, *303*(5654), pp.95-98.

Lydeard, J.R., Schulman, B.A. and Harper, J.W., 2013. Building and remodelling Cullin–RING E3 ubiquitin ligases. *EMBO reports*, *14*(12), pp.1050-1061.

Lyons, J.F., Wilhelm, S., Hibner, B. and Bollag, G., 2001. Discovery of a novel RAF kinase inhibitor. *Endocrine-related cancer*, *8*(3), pp.219-225.

Ma, L., Broomfield, S., Lavery, C., Lin, S.L., Xiao, W. and Bacchetti, S., 1998. Up-regulation of CIR1/CROC1 expression upon cell immortalization and in tumor-derived human cell lines. *Oncogene*, *17*(10), pp.1321-1326.

Malone, C.D. and Hannon, G.J., 2009. Small RNAs as guardians of the genome. *Cell*, *136*(4), pp.656-668.

Mani, A. and Gelmann, E.P., 2005. The ubiquitin-proteasome pathway and its role in cancer. *Journal of Clinical Oncology*, *23*(21), pp.4776-4789.

Maniataki, E. and Mourelatos, Z., 2005. Human mitochondrial tRNAMet is exported to the cytoplasm and associates with the Argonaute 2 protein. *Rna*, *11*(6), pp.849-852.

Martinez, J. and Tuschl, T., 2004. RISC is a 5′ phosphomonoester-producing RNA endonuclease. *Genes & development*, *18*(9), pp.975-980.

Martinez, J., Patkaniowska, A., Urlaub, H., Lührmann, R. and Tuschl, T., 2002. Single-stranded antisense siRNAs guide target RNA cleavage in RNAi. *Cell*, *110*(5), pp.563-574.

Mason, C.S., Springer, C.J., Cooper, R.G., Superti-Furga, G., Marshall, C.J. and Marais, R., 1999. Serine and tyrosine phosphorylations cooperate in RAF‐1, but not B‐RAF activation. The EMBO journal, 18(8), pp.2137-2148.

Matranga, C., Tomari, Y., Shin, C., Bartel, D.P. and Zamore, P.D., 2005. Passenger-strand cleavage facilitates assembly of siRNA into Ago2-containing RNAi enzyme complexes. *Cell*, *123*(4), pp.607-620.

Matzke, M.A. and Birchler, J.A., 2005. RNAi-mediated pathways in the nucleus. *Nature Reviews Genetics*, *6*(1), pp.24-35.

Mayer, M.P., Nikolay, R. and Bukau, B., 2002. Aha, another regulator for HSP90 chaperones. *Molecular cell*, *10*(6), pp.1255-1256.

Mayer, M.P., Prodromou, C. and Frydman, J., 2009. The HSP90 mosaic: a picture emerges. *Nature structural & molecular biology*, *16*(1), pp.2-6.

McGill, M.A. and McGlade, C.J., 2003. Mammalian numb proteins promote Notch1 receptor ubiquitylation and degradation of the Notch1 intracellular domain. *Journal of Biological Chemistry*, *278*(25), pp.23196-23203.

McKenna, S., Moraes, T., Pastushok, L., Ptak, C., Xiao, W., Spyracopoulos, L. and Ellison, M.J., 2003. An NMR-based Model of the Ubiquitin-bound Human Ubiquitin Conjugation Complex Mms2· Ubc13 THE STRUCTURAL BASIS FOR LYSINE 63 CHAIN CATALYSIS. *Journal of Biological Chemistry*, *278*(15), pp.13151-13158.

McKenna, S., Spyracopoulos, L., Moraes, T., Pastushok, L., Ptak, C., Xiao, W. and Ellison, M.J., 2001. Noncovalent interaction between ubiquitin and the human DNA repair protein Mms2 is required for Ubc13-mediated polyubiquitylation. *Journal of Biological Chemistry*, *276*(43), pp.40120-40126.

McLaughlin, S.H., Ventouras, L.A., Lobbezoo, B. and Jackson, S.E., 2004. Independent ATPase activity of HSP90 subunits creates a flexible assembly platform. *Journal of molecular biology*, *344*(3), pp.813-826.

McPherson, R.A., Harding, A., Roy, S., Lane, A. and Hancock, J.F., 1999. Interactions of c-RAF-1 with phosphatidylserine and 14-3-3. *Oncogene*, *18*(26), pp. 3862–3869.

Meacham, G.C., Patterson, C., Zhang, W., Younger, J.M. and Cyr, D.M., 2001. The Hsc70 co-chaperone CHIP targets immature CFTR for proteasomal degradation. *Nature cell biology*, *3*(1), pp.100-105.

Mehrpour, M., Esclatine, A., Beau, I. and Codogno, P., 2010. Autophagy in health and disease. 1. Regulation and significance of autophagy: an overview. *American Journal of Physiology-Cell Physiology*, *298*(4), pp.C776-C785.

Mehta, P.P., Kung, P.P., Yamazaki, S., Walls, M., Shen, A., Nguyen, L., Gehring, M.R.,

Los, G., Smeal, T. and Yin, M.J., 2011. A novel class of specific HSP90 small molecule inhibitors demonstrate in vitro and in vivo anti-tumor activity in human melanoma cells. *Cancer letters*, *300*(1), pp.30-39.

Meimaridou, E., Gooljar, S.B., Ramnarace, N., Anthonypillai, L., Clark, A.J. and Chapple, J.P., 2011. The cytosolic chaperone Hsc70 promotes traffic to the cell surface of intracellular retained melanocortin-4 receptor mutants.*Molecular Endocrinology*, *25*(9), pp.1650-1660.

Meister, G. and Tuschl, T., 2004. Mechanisms of gene silencing by double-stranded RNA. *Nature*, *431*(7006), pp.343-349.

Meister, G., 2013. Argonaute proteins: functional insights and emerging roles. *Nature Reviews Genetics*, *14*(7), pp.447-459.

Meyer, P., Prodromou, C., Hu, B., Vaughan, C., Roe, S.M., Panaretou, B., Piper, P.W. and Pearl, L.H., 2003. Structural and functional analysis of the middle segment of HSP90: implications for ATP hydrolysis and client protein and cochaperone interactions. *Molecular cell*, *11*(3), pp.647-658.

Meyer, P., Prodromou, C., Liao, C., Hu, B., Roe, S.M., Vaughan, C.K., Vlasic, I., Panaretou, B., Piper, P.W. and Pearl, L.H., 2004. Structural basis for recruitment of the ATPase activator AHA1 to the HSP90 chaperone machinery. *The EMBO journal*, *23*(3), pp.511-519.

Michaud, N.R., Fabian, J.R., Mathes, K.D. and Morrison, D.K., 1995. 14-3-3 is not essential for RAF-1 function: identification of RAF-1 proteins that are biologically activated in a 14-3-3-and Ras-independent manner. *Molecular and Cellular Biology*, *15*(6), pp.3390-3397.

Mikolajczyk, M. and Nelson, M.A., 2004. Regulation of stability of cyclin-dependent kinase CDK11p110 and a caspase-processed form, CDK11p46, by HSP90. *Biochemical Journal*, *384*(3), pp.461-467.

Minami, Y., Kimura, Y., Kawasaki, H., Suzuki, K. and Yahara, I., 1994. The carboxy-terminal region of mammalian HSP90 is required for its dimerization and function in vivo. *Molecular and Cellular Biology*, *14*(2), pp.1459-1464.

Miyata, Y. and Nishida, E., 2004. CK2 controls multiple protein kinases by phosphorylating a kinase-targeting molecular chaperone, CDC37. *Molecular and cellular biology*, *24*(9), pp.4065-4074.

Mizushima, N. and Komatsu, M., 2011. Autophagy: renovation of cells and tissues. *Cell*, *147*(4), pp.728-741.

Mizushima, N., 2007. Autophagy: process and function. *Genes & development*, *21*(22), pp.2861-2873.

Modi, S., Stopeck, A.T., Gordon, M.S., Mendelson, D., Solit, D.B., Bagatell, R., Ma, W., Wheler, J., Rosen, N., Norton, L. and Cropp, G.F., 2007. Combination of trastuzumab and tanespimycin (17-AAG, KOS-953) is safe and active in trastuzumab-refractory HER-2–overexpressing breast cancer: a phase I dose-escalation study. *Journal of Clinical Oncology*, *25*(34), pp.5410-5417.

Mollapour, M., Tsutsumi, S., Truman, A.W., Xu, W., Vaughan, C.K., Beebe, K., Konstantinova, A., Vourganti, S., Panaretou, B., Piper, P.W. and Trepel, J.B., 2011. Threonine 22 phosphorylation attenuates HSP90 interaction with cochaperones and affects its chaperone activity. *Molecular cell*, *41*(6), pp.672-681.

Moodie, S.A., Paris, M.J., Kolch, W. and Wolfman, A., 1994. Association of MEK1 with p21ras. GMPPNP is dependent on B-RAF. *Molecular and Cellular Biology*, *14*(11), pp.7153-7162.

Moraes, T.F., Edwards, R.A., McKenna, S., Pastushok, L., Xiao, W., Glover, J.M. and Ellison, M.J., 2001. Crystal structure of the human ubiquitin conjugating enzyme complex, hMms2–hUbc13. *Nature Structural & Molecular Biology*, *8*(8), pp.669-673.

Mort-Bontemps-Soret, M., Facca, C. and Faye, G., 2002. Physical interaction of Cdc28 with CDC37 in Saccharomyces cerevisiae. *Molecular Genetics and Genomics*, *267*(4), pp.447-458.

Mudgil, Y., Shiu, S.H., Stone, S.L., Salt, J.N. and Goring, D.R., 2004. A large complement of the predicted Arabidopsis ARM repeat proteins are members of the U-box E3 ubiquitin ligase family. *Plant Physiology*, *134*(1), pp.59-66.

Murata, S., Minami, Y., Minami, M., Chiba, T. and Tanaka, K., 2001. CHIP is a

chaperone-dependent E3 ligase that ubiquitylates unfolded protein. EMBO reports, 2(12), pp.1133-1138.

Muslin, A.J. and Xing, H., 2000. 14-3-3 proteins: regulation of subcellular localization by molecular interference. *Cellular signalling*, *12*(11), pp.703-709.

Muslin, A.J., Tanner, J.W., Allen, P.M. and Shaw, A.S., 1996. Interaction of 14-3-3 with signaling proteins is mediated by the recognition of phosphoserine. *Cell*, *84*(6), pp.889-897.

Nagengast, W.B., de Korte, M.A., Munnink, T.H.O., Timmer-Bosscha, H., den Dunnen, W.F., Hollema, H., de Jong, J.R., Jensen, M.R., Quadt, C., Garcia-Echeverria, C. and van Dongen, G.A., 2010. 89Zr-bevacizumab PET of early antiangiogenic tumor response to treatment with HSP90 inhibitor NVP-AUY922. *Journal of Nuclear Medicine*, *51*(5), pp.761-767.

Nakatogawa, H., Suzuki, K., Kamada, Y. and Ohsumi, Y., 2009. Dynamics and diversity in autophagy mechanisms: lessons from yeast. *Nature reviews Molecular cell biology*, *10*(7), pp.458-467.

Nathan, D.F., Vos, M.H. and Lindquist, S., 1999. Identification of SSF1, CNS1, and HCH1 as multicopy suppressors of a Saccharomyces cerevisiae HSP90 loss-of-function mutation. *Proceedings of the National Academy of Sciences*, *96*(4), pp.1409-1414.

Neckers, L. and Workman, P., 2012. HSP90 molecular chaperone inhibitors: are we there yet?. *Clinical Cancer Research*, *18*(1), pp.64-76.

Nelson, D.E., Randle, S.J. and Laman, H., 2013. Beyond ubiquitylation: the atypical functions of Fbxo7 and other F-box proteins. *Open biology*, *3*(10), p.130131.

Nollen, E.A. and Morimoto, R.I., 2002. Chaperoning signaling pathways: molecular chaperones as stress-sensingheat shock'proteins. *Journal of cell science*, *115*(14), pp.2809-2816.

Nony, P., Gaude, H., Rossel, M., Fournier, L., Rouault, J.P. and Billaud, M., 2003. Stability of the Peutz–Jeghers syndrome kinase LKB1 requires its binding to the molecular chaperones HSP90/CDC37. *Oncogene*, *22*(57), pp.9165-9175.

Nykänen, A., Haley, B. and Zamore, P.D., 2001. ATP requirements and small

interfering RNA structure in the RNA interference pathway. *Cell*, *107*(3), pp.309-321.

Obermann, W.M., Sondermann, H., Russo, A.A., Pavletich, N.P. and Hartl, F.U., 1998. In vivo function of HSP90 is dependent on ATP binding and ATP hydrolysis. *The Journal of cell biology*, *143*(4), pp.901-910.

Ogier-Denis, E., Houri, J.J., Bauvy, C. and Codogno, P., 1996. Guanine nucleotide exchange on heterotrimeric Gi3 protein controls autophagic sequestration in HT-29 cells. *Journal of Biological Chemistry*, *271*(45), pp.28593-28600.

Ogunjimi, A.A., Briant, D.J., Pece-Barbara, N., Le Roy, C., Di Guglielmo, G.M., Kavsak, P., Rasmussen, R.K., Seet, B.T., Sicheri, F. and Wrana, J.L., 2005. Regulation of Smurf2 ubiquitin ligase activity by anchoring the E2 to the HECT domain. *Molecular cell*, *19*(3), pp.297-308.

Ohi, M.D., Vander Kooi, C.W., Rosenberg, J.A., Chazin, W.J. and Gould, K.L., 2003. Structural insights into the U-box, a domain associated with multi-ubiquitylation. *Nature Structural & Molecular Biology*, *10*(4), pp.250-255.

Ohi, M.D., Vander Kooi, C.W., Rosenberg, J.A., Ren, L., Hirsch, J.P., Chazin, W.J., Walz, T. and Gould, K.L., 2005. Structural and functional analysis of essential pre-mRNA splicing factor Prp19p. *Molecular and cellular biology*, *25*(1), pp.451-460.

Okumura, F., Joo-Okumura, A., Nakatsukasa, K. and Kamura, T., 2016. The role of cullin 5-containing ubiquitin ligases. *Cell division*, *11*(1).

Okumura, F., Matsuzaki, M. and andTakumi Kamura, K.N., 2012. The role of elongin BC-containing ubiquitin ligases. *The key role of ubiquitylation and sumoylation in signaling and cancer*, *Front Oncol, 2*(10).

Pacey, S., Banerj, U., Judson, I. and Workman, P., 2006. HSP90 inhibitors in the clinic. *Handb Exp Pharmacol, 172*, pp.331-358.

Palacios, C., López-Pérez, A.I. and López-Rivas, A., 2010. Down-regulation of RIP expression by 17-dimethylaminoethylamino-17-demethoxygeldanamycin promotes TRAIL-induced apoptosis in breast tumor cells. *Cancer letters*, *287*(2), pp.207-215.

Pan, Z.Q., Kentsis, A., Dias, D.C., Yamoah, K. and Wu, K., 2004. Nedd8 on cullin: building an expressway to protein destruction. *Oncogene*, *23*(11), pp.1985-1997.

Panaretou, B., Prodromou, C., Roe, S.M., O'Brien, R., Ladbury, J.E., Piper, P.W. and Pearl, L.H., 1998. ATP binding and hydrolysis are essential to the function of the HSP90 molecular chaperone in vivo. *The EMBO journal*, *17*(16), pp.4829-4836.

Panaretou, B., Siligardi, G., Meyer, P., Maloney, A., Sullivan, J.K., Singh, S., Millson, S.H., Clarke, P.A., Naaby-Hansen, S., Stein, R. and Cramer, R., 2002. Activation of the ATPase activity of HSP90 by the stress-regulated cochaperone AHA1. *Molecular cell*, *10*(6), pp.1307-1318.

Park, K.S., Oh, B., Lee, M.H., Nam, K.Y., Jin, H.R., Yang, H., Choi, J., Kim, S.W. and Lee, D.H., 2016. The HSP90 inhibitor, NVP-AUY922, sensitizes KRAS-mutant non-small cell lung cancer with intrinsic resistance to MEK inhibitor, trametinib. *Cancer letters*, *372*(1), pp.75-81.

Passmore, L.A., McCormack, E.A., Au, S.W., Paul, A., Willison, K.R., Harper, J.W. and Barford, D., 2003. Doc1 mediates the activity of the anaphase‐promoting complex by contributing to substrate recognition. *The EMBO journal*, *22*(4), pp.786-796.

Pastushok, L., Moraes, T.F., Ellison, M.J. and Xiao, W., 2005. A single Mms2 “key” residue insertion into a Ubc13 pocket determines the interface specificity of a human Lys63 ubiquitin conjugation complex. *Journal of Biological Chemistry*, *280*(18), pp.17891-17900.

Patton, E.E., Willems, A.R., Sa, D., Kuras, L., Thomas, D., Craig, K.L. and Tyers, M., 1998. Cdc53 is a scaffold protein for multiple Cdc34/Skp1/F-box protein complexes that regulate cell division and methionine biosynthesis in yeast. *Genes & Development*, *12*(5), pp.692-705.

Pearl, L.H. and Prodromou, C., 2001. Structure, function, and mechanism of the HSP90 molecular chaperone. *Advances in protein chemistry*, *59*, pp.157-186.

Pearl, L.H. and Prodromou, C., 2006. Structure and mechanism of the HSP90 molecular chaperone machinery. *Annu. Rev. Biochem*, *75*, pp.271-294.

Pei, X.H., Bai, F., Li, Z., Smith, M.D., Whitewolf, G., Jin, R. and Xiong, Y., 2011. Cytoplasmic CUL9/PARC ubiquitin ligase is a tumor suppressor and promotes p53-dependent apoptosis. *Cancer research*, *71*(8), pp.2969-2977.

Peng, H.M., Morishima, Y., Jenkins, G.J., Dunbar, A.Y., Lau, M., Patterson, C., Pratt, W.B. and Osawa, Y., 2004. Ubiquitylation of neuronal nitric-oxide synthase by CHIP, a chaperone-dependent E3 ligase. *Journal of Biological Chemistry*, *279*(51), pp.52970-52977.

Petosa, C., Masters, S.C., Bankston, L.A., Pohl, J., Wang, B., Fu, H. and Liddington, R.C., 1998. 14-3-3 binds a phosphorylated RAF peptide and an unphosphorylated peptide via its conserved amphipathic groove. *Journal of Biological Chemistry*, *273*(26), pp.16305-16310.

Petroski, M.D. and Deshaies, R.J., 2005. Function and regulation of cullin–RING ubiquitin ligases. *Nature reviews Molecular cell biology*, *6*(1), pp.9-20.

Petrucelli, L., Dickson, D., Kehoe, K., Taylor, J., Snyder, H., Grover, A., De Lucia, M., McGowan, E., Lewis, J., Prihar, G. and Kim, J., 2004. CHIP and HSP70 regulate tau ubiquitylation, degradation and aggregation. *Human molecular genetics*, *13*(7), pp.703-714.

Pham, J.W., Pellino, J.L., Lee, Y.S., Carthew, R.W. and Sontheimer, E.J., 2004. A Dicer-2-dependent 80s complex cleaves targeted mRNAs during RNAi in Drosophila. *Cell*, *117*(1), pp.83-94.

Pick, E., Kluger, Y., Giltnane, J.M., Moeder, C., Camp, R.L., Rimm, D.L. and Kluger, H.M., 2007. High HSP90 expression is associated with decreased survival in breast cancer. *Cancer research*, *67*(7), pp.2932-2937.

Piessevaux, J., Lavens, D., Peelman, F. and Tavernier, J., 2008. The many faces of the SOCS box. *Cytokine & growth factor reviews*, *19*(5), pp.371-381.

Polier, S., Samant, R.S., Clarke, P.A., Workman, P., Prodromou, C. and Pearl, L.H., 2013. ATP-competitive inhibitors block protein kinase recruitment to the HSP90-CDC37 system. *Nature chemical biology*, *9*(5), pp.307-312.

Powers, M.V. and Workman, P., 2006. Targeting of multiple signalling pathways by heat shock protein 90 molecular chaperone inhibitors. *Endocrine-Related Cancer*, *13*(Supplement 1), pp.S125-S135.

Pratt, W.B., Galigniana, M.D., Morishima, Y. and Murphy, P.J., 2004. Role of

molecular chaperones in steroid receptor action. *Essays in biochemistry*, *40*, pp.41-58.

Pratt, W.B., Morishima, Y., Murphy, M. and Harrell, M., 2006. Chaperoning of glucocorticoid receptors. *Handb Exp Pharmacol, 172*, pp.111-138.

Prince, T. and Matts, R.L., 2004. Definition of protein kinase sequence motifs that trigger high affinity binding of HSP90 and CDC37. *Journal of Biological Chemistry*, *279*(38), pp.39975-39981.

Pritchard, C.A., Samuels, M.L., Bosch, E. and McMahon, M., 1995. Conditionally oncogenic forms of the A-RAF and B-RAF protein kinases display different biological and biochemical properties in NIH 3T3 cells. *Molecular and cellular biology*, *15*(11), pp.6430-6442.

Prodromou, C., 2012. The 'active life'of HSP90 complexes. *Biochimica et Biophysica Acta (BBA)-Molecular Cell Research*, *1823*(3), pp.614-623.

Prodromou, C., Panaretou, B., Chohan, S., Siligardi, G., O'Brien, R., Ladbury, J.E., Roe, S.M., Piper, P.W. and Pearl, L.H., 2000. The ATPase cycle of HSP90 drives a molecular 'clamp'via transient dimerization of the N‐terminal domains. *The EMBO Journal*, *19*(16), pp.4383-4392.

Prodromou, C., Roe, S.M., O'Brien, R., Ladbury, J.E., Piper, P.W. and Pearl, L.H., 1997a. Identification and structural characterization of the ATP/ADP-binding site in the HSP90 molecular chaperone. *Cell*, *90*(1), pp.65-75.

Prodromou, C., Roe, S.M., Piper, P.W. and Pearl, L.H., 1997b. A molecular clamp in the crystal structure of the N-terminal domain of the yeast HSP90 chaperone. *Nature Structural & Molecular Biology*, *4*(6), pp.477-482.

Prodromou, C., Siligardi, G., O'Brien, R., Woolfson, D.N., Regan, L., Panaretou, B., Ladbury, J.E., Piper, P.W. and Pearl, L.H., 1999. Regulation of Hsp90 ATPase activity by tetratricopeptide repeat (TPR)‐domain co‐chaperones. *The EMBO journal*, *18*(3), pp.754-762.

Rabut, G. and Peter, M., 2008. Function and regulation of protein neddylation. *EMBO reports*, *9*(10), pp.969-976.

Ramsey, A.J., Russell, L.C., Whitt, S.R. and Chinkers, M., 2000. Overlapping sites of

tetratricopeptide repeat protein binding and chaperone activity in heat shock protein 90. *Journal of Biological Chemistry*, *275*(23), pp.17857-17862.

Ran, F., Gadura, N. and Michels, C.A., 2010. HSP90 cochaperone AHA1 is a negative regulator of the Saccharomyces MAL activator and acts early in the chaperone activation pathway. *Journal of Biological Chemistry*, *285*(18), pp.13850-13862.

Rapp, U.R., Goldsborough, M.D., Mark, G.E., Bonner, T.I., Groffen, J., Reynolds, F.H. and Stephenson, J.R., 1983. Structure and biological activity of v-RAF, a unique oncogene transduced by a retrovirus. *Proceedings of the National Academy of Sciences*, *80*(14), pp.4218-4222.

Resnier, P., Montier, T., Mathieu, V., Benoit, J.P. and Passirani, C., 2013. A review of the current status of siRNA nanomedicines in the treatment of cancer. *Biomaterials*, *34*(27), pp.6429-6443.

Retzlaff, M., Hagn, F., Mitschke, L., Hessling, M., Gugel, F., Kessler, H., Richter, K. and Buchner, J., 2010. Asymmetric activation of the HSP90 dimer by its cochaperone AHA1. *Molecular cell*, *37*(3), pp.344-354.

Riedl, B., Lowinger, T.B., Bankston, D., Barbosa, J., Brittelli, D.R., Carlson, R., Dumas, J., Hibner, B., Kadono, H., Katz, M. and Kennure, N., 2001. Potent RAF kinase inhibitors from the diphenylurea class: structure activity relationships. *Clin. Cancer Res*, *20*, p.83a.

Riggs, D.L., Cox, M.B., Cheung-Flynn, J., Prapapanich, V., Carrigan, P.E. and Smith, D.F., 2004. Functional specificity of co-chaperone interactions with HSP90 client proteins. *Critical reviews in biochemistry and molecular biology*, *39*(5-6), pp.279-295.

Roberts, E.A. and Deretic, V., 2008. Autophagic proteolysis of long-lived proteins in nonliver cells. *Autophagosome and Phagosome*, *445*, pp.111-117.

Roberts, P.J. and Der, C.J., 2007. Targeting the RAF-MEK-ERK mitogen-activated protein kinase cascade for the treatment of cancer. *Oncogene*, *26*(22), pp.3291-3310.

Roe, S.M., Ali, M.M., Meyer, P., Vaughan, C.K., Panaretou, B., Piper, P.W., Prodromou, C. and Pearl, L.H., 2004. The mechanism of HSP90 regulation by the protein kinase-specific cochaperone p50 CDC37. *Cell*, *116*(1), pp.87-98.

Roe, S.M., Prodromou, C., O'Brien, R., Ladbury, J.E., Piper, P.W. and Pearl, L.H., 1999. Structural basis for inhibition of the HSP90 molecular chaperone by the antitumor antibiotics radicicol and geldanamycin. *Journal of medicinal chemistry*, *42*(2), pp.260-266.

Rommel, C., Radziwill, G., Lovrić, J., Noeldeke, J., Heinicke, T., Jones, D., Aitken, A. and Moelling, K., 1996. Activated Ras displaces 14-3-3 protein from the amino terminus of c-RAF-1. *Oncogene*, *12*(3), pp.609-619.

Rothofsky, M.L. and Lin, S.L., 1997. CROC-1 encodes a protein which mediates transcriptional activation of the human FOS promoter. *Gene*, *195*(2), pp.141-149.

Rotin, D. and Kumar, S., 2009. Physiological functions of the HECT family of ubiquitin ligases. *Nature reviews Molecular cell biology*, *10*(6), pp.398-409.

Roy, S., McPherson, R.A., Apolloni, A., Yan, J., Lane, A., Clyde-Smith, J. and Hancock, J.F., 1998. 14-3-3 facilitates Ras-dependent RAF-1 activation in vitro and in vivo. *Molecular and cellular biology*, *18*(7), pp.3947-3955.

Russell, L.C., Whitt, S.R., Chen, M.S. and Chinkers, M., 1999. Identification of conserved residues required for the binding of a tetratricopeptide repeat domain to heat shock protein 90. *Journal of Biological Chemistry*, *274*(29), pp.20060-20063.

Samant, R.S., Clarke, P.A. and Workman, P., 2014. E3 ubiquitin ligase Cullin-5 modulates multiple molecular and cellular responses to heat shock protein 90 inhibition in human cancer cells. *Proceedings of the National Academy of Sciences*, *111*(18), pp.6834-6839.

Sancho, E., Vilá, M.R., Sánchez-Pulido, L., Lozano, J.J., Paciucci, R., Nadal, M., Fox, M., Harvey, C., Bercovich, B., Loukili, N. and Ciechanover, A., 1998. Role of UEV-1, an inactive variant of the E2 ubiquitinconjugating enzymes, in in vitro differentiation and cell cycle behavior of HT-29-M6 intestinal mucosecretory cells. *Molecular and cellular biology*, *18*(1), pp.576-589.

Sato, S., Fujita, N. and Tsuruo, T., 2000. Modulation of Akt kinase activity by binding to HSP90. *Proceedings of the National Academy of Sciences*, *97*(20), pp.10832-10837.

Sausville, E.A., Tomaszewski, J.E. and Ivy, P., 2003. Clinical development of 17-

allylamino, 17-demethoxygeldanamycin. *Current cancer drug targets*, *3*(5), pp.377-383.

Scheffner, M., Huibregtse, J.M., Vierstra, R.D. and Howley, P.M., 1993. The HPV-16 E6 and E6-AP complex functions as a ubiquitin-protein ligase in the ubiquitylation of p53. *Cell*, *75*(3), pp.495-505.

Schiapparelli, L.M., McClatchy, D.B., Liu, H.H., Sharma, P., Yates III, J.R. and Cline, H.T., 2014. Direct detection of biotinylated proteins by mass spectrometry. *Journal of proteome research*, *13*(9), pp.3966-3978.

Schlesinger, D.H., Goldstein, G. and Niall, H.D., 1975. Complete amino acid sequence of ubiquitin, an adenylate cyclase stimulating polypeptide probably universal in living cells. *Biochemistry*, *14*(10), pp.2214-2218.

Schreck, R. and Rapp, U.R., 2006. RAF kinases: oncogenesis and drug discovery. *International journal of cancer*, *119*(10), pp.2261-2271.

Schulman, B.A. and Harper, J.W., 2009. Ubiquitin-like protein activation by E1 enzymes: the apex for downstream signalling pathways. *Nature reviews Molecular cell biology*, *10*(5), pp.319-331.

Schulte, T.W., Blagosklonny, M.V., Ingui, C. and Neckers, L., 1995. Disruption of the RAF-1-HSP90 molecular complex results in destabilization of RAF-1 and loss of RAF-1-Ras association. *Journal of Biological Chemistry*, *270*(41), pp.24585-24588.

Schulze, A., Beliu, G., Helmerich, D.A., Schubert, J., Pearl, L.H., Prodromou, C. and Neuweiler, H., 2016. Cooperation of local motions in the HSP90 molecular chaperone ATPase mechanism. *Nature Chemical Biology, 12,* pp.628-635.

Scroggins, B.T., Prince, T., Shao, J., Uma, S., Huang, W., Guo, Y., Yun, B.G., Hedman, K., Matts, R.L. and Hartson, S.D., 2003. High affinity binding of HSP90 is triggered by multiple discrete segments of its kinase clients. *Biochemistry*, *42*(43), pp.12550-12561.

Shao, J., Irwin, A., Hartson, S.D. and Matts, R.L., 2003a. Functional dissection of CDC37: characterization of domain structure and amino acid residues critical for protein kinase binding. *Biochemistry*, *42*(43), pp.12577-12588.

Shao, J., Prince, T., Hartson, S.D. and Matts, R.L., 2003b. Phosphorylation of serine 13 is required for the proper function of the HSP90 co-chaperone, CDC37. *Journal of*

Biological Chemistry, *278*(40), pp.38117-38120.

Sharp, S. and Workman, P., 2006. Inhibitors of the HSP90 molecular chaperone: current status. *Advances in cancer research*, *95*, pp.323-348.

Sharp, S.Y., Prodromou, C., Boxall, K., Powers, M.V., Holmes, J.L., Box, G., Matthews, T.P., Cheung, K.M.J., Kalusa, A., James, K. and Hayes, A., 2007b. Inhibition of the heat shock protein 90 molecular chaperone in vitro and in vivo by novel, synthetic, potent resorcinylic pyrazole/isoxazole amide analogues. *Molecular Cancer Therapeutics*, *6*(4), pp.1198-1211.

Shiau, A.K., Harris, S.F., Southworth, D.R. and Agard, D.A., 2006. Structural analysis of E. coli HSP90 reveals dramatic nucleotide-dependent conformational rearrangements. *Cell*, *127*(2), pp.329-340.

Shimura, H., Schwartz, D., Gygi, S.P. and Kosik, K.S., 2004. CHIP-Hsc70 complex ubiquitinates phosphorylated tau and enhances cell survival. *Journal of Biological Chemistry*, *279*(6), pp.4869-4876.

Sidera, K. and Patsavoudi, E., 2008. Extracellular HSP90: conquering the cell surface. *Cell Cycle*, *7*(11), pp.1564-1568.

Siligardi, G., Panaretou, B., Meyer, P., Singh, S., Woolfson, D.N., Piper, P.W., Pearl, L.H. and Prodromou, C., 2002. Regulation of HSP90 ATPase activity by the co-chaperone CDC37p/p50 CDC37. *Journal of Biological Chemistry*, *277*(23), pp.20151-20159.

Simpson, M.V., 1953. The release of labeled amino acids from the proteins of rat liver slices. *Journal of Biological Chemistry*, *201*, pp.143-154.

Smith, J.R., Clarke, P.A., de Billy, E. and Workman, P., 2009. Silencing the cochaperone CDC37 destabilizes kinase clients and sensitizes cancer cells to HSP90 inhibitors. *Oncogene*, *28*(2), pp.157-169.

Smith, J.R., de Billy, E., Hobbs, S., Powers, M., Prodromou, C., Pearl, L., Clarke, P.A. and Workman, P., 2015. Restricting direct interaction of CDC37 with HSP90 does not compromise chaperoning of client proteins. *Oncogene*, *34*(1), pp.15-26.

Smith, R.A., Barbosa, J., Blum, C.L., Bobko, M.A., Caringal, Y.V., Dally, R., Johnson,

J.S., Katz, M.E., Kennure, N., Kingery-Wood, J. and Lee, W., 2001. Discovery of heterocyclic ureas as a new class of RAF kinase inhibitors: identification of a second generation lead by a combinatorial chemistry approach. *Bioorganic & medicinal chemistry letters*, *11*(20), pp.2775-2778.

Smith, R.A., Dumas, J., Adnane, L. and Wilhelm, S.M., 2006. Recent advances in the research and development of RAF kinase inhibitors. *Current topics in medicinal chemistry*, *6*(11), pp.1071-1089.

Soucy, T.A., Dick, L.R., Smith, P.G., Milhollen, M.A. and Brownell, J.E., 2010. The NEDD8 conjugation pathway and its relevance in cancer biology and therapy. *Genes & cancer*, *1*(7), pp.708-716.

Southworth, D.R. and Agard, D.A., 2008. Species-dependent ensembles of conserved conformational states define the HSP90 chaperone ATPase cycle. *Molecular cell*, *32*(5), pp.631-640.

Spana, E.P. and Doe, C.Q., 1996. Numb antagonizes Notch signaling to specify sibling neuron cell fates. *Neuron*, *17*(1), pp.21-26.

Spratt, D.E., Walden, H. and Shaw, G.S., 2014. RBR E3 ubiquitin ligases: new structures, new insights, new questions. *Biochemical Journal*, *458*(3), pp.421-437.

Stancato, L.F., Chow, Y.H., Hutchison, K.A., Perdew, G.H., Jove, R. and Pratt, W.B., 1993. RAF exists in a native heterocomplex with HSP90 and p50 that can be reconstituted in a cell-free system. *Journal of Biological Chemistry*, *268*(29), pp.21711-21716.

Stancato, L.F., Silverstein, A.M., Owens-Grillo, J.K., Chow, Y.H., Jove, R. and Pratt, W.B., 1997. The HSP90-binding antibiotic geldanamycin decreases RAF levels and epidermal growth factor signaling without disrupting formation of signaling complexes or reducing the specific enzymatic activity of RAF kinase. *Journal of Biological Chemistry*, *272*(7), pp.4013-4020.

Stebbins, C.E., Russo, A.A., Schneider, C., Rosen, N., Hartl, F.U. and Pavletich, N.P., 1997. Crystal structure of an HSP90–geldanamycin complex: targeting of a protein chaperone by an antitumor agent. *Cell*, *89*(2), pp.239-250.

Stepanova, L., Leng, X., Parker, S.B. and Harper, J.W., 1996. Mammalian p50CDC37 is a protein kinase-targeting subunit of HSP90 that binds and stabilizes CDK4. *Genes & development*, *10*(12), pp.1491-1502.

Stingl, L., Stühmer, T., Chatterjee, M., Jensen, M.R., Flentje, M. and Djuzenova, C.S., 2010. Novel HSP90 inhibitors, NVP-AUY922 and NVP-BEP800, radiosensitise tumour cells through cell-cycle impairment, increased DNA damage and repair protraction. *British journal of cancer*, *102*(11), pp.1578-1591.

Stokoe, D., Macdonald, S.G., Cadwallader, K., Symons, M. and Hancock, J.F., 1994. Activation of RAF as a result of recruitment to the plasma membrane. *Science*, *264*(5164), pp.1463-1467.

Sturm, R.A., Duffy, D.L., Zhao, Z.Z., Leite, F.P., Stark, M.S., Hayward, N.K., Martin, N.G. and Montgomery, G.W., 2008. A single SNP in an evolutionary conserved region within intron 86 of the HERC2 gene determines human blue-brown eye color. *The American Journal of Human Genetics*, *82*(2), pp.424-431.

Suen, K.L., Bustelo, X.R. and Barbacid, M., 1995. Lack of evidence for the activation of the Ras/RAF mitogenic pathway by 14-3-3 proteins in mammalian cells. *Oncogene*, *11*(5), pp.825-831.

Sun, F., Mi, Z., Condliffe, S.B., Bertrand, C.A., Gong, X., Lu, X., Zhang, R., Latoche, J.D., Pilewski, J.M., Robbins, P.D. and Frizzell, R.A., 2008. Chaperone displacement from mutant cystic fibrosis transmembrane conductance regulator restores its function in human airway epithelia. *The FASEB Journal*, *22*(9), pp.3255-3263.

Sun, L., Prince, T., Manjarrez, J.R., Scroggins, B.T. and Matts, R.L., 2012. Characterization of the interaction of AHA1 with components of the HSP90 chaperone machine and client proteins. *Biochimica et Biophysica Acta (BBA)-Molecular Cell Research*, *1823*(6), pp.1092-1101.

Sutrave, P., Bonner, T.I., Rapp, U.R., Jansen, H.W., Patschinsky, T. and Bister, K., 1984. Nucleotide sequence of avian retroviral oncogene v-mil: homologue of murine retroviral oncogene v-RAF. *Nature*, *309*(5963), pp.85–88.

Swick, L. and Kapatos, G., 2006. A yeast 2‐hybrid analysis of human GTP cyclohydrolase I protein interactions. *Journal of neurochemistry*, *97*(5), pp.1447-1455.

Swingle, M.R., Honkanen, R.E. and Ciszak, E.M., 2004. Structural basis for the catalytic activity of human serine/threonine protein phosphatase-5. *Journal of Biological Chemistry*, *279*(32), pp.33992-33999.

Tai, H.C. and Schuman, E.M., 2008. Ubiquitin, the proteasome and protein degradation in neuronal function and dysfunction. *Nature Reviews Neuroscience*, *9*(11), pp.826-838.

Taipale, M., Krykbaeva, I., Koeva, M., Kayatekin, C., Westover, K.D., Karras, G.I. and Lindquist, S., 2012. Quantitative analysis of HSP90-client interactions reveals principles of substrate recognition. *Cell*, *150*(5), pp.987-1001.

Taldone, T., Sun, W. and Chiosis, G., 2009. Discovery and development of heat shock protein 90 inhibitors. *Bioorganic & medicinal chemistry*, *17*(6), pp.2225-2235.

Tatebe, H. and Shiozaki, K., 2003. Identification of CDC37 as a novel regulator of the stress-responsive mitogen-activated protein kinase. *Molecular and cellular biology*, *23*(15), pp.5132-5142.

Tenno, T., Fujiwara, K., Tochio, H., Iwai, K., Morita, E.H., Hayashi, H., Murata, S., Hiroaki, H., Sato, M., Tanaka, K. and Shirakawa, M., 2004. Structural basis for distinct roles of Lys63‐and Lys48‐linked polyubiquitin chains. *Genes to Cells*, *9*(10), pp.865-875.

Terasawa, K. and Minami, Y., 2005. A client‐binding site of CDC37. *FEBS Journal*, *272*(18), pp.4684-4690.

Thorson, J.A., Lily, W.K., Hsu, A.L., Shih, N.Y., Graves, P.R., Tanner, J.W., Allen, P.M., Piwnica-Worms, H. and Shaw, A.S., 1998. 14-3-3 proteins are required for maintenance of RAF-1 phosphorylation and kinase activity. *Molecular and cellular biology*, *18*(9), pp.5229-5238.

Toft, D.O., 1998. Recent advances in the study of HSP90 structure and mechanism of action. *Trends in Endocrinology & Metabolism*, *9*(6), pp.238-243.

Tomari, Y. and Zamore, P.D., 2005. Perspective: machines for RNAi. *Genes & development*, *19*(5), pp.517-529.

Tomari, Y., Matranga, C., Haley, B., Martinez, N. and Zamore, P.D., 2004. A protein sensor for siRNA asymmetry. *Science*, *306*(5700), pp.1377-1380.

Trepel, J., Mollapour, M., Giaccone, G. and Neckers, L., 2010. Targeting the dynamic HSP90 complex in cancer. *Nature Reviews Cancer*, *10*(8), pp.537-549.

Tsunematsu, R., Nishiyama, M., Kotoshiba, S., Saiga, T., Kamura, T. and Nakayama, K.I., 2006. Fbxw8 is essential for Cul1-Cul7 complex formation and for placental development. *Molecular and cellular biology*, *26*(16), pp.6157-6169.

Tzivion, G., Luo, Z. and Avruch, J., 1998. A dimeric 14-3-3 protein is an essential cofactor for RAF kinase activity. *Nature*, *394*(6688), pp.88-92.

Ueno, T., Tsukuda, K., Toyooka, S., Ando, M., Takaoka, M., Soh, J., Asano, H., Maki, Y., Muraoka, T., Tanaka, N. and Shien, K., 2012. Strong anti-tumor effect of NVP-AUY922, a novel HSP90 inhibitor, on non-small cell lung cancer. *Lung cancer*, *76*(1), pp.26-31.

Vaughan, C.K., Gohlke, U., Sobott, F., Good, V.M., Ali, M.M., Prodromou, C., Robinson, C.V., Saibil, H.R. and Pearl, L.H., 2006. Structure of an HSP90-CDC37-CDK4 complex. *Molecular cell*, *23*(5), pp.697-707.

Vaughan, C.K., Mollapour, M., Smith, J.R., Truman, A., Hu, B., Good, V.M., Panaretou, B., Neckers, L., Clarke, P.A., Workman, P. and Piper, P.W., 2008. HSP90-dependent activation of protein kinases is regulated by chaperone-targeted dephosphorylation of CDC37. *Molecular cell*, *31*(6), pp.886-895.

Verba, K.A., Wang, R.Y.R., Arakawa, A., Liu, Y., Shirouzu, M., Yokoyama, S. and Agard, D.A., 2016. Atomic structure of HSP90-CDC37-CDK4 reveals that HSP90 traps and stabilizes an unfolded kinase. *Science*, *352*(6293), pp.1542-1547.

Verdecia, M.A., Joazeiro, C.A., Wells, N.J., Ferrer, J.L., Bowman, M.E., Hunter, T. and Noel, J.P., 2003. Conformational flexibility underlies ubiquitin ligation mediated by the WWP1 HECT domain E3 ligase. *Molecular cell*, *11*(1), pp.249-259.

Wan, P.T., Garnett, M.J., Roe, S.M., Lee, S., Niculescu-Duvaz, D., Good, V.M., Project, C.G., Jones, C.M., Marshall, C.J., Springer, C.J. and Barford, D., 2004. Mechanism of activation of the RAF-ERK signaling pathway by oncogenic mutations of B-RAF. *Cell*, *116*(6), pp.855-867.

Wang, H., Chen, Y., Lin, P., Li, L., Zhou, G., Liu, G., Logsdon, C., Jin, J., Abbruzzese,

J.L., Tan, T.H. and Wang, H., 2014. The CUL7/F-box and WD repeat domain containing 8 (CUL7/Fbxw8) ubiquitin ligase promotes degradation of hematopoietic progenitor kinase 1. *Journal of Biological Chemistry*, *289*(7), pp.4009-4017.

Wang, H.G., Takayama, S., Rapp, U.R. and Reed, J.C., 1996. Bcl-2 interacting protein, BAG-1, binds to and activates the kinase RAF-1. *Proceedings of the National Academy of Sciences*, *93*(14), pp.7063-7068.

Wang, X., Venable, J., LaPointe, P., Hutt, D.M., Koulov, A.V., Coppinger, J., Gurkan, C., Kellner, W., Matteson, J., Plutner, H. and Riordan, J.R., 2006. HSP90 cochaperone AHA1 downregulation rescues misfolding of CFTR in cystic fibrosis. *Cell*, *127*(4), pp.803-815.

Welcker, M. and Clurman, B.E., 2008. FBW7 ubiquitin ligase: a tumour suppressor at the crossroads of cell division, growth and differentiation. *Nature Reviews Cancer*, *8*(2), pp.83-93.

Wellbrock, C., Karasarides, M. and Marais, R., 2004. The RAF proteins take centre stage. *Nature Reviews Molecular Cell Biology*, *5*(11), pp.875-885.

Wendel, T., Zhen, Y., Suo, Z., Bruheim, S. and Wiedlocha, A., 2016. The novel HSP90 inhibitor NVP-AUY922 shows synergistic anti-leukemic activity with cytarabine in vivo. *Experimental cell research*, *340*(2), pp.220-226.

Westbrook, T.F., Martin, E.S., Schlabach, M.R., Leng, Y., Liang, A.C., Feng, B., Zhao, J.J., Roberts, T.M., Mandel, G., Hannon, G.J. and DePinho, R.A., 2005. A genetic screen for candidate tumor suppressors identifies REST.*Cell*, *121*(6), pp.837-848.

Whitesell, L., Mimnaugh, E.G., De Costa, B., Myers, C.E. and Neckers, L.M., 1994. Inhibition of heat shock protein HSP90-pp60v-src heteroprotein complex formation by benzoquinone ansamycins: essential role for stress proteins in oncogenic transformation. *Proceedings of the National Academy of Sciences*, *91*(18), pp.8324-8328.

Whitesell, L., Sutphin, P., An, W.G., Schulte, T., Blagosklonny, M.V. and Neckers, L., 1997. Geldanamycin-stimulated destabilization of mutated p53 is mediated by the proteasome in vivo. *Oncogene*, *14*(23).

Wiech, H., Buchner, J., Zimmermann, R. and Jakob, U., 1992. HSP90 chaperones

protein folding in vitro. *Nature*, *358*(6382), pp.169-170.

Wilhelm, S. and Chien, D.S., 2002. BAY 43-9006: preclinical data. *Current pharmaceutical design*, *8*(25), pp.2255-2257.

Wilhelm, S., Carter, C., Lynch, M., Lowinger, T., Dumas, J., Smith, R.A., Schwartz, B., Simantov, R. and Kelley, S., 2006. Discovery and development of Sorafenib: a multikinase inhibitor for treating cancer. *Nature reviews Drug discovery*, *5*(10), pp.835-844.

Wilhelm, S.M., Carter, C., Tang, L., Wilkie, D., McNabola, A., Rong, H., Chen, C., Zhang, X., Vincent, P., McHugh, M. and Cao, Y., 2004. BAY 43-9006 exhibits broad spectrum oral antitumor activity and targets the RAF/MEK/ERK pathway and receptor tyrosine kinases involved in tumor progression and angiogenesis. *Cancer research*, *64*(19), pp.7099-7109.

Wilkinson, K.D., Urban, M.K. and Haas, A.L., 1980. Ubiquitin is the ATP-dependent proteolysis factor I of rabbit reticulocytes. *Journal of Biological Chemistry*, *255*(16), pp.7529-7532.

Wojnowski, L., Stancato, L.F., Larner, A.C., Rapp, U.R. and Zimmer, A., 2000. Overlapping and specific functions of BRAF and CRAF-1 proto-oncogenes during mouse embryogenesis. *Mechanisms of development*, *91*(1), pp.97-104.

Workman, P., Burrows, F., Neckers, L.E.N. and Rosen, N., 2007. Drugging the cancer chaperone HSP90. *Annals of the New York Academy of Sciences*, *1113*(1), pp.202-216.

Wu, K., Fuchs, S.Y., Chen, A., Tan, P., Gomez, C., Ronai, Z.E. and Pan, Z.Q., 2000. The SCFHOS/β-TRCP-ROC1 E3 ubiquitin ligase utilizes two distinct domains within CUL1 for substrate targeting and ubiquitin ligation. *Molecular and Cellular Biology*, *20*(4), pp.1382-1393.

Xiao, W., Broomfield, S., Chow, B.L., Lin, S.L. and Wei, Y.F., 1998. The products of the yeast MMS2 and two human homologs (hMMS2 and CROC-1) define a structurally and functionally conserved Ubc-like protein family. *Nucleic acids research*, *26*(17), pp.3908-3914.

Xie, Z., Johansen, L.K., Gustafson, A.M., Kasschau, K.D., Lellis, A.D., Zilberman, D.,

Jacobsen, S.E. and Carrington, J.C., 2004. Genetic and functional diversification of small RNA pathways in plants. *PLoS Biol*, *2*(5), p.e104.

Xu, W., Marcu, M., Yuan, X., Mimnaugh, E., Patterson, C. and Neckers, L., 2002. Chaperone-dependent E3 ubiquitin ligase CHIP mediates a degradative pathway for c-ErbB2/Neu. *Proceedings of the National Academy of Sciences*, *99*(20), pp.12847-12852.

Xu, W., Mollapour, M., Prodromou, C., Wang, S., Scroggins, B.T., Palchick, Z., Beebe, K., Siderius, M., Lee, M.J., Couvillon, A. and Trepel, J.B., 2012. Dynamic Tyrosine Phosphorylation Modulates Cycling of the HSP90-P50 CDC37-AHA1 Chaperone Machine. *Molecular cell*, *47*(3), pp.434-443.

Xu, X., Sarikas, A., Dias-Santagata, D.C., Dolios, G., Lafontant, P.J., Tsai, S.C., Zhu, W., Nakajima, H., Nakajima, H.O., Field, L.J. and Wang, R., 2008. The CUL7 E3 ubiquitin ligase targets insulin receptor substrate 1 for ubiquitin-dependent degradation. *Molecular cell*, *30*(4), pp.403-414.

Xu, Y. and Lindquist, S., 1993. Heat-shock protein HSP90 governs the activity of pp60v-src kinase. *Proceedings of the National Academy of Sciences*, *90*(15), pp.7074-7078.

Yaffe, M.B., Rittinger, K., Volinia, S., Caron, P.R., Aitken, A., Leffers, H., Gamblin, S.J., Smerdon, S.J. and Cantley, L.C., 1997. The structural basis for 14-3-3: phosphopeptide binding specificity. *Cell*, *91*(7), pp.961-971.

Yamamori, B., Kuroda, S., Shimizu, K., Fukui, K., Ohtsuka, T. and Takai, Y., 1995. Purification of a Ras-dependent mitogen-activated protein kinase kinase kinase from bovine brain cytosol and its identification as a complex of B-RAF and 14-3-3 proteins. *Journal of Biological Chemistry*, *270*(20), pp.11723-11726.

Yi, R., Qin, Y., Macara, I.G. and Cullen, B.R., 2003. Exportin-5 mediates the nuclear export of pre-microRNAs and short hairpin RNAs. *Genes & development*, *17*(24), pp.3011-3016.

YIP-SCHNEIDER, M.T., Wenyan, M.I.A.O., Amy, L.I.N., BARNARD, D.S., TZIVION, G. and MARSHALL, M.S., 2000. Regulation of the RAF-1 kinase domain by phosphorylation and 14-3-3 association. *Biochemical Journal*, *351*(1), pp.151-159.

Young, J.C. and Hartl, F.U., 2000. Polypeptide release by HSP90 involves ATP hydrolysis and is enhanced by the co‐chaperone p23. *The EMBO journal*, *19*(21), pp.5930-5940.

Younger, J.M., Ren, H.Y., Chen, L., Fan, C.Y., Fields, A., Patterson, C. and Cyr, D.M., 2004. A foldable CFTR Δ F508 biogenic intermediate accumulates upon inhibition of the Hsc70‐CHIP E3 ubiquitin ligase. *The Journal of cell biology*, *167*(6), pp.1075-1085.

Yu, J., Lan, J., Zhu, Y., Li, X., Lai, X., Xue, Y., Jin, C. and Huang, H., 2008. The E3 ubiquitin ligase HECTD3 regulates ubiquitylation and degradation of Tara. *Biochemical and biophysical research communications*, *367*(4), pp.805-812.

Zhang, A., He, X., Zhang, L., Yang, L., Woodman, P. and Li, W., 2014. Biogenesis of lysosome-related organelles complex-1 subunit 1 (BLOS1) interacts with sorting nexin 2 and the endosomal sorting complex required for transport-I (ESCRT-I) component TSG101 to mediate the sorting of epidermal growth factor receptor into endosomal compartments. *Journal of Biological Chemistry*, *289*(42), pp.29180-29194.

Zhang, H., Wu, W., Du, Y., Santos, S.J., Conrad, S.E., Watson, J.T., Grammatikakis, N. and Gallo, K.A., 2004. HSP90/p50CDC37 is required for mixed-lineage kinase (MLK) 3 signaling. *Journal of Biological Chemistry*, *279*(19), pp.19457-19463.

Zhang, L., Kang, L., Bond, W. and Zhang, N., 2009. Interaction between syntaxin 8 and HECTD3, a HECT domain ligase. *Cellular and molecular neurobiology*, *29*(1), pp.115-121.

Zhang, M., Kadota, Y., Prodromou, C., Shirasu, K. and Pearl, L.H., 2010. Structural basis for assembly of HSP90-Sgt1-CHORD protein complexes: implications for chaperoning of NLR innate immunity receptors. *Molecular cell*, *39*(2), pp.269-281.

Zhang, M., Windheim, M., Roe, S.M., Peggie, M., Cohen, P., Prodromou, C. and Pearl, L.H., 2005. Chaperoned ubiquitylation—crystal structures of the CHIP U box E3 ubiquitin ligase and a CHIP-Ubc13-Uev1a complex. *Molecular cell*, *20*(4), pp.525-538.

Zhao, Q., Boschelli, F., Caplan, A.J. and Arndt, K.T., 2004. Identification of a conserved sequence motif that promotes CDC37 and cyclin D1 binding to CDK4.

Journal of Biological Chemistry, *279*(13), pp.12560-12564.

Zhong, Q., Gao, W., Du, F. and Wang, X., 2005. Mule/ARF-BP1, a BH3-only E3 ubiquitin ligase, catalyzes the polyubiquitylation of Mcl-1 and regulates apoptosis. *Cell*, *121*(7), pp.1085-1095.

Zhong, X.Y., Ding, J.H., Adams, J.A., Ghosh, G. and Fu, X.D., 2009. Regulation of SR protein phosphorylation and alternative splicing by modulating kinetic interactions of SRPK1 with molecular chaperones. *Genes & development*, *23*(4), pp.482-495.

Zhou, P., Fernandes, N., Dodge, I.L., Reddi, A.L., Rao, N., Safran, H., DiPetrillo, T.A., Wazer, D.E., Band, V. and Band, H., 2003. ErbB2 degradation mediated by the co-chaperone protein CHIP. *Journal of Biological Chemistry*, *278*(16), pp.13829-13837.

Zou, X., Levy-Cohen, G. and Blank, M., 2015. Molecular functions of NEDD4 E3 ubiquitin ligases in cancer. *Biochimica et Biophysica Acta (BBA)-Reviews on Cancer*, *1856*(1), pp.91-106.

Appendix 1

Appendix 1.1 The full-length human CRAF

Item 1: Gene Synthesis
Gene Name: RAF1, Length: 1991bp, Vector Name: pUC57, Codon Optimization: No
Start with: GCTAGCCTCGAGCC
Sequence:
ATGGAGCACATACAGGGAGCTTGGAAGACGATCAGCAATGGTTTTGGATTCAAAGATGCCGTGTTTG
ATGGCTCCAGCTGCATCTCTCCTACAATAGTTCAGCAGTTTGGCTATCAGCGCCGGGCATCAGATGA
TGGCAAACTCACAGATCCTTCTAAGACAAGCAACACTATCCGTGTTTTCTTGCCGAACAAGCAAAGA
ACAGTGGTCAATGTGCGAAATGGAATGAGCTTGCATGACTGCCTTATGAAAGCACTCAAGGTGAGGG
GCCTGCAACCAGAGTGCTGTGCAGTGTTCAGACTTCTCCACGAACACAAAGGTAAAAAAGCACGCTT
AGATTGGAATACTGATGCTGCGTCTTTGATTGGAGAAGAACTTCAAGTAGATTTCCTGGATCATGTT
CCCCTCACAACACACAACTTTGCTCGGAAGACGTTCCTGAAGCTTGCCTTCTGTGACATCTGTCAGA
AATTCCTGCTCAATGGATTTCGATGTCAGACTTGTGGCTACAAATTTCATGAGCACTGTAGCACCAA
AGTACCTACTATGTGTGTGGACTGGAGTAACATCAGACAACTCTTATTGTTTCCAAATTCCACTATT
GGTGATAGTGGAGTCCCAGCACTACCTTCTTTGACTATGCGTCGTATGCGAGAGTCTGTTTCCAGGA
TGCCTGTTAGTTCTCAGCACAGATATTCTACACCTCACGCCTTCACCTTTAACACCTCCAGTCCCTC
ATCTGAAGGTTCCCTCTCCCAGAGGCAGAGGTCGACATCCACACCTAATGTCCACATGGTCAGCACC
ACGCTGCCTGTGGACAGCAGGATGATTGAGGATGCAATTCGAAGTCACAGCGAATCAGCCTCACCTT
CAGCCCTGTCCAGTAGCCCCAACAATCTGAGCCCAACAGGCTGGTCACAGCCGAAAACCCCCGTGCC
AGCACAAAGAGAGCGGGCACCAGTATCTGGGACCCAGGAGAAAAACAAAATTAGGCCTCGTGGACAG
AGAGATTCAAGCTATTATTGGGAAATAGAAGCCAGTGAAGTGATGCTGTCCACTCGGATTGGGTCAG
GCTCTTTTGGAACTGTTTATAAGGGTAAATGGCACGGAGATGTTGCAGTAAAGATCCTAAAGGTTGT
CGACCCAACCCCAGAGCAATTCCAGGCCTTCAGGAATGAGGTGGCTGTTCTGCGCAAAACACGGCAT
GTGAACATTCTGCTTTTCATGGGGTACATGACAAAGGACAACCTGGCAATTGTGACCCAGTGGTGCG
AGGGCAGCAGCCTCTACAAACACCTGCATGTCCAGGAGACCAAGTTTCAGATGTTCCAGCTAATTGA
CATTGCCCGGCAGACGGCTCAGGGAATGGACTATTTGCATGCAAAGAACATCATCCATAGAGACATG
AAATCCAACAATATATTTCTCCATGAAGGCTTAACAGTGAAAATTGGAGATTTTGGTTTGGCAACAG
TAAAGTCACGCTGGAGTGGTTCTCAGCAGGTTGAACAACCTACTGGCTCTGTCCTCTGGATGGCCCC
AGAGGTGATCCGAATGCAGGATAACAACCCATTCAGTTTCCAGTCGGATGTCTACTCCTATGGCATC
GTATTGTATGAACTGATGACGGGGGAGCTTCCTTATTCTCACATCAACAACCGAGATCAGATCATCT
TCATGGTGGGCCGAGGATAtGCCTCCCCAGATCTTAGTAAGCTATATAAGAACTGCCCCAAAGCAAT
GAAGAGGCTGGTAGCTGACTGTGTGAAGAAAGTAAAGGAAGAGAGGCCTCTTTTTCCCCAGATCCTG
TCTTCCATTGAGCTGCTCCAACACTCTCTACCGAAGATCAACCGGAGCGCTTCCGAGCCATCCTTGC
ATCGGGCAGCCCACACTGAGGATATtAATGCTTGCACGCTGACCACGTCCCCGAGGCTGCCTGTCTT
CTAG
End with: GGATCCGAATTCTCTAGACTGCAGACCGGT

Appendix 2

Appendix 2.1 The table of primary antibodies

Dilution factor of primary and secondary antibodies used in western blot analyses.

Name of Antibody	Product code	Company	Dilution
RAF-1	sc-133	santa cruz biotechnology	1:300
RAF-1	sc-7267	santa cruz biotechnology	1:300
RAF-B	sc-5284	santa cruz biotechnology	1:300
PDK1	sc-7140	santa cruz biotechnology	1:300
RIP	sc-7881	santa cruz biotechnology	1:300
CDK4	sc-601	santa cruz biotechnology	1:2000
Ub	sc-8017	santa cruz biotechnology	1:500
GAPDH	MA5-15738	Thermo Fisher	1:10000
MASTL	A302-190A	BETHYL	1:1250
HECTD3	ab173122	Abcam	1:700
Biotin	ab53494	Abcam	1:2000
LKB1	ab15095	Abcam	1:1000
HSP90	ab13492	Abcam	1:2000
Phospho-p44/42 MAPK	9101s	Cell Signalling	1:1000
HER2/erbB2	2242L	Cell Signalling	1:300
GFP	2555s	Cell Signalling	1:2000
Src	2108s	Cell Signalling	1:1000

Appendix 3

Appendix 3.1 The Human Ubiquitin conjugation Subset1

Dharmacon® RTF SMART pool® siRNA Library- Human Ubiquitin Conjugation Subset 1		
H-105615 Lot 12115		
Plate	**Well**	**Gene Symbol**
Plate 1	A01	Dharmacon ON-TARGET*plus*® Non-Targeting Control siRNA #1
Plate 1	A02	UBE2C
Plate 1	A02	UBE2C
Plate 1	A02	UBE2C
Plate 1	A02	UBE2C
Plate 1	A03	SMURF1
Plate 1	A03	SMURF1
Plate 1	A03	SMURF1
Plate 1	A03	SMURF1
Plate 1	A04	EDD1
Plate 1	A04	EDD1
Plate 1	A04	EDD1
Plate 1	A04	EDD1
Plate 1	A05	HIP2
Plate 1	A05	HIP2
Plate 1	A05	HIP2
Plate 1	A05	HIP2
Plate 1	A06	HECTD1
Plate 1	A06	HECTD1
Plate 1	A06	HECTD1
Plate 1	A06	HECTD1
Plate 1	A07	UBE2T
Plate 1	A07	UBE2T
Plate 1	A07	UBE2T
Plate 1	A07	UBE2T
Plate 1	A08	CDC34
Plate 1	A08	CDC34
Plate 1	A08	CDC34
Plate 1	A08	CDC34
Plate 1	A09	FLJ34154
Plate 1	A09	FLJ34154
Plate 1	A09	FLJ34154
Plate 1	A09	FLJ34154
Plate 1	A10	DCUN1D1
Plate 1	A10	DCUN1D1
Plate 1	A10	DCUN1D1
Plate 1	A10	DCUN1D1
Plate 1	A11	CUL2
Plate 1	A11	CUL2
Plate 1	A11	CUL2
Plate 1	A11	CUL2
Plate 1	B01	Dharmacon ON-TARGET*plus*® Non-Targeting Control siRNA #2
Plate 1	B02	HERC3
Plate 1	B02	HERC3

Plate 1	B02	HERC3
Plate 1	B02	HERC3
Plate 1	B03	UBE2W
Plate 1	B03	UBE2W
Plate 1	B03	UBE2W
Plate 1	B03	UBE2W
Plate 1	B04	UBE2V2
Plate 1	B04	UBE2V2
Plate 1	B04	UBE2V2
Plate 1	B04	UBE2V2
Plate 1	B05	DCUN1D5
Plate 1	B05	DCUN1D5
Plate 1	B05	DCUN1D5
Plate 1	B05	DCUN1D5
Plate 1	B06	HERC2
Plate 1	B06	HERC2
Plate 1	B06	HERC2
Plate 1	B06	HERC2
Plate 1	B07	UBE2N
Plate 1	B07	UBE2N
Plate 1	B07	UBE2N
Plate 1	B07	UBE2N
Plate 1	B08	UBE2Z
Plate 1	B08	UBE2Z
Plate 1	B08	UBE2Z
Plate 1	B08	UBE2Z
Plate 1	B09	UBE2L3
Plate 1	B09	UBE2L3
Plate 1	B09	UBE2L3
Plate 1	B09	UBE2L3
Plate 1	B10	HERC5
Plate 1	B10	HERC5
Plate 1	B10	HERC5
Plate 1	B10	HERC5
Plate 1	B11	UBE2NL
Plate 1	B11	UBE2NL
Plate 1	B11	UBE2NL
Plate 1	B11	UBE2NL
Plate 1	B12	Dharmacon GFP Duplex I
Plate 1	C01	Dharmacon ON-TARGET*plus*® Non-Targeting Control siRNA #3
Plate 1	C02	DCUN1D3
Plate 1	C02	DCUN1D3
Plate 1	C02	DCUN1D3
Plate 1	C02	DCUN1D3
Plate 1	C03	BIRC6
Plate 1	C03	BIRC6
Plate 1	C03	BIRC6
Plate 1	C03	BIRC6
Plate 1	C04	UBE2J2
Plate 1	C04	UBE2J2
Plate 1	C04	UBE2J2
Plate 1	C04	UBE2J2
Plate 1	C05	HECW1
Plate 1	C05	HECW1
Plate 1	C05	HECW1

Plate 1	C05	HECW1
Plate 1	C06	UBE1L
Plate 1	C06	UBE1L
Plate 1	C06	UBE1L
Plate 1	C06	UBE1L
Plate 1	C07	UBE1
Plate 1	C07	UBE1
Plate 1	C07	UBE1
Plate 1	C07	UBE1
Plate 1	C08	HERC1
Plate 1	C08	HERC1
Plate 1	C08	HERC1
Plate 1	C08	HERC1
Plate 1	C09	HACE1
Plate 1	C09	HACE1
Plate 1	C09	HACE1
Plate 1	C09	HACE1
Plate 1	C10	CUL7
Plate 1	C10	CUL7
Plate 1	C10	CUL7
Plate 1	C10	CUL7
Plate 1	C11	UBE2S
Plate 1	C11	UBE2S
Plate 1	C11	UBE2S
Plate 1	C11	UBE2S
Plate 1	D01	Dharmacon ON-TARGET*plus*® Non-Targeting Control siRNA #4
Plate 1	D02	CUL3
Plate 1	D02	CUL3
Plate 1	D02	CUL3
Plate 1	D02	CUL3
Plate 1	D03	ITCH
Plate 1	D03	ITCH
Plate 1	D03	ITCH
Plate 1	D03	ITCH
Plate 1	D04	HUWE1
Plate 1	D04	HUWE1
Plate 1	D04	HUWE1
Plate 1	D04	HUWE1
Plate 1	D05	CAND2
Plate 1	D05	CAND2
Plate 1	D05	CAND2
Plate 1	D05	CAND2
Plate 1	D06	UBE2D3
Plate 1	D06	UBE2D3
Plate 1	D06	UBE2D3
Plate 1	D06	UBE2D3
Plate 1	D07	NEDD4
Plate 1	D07	NEDD4
Plate 1	D07	NEDD4
Plate 1	D07	NEDD4
Plate 1	D08	UBE1DC1
Plate 1	D08	UBE1DC1
Plate 1	D08	UBE1DC1
Plate 1	D08	UBE1DC1
Plate 1	D09	UBE2M

Plate 1	D09	UBE2M
Plate 1	D09	UBE2M
Plate 1	D09	UBE2M
Plate 1	D10	UEVLD
Plate 1	D10	UEVLD
Plate 1	D10	UEVLD
Plate 1	D10	UEVLD
Plate 1	D11	UBE2F
Plate 1	D11	UBE2F
Plate 1	D11	UBE2F
Plate 1	D11	UBE2F
Plate 1	E01	Dharmacon ON-TARGET*plus*® Non-Targeting Control Pool
Plate 1	E02	DCUN1D2
Plate 1	E02	DCUN1D2
Plate 1	E02	DCUN1D2
Plate 1	E02	DCUN1D2
Plate 1	E03	CUL1
Plate 1	E03	CUL1
Plate 1	E03	CUL1
Plate 1	E03	CUL1
Plate 1	E04	UBE3B
Plate 1	E04	UBE3B
Plate 1	E04	UBE3B
Plate 1	E04	UBE3B
Plate 1	E05	UBE2A
Plate 1	E05	UBE2A
Plate 1	E05	UBE2A
Plate 1	E05	UBE2A
Plate 1	E06	UBE2E2
Plate 1	E06	UBE2E2
Plate 1	E06	UBE2E2
Plate 1	E06	UBE2E2
Plate 1	E07	HECTD3
Plate 1	E07	HECTD3
Plate 1	E07	HECTD3
Plate 1	E07	HECTD3
Plate 1	E08	UBE2I
Plate 1	E08	UBE2I
Plate 1	E08	UBE2I
Plate 1	E08	UBE2I
Plate 1	E09	UBE2Q2
Plate 1	E09	UBE2Q2
Plate 1	E09	UBE2Q2
Plate 1	E09	UBE2Q2
Plate 1	E10	HERC6
Plate 1	E10	HERC6
Plate 1	E10	HERC6
Plate 1	E10	HERC6
Plate 1	E11	WWP1
Plate 1	E11	WWP1
Plate 1	E11	WWP1
Plate 1	E11	WWP1
Plate 1	F01	Dharmacon ON-TARGET*plus*® Cyclophilin B Control Pool
Plate 1	F02	UBE2O
Plate 1	F02	UBE2O
Plate 1	F02	UBE2O

Plate 1	F02	UBE2O
Plate 1	F03	UBE2V1
Plate 1	F03	UBE2V1
Plate 1	F03	UBE2V1
Plate 1	F03	UBE2V1
Plate 1	F04	UBE2R2
Plate 1	F04	UBE2R2
Plate 1	F04	UBE2R2
Plate 1	F04	UBE2R2
Plate 1	F05	AKTIP
Plate 1	F05	AKTIP
Plate 1	F05	AKTIP
Plate 1	F05	AKTIP
Plate 1	F06	UBE2E1
Plate 1	F06	UBE2E1
Plate 1	F06	UBE2E1
Plate 1	F06	UBE2E1
Plate 1	F07	UBE3C
Plate 1	F07	UBE3C
Plate 1	F07	UBE3C
Plate 1	F07	UBE3C
Plate 1	F08	TSG101
Plate 1	F08	TSG101
Plate 1	F08	TSG101
Plate 1	F08	TSG101
Plate 1	F09	UBE2G2
Plate 1	F09	UBE2G2
Plate 1	F09	UBE2G2
Plate 1	F09	UBE2G2
Plate 1	F10	SMURF2
Plate 1	F10	SMURF2
Plate 1	F10	SMURF2
Plate 1	F10	SMURF2
Plate 1	F11	NEDD4L
Plate 1	F11	NEDD4L
Plate 1	F11	NEDD4L
Plate 1	F11	NEDD4L
Plate 1	G02	UBE1C
Plate 1	G02	UBE1C
Plate 1	G02	UBE1C
Plate 1	G02	UBE1C
Plate 1	G03	UBE2E3
Plate 1	G03	UBE2E3
Plate 1	G03	UBE2E3
Plate 1	G03	UBE2E3
Plate 1	G04	UBE2D1
Plate 1	G04	UBE2D1
Plate 1	G04	UBE2D1
Plate 1	G04	UBE2D1
Plate 1	G05	UBE3A
Plate 1	G05	UBE3A
Plate 1	G05	UBE3A
Plate 1	G05	UBE3A
Plate 1	G06	TRIP12
Plate 1	G06	TRIP12
Plate 1	G06	TRIP12

Plate 1	G06	TRIP12
Plate 1	G07	HECTD2
Plate 1	G07	HECTD2
Plate 1	G07	HECTD2
Plate 1	G07	HECTD2
Plate 1	G08	CUL4A
Plate 1	G08	CUL4A
Plate 1	G08	CUL4A
Plate 1	G08	CUL4A
Plate 1	G09	HERC4
Plate 1	G09	HERC4
Plate 1	G09	HERC4
Plate 1	G09	HERC4
Plate 1	G10	HECW2
Plate 1	G10	HECW2
Plate 1	G10	HECW2
Plate 1	G10	HECW2
Plate 1	G11	UBE2B
Plate 1	G11	UBE2B
Plate 1	G11	UBE2B
Plate 1	G11	UBE2B
Plate 1	H02	UBE2U
Plate 1	H02	UBE2U
Plate 1	H02	UBE2U
Plate 1	H02	UBE2U
Plate 1	H03	TIP120A
Plate 1	H03	TIP120A
Plate 1	H03	TIP120A
Plate 1	H03	TIP120A
Plate 1	H04	KIAA0317
Plate 1	H04	KIAA0317
Plate 1	H04	KIAA0317
Plate 1	H04	KIAA0317
Plate 1	H05	UBE2D4
Plate 1	H05	UBE2D4
Plate 1	H05	UBE2D4
Plate 1	H05	UBE2D4
Plate 1	H06	DCUN1D4
Plate 1	H06	DCUN1D4
Plate 1	H06	DCUN1D4
Plate 1	H06	DCUN1D4
Plate 1	H07	CUL4B
Plate 1	H07	CUL4B
Plate 1	H07	CUL4B
Plate 1	H07	CUL4B
Plate 1	H08	UBE2L6
Plate 1	H08	UBE2L6
Plate 1	H08	UBE2L6
Plate 1	H08	UBE2L6
Plate 1	H09	UBE2J1
Plate 1	H09	UBE2J1
Plate 1	H09	UBE2J1
Plate 1	H09	UBE2J1
Plate 1	H10	FLJ25076
Plate 1	H10	FLJ25076
Plate 1	H10	FLJ25076

Plate 1	H10	FLJ25076
Plate 1	H11	UBE2Q1
Plate 1	H11	UBE2Q1
Plate 1	H11	UBE2Q1
Plate 1	H11	UBE2Q1
Plate 2	A01	Dharmacon ON-TARGET*plus*® Non-Targeting Control siRNA #1
Plate 2	A02	UBE2G1
Plate 2	A02	UBE2G1
Plate 2	A02	UBE2G1
Plate 2	A02	UBE2G1
Plate 2	A03	UBE2H
Plate 2	A03	UBE2H
Plate 2	A03	UBE2H
Plate 2	A03	UBE2H
Plate 2	A04	CUL5
Plate 2	A04	CUL5
Plate 2	A04	CUL5
Plate 2	A04	CUL5
Plate 2	A05	ARIH1
Plate 2	A05	ARIH1
Plate 2	A05	ARIH1
Plate 2	A05	ARIH1
Plate 2	A06	UBE1L2
Plate 2	A06	UBE1L2
Plate 2	A06	UBE1L2
Plate 2	A06	UBE1L2
Plate 2	A07	UBE2D2
Plate 2	A07	UBE2D2
Plate 2	A07	UBE2D2
Plate 2	A07	UBE2D2
Plate 2	A08	WWP2
Plate 2	A08	WWP2
Plate 2	A08	WWP2
Plate 2	A08	WWP2
Plate 2	A09	C10ORF46
Plate 2	A09	C10ORF46
Plate 2	A09	C10ORF46
Plate 2	A09	C10ORF46
Plate 2	B01	Dharmacon ON-TARGET*plus*® Non-Targeting Control siRNA #2
Plate 2	B12	Dharmacon GFP Duplex I
Plate 2	C01	Dharmacon ON-TARGET*plus*® Non-Targeting Control siRNA #3
Plate 2	D01	Dharmacon ON-TARGET*plus*® Non-Targeting Control siRNA #4
Plate 2	E01	Dharmacon ON-TARGET*plus*® Non-Targeting Control Pool
Plate 2	F01	Dharmacon ON-TARGET*plus*® Cyclophilin B Control Pool

Appendix 3.2 The list of siRNA

NAME:	Catlog:
ON-TARGETplus Human Ubiquitin Conjugation Subset 1 - SMARTpool	G-105615-01
ON-TARGETplus Human SOCS1- Individual	J-011511-10-0002
ON-TARGETplus Human SOCS2- Individual	J-017604-05-0002
ON-TARGETplus Human SOCS3- Individual	J-004299-09-0002
ON-TARGETplus Human SOCS4- Individual	J-009037-07-0002
ON-TARGETplus Human SOCS5- Individual	J-017374-05-0002
ON-TARGETplus Human SOCS6- Individual	J-017375-05-0002
ON-TARGETplus Human SOCS7- Individual	J-027197-05-0002
ON-TARGETplus Human CUL3- SMARTpool	L-010224-00-0005
ON-TARGETplus Human CUL5- SMARTpool	L-019553-00-0005
ON-TARGETplus Human HECTD3- SMARTpool	L-027468-00-0005
ON-TARGETplus Human HECTD3- Individual	J-027468-09-0002
ON-TARGETplus Human HECTD3- Individual	J-027468-10-0005
ON-TARGETplus Human HECTD3- Individual	J-027468-11-0005
ON-TARGETplus Human HECTD3- Individual	J-027468-12-0005
ON-TARGETplus Human UBA1- SMARTpool	L-004509-00-0005
ON-TARGETplus Human HERC3- SMARTpool	L-007179-00-0005
ON-TARGETplus Human CUL4B- SMARTpool	L-017965-00-0005
ON-TARGETplus Human TRIP12- SMARTpool	L-007182-00-0005
ON-TARGETplus Human UBE2E1- SMARTpool	L-008850-00-0005
ON-TARGETplus Human UBE2E1- Individual	J-008850-07-0005
ON-TARGETplus Human UBA1- Individual	J-004509-05-0002
ON-TARGETplus Human TCEB1- Individual	J-010541-09-0002
ON-TARGETplus Human TCEB2- Individual	J-012376-08-0002
ON-TARGETplus Human STIP1- Individual	J-019802-05-0020
ON-TARGETplus Human UBE2G1- Individual	J-010154-06-

	0005
ON-TARGETplus Human UBE2D3- Individual	J-008478-10-0005
ON-TARGETplus Human NEDD4- Individual	J-007178-08-0005
ON-TARGETplus Human NEDD4- Individual	J-007178-06-0005
ON-TARGETplus Human STUB1- Individual	J-007201-07-0002
ON-TARGETplus Human UBA5- Individual	J-006405-05-0002
ON-TARGETplus Human UBA6- Individual	J-006403-09-0002
ON-TARGETplus Non-targeting Pool	D-001810-10-05
GFP Duplex I	P-002048-01-20

Note: The siRNA sequence is not available due to the policy of the company.

Appendix 3.2 The customized siRNA sequence for CUL5 and HECTD3

Custom siRNA:	**Sequence:**
CUL5-01:	CAGCTGGTTATTGGAGTAAGA
CUL5-02:	CTGGAGGACTTGATACCGGAA
CUL5-03:	CAGGTTTGAATCAGTCACCTA
CUL5-04:	CCAGCTGATTCAGTTATTATA
HECTD3-01:	GCGGGAACUAGGGUUGAAUUU
HECTD3-02:	GGUAUUUCACCUCUUAAGAUU

Appendix 4

Appendix 4.1 Macros for PLA foci counting

Plugins => Macros => Run

```
// Macro to perform foci analysis using 2 input image stacks

if (nImages != 2) {
	exit("Require 2 input images");
}

selectImage(1);
spots = getTitle();
getDimensions(w1,h1,c1,s1,f1);
selectImage(2);
dapi = getTitle();
getDimensions(w2,h2,c2,s2,f2);

print(spots);

if (w1!=w2 || h1!=h2) {
	exit("Images should be the same width & height");
}

// Detect which is the first channel (spots) and second channel (DAPI)
if (endsWith(spots, '0.tif')) {
	tmp = dapi;
	dapi = spots;
```

```
        spots = tmp;
} else if (!endsWith(spots, '1.tif')) {
        exit("Images should have [01].tif at the end of the title");
}

// SD project the spots
selectWindow(spots);
run("Z Project...", "start=1 end="+nSlices+" projection=[Standard Deviation]");
rename("Spots");
run("Find Maxima...", "noise=5 output=[Point Selection]");

// MAX project the DAPI
selectWindow(dapi);
run("Z Project...", "start=1 end="+nSlices+" projection=[Max Intensity]");
rename("DAPI");
setAutoThreshold("Default dark");
run("Threshold...");

// Allow manual adjustment of the threshold
waitForUser("Click to continue when thresholding is complete...");

setOption("BlackBackground", true);
run("Convert to Mask");

// Remove noise
run("Open");
run("Fill Holes");
run("Gaussian Blur...", "sigma=2");
run("Make Binary");
```

```
run("Watershed");

// Allow manual adjustment of the segregation
waitForUser("Click to continue when segregation is complete...");

// Get the spots and put them on the DAPI mask
selectWindow("Spots");
selectWindow("DAPI");
run("Restore Selection");

run("Assign Foci to Objects", "foci=ROI radius=30 min_size=50 max_size=0 remove_small_objects");

if (getBoolean("Analysis complete. Close all images?")) {
	run("Close All");
}
```

Appendix 5

Appendix 5.1 The expression $BRAF^{V600E}$-eYFP

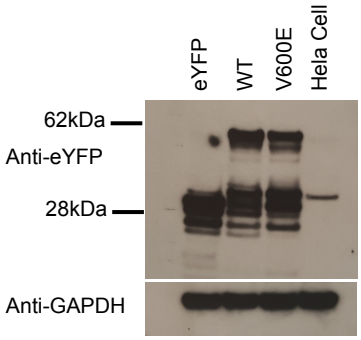

The expression of pEYFP-C1 vector, WT and V600E BRAF kinase domain in Hela cells. Empty pEYFP-C1, pEYFP-$BRAF^{WT}$ kinase domain, pEYFP-$BRAF^{V600E}$ kinase domain were respectively transfected into Hela cells. The expression of the protein was detected by α-GFP antibody after 24 hrs transfection. The GAPDH was used as the loading control for each sample. Free eYFP protein was detected from both pEYFP-$BRAF^{WT}$ and pEYFP-$BRAF^{V600E}$ transfected cells.